Convention on Long-range Transboundary Air Pollution

emep

Co-operative programme for monitoring and evaluation of the long-range transmission of air pollutants in Europe

STATUS REPORT
2/2019 July 2019

Assessment of transboundary pollution by toxic substances: Heavy metals and POPs

Status Report 2/2019

msc-e & ccc & ceip & ineris

Clean Air 40 YEARS

EMEP Status Report 2/2019

July 2019

Assessment of transboundary pollution by toxic substances: Heavy metals and POPs

METEOROLOGICAL SYNTHESIZING CENTRE - EAST

A. Gusev, I. Ilyin, V. Shatalov, O. Travnikov, N. Batrakova, O. Rozovskaya, I. Strijkina

CHEMICAL CO-ORDINATING CENTRE

K.Brevik, Nizzetto P.B., W. Aas

CEIP/Umweltbundesamt Austria

K. Mareckova, S. Poupa, C. Sosa, M. Tista, R. Wankmueller

FRENCH NATIONAL INSTITUTE FOR INDUSTRIAL ENVIRONMENT AND RISKS
F. Couvidat

MCS-E

Meteorological Synthesizing Centre - East

2nd Roshchinsky proezd, 8/5
115419 Moscow
Russia
Phone.: +7 926 906 91 78
Fax: +7 495 956 19 44
E-mail: msce@msceast.org
www.msceast.org

CCC

Norwegian Institute for Air Research (NILU)

P.O. Box 100
NO-2027 Kjeller
Norway
Phone: +47 63 89 80 00
Fax: +47 63 89 80 50
E-mail: kjetil.torseth@nilu.no
www.nilu.no

CEIP

Umweltbundesamt GmbH

Spittelauer Lände 5
1090 Vienna Austria
Phone:+43-(0)1-313 04
Fax: +43-(0)1-313 04/5400
E-mail:
emep.emissions@umweltbundesamt.at
www.umweltbundesamt.at

INERIS

French National Institute for Industrial Environment and Risks

Parc Technologique ALATA
BP 2, 60550 Verneuil-en-Halatte,
Paris, France
Tél. : 03 44 55 66 77
Fax : 03 44 55 66 99
www.ineris.fr

EXECUTIVE SUMMARY

Heavy metals and persistent organic pollutants (POPs) are toxic substances, which are within the scope of various international bodies including the UNECE Convention on Long-range Transboundary Air Pollution (hereafter, CLRTAP or the Convention). Despite continuous decrease of emissions of these pollutants in the past decades, these substances still cause adverse effects on human health and ecosystems (the Long-term Strategy of the Convention, ECE/EB.AIR/2018/1/Rev.1). The priority heavy metals targeted by the Convention are lead (Pb), cadmium (Cd) and mercury (Hg). The list of considered POPs includes polychlorinated biphenyls (PCBs), polychlorinated dibenzo(p)dioxins and dibenzofurans (PCDD/Fs), hexachlorobenzene (HCB), and polyaromatic hydrocarbons (PAHs). The priority PAHs are benzo(a)pyrene (B(a)P), benzo(b)fluoranthene (B(b)F), benzo(k)fluoranthene (B(k)F), and indeno(1,2,3-cd)pyrene (IP). Research and operational assessment of heavy metal and POP pollution are carried out by relevant EMEP Centres – the Centre of Emission Inventories and Projections (CEIP), the Chemical Coordinating Centre (CCC), the Meteorological Synthesizing Centre – East (MSC-E).

The purpose of the present Status Report is to provide an overview of the EMEP Centres activities in the field of heavy metals and POPs carried out in accordance with the bi-annual workplan of the Convention for 2018-2019 [ECE/EB.AIR/GE.1/2017/20-ECE/EB.AIR/WG.1/2017/13]. The report includes information on emissions, monitoring, and model assessment of heavy metal and POP pollution in 2017; research activities and co-operation with subsidiary bodies to the Convention and international organizations. Detailed technical information aimed to support the Status Report is available in the Supplementary Data Reports on heavy metals [*Ilyin et al.,* 2019] and POPs [*Gusev et al.,* 2019] as well as at the MSC-E website (www.msceast.org).

Emissions

Quality of emissions data reported by countries has been improved significantly. In 2019 emission inventories for heavy metals and POPs were submitted by 45 of 51 Parties. Completeness and consistency of the reported data affects significantly estimated emissions trends in various parts of the EMEP region. Emissions of heavy metals in the western part of the EMEP region show a rather smooth declining trend. In contrast, long-term trend of heavy metal emissions in the eastern part of the region as well as trend of POP emissions exhibit strong variations due to incomplete reporting or effect of inconsistent data from individual countries. In order to improve consistency of the time series the countries recalculate previously reported data. For instance, emissions data for 2016 were considerably (more than 15% difference) changed by 22 countries. Gridded emissions data on the new EMEP grid were reported by 29 countries. Final emissions fields for modelling were generated by MSC-E based on reported emissions data collected and gap-filled by CEIP and supplemented by additional information on vertical distribution, seasonal variation and chemical speciation of heavy metal and POP emissions.

Monitoring

Measurements of heavy metal and POP pollution levels were performed at sites of the EMEP monitoring network under methodological guidance of CCC. Observed concentrations of Pb and Cd in air or precipitation in 2017 were reported from 65 measurement sites. Besides, 28 sites were measuring Hg in either air or precipitation. The PAHs measurements were carried out at 36 stations, and other POPs were observed at 12 sites. The lowest concentrations for heavy metals were generally found in Scandinavia, whereas the highest values were commonly observed in Central and Western Europe. The highest PAH and PCB levels took place at sites located in the central part of Europe, while the highest HCB levels are noted for the Arctic stations (Spitsbergen, Greenland). The analysis of seasonal variability reveals that lighter PCB congeners have higher contribution to total sum of PCBs in summer compared to the heavier congeners. It was also shown that HCB air concentrations are the lowest in summer and the highest in winter. The exception is stations located in the high Arctic (e.g., Zeppelin).

Transition to finer spatial resolution makes possible more thorough analysis of heavy metal and POP levels in highly populated and urbanized areas. In order to refine modelling results and facilitate evaluation of the model performance MSC-E utilized supplementary data from AIRBASE database by European Environmental Agency (EEA). Information on air concentrations of Pb, Cd, Hg and B(a)P from more than 700 European sites was involved into the analysis.

Status of pollution levels in 2017

Model assessment of transboundary pollution of the EMEP countries by heavy metals and POPs in 2017 was carried out by MSC-E. Main results of the assessment are based on the most recent heavy metal and POP emissions dataset for 2016 available at the moment of the study. Updated results based on the new emissions reporting for 2017, which became available in the meantime, will be presented at the website along with updated information for the EMEP countries.

The performed analysis shows that the highest levels of Pb, Cd, and Hg deposition take place in the Balkan countries, Central and Eastern Europe. Considerable deposition also occurs along windward slopes of mountain regions (the western part of Norway, the Alpine and Balkan regions, the south-eastern part of Kazakhstan and north of Kyrgyzstan). Elevated Hg deposition fluxes are also predicted in the high Arctic as a result of intensive Hg oxidation during springtime.

High levels of B(a)P concentration, which exceed the air quality guidelines, take place in the countries of Central and Eastern Europe. Countries of Central Europe (Poland, Slovakia, and Hungary) as well as Romania, Northern Italy, Russia, and Turkey are characterized by elevated concentrations of PCDD/Fs. For PCB-153 the areas of relatively high concentrations comprise countries of Western and, partly, Southern Europe (e.g. Germany, France, Belgium, and Italy). In case of HCB, higher levels are indicated for countries of Central, Southern, and Eastern Europe. Contrary to other POPs, HCB levels in air are more homogeneous indicating its higher persistence in the atmosphere. Spatial

distributions of annual deposition fluxes of HCB, PCDD/Fs, and PCB-153 are similar to those of air concentrations.

Modelled air concentrations of heavy metals generally agree with the levels observed at the EMEP monitoring network. The mean relative bias between the annual average modelled and observed concentrations does not exceed 1% and 12% for Pb and Cd, respectively. The corresponding spatial correlation coefficients are as large as 0.8. Deviation between the modelled and observed Hg^0 air concentrations does not exceed ±15%. Simulated wet deposition of heavy metals agrees with observations within a factor of 2. The modelling results for PAH reproduce the EMEP observations with the mean relative bias for the sum of 4 PAHs about -17% and high spatial correlation (0.8). Validation of individual PAH compounds indicates some under-prediction of observed B(a)P, B(k)F, and IP air concentrations, and over-prediction of B(b)F concentrations. The model tends to under-predict by 40% non-EMEP B(a)P measurements at rural and suburban monitoring sites available from AIRBASE. Simulations of PCB-153 are generally consistent with measured pollution levels in the countries of Northern and Central Europe. For more than a half of monitoring sites the difference between measured and modelled concentrations is within a factor of 2 and spatial correlation coefficient is 0.8. There is a general tendency of under-prediction of observed HCB concentrations by the modelling results with mean bias about -50%.

Main contributors to atmospheric deposition of Pb and Cd in the EMEP countries are anthropogenic sources and wind re-suspension. The contribution of non-EMEP sources is relatively low except for the countries located close to the borders of the EMEP region. Regional anthropogenic emissions sources contribute on average 22% of Hg deposition in the EMEP countries, whereas contribution of intercontinental transport exceeds 75%. However, this large estimate contains implicit contribution of EMEP emissions that flew out through the boundaries and returned back to the region. The contribution of transboundary transport exceeds deposition form national sources in 37, 39 and 36 of 51 EMEP countries for Pb, Cd and Hg, respectively.

Deposition of PAH from foreign sources exceeds deposition form national sources in a half of the 51 EMEP countries. Similar prevalence of transboundary transport over national emissions in deposition of other POPs is estimated in a number of countries varying from 22 for PCDD/Fs to 38 for HCB. Secondary emission sources of PCDD/Fs, PCB-153, and HCB contributed about 50-70% to deposition of these pollutants in the EMEP countries.

Additional information products

Regular model assessment provides valuable information on heavy metal and POP pollution levels as well as the source-receptor relationships. Variety of additional information can be produced to support the policy making process both within the Convention and in other international bodies. It includes evaluation of ecosystem-specific deposition, atmospheric loads to major regional watersheds, marginal seas and remote regions (the Arctic), estimates of exceedances of air quality standards, and pollution assessment on a global scale.

Model estimates of heavy metal deposition to various types of the surface land cover (forests,

grasslands, crops, water bodies, etc.) are performed on a regular base and available at the MSC-E website. These estimates of ecosystem-specific deposition are aimed to support activities within the Working Group on Effects (WGE) and, in particular, evaluation of critical loads exceedences. This relevant information is widely used in the Convention to characterize levels of adverse effects on human health and biota. Future work in this direction requires updating both deposition estimates and the critical loads for heavy metals and POPs.

Aquatic ecosystems are among the most vulnerable receptors of heavy metals and POP pollution, which undergo long-term accumulation and bio-magnification of the contaminants. In many cases, direct atmospheric deposition to the water surface cannot completely characterize contamination of the water body due to additional input of the pollution with ground and surface water run-off from the adjacent territory. Therefore, deposition fluxes of the considered heavy metals and POPs to major watersheds of rivers, lakes and coastal drainage areas within the EMEP region have been calculated and analysed. Among the major rivers in Europe and Central Asia the largest atmospheric load of Hg and B(a)P is to watersheds of the Vistula and Oder rivers in Central Europe. In contrast, the watersheds of the Ugra and Oka rivers located in Russia are the most significantly affected by Cd deposition.

Some PAHs, such as B(a)P, are characterized by toxic properties and are considered as carcinogens, mutagens, and teratogens. Exceedances of the target value adopted within the European Union for annual mean B(a)P air concentrations (1 ng/m^3) has been estimated based on the modelling results for the EMEP region. About 12% of total population of the EMEP countries lived in 2017 on territories characterized by the exceeded EU target level. The information on the target level exceedances is expected to support activities of the Task Force on Health and WGE with regard to the analysis of population exposure to toxic substances and their impacts on human health and ecosystems.

In addition, information on heavy metal and POP deposition to the marginal seas (Baltic, North, Mediterranean, Black, and Caspian) was prepared along with source apportionment for 2017. Similar information was also produced for the Arctic sector covered by the EMEP domain. Finally, the regional model assessment was supported by global scale simulations using the GLEMOS multi-scale modelling system to take into account the effect of inter-regional and intercontinental transport on pollution of the EMEP countries. It was noted that improvement of the global scale assessment requires closer co-operation of the LRTAP Convention with other international bodies (UN Environment, Stockholm Convention, Minamata Convention) in order to facilitate development of global emissions inventories for heavy metals and POPs.

Research activities

Research activities of MSC-E were carried out in accordance with the priorities of the long-term strategy for the Convention and were aimed at improvement of the pollution assessment quality and further development of the modelling tools. The main directions of the research included country-scale pollution assessments for B(a)P (France) and heavy metals (Germany), analysis of key emission sources and trends of B(a)P pollution, evaluation of a new mechanism of Hg photo-reduction in the atmosphere, and further development of the multi-media approach for POPs and Hg.

The current stage of a pilot study for B(a)P on regional and national scales is focused on evaluation of various parameterizations of the key processes governing B(a)P fate in the atmosphere. Two chemical transport models (GLEMOS and CHIMERE) are involved to the study. The analysis of the model simulations is carried out in close cooperation with national experts from France and Spain. Results of study show the critical role of the parameterization of B(a)P degradation in air for evaluation of its long-range transport. Thus, further refinement of the parameterizations of particle-bound B(a)P degradation and gas-particle partitioning processes is needed.

A new study of heavy metal pollution on a country scale has been started this year for Germany. The main objective of the study is generation of detailed information on levels and spatial distribution of atmospheric deposition of three heavy metals (Pb, Cd, Hg) in the country for the period from 2014 to 2016. This year activities include preparation of input information, pilot simulations of heavy metal pollution in the country, and preliminary evaluation against observations. Further work within the study will include finalizing the model assessment of pollution levels, joint analysis of assessment results with national experts, evaluation of national emissions based on both modelling and measurement data, and formulation of recommendations for improvement of the assessment quality both on national and regional scales.

In spite of significant improvements in understanding of Hg oxidation and reduction mechanisms, current knowledge on Hg atmospheric chemistry remains incomplete. An experimental version of the GLEMOS model was applied to test a new mechanism of Hg photo-reduction in gaseous phase over the global scale. The performed analysis of the modelling results shows that the new mechanism applied along with the Br-initiated oxidation chemistry provides reasonable agreement of modelling results with observations. However, remaining discrepancies of modelling results with measurements require further in-depth study of the Br oxidation/reduction chemistry.

Environmental dispersion of some POPs (HCB, PCDD/Fs, PCBs) and Hg is characterized by intensive cycling between various environmental media (atmosphere, ocean, soil, vegetation). This cycling determines a complex character of their dispersion and leads to legacy effect of historical emissions on contemporary pollution levels. To take this phenomenon into account a multi-media modelling approach has been developed and applied in the GLEMOS model for simulation of POP pollution both on regional and global scales. Besides, the approach was recently adapted for multi-media modelling of Hg. New developments of the multi-media approach include refining information on physical-chemical properties and update of the model parameterizations for HCB. For this purpose, sensitivity of the modelling results to parameterizations of HCB air-soil exchange has been studied. Simplified version of GLEMOS was also applied to simulate Hg multi-media cycling on a global scale for the period from the beginning of the 19th century to nowadays. The process of Hg accumulation in different media was studied and contemporary level in the atmosphere and seawater were evaluated against observations.

Analysis of long-term trends of B(a)P pollution was carried out for the period from 2007-2017 to support evaluation of effectiveness of the measures on PAH pollution reduction. Simulated changes of B(a)P air concentrations were compared with observations from the EMEP monitoring network and AIRBASE. It was shown that B(a)P levels demonstrate statistically significant decrease at 30% of sites and statistically significant increase at 7% of sites. Further activity will be focused on the

detailed analysis of temporal trends at particular stations including source apportionment and contribution of various emission sectors.

Cooperation with subsidiary bodies of the Convention and other international bodies

Scientific co-operation is an important part of MSC-E activities aimed at support and improvement of heavy metal and POP pollution assessment within EMEP as well as dissemination of the assessment results to wider international audience. Results of current research activities and future plans of MSC-E were discussed at the recent meeting of the Task Force on Measurements and Modelling (TFMM). The Centre also contributed to the work of the Task Force on Techno-Economical Issues (TF TEI) aimed at promoting the ratification of the CLRTAP Protocols by the EECCA countries. In co-operation with the Arctic Monitoring and Assessment Programme (AMAP) the Centre takes part in the new AMAP Assessments on the Arctic pollution by Hg and POPs. Besides, regular evaluation of airborne pollution load of heavy metals and POPs to the Baltic Sea is carried out in the framework of cooperation with the Helsinki Commission (HELCOM). Finally, MSC-E continues collaboration with the UN Environment as well as Minamata and Stockholm Conventions.

Main challenges and directions of future research

Future directions of the EMEP centre's activities will be aimed at improvement of heavy metal and POP pollution assessment in the EMEP region. The country-scale study for Germany will be continued focusing on detailed analysis of the modelling results and deriving recommendations for improvement of the assessment quality both on national and regional scales. Besides, detailed assessment of PAH pollution in Poland will be launched. A multi-model analysis for B(a)P pollution is planned in the framework of the EMEP EuroDelta-Carb intercomparison exercise in co-operation with TFMM and national experts. The major mechanisms of Hg oxidation and reduction in the atmosphere will be further studied and evaluated. Attribution of long-term changes of Hg and POP pollution to regional and extra-regional (global and secondary) sources will be performed. Finally, MSC-E will continue long-term co-operation with WGE focusing on joint analysis of heavy metal measurements in moss, preparation of information on Hg deposition to water bodies/watersheds, and B(a)P exceedances of air quality guidelines.

CONTENTS

INTRODUCTION

Heavy metals and persistent organic pollutants (POPs) are toxic substances, which are within the scope of various international bodies including the UNECE Convention on Long-range Transboundary Air Pollution (hereafter, CLRTAP or the Convention). Despite continuous decrease of emissions of these pollutants in the past decades, these substances still cause adverse effects on human health and ecosystems (the Long-term Strategy of the Convention, ECE/EB.AIR/2018/1/Rev.1). The priority heavy metals targeted by the Convention are lead (Pb), cadmium (Cd) and mercury (Hg). The list of considered POPs includes polychlorinated biphenyls (PCBs), polychlorinated dibenzo(p)dioxins and dibenzofurans (PCDD/Fs), hexachlorobenzene (HCB), and polyaromatic hydrocarbons (PAHs). The priority PAHs are benzo(a)pyrene (B(a)P), benzo(b)fluoranthene (B(b)F), benzo(k)fluoranthene (B(k)F), and indeno(1,2,3-cd)pyrene (IP).

The Co-operative Programme for Monitoring and Evaluation of Long-range Transmission of Air Pollutants in Europe (EMEP, www.emep.int) provides scientific support of the Convention in terms of emission inventories, monitoring, modelling and integrated assessment of transboundary pollution by various contaminants. Research and operational assessment of heavy metal and POP pollution are carried out by relevant EMEP Centres – the Centre on Emission Inventories and Projections (CEIP), the Chemical Coordinating Centre (CCC), the Meteorological Synthesizing Centre – East (MSC-E).

The purpose of the present Status Report is to provide an overview of the EMEP Centres activities in the field of heavy metals and POPs carried out in accordance with the bi-annual workplan of the Convention for 2018-2019 [ECE/EB.AIR/GE.1/2017/20-ECE/EB.AIR/WG.1/2017/13]. The report consists of six chapters. Chapter 1 presents the status of heavy metal and POP emissions reporting by the EMEP countries and preparation of emissions data for modelling. Chapter 2 overviews observations of these pollutants in the EMEP monitoring network and other measurement initiatives. Assessment of the current status of heavy metal and POP pollution in the EMEP region is presented in Chapter 3. Chapter 4 summarizes results of research and development activities. Cooperation of MSC-E with subsidiary bodies of the Convention, international organizations and national experts is discussed in Chapter 5. Main challenges and plans for future activities are formulated in Chapter 6.

Detailed technical information aimed to support the Status Report is available in the Supplementary Data Reports on heavy metals [*Ilyin et al*., 2019] and POPs [*Gusev et al*., 2019] as well as at the MSC-E website [www.msceast.org]. Main results of the assessment are based on the most recent heavy metal and POP emissions dataset available at the moment of the study, which was prepared by CEIP for 2016. Results of the model assessment based on the new emissions reporting for 2017, which became available in the meantime, will be presented at the website along with updated information for the EMEP countries.

1. EMISSIONS OF HEAVY METALS AND POPs

Emission data is one o the key components of air pollution assessment. Status of official emission data on heavy metals and POPs including reporting by the EMEP countries, long-term changes, re-calculations between 2016 and 2017 and gap filing is overviewed. Besides, regional-scale and global-scale emissions used in the model assessment are described.

1.1. Official emission data for 2017

The EMEP Reporting guidelines [*UNECE*, 2014] request all Parties to the *LRTAP Convention* to report annually emissions and activity data of air pollutants (SO_x, NO_x, NMVOCs, NH_3, CO, heavy metals[1], POPs[2], PM (and voluntary BC). Further, every four years, projection data, gridded data and information on large point sources (LPS) have to be reported to the EMEP Centre on Emission Inventories and Projections (CEIP).

1.1.1. Reporting of emission inventories in 2019

Completeness and consistency of submitted data have improved significantly since EMEP is collecting information on emissions. Data of at least 45 Parties each year were submitted to CEIP for the last seven years (compare Fig.1.1). 45 Parties (88 %) submitted inventories[3] in 2019; six Parties[4] did not submit any data. 41 Parties provided time series of priority heavy metals (Cd, Hg, Pb), 3 Parties reported only 2017 data, 38 Parties reported data on 5 additional heavy metals (Arsenic (As), chromium (Cr), copper (Cu), nickel (Ni), selenium (Se), zinc (Zn) and their compounds). 43 Parties reported data on POPs (total PAHs, PCDD/Fs, HCB, PCBs) five from which reported only 2017 emissions [*EEA/CEIP*, 2019].

---

[1] *Heavy metals (Cd- Cadmium, Hg- Mercury, Pb-Lead) and its compounds.*

[2] *Persistent Organic Pollutants (Total PAHs, PCDD/Fs, HCB, PCBs).*

> *(j) Polycyclic aromatic hydrocarbons (PAHs). For the purposes of emission inventories, the following four indicator compounds shall be used: benzo(a)pyrene, benzo(b)fluoranthene, benzo(k)fluoranthene, and indeno(1,2,3_cd)pyrene;*
>
> *(k) "Dioxins and furans" (PCDD/F), which are polychlorinated dibenzo p dioxins (PCDD) and polychlorinated dibenzofurans (PCDF), tricyclic, aromatic compounds formed by two benzene rings, connected by two oxygen atoms in PCDD and by one oxygen atom in PCDF, and the hydrogen atoms of which may be replaced by up to eight chlorine atoms;*
>
> *(l) "Polychlorinated biphenyls" (PCBs), which means aromatic compounds formed in such a manner that the hydrogen atoms on the biphenyl molecule (two benzene rings bonded together by a single carbon-carbon bond) may be replaced by up to 10 chlorine atoms.*

[3] *The original submissions from the Parties can be accessed via the CEIP homepage on http://www.ceip.at/status_reporting/2019_submissions.*

[4] *Greece, Bosnia and Herzegovina, Kazakhstan, Liechtenstein, the Republic of Moldova, and Montenegro.*

The quality of submitted data across countries differs quite significantly. By compiling the inventories, countries have to use the newest available version of the EMEP/EEA *air pollutant emission inventory guidebook*, which is the version of 2016 [*EMEP/EEA Guidebook 2016*]. However, many countries still use the Guidebook 2013 [*EMEP/EEA Guidebook 2013*] or older versions. Uncertainty of reported data (national totals, sectoral data) is considered relatively high – the completeness of reported data has not turned out satisfactory for all pollutants and sectors neither. Detailed information on recalculations, completeness and key categories, plus additional review findings can be found in the annual EEA & CEIP technical inventory review reports and its Annexes[5].

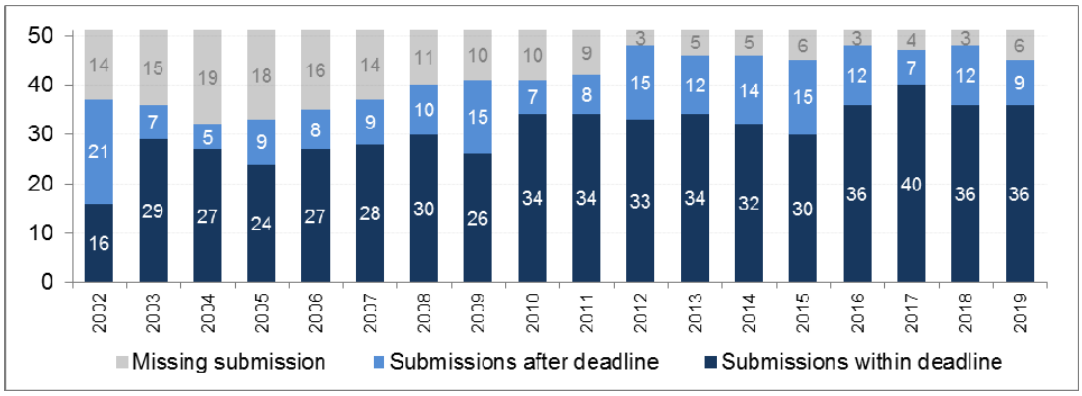

Fig.1.1. *Parties reporting emission data to EMEP since 2002, as of 4 June 2019*

1.1.2. Emission Trends in the EMEP area – reported data

For priority heavy metals and POPs the emission trends and completeness of reported data show different pictures for EMEP-East and EMEP-West regions. EMEP-West region includes EU28 countries, Monaco, Albania, Bosnia & Herzegovina, North Macedonia, Montenegro, Serbia, Iceland, Liechtenstein, Norway and Switzerland. The EECCA countries and Turkey are related to the EMEP-East region [*www.ceip.at/emep_countries*].

[5] *http://www.ceip.at/review_proces_intro/review_reports*

EMEP West area - POPs

The strong fluctuations in emission trends of POPs for the EMEP-West region are mostly due to the reporting of single countries (Fig. 1.2). The high reductions of HCB from 2001 to 2002 are due to the strong drop of emissions reported by Germany and the peak in 2009 is mainly due the reporting of Albania. The high increase from 2000 to 2006 and the strong drop in 2007 of PAHs and B(a)P is due to the reporting of Bulgaria whereas the trend of PAHs and B(a)P emissions in the period 2007-2017 is dominated by Portugal. The strong drop in 2017 PAH emissions and its four compounds is mainly due to the gap in reporting of Greece. The drop in PCB emissions for 2000 – 2002 is mainly due to the reporting of Portugal. The drop in B(k)F emissions for 2007-2008 is mainly due to the reporting of Poland. It has to be mentioned that Austria, Spain, Italy and Finland report total PAH emissions but do not report the four PAH compounds B(a)P, B(b)F, B(k)F and IP.

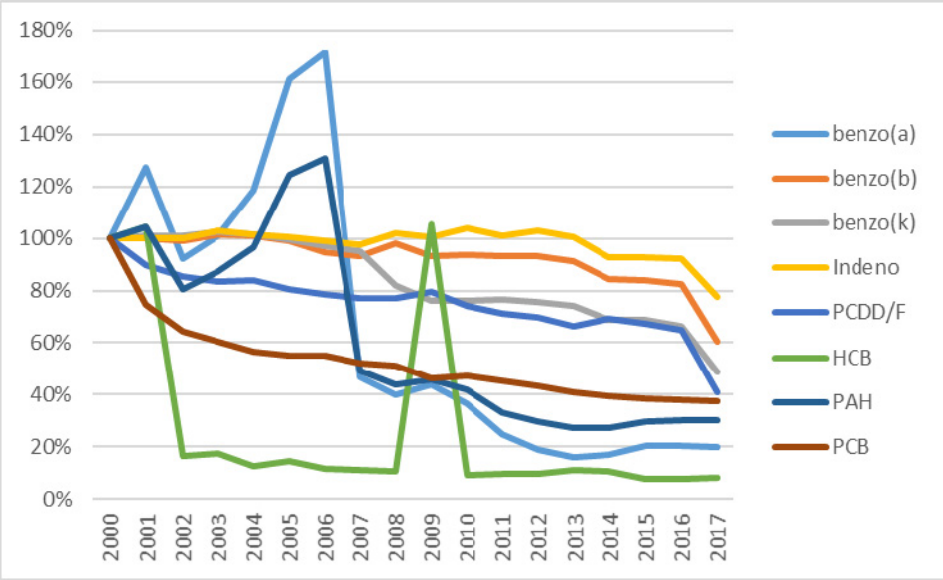

Fig. 1.2. *Emission trends of POPs 2000-2017 in the EMEP West area (reported data)*

EMEP East area - POPs

Reporting of POPs in the EMEP East region is quite incomplete and shows high peaks and inconsistent time series. The Russian Federation reported some POPs for the years 2000 and 2005 only and Turkey did not report any POPs at all. Belarus did not report data for the year 2000 and incomplete data for 2001. Ukraine reported very high levels of POPs for the years from 2010 to 2013 (constant values) and 2017 only. The following figure (Fig. 1.3) shows 2002 to 2017 POPs emissions for EMEP East without emissions of Ukraine. The strong peak of PCDD/F and HCB emissions in 2005 is mainly due to the reporting of Russia. The drop in PCB and PAH emissions 2017 is mainly due to missing data of Kazakhstan for this year.

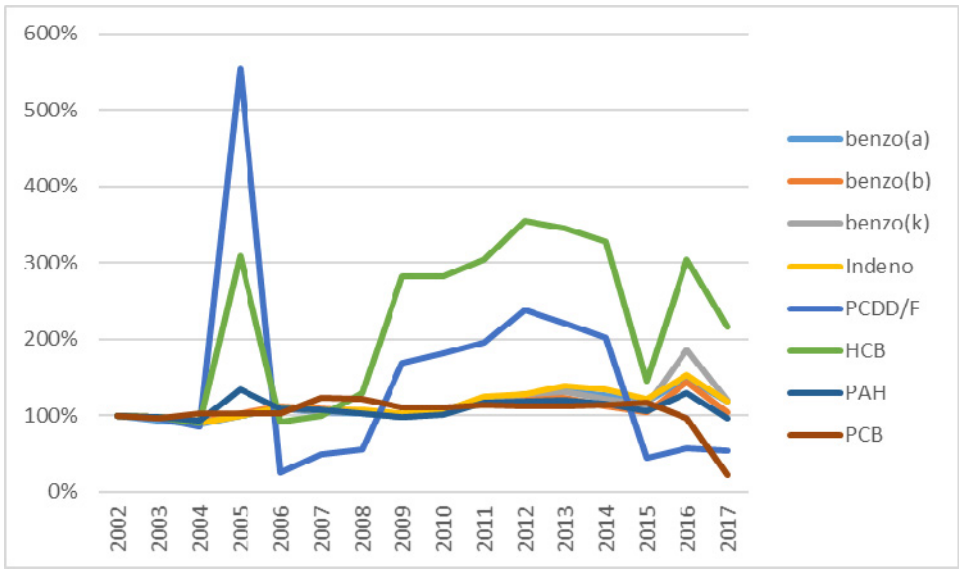

Fig. 1.3. *Emission trends of POPs 2002-2017 in the EMEP East area (reported data) without Ukraine*

EMEP West area – priority heavy metals

Priority heavy metals of the EMEP West area show a rather smooth down trend and a dip for the year 2009 which reflects the economic and industrial production downturn in that year (Fig. 1.4). The strong decrease of Pb emissions from 2000 to 2002 is mainly due to lower emissions in the transport sector of Italy and Spain.

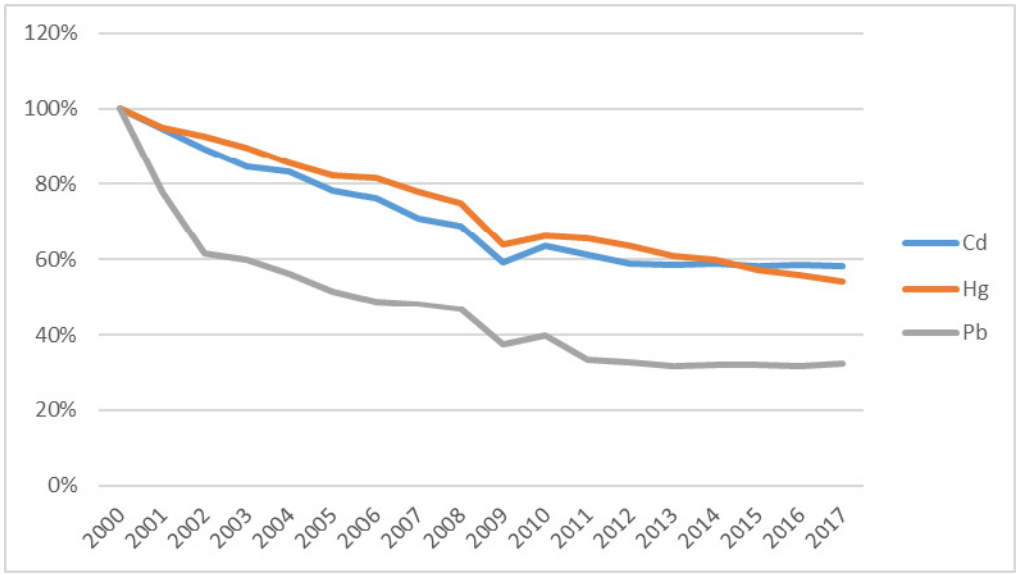

Fig. 1.4. *Emission trends of priority heavy metals 2000-2017 in the EMEP West area (reported data)*

EMEP East area – priority heavy metals

Unlike for EMEP West, *priority heavy metals of the EMEP East area show an unstable trend from 2000 to 2007*, which is mainly due to incomplete reporting (Fig. 1.5). The dip of 2001 Pb and Cd emissions is mainly due to a gap in reporting of the Russian Federation, which reports for 2000, 2002-2006 and 2009 (jump in Cd emissions) only. The drop in 2017 emissions is mainly due to missing data from Kazakhstan. Ukraine and Belarus do not report data for 2001. Azerbaijan and Turkey are the only countries, which report complete time series for all three heavy metals.

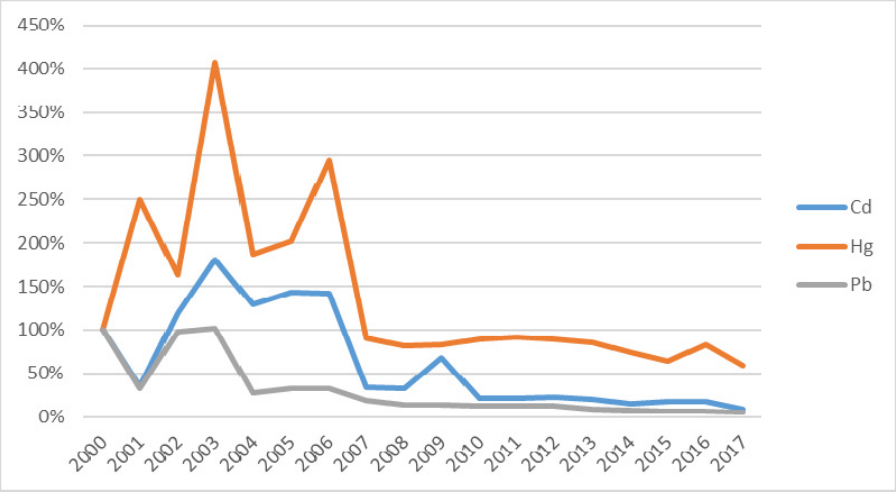

Fig. 1.5. *Emission trends of priority heavy metals 2000-2017 in the EMEP East area (reported data)*

1.1.3. Comparison of 2016 data reported in 2018 and in 2019

Reported data of 2016 emissions (reported in 2019) with 2016 emissions (reported in 2018) were compared. For 22 countries, data changed by more than 15 % for one or several pollutants (see Fig. 1.6 and Appendix 2). For 11 countries, 2016 data is unchanged or nearly unchanged (< 1 %).

Bulgaria and Malta showed the largest relative recalculations (see right part of Fig. 1.6.) with changes up to almost 4500% (Malta, HCB).

For **B(a)P, PAHs and PCB**, the recalculations of Portugal (-51%, -45%, -92%) contributed the most share to overall recalculations in the EMEP area.

Beside Portugal, the **PAH** recalculations of Bulgaria (+564%) and Spain (-46%) also contributed to a large extend to overall recalculations in the EMEP area.

For **PCDD/Fs**, the recalculations of Azerbaijan (-99%) contributed the most share to overall recalculations in the EMEP area.

For **Pb**, the recalculations of Poland (-29%) contributed the most share to overall recalculations in the EMEP area.

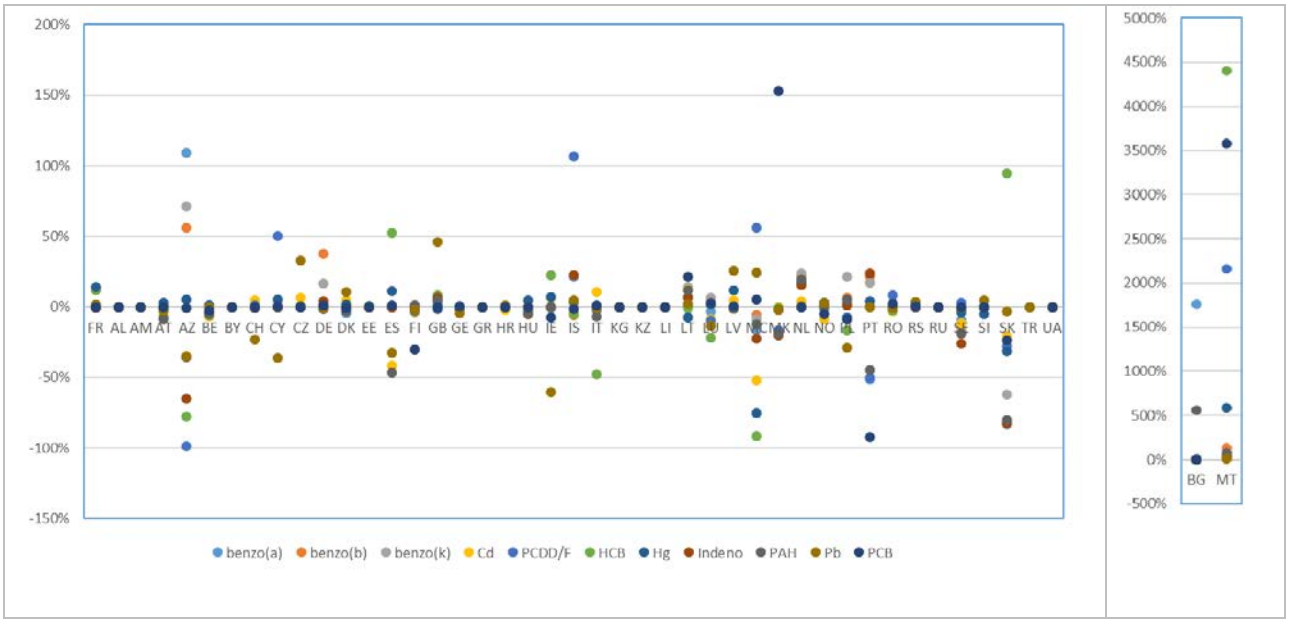

Fig. 1.6. *Recalculations between the 2019 and 2018 submission for year 2016 values (reported data). The separate chart at the right side shows countries with recalculations > 200% or <-200%.*

1.1.4. Data sets for modelers in 2019

Data used by CEIP were reported by the Parties to the LRTAP Convention as sectoral emissions (NFR14) and National Total emissions according to the UNECE guidelines for reporting emissions and projections data under the LRTAP Convention, Annex I [*UNECE*, 2014].

Reported (NFR[6]) sector data were aggregated to 13 GNFR sectors. In several cases, no data were submitted by the countries, or the reporting is not complete or contains errors. Before such emission data can be used by modellers, missing or erroneous information have to be filled in or replaced by expert estimates. To gap-fill missing/erroneous data, CEIP typically applies different methods. The gap-filling procedure annually is fully documented in technical reports (Technical reports CEIP 02/2019 and 03/2019), which can be downloaded from the CEIP website[7]. After the gap-filling, sector emissions are used for spatial distribution (mapping) to the EMEP grids.

The Parties, where reported data were (partly) replaced in 2019 are Albania, Armenia, Azerbaijan, Bulgaria, Germany, Finland, Portugal, Romania, Serbia, Turkey and Ukraine (see Appendix 3 or Technical report CEIP 02/2019 and 03/2019).

[6] NFR – Nomenclature for Reporting

[7] http://www.ceip.at/ceip_reports

Contribution of individual sectors to total EMEP heavy metals and POPs emissions

Fig. *1.7* shows the *contribution of each GNFR sector to the total emissions of individual air pollutants* (Cd, Hg, Pb, B(a)P, B(b)F, B(k)F, IP, PAHs, PCDD/F, HCB, PCB). To provide as complete a picture as possible of the situation of the individual sectors to total EMEP emissions, data as used for EMEP models (i.e. gap-filled data) were used for the calculations. The analysis does not include sea regions.

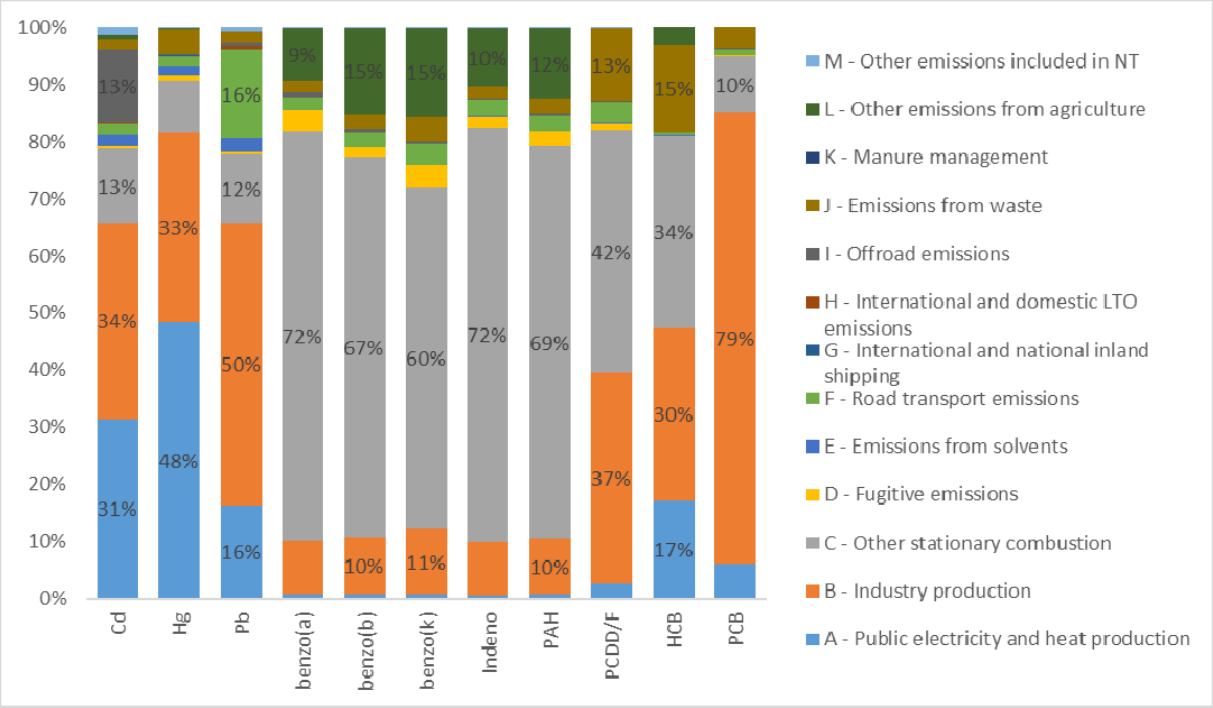

Fig. 1.7. *GNFR sector contribution to national total emissions in 2017, EMEP extended area without sea regions (only percentages above 10% are shown)*

It is evident that the combustion of fossil fuels and processing of raw materials is responsible for a significant part of heavy metals and POPs emissions.

Industry production emits about 34% of **Cd** emissions, followed by 31% from public power and heat plants.

Energy industries emit about 48% of total **Hg** emissions, mainly from coal power plants, followed by the industry production sector, which released 33% of total emissions.

About 50% of **Pb** emissions have been released by the industry production sector, while each of the other sectors contributes to a maximum of about 16%. Road transport (leaded gasoline) only contributes to 16%.

The largest source of **PAHs** and its compounds (B(a)P, B(b)F, B(k)F, IP) is the 'other stationary combustion' sector, which contributes to 69% of total emissions. The main source of PAH emissions are coal and wood stoves/boilers in households. 12% of PAH emissions are released by the agriculture sector, mainly from field burning of agriculture residues.

With 42% of total emissions, the 'other stationary combustion' sector contributes most to **PCDD/F** emissions. The main source of PCDD/F emissions are coal and wood stoves/boilers in households. Industry production plants (metal industries) contribute to 37% of total PCDD/F emissions and the waste sector (mainly waste incineration) contributes to about 13%.

With 34% of total emissions, the 'other stationary combustion' sector also contributes most of **HCB** emissions, followed by industry production with 30% and the energy sector with 17%.

The dominating sector for **PCB** emissions is the industrial sector, which contributes 79% to total emissions.

Fig. ***1.8.*** illustrates the sector contribution for the sum of total emissions in the EMEP West region and the EMEP East region. North Africa is included in the EMEP East region. The comparison of both graphs highlights some significant differences between West and East.

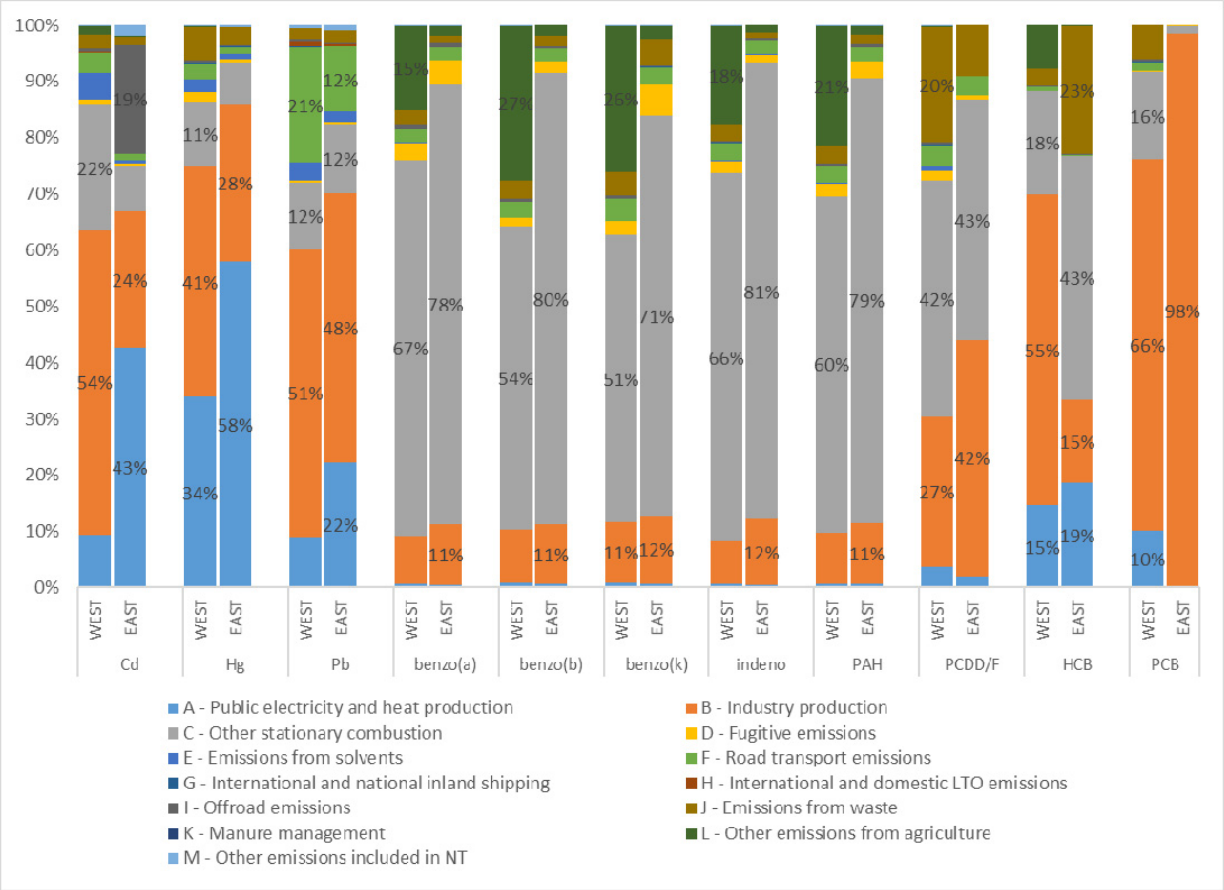

Fig. 1.8. *GNFR sector contribution to national total emissions in 2017 for the EMEP West and EMEP East areas (Only percentages above 10% are visible. 'Remaining Asian Areas' are included in the EMEP East region and North Africa is included in the EMEP West region)*

Reporting of gridded data

2017 was the first year with reporting obligation of gridded emissions in the new grid resolution of 0.1°x0.1° (long/lat). Twenty-nine of the 48 countries which are considered to be part of the extended EMEP area did report sectoral gridded heavy metal and POP emissions in the new resolution until June 2019 and one country reported only gridded national total values (instead of sectoral data). *The majority of gridded sectoral emissions in 0.1°x0.1° (long/lat) resolution have been reported for the year 2015 (28 countries).* For the year 2017, gridded sectoral emissions have been reported by three countries only.

Twelve countries reported gridded emissions additionally for previous years (one country for the whole time series from 1980 to 2017; one country for the whole time series from 1990 to 2017; three countries for the years 1990, 1995, 2000, 2005 and 2010; one country for the years 1990, 2000, 2005 and 2010; one country for the years 2005 and 2010; one country for the year 2005; one country for the year 2010; and three countries for the year 2014).

Reported gridded sectoral data in 0.1°x0.1° (long/lat) resolution, which can be used for the preparation of gridded emissions for modellers, covers less than 20 % of the cells within the geographic EMEP area. For remaining areas missing emissions are gap-filled and spatially distributed by expert estimates. Reported grid data can be downloaded from the CEIP website[8].

Gridded data 2017 in new resolution 0.1° x 0.1° (long/lat)

For this year it was agreed with the modellers to perform gap-filling and gridding for the year 2017 in 0.1° x 0.1° longitude/latitude resolution on GNFR sector level.

The 0.1° x 0.1° GNFR grids of heavy metals (Cd, Hg, Pb) and POPs (B(a)P, B(b)F, B(k)F, IP, PCDD/Fs, HCB) were spatially distributed based on the gridding system developed by CEIP. Map of Pb total emissions in 2017 is shown in Fig. 1.9 as an example. The system is module based and uses as a first step reported gridded emission data for each country and sector where it is available and usable. If no reported gridded data in the 0.1° x 0.1° (long/lat) resolution is available, reported gridded PM data is used as proxy for spatial disaggregation. If reported PM data is also not available PM data from the Copernicus Atmospheric Monitoring Service (CAMS-81, CAMS-REG-AP-v2.2) and the Emission Database for Global Atmospheric Research (EDGAR) is used as proxy.

Reported gridded data in 0.1° x 0.1° (long/lat) resolution was used from Austria, Belgium, Bulgaria, Croatia, Czech Republic, Denmark, Finland, France, Georgia, Greece, Hungary, Ireland, Latvia, Luxembourg, Malta, Monaco, Netherlands, North Macedonia, Norway, Poland, Portugal, Romania, Slovakia, Slovenia, Spain, Sweden, Switzerland and United Kingdom. For Poland, Portugal and Spain the spatial disaggregation of sector 'F – Road Transport' had to be replaced by CAMS proxies. Reported gridded data from Italy had to be completely replaced by CAMS and EDGAR proxies.

[8] http://www.ceip.at/status_reporting

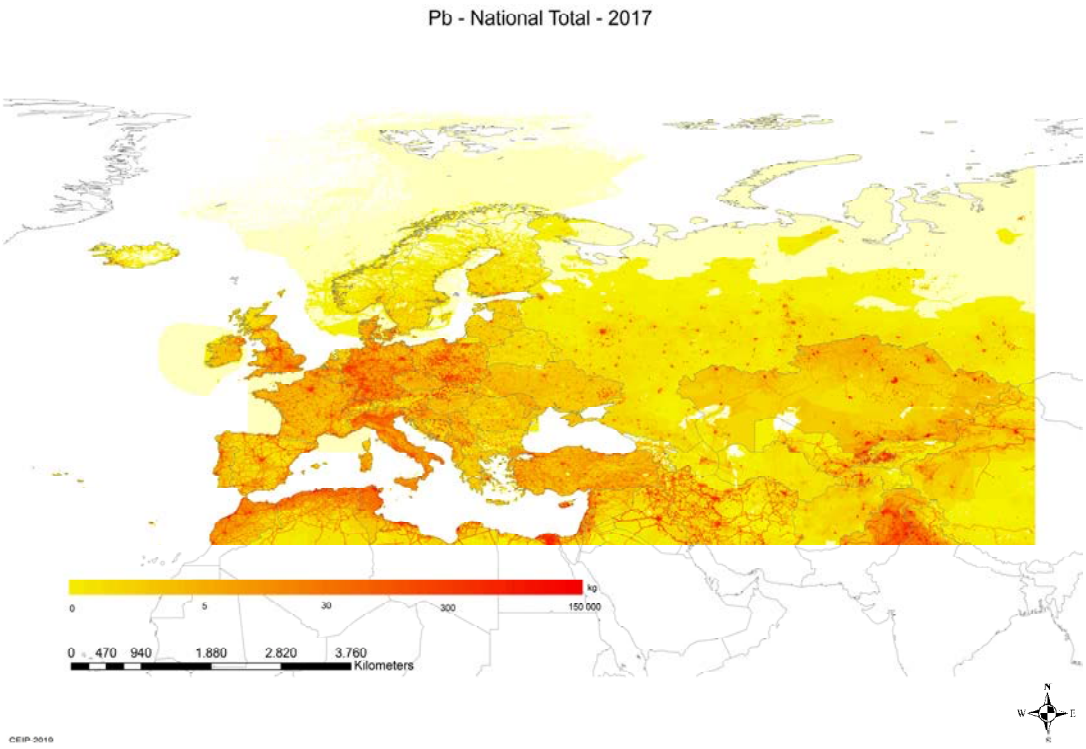

Fig. 1.9. *Visualized gap-filled and gridded Pb emissions in 0.1°x0.1° long-lat resolution*

1.2. Emissions data for modelling

Regional emissions

Model assessment of heavy metals and POPs pollution in the EMEP domain was made on the basis of gridded emission data with spatial resolution 0.1°x0.1° provided by CEIP (*http://www.ceip.at*). Pollution levels of heavy metals and POPs in 2017 were evaluated on the basis of emissions reported for the previous year 2016 due to availability of necessary gridded emission data[9]. Detailed description of estimated heavy metal and POP emissions in the EMEP countries, gap-filling methods, and expert estimates applied for preparation of emission inventory, can be found in the Technical reports of CEIP [*Tista et al.,* 2018a,b].

Gridded emission data for PCB modelling were based on the available expert estimates and officially reported data of the EMEP countries. Model assessment of PCB pollution levels (total and congener specific) requires definition of emissions of particular PCB congeners. However, currently reported national inventories of PCB emissions provide total releases of PCBs without distribution by particular congeners. Therefore, to evaluate transport and fate of individual PCB congeners, congener specific emission inventory of *Breivik et al*. [2007] was used for modelling. The indicator congener PCB-153 was selected to characterize transboundary transport and pollution by PCBs. Spatial distribution of PCB-153 emissions was constructed on the base of gridded PCB emissions officially provided by the

[9] *Update of the modelling results based on the new emission data for 2017 is available at the MSC-E web site [www.msceast.org].*

EMEP countries. For other EMEP countries, which did not report gridded emission data, gridded population density was used for allocation of emissions.

Estimates of PCDD/F emissions officially reported by the EMEP countries are most likely subject to considerable uncertainties due to underestimation of releases from some source categories (e.g. 'Residential combustion', 'Open burning of wastes') and incomplete coverage of all potential sources [*Breivik et al.*, 2004; *Fiedler*, 2007; *Pulles et al.*, 2005; *Pulles et al.*, 2006]. For this reason emission scenario, representing maximum level of PCDD/F releases to the atmosphere was used in the model simulations. The maximum emission scenario was prepared on the basis of the uncertainty range reported by 12 EMEP countries in their inventory information reports (namely, Belarus, Belgium, Croatia, Cyprus, Denmark, Estonia, Finland, France, Latvia, Poland, Sweden, and the UK). Difference between the maximum and average estimates of PCDD/F emissions in these countries varied from a factor of 1.5 for the UK up to a factor of 4.2 for Denmark. For other EMEP countries, which did not report uncertainty range in their inventories, the maximum level of national PCDD/F emissions was assumed to be 3-fold higher compared to the officially reported emissions in accordance with the expert estimates [*Pulles et al.*, 2006; *Bogdal et al.*, 2014]. Thus, total PCDD/F emission in the EMEP countries according to the maximum emission scenario exceeded reported data in the inventories by a factor of 3.5 on average. This approach has already been applied in the model assessment for previous year [*Gusev et al*., 2018].

Maps illustrating spatial distributions of the pollutants, namely, Pb, Cd, Hg, B[a]P, sum of 4 PAHs, PCDD/Fs, HCB and PCB-153 emission fluxes from anthropogenic sources in the EMEP region, used in the model simulations for 2017, are presented in Figs. 1.10.

Along with gridded emission data the GLEMOS modelling system requires additional information on heavy metal and POP emissions, namely, intra-annual variations, distribution of emissions with height and chemical speciation of Hg emissions. Necessary vertical and temporal disaggregation of the emissions was generated using emission pre-processing tool, developed by MSC-E for the GLEMOS modelling system. More detailed information on the emission pre-processing procedure is presented in the heavy metal Status Report [*Ilyin et al*., 2018].

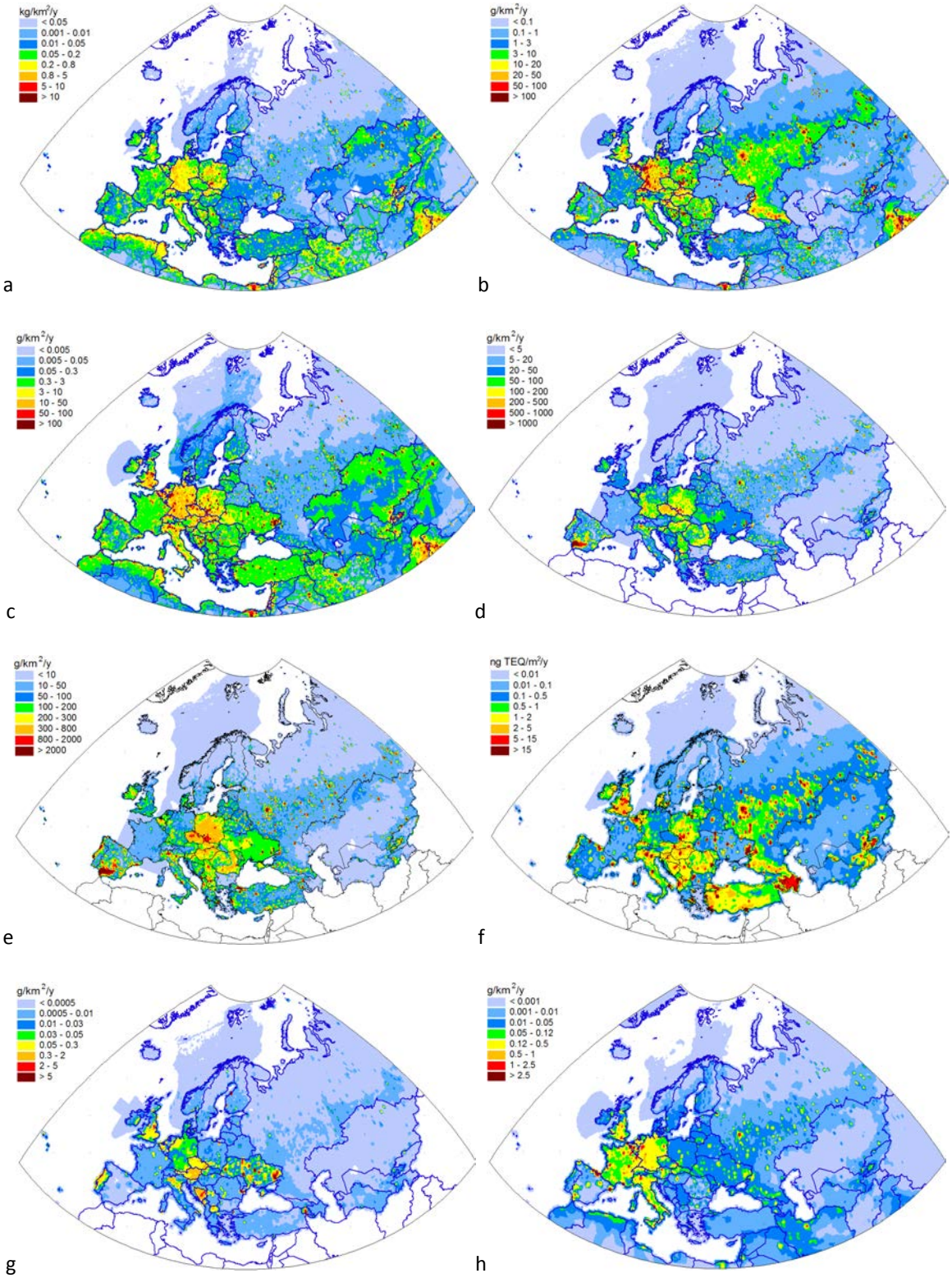

Fig. 1.10. *Spatial distribution of Pb (a), Cd (b), Hg (c), B(a)P (d), sum of 4 PAHs (e), PCDD/Fs (f), HCB (g) and PCB-153 (h) emissions in the EMEP region used in model simulations for 2017*

Global emissions

A number of pollutants, such as mercury and some POPs, are known for their ability to disperse in the atmosphere over the global scale. In order to take into account contribution of intercontinental transport to pollution levels in the EMEP countries and to evaluate boundary conditions required for regional EMEP modelling, global-scale model simulations are carried out.

Global-scale modelling of Hg is based on gridded emission data produced in the framework of the UNEP Global Mercury Assessment 2013 [*AMAP/UNEP*, 2013] and related to 2010. Intercontinental transport of PAHs is simulated based on emissions, produced by the research group of Peking University [*Shen et al*., 2013]. Global PAH emission inventories with 0.1°x0.1° spatial resolution were developed using a bottom-up approach for the period from 1960 to 2014. For the evaluation of global-scale transport and fate of PCDD/Fs, HCB, and PCBs expert estimates of global emissions were applied. In particular, global gridded emissions of PCDD/Fs to the atmosphere and soil were prepared using the national emission inventories reported by countries to the Stockholm Convention [*Gusev et al.*, 2014; *Shatalov et al.*, 2014]. Model simulations of HCB global-scale transport were carried out on the basis of experimental emission scenario of historical HCB releases during the period covering several recent decades [*Shatalov et al.*, 2010]. For PCB-153 modelling, data on global emissions were derived from the inventory of *Breivik et al.* [2007]. Spatial distributions of Hg and PCB-153 emissions, used in the global-scale model simulations for 2017, are shown in Fig. 1.11.

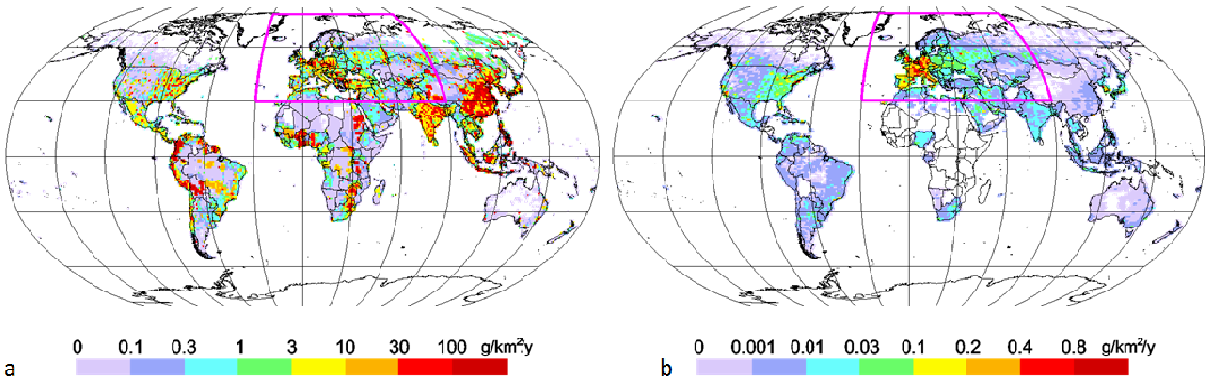

Fig. 1.11. *Spatial distribution of global annual emissions of Hg, g/km^2/y (a) and PCB-153, g/km^2/y (b) with spatial resolution 1°x1°, used in the model simulations for 2017*

2. MEASUREMENTS of HEAVY METALS and POPs

Information about actual pollution levels and their temporal changes is obtained by means of monitoring. Current levels of heavy metals and POPs in air and precipitation measured at the EMEP stations are overviewed. Supplementary measurement information including the data derived from AIRBASE data base and results of regular moss surveys is described.

2.1. EMEP measurements in 2017

Heavy metals and persistent organic pollutants (POPs) were included in the EMEP's monitoring program in 1999. However, earlier data have been reported and are available. A number of countries have been reporting heavy metals and POPs within the EMEP area in connection with different national and international programmes such as HELCOM, AMAP and OSPAR. I.e. for 2017, the Russian site Amderma has been reporting data to AMAP, and these data are also included in this year EMEP report.

The EMEP monitoring strategy for 2010–2019 [*UNECE*, 2009] defines the monitoring obligations for the Parties. For POPs, polycyclic aromatic hydrocarbons (PAHs), polychlorinated biphenyls (PCBs), hexachlorobenzene (HCB), chlordanes (CHLs), lindane/γ-hexachlorohexane (γ-HCH), α-HCH, and DDT/DDE are part of the compulsory monitoring programme, while for heavy metals, Hg, Cd and Pb are the 1st priority elements while Cu, Zn, As, Cr, Ni are the 2nd priority. In addition to these compounds, several parties report other POPs and trace elements. All the data are available from the EBAS database (http://ebas.nilu.no/), and more detailed information about the sites and the measurement methods are found in EMEP/CCC's data report on heavy metals and POPs [*Aas et al*., 2019].

In the suggested new monitoring strategy for 2020-2029, which will be adopted this autumn (2019), the monitoring programme will continue as it is now. Further, it is recommended to increase the attention on organic contaminants of emerging concern (CECs), thus these are included at level 3 sites, which is the voluntary part of the monitoring activity in EMEP. The monitoring of CECs is important to better understand the CECs' potential for long-range transport and to help authorities in determining adequate policy measures and if necessary, make national or international regulations come into place. Initial monitoring of CECs in background air have shown that many CECs are present in concentrations exceeding the concentrations of the legacy POPs with up to 1000 times

2.1.1. Monitoring of POPs in 2017

The spatial coverage of POP monitoring in Europe is still scarce and POP (not including PAH) data in air are only available from maximum eight Parties (12 sites) in 2017 (Fig. 2.1a). For PAHs (i.e. benzo(a)pyrene, B(a)P), the spatial coverage is better with data in air reported from 15 Parties (36 sites) (Fig. 2.1b).

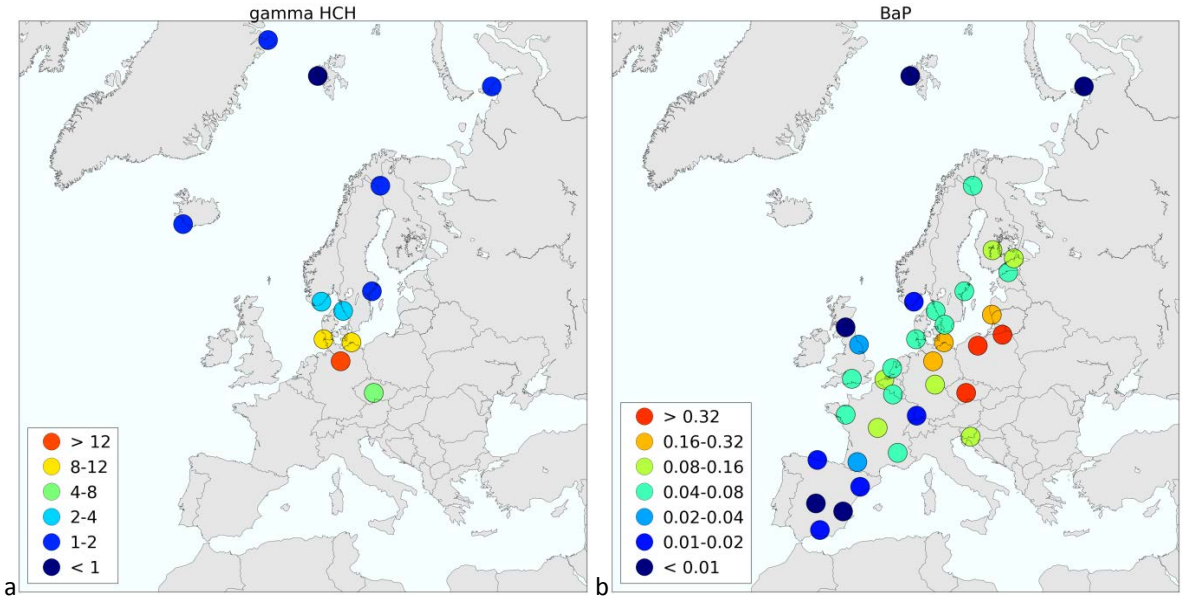

Fig. 2.1. *Spatial coverage of the monitoring network of POPs versus PAHs (i.e. B(a)P) in EMEP in 2017. The colors represent the annual mean concentrations in air for γ-HCH (a), pg/m^3 and B(a)P (b), ng/m^3*

Most POPs are semi-volatile substances, e.g. they may occur in both gaseous and particulate states in the atmosphere. Their gas-particle partitioning is strongly temperature-dependent, and hence partitioning may vary both temporally (diurnal, seasonal) and spatially (e.g. by altitude, latitude). Several POPs furthermore have a significant potential for reversible atmospheric deposition. POP exchange between the atmosphere and various surface media is strongly temperature-dependent as well. Hence, measured concentrations of POPs in air may in part be a result of volatilization from environmental surfaces as contaminated in the past, i.e. secondary emissions. Primary diffusive emissions of intentionally produced semi-volatile POPs (industrial chemicals, organochlorine pesticides) are often temperature-dependent as well. Thus, concentrations of POPs tend to be elevated in air during summer because of elevated primary and/or secondary emissions. To complicate matters, any correlation between air temperature and elevated concentrations of POPs in air at northern background sites may also be a reflection of long-range atmospheric transport (LRAT) from warmer regions with higher emissions. In this year's report, the main focus is on seasonal variability of selected POPs in air in an attempt to (i) highlight the importance of continued long-term seasonally resolved monitoring within EMEP and (ii) identify and discuss some issues which may merit further attention in terms of sources, processes and control strategies.

Polychlorinated Biphenyls (PCBs)

The environmental occurrence of Polychlorinated Biphenyls (PCBs) is mainly a result of historical intentional production. Production peaked around 1970, followed by various control measures on production and/or new use in various countries and jurisdictions. PCBs are among the initial POPs included under the Aarhus protocol on POPs and the Stockholm Convention on POPs. They are also among the POPs more extensively reported to EMEP and other monitoring programs. Annual mean

concentrations for selected PCBs in air in 2017 are shown in Fig. 2.2. The four congeners shown in Fig. 2.2 are among the seven so-called indicator PCBs (or "Dutch PCBs"). These were abundant in various technical mixtures of PCBs produced, and are among the congeners more frequently analyzed and reported to EMEP.

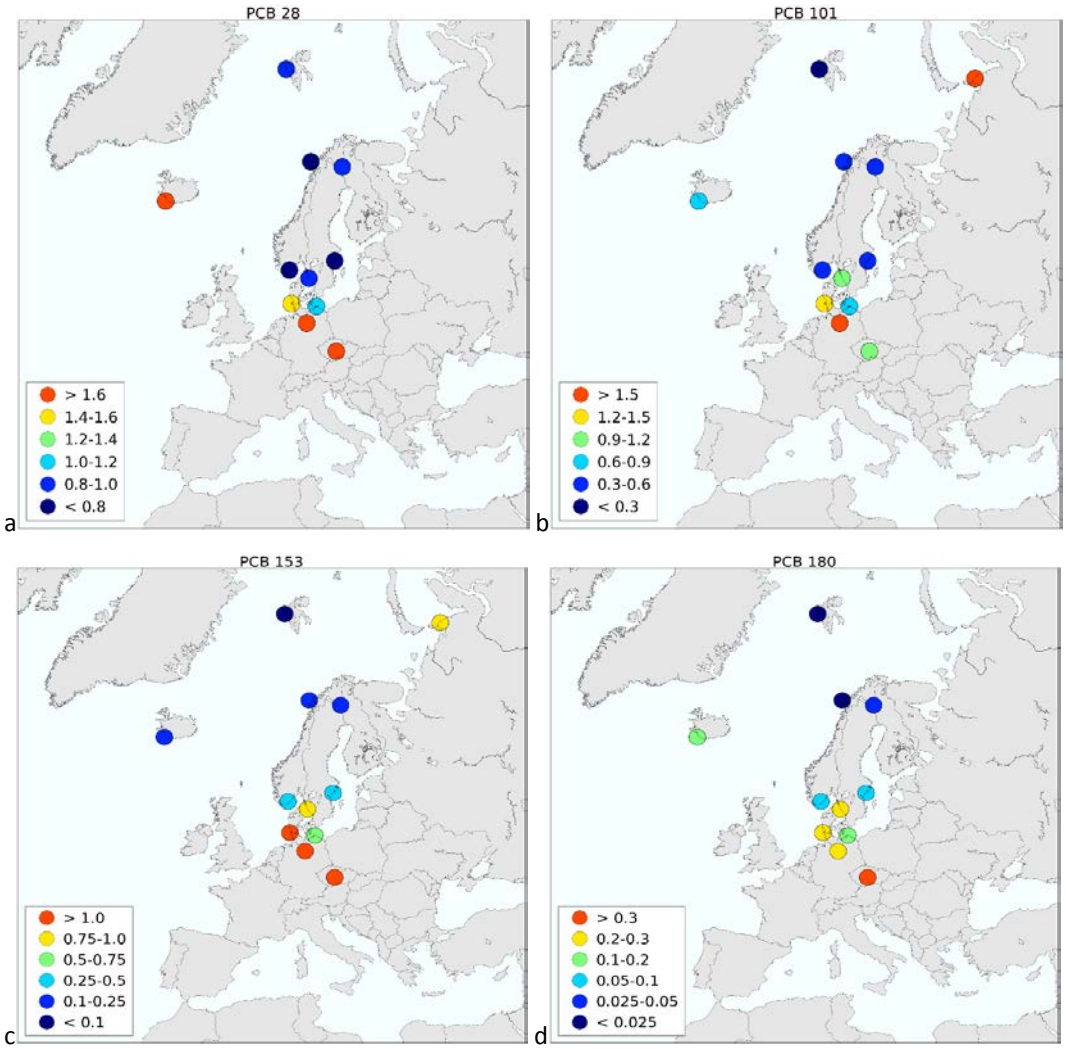

Fig. 2.2. *Annual mean concentrations in air for selected polychlorinated biphenyls (PCBs) in 2017 (pg/m^3): PCB-28(a), PCB-101 (b), PCB-153 (c) and PCB-180 (d)*

More than half of the amount of PCBs ever produced was used in electrical equipment (transformers and capacitors). PCBs were also used in various building materials, such as paints and as window sealants. Many of these products still remain in use, causing continuing primary emissions to air and other environmental media even today. While primary emissions are expected to have experienced a general decline over the last decades, as also seen in the EMEP monitoring data, primary emissions may still persist due to the long lifetime of products and material containing PCBs. Primary emissions may also occur during the disposal/recycling stages, e.g. when buildings are demolished, or when discarded electrical equipment (e.g. capacitors) is not properly recycled and/or disposed.

The potential for POPs to undergo LRAT is limited by either atmospheric reaction or (net) atmospheric deposition. Theoretical studies have suggested that the potential for LRAT varies significantly among individual PCB congeners [*Wania and Daly*, 2002]. Atmospheric reaction is predicted to be more efficient in limiting LRAT for the lighter and more volatile PCBs (e.g. PCB-28), whereas atmospheric deposition is suggested to be the limiting factor for the heavier and less-volatile PCBs (e.g. PCB-180) . The latter effect, i.e. limited LRAT potential due to deposition, may help to explain why PCB-180 appears to experience elevated concentrations in air in more central parts of Europe, compared to more remote sites (Fig. 2.2).

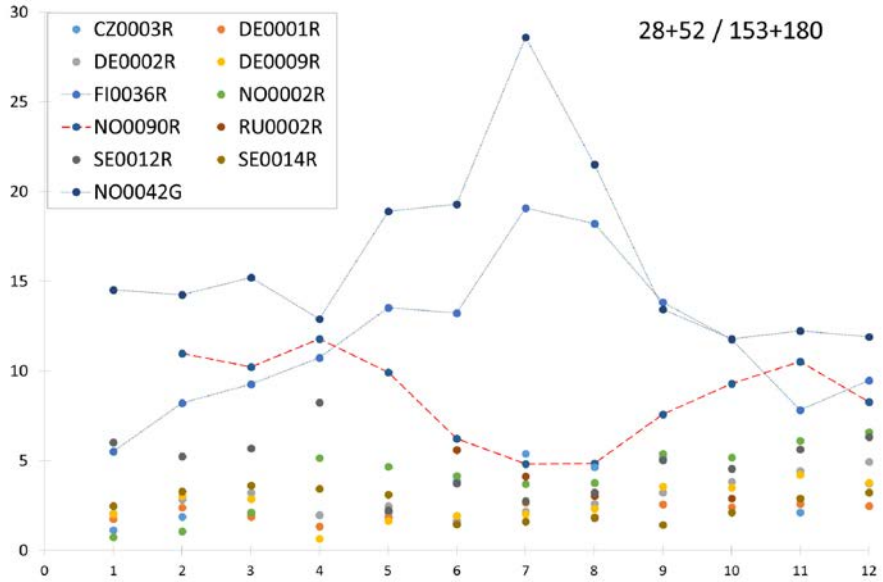

Fig. 2.3. *Ratio between monthly concentrations in air for PCB-28 + PCB-52, divided by PCB-153 + PCB-180 at EMEP sites*

Another way to analyze the relative significance of reaction and deposition is to look at the ratio between lighter and heavier PCBs over the time course of a year. This is shown in Fig. 2.3, where we have calculated the monthly ratio between PCB-28 + PCB-52, divided by PCB-153 + PCB-180. There are two sites, highlighted with stipulated lines, which are showing distinctively elevated ratios during summer. These are the remote northern sites Zeppelin (NO0042G) and Pallas (FI0036R). A possible explanation for this pattern might be a relative increase in lighter PCBs as a result of warmer temperatures in air during summer, causing enhanced volatilization of the more volatile congeners (PCB-28 and PCB-52). Or, the relatively cold air temperatures experienced during summer do not lead to any enhanced degradation even for the lighter PCBs. This seasonal pattern may also be affected by cold temperatures during winter, which may favor enhanced atmospheric deposition of the less volatiles congeners (PCB-153 and PCB-180) at the expense of the more volatile congeners. In the case of Zeppelin, a closer look at the data, comparing monthly concentrations in air divided by the annual mean, suggest that PCB-180 is the congener showing the more significant seasonal variability in air (data not shown). In other words, the seasonal pattern for PCB-180 at this site may in part be explained by enhanced atmospheric deposition of PCB-180 during winter. The seasonal pattern for Andøya (NO0090R) is showing the opposite pattern, with a lower ratio observed during summer. In this case, the pattern is largely explained by a stronger influence caused by lower

concentrations of lighter PCBs in air during summer, more than seasonal variability for heavier PCBs (data not shown). One possibility for the seasonal pattern observed for Andøya could be enhanced degradation of lighter PCBs during summer. For the other sites included in Fig. 2.3, seasonal patterns are less distinctive. For many of the other EMEP sites, we suspect the lack of strong seasonal patterns is a reflection of proximity to source regions. Under such circumstances, processes as atmospheric reaction and deposition may not have altered the measured PCB fingerprint at EMEP sites, compared to the original fingerprint from PCB emission sources.

However, the reasoning above rest on the critical assumption of measured concentrations at the sites specifically discussed are mainly attributed to LRAT from distant sources and source regions. Another feature associated with PCBs is their potential to undergo reversible atmospheric deposition, i.e. due to secondary emissions from environmental reservoirs as contaminated in the past [*Wania and Mackay*, 1996. Hence, it cannot be excluded the seasonal pattern seen at Zeppelin and Pallas in Fig. 2.3 is partly caused by enhanced secondary volatilization of the more volatile congeners during summertime. As it is well established Arctic regions are more prone to experience an increase in temperatures as result of climate change, enhanced re-volatilization of POPs have been hypothesized [*Ma et al*., 2011].

Hexachlorobenzene

Hexachlorobenzene (HCB) is characterized by a relatively high volatility and a long lifetime in air (approx. 1 year), compared to many other POPs. Hence, HCB does not readily degrade nor deposit, and the spatial variability is therefore anticipated to be relatively small as any fresh signal from emissions are likely to be buffered against the background concentration in air. Yet, the observed annual mean concentration and seasonal patterns are indeed observed to be spatially variable (Fig. 2.4a). However, concentrations of HCB in air might be underestimated due to breakthrough during active air sampling. Such sampling artefacts may possibly affect spatial patterns in particular, dependent on specific air sampling strategies as well as temperatures at individual sites.

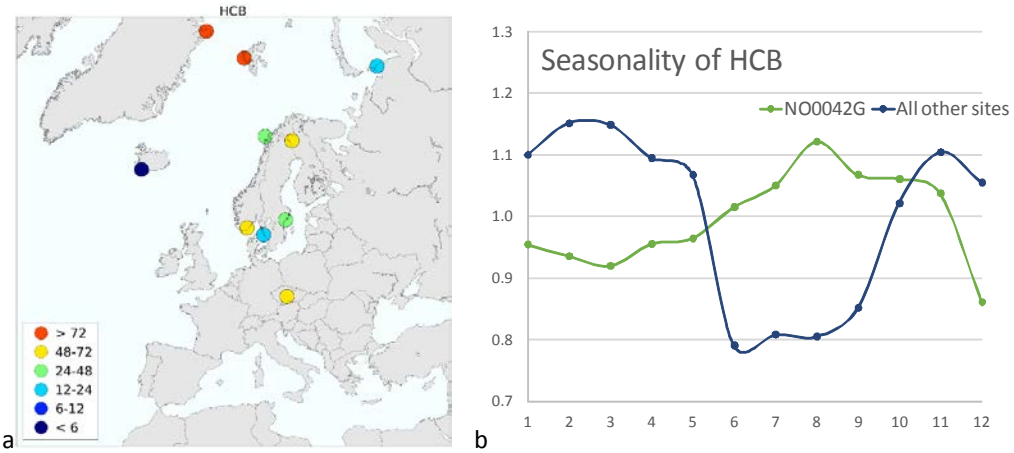

a b

Fig. 2.4. *Spatial pattern of annual average concentrations of HCB in air (pg/m^3) (a), and seasonal variability in atmospheric concentrations for Zeppelin versus all other EMEP sites combined (b). The latter was calculated as the monthly average concentration in air, divided by the annual mean*

Again, a closer look at seasonal patterns may reveal insights into sources and processes controlling concentrations of HCB in air. In this case, however, degradation is a very slow removal mechanism from the atmosphere. Hence, air-surface exchange processes are assumed to be more influential as a removal process, irrespective of whether surface to air fluxes are due to primary and/or secondary emissions. In Fig. 2.4b we have plotted the seasonality of HCB concentrations expressed as monthly mean divided by annual average concentrations in an attempt to minimize possible influence from sampling artefacts mentioned above. Furthermore, we have singled out the seasonality for Zeppelin (NO0042G), whereas all other EMEP sites are lumped into one lumped seasonal pattern. This was done to simplify the picture as most stations (with the exception of Zeppelin and to some extent the Danish station at Greenland (Villum Research Station, Station Nord) exhibited a seasonal pattern which tended to exhibit higher concentrations during winter, compared to summer. Of course, a possible explanation for this pattern could be that emissions are higher during winter compared to summer. However, as the annual mean concentration in air of HCB is the highest at the most remote Arctic sites, it seems unlikely primary emissions in these remote regions would be higher than the other European sites. Taken together, it cannot be ruled out concentrations of HCB in air at Zeppelin during summer and fall is largely affected by re-volatilization from environmental reservoirs.

DDTs

DDT is an insecticide extensively used in the past, yet which continues to be used in some tropical regions to combat mosquitoes carrying malaria viruses. The DDT technical mixture used as insecticide contains about 80% or more of the p,p'-DDT isomer. The highest annual mean concentration of p,p'-DDT in air was measured at Zingst (DE0009R: 5.9 pg/m^3). The atmospheric burden at Zingst was more than twice the annual mean concentration measured at the AMAP site Amderma (RU0002R: 2.6 pg/m^3), and the EMEP sites Hof (DE0002R: 2.4 pg/m^3) and Kosetice (CZ0003R: 2.3 pg/m^3). The annual mean concentration at other sites was 0.9 pg/m^3 (DE0001R) or less [*Aas et al.*, 2019]. The monthly mean concentrations of p,p'-DDT at EMEP sites are plotted in Fig. 2.5a. A seasonal pattern showing elevated concentrations in air during summer is expected as emissions are anticipated to be more significant during this time of year. However, the seasonal pattern of p,p'-DDT in air alone do not provide sufficient information which helps to discriminate between primary and secondary emissions.

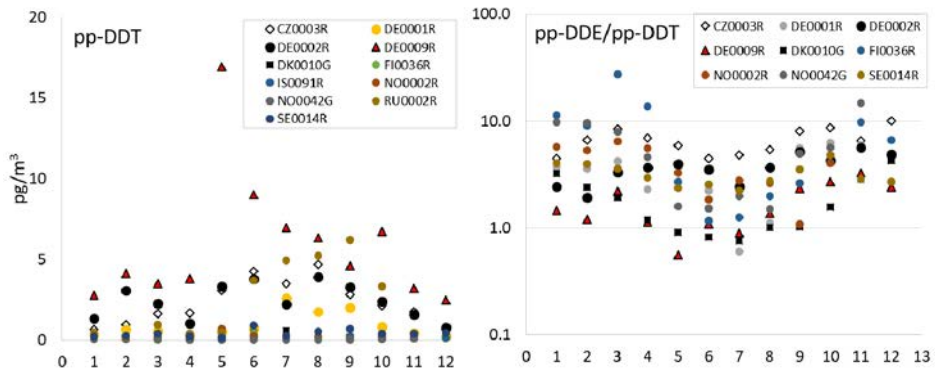

a b

Fig. 2.5. *Monthly mean concentrations of pp-DDT in pg/m^3 (a), along with monthly mean concentration ratios for p,p'-DDE/p,p'-DDT (b) in air at EMEP sites in 2017*

Once in the environment, p,p'-DDT will gradually be converted into the p,p'-DDE isomer. Hence, the relative difference between these two isomers in the environment may provide valuable insights as to whether samples are affected by fresh input of DDT (high p,p'-DDT, low p,p'-DDE), or a weathered signal (high p,p'-DDE, low p,p'-DDT). Hence, the ratio between p,p'-DDE to p,p'-DDT is often analyzed in environmental samples as shown in Fig. 2.5b. Zingst, which experienced a combination of both high concentrations of p,p'-DDT (left) and a low p,p'-DDE/p,p'-DDT ratio in 2017 appears to be influenced by fresh inputs of DDT during summer [triangles in Fig. 2.5]. In contrast, Kosetice, which is among the sites experiencing elevated concentrations during summer (Fig. 2.5a), have a calculated p,p'-DDE/p,p'-DDT ratio (Fig. 2.5b) which suggest a weathered signal. Interestingly, the site at Greenland (DK0010G) had very low concentrations of p,p'-DDE, albeit a low ratio, indicating possible influence by LRAT from areas affected by recent use of technical DDTs. While such ratios should be interpreted with a healthy skepticism, a combination of concentrations and analysis of POP fingerprints may offer useful information nonetheless. Such inferences would be difficult to infer without continued seasonal monitoring of POPs in air within the EMEP programme. However, a more detailed analysis of possible source-receptor relationships to assess recent use of technical DDT in controlling atmospheric samples requires a more in-depth model based analysis of individual air samples.

2.1.2. Monitoring of heavy metals in 2017

In 2017, there were 39 sites measuring heavy metals (Cd or Pb) in both aerosols and precipitation, and altogether there were 65 measurement sites. 28 sites were measuring Hg in either air and precipitation, 13 of these with co-current measurements in air and precipitation. In total, 22 Parties to the Convention reports heavy metal data to EMEP.

Annual averages of Pb , Cd and Hg concentrations in precipitation and in air in 2017 are presented in Fig. 2.6-2.8. The lowest concentrations for all elements are generally found in Scandinavia, and the highest depends on compounds and compartment, aerosol or precipitation.

For Pb, the highest concentration in aerosols is observed in Hungary followed by sites in Slovakia, and in the Benelux. In precipitation, the highest volume weighted annual mean is observed in Slovakia followed by sited Spain and France. For Cd, the highest concentration in aerosols in observed in Hungary followed by sites in Belgium and Spain, while in precipitation, the highest level is seen in France, Spain and Estonia. For total gaseous and elemental Hg the highest concentration is seen in Germany, while in precipitation, the highest levels are seen in Latvia and the Czech Republic.

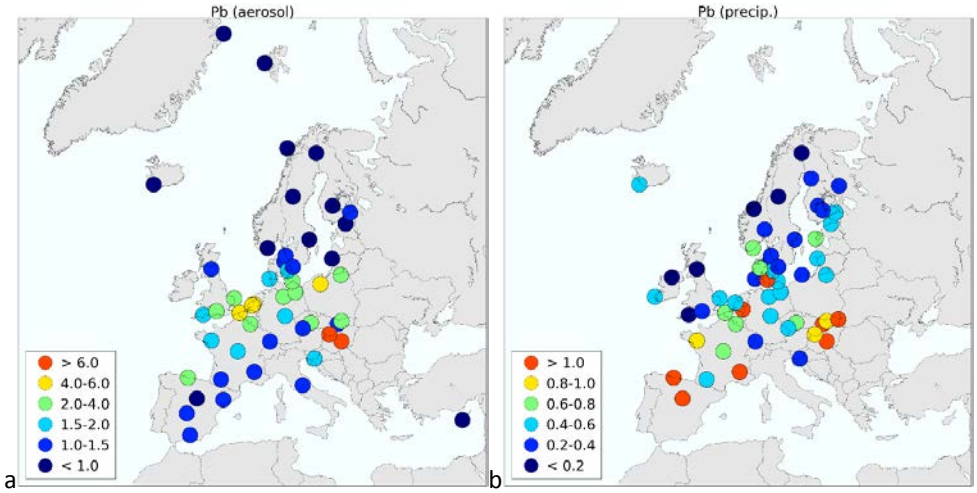

a b

Fig. 2.6. *Annual mean concentrations of Pb and in aerosols (a), ng/m^3 and precipitation (b), µg/L in 2017*

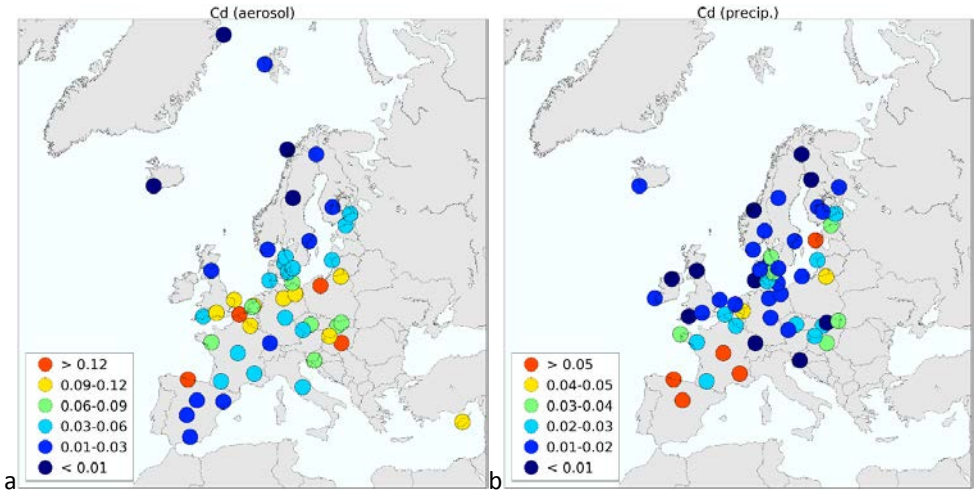

a b

Fig. 2.7. *Annual mean concentrations of Cd in aerosols (a), ng/m^3 and precipitation (b), µg/L in 2017*

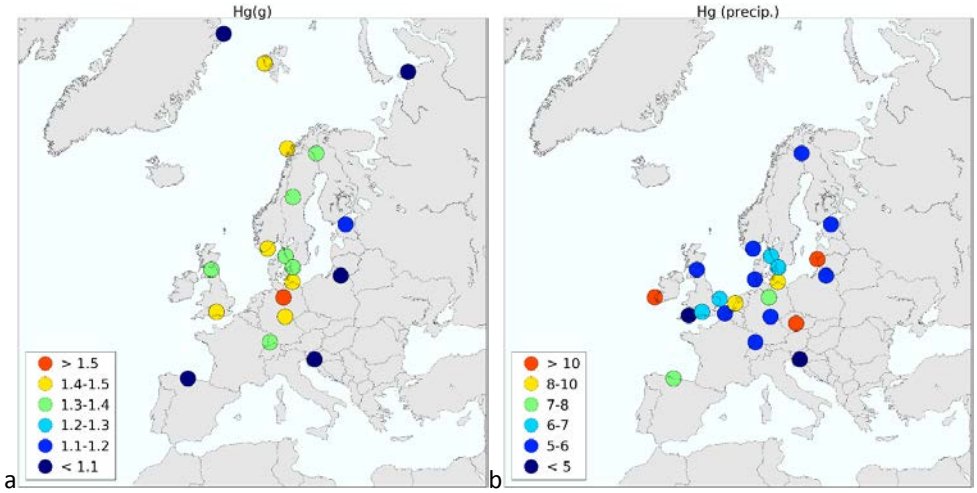

a b

Fig.2.8. *Annual mean concentrations of Hg in air (a), ng/m^3 and precipitation (b), ng/L in 2017*

2.2. Supplementary measurements

EMEP monitoring stations are mostly located in areas remote from main anthropogenic sources. However, transition to finer spatial resolution makes possible to better reproduce concentrations and deposition of heavy metals and POPs in more polluted regions such as urban areas and hot spots. In order to characterise pollution patterns over the EMEP region and evaluate modelling results against observed levels EMEP monitoring data can be supplemented with the information regularly reported by European Environmental Agency (EEA). EEA collects and makes available monitoring data on various pollutants including Pb, Cd, Hg, B(a)P and second priority metals (e.g., As, Ni) obtained at national monitoring networks of EU countries-members. These data as well as metadata are summarized in AIRBASE (AQ-e-Reporting) database and are available online (*https://www.eea.europa.eu/data-and-maps/data/aqereporting-8*).

Available data on heavy metals and POPs were derived from the AIRBASE database by MSC-E. In 2017 information on measured concentrations of Pb, Cd and Hg in air was reported by about 700, 850 and 26 stations, respectively (Fig. 2.9a,b). Results of B(a)P monitoring were reported from about 860 stations (Fig. 2.9c). Obviously, these data provide denser spatial coverage compared to EMEP stations. Besides, AIRBASE data are reported for regions where measurements of EMEP are scare or not available (e.g., Romania, Bulgaria, Italy etc.).

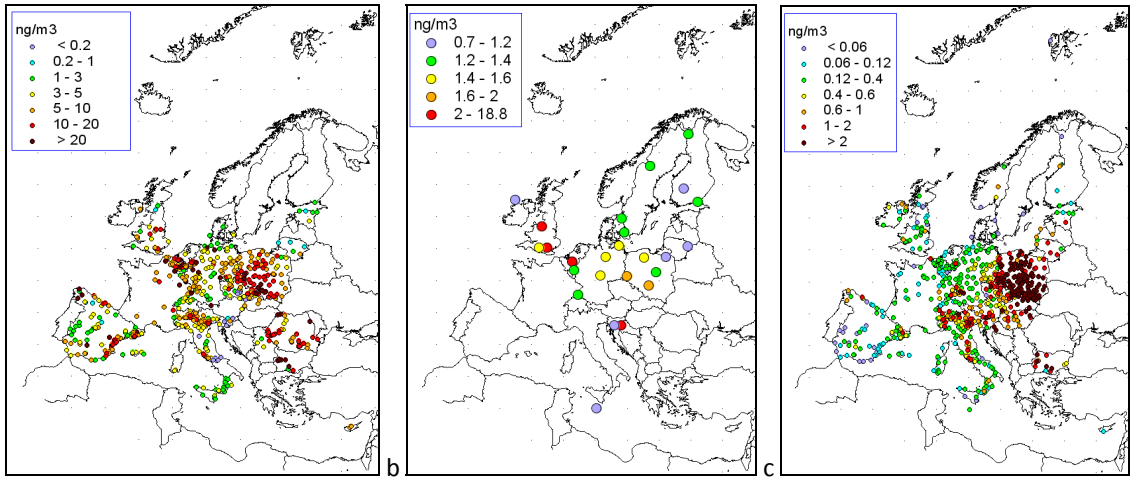

Fig. 2.9. *Concentrations of Pb (a), Hg (b) and B(a)P (c) in the EMEP region form AIRBASE database (circles)*

According to classification used within European Union, measurement stations in Europe are subdivided according to type of area where stations are located, and from viewpoint of predominant sources affecting the stations [*Larssen et al*., 1999]. Area types include urban (almost or completely built-up area), suburban (built-up area mixed with agricultural lands, woods etc) and rural. Rural stations additionally subdivided into the following categories:

- Rural-Near city (area within 10 km from the border of an urban or suburban area),
- Rural-Regional (10-50 km from major sources/source areas),

- Rural-Remote (50 km from major sources/source areas).

Subdivision of stations regarding to predominant emission sources includes the following types:

- Traffic (located in close proximity to a road and strongly influenced by traffic emissions),
- Industrial (located near single industrial sources or industrial areas),
- Background (not dominated by single emission source; representative of a wider area of at least several square kilometers).

Mean levels and their range may significantly differ depending on type of a station. The lowest (4.2 ng/m^3) air concentrations of Pb take place at background rural stations (Fig. 2.10a), followed by traffic (8.7 ng/m^3) and background urban (12.4 ng/m^3) stations. The highest concentrations (22 ng/m^3) are measured at industrial stations. Similar distribution is noted for Cd concentrations in air. Average concentration of mercury at background rural stations is 1.35 ng/m^3, at background urban stations – 1.79 ng/m^3 and at industrial stations – around 20 ng/m^3.

Statistical distribution of B(a)P concentrations differs from that of heavy metals. The lowest annual mean levels are noted for background rural (0.4 ng/m^3) and industrial (0.7 ng/m^3) stations (Fig. 2b). The highest concentrations are measured at background urban stations (2.0 ng/m^3).

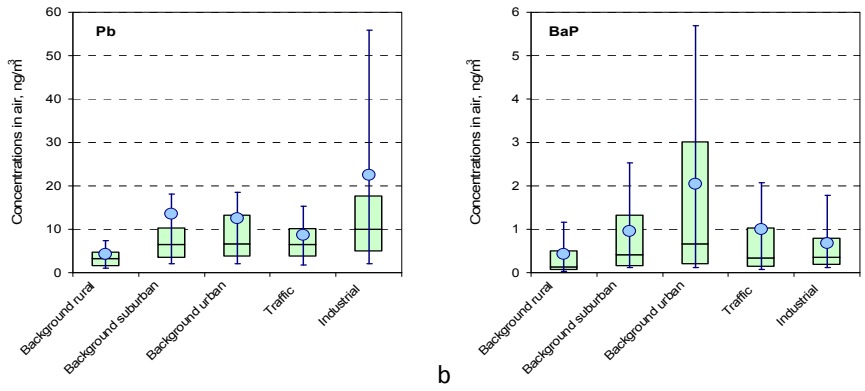

Fig. 2.10. *Frequency distributions of observed concentrations of Pb (a) and B(a)P (b) in 2017 available in AIRBASE data base. Boxes: 25th, 75th percentiles and median; circles: arithmetic mean; whiskers: range between 10th and 90th percentiles*

Another type of supplementary information used for analysis of heavy metal pollution levels is data on concentrations of heavy metals in terrestrial mosses [e.g., *Schroder et al*., 2015, *Lequy et al*., 2017, *Nickel et al*., 2017]. Moss monitoring surveys are carried every five years out in European countries [*Harmens et al*., 2016] under supervision of International Cooperative Programme on Vegetation (ICP-Vegetation) of Working Group on Effects. These surveys include both priority (Pb, Cd, Hg) as well as other metals, e.g. As, Ni, Cu, Cr and Zn.

Measurements of heavy metals in mosses are characterized by higher spatial density compared to EMEP monitoring network. Besides, these measurements are often organized in countries where

EMEP network is scarce, e.g. in the Caucasus region, Russia and Central Asia (Fig. 2.11). However, it should be noted that concentrations in mosses depend not only on atmospheric deposition but also on other environmental factors (particular moss species, proximity to sea shore etc.). Therefore, these data can be used in the assessment of pollution levels and verification of modelling results with caution.

a 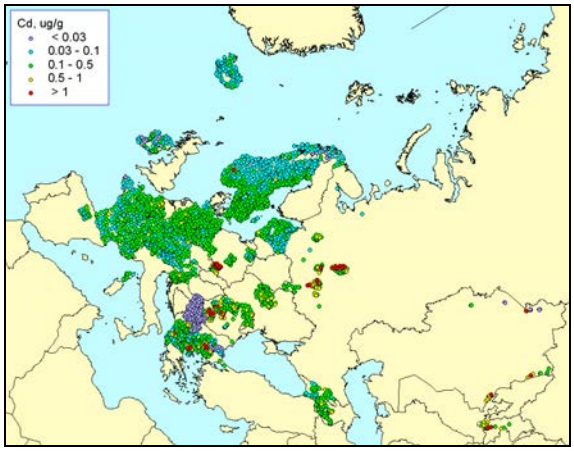

b 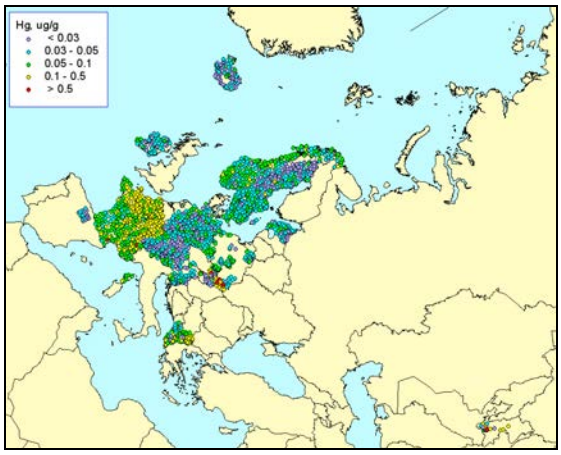

Fig. 2.11. *Concentrations of Cd (a) and Hg(b) in mosses measured in 2015*

3. STATUS of HEAVY METALS and POP AIR POLLUTION in 2017

Results of assessment of heavy metal and POP pollution levels in the EMEP region are presented. In accordance with the mandate of EMEP, deposition, concentration and transboundary transport of the considered pollutants was evaluated. Various additional types of information such as ecosystem-depended deposition, atmospheric pollution of watersheds, marginal seas, the Arctic region as well as the results of global-scale model simulations are described. Finally, meteorological conditions in 2017 and their changes compared to previous (2016) year are overviewed.

3.1. Meteorological conditions of 2017

Long-range atmospheric transport and deposition of heavy metals and persistent organic pollutants is strongly affected by meteorological conditions. Atmospheric circulation and vertical exchange of air masses are responsible for transport of the pollutants. Wet scavenging is controlled by atmospheric precipitation. Processes in the surface layer of the atmosphere influence dry deposition velocity of pollutants and the intensity of gaseous exchange. Soil moisture and wind velocity are the key meteorological factors responsible for dust suspension.

It is obvious that meteorological conditions change from one year to another. It can be caused by relatively slow long-term processes of climatic changes as well as inter-annual variability of the atmosphere. Therefore, meteorological conditions of 2017 are characterized via comparison with climatic mean values. Besides, the conditions in 2017 are compared with those taken place in previous (2016) year. This comparison is helpful for analysis of changes in pollution levels between 2016 and 2017.

The year 2017 is considered as the fifth warmest year starting from the middle of 19th century [*Blunden et al*., 2018]. Near-surface air temperatures in 2017 are higher than climatic mean (average in the period from 1961 to 1990) over the entire Europe (Fig. 3.1). Average value of the anomaly is 1.3°C [*Blunden et al*., 2018, *WMO*, 2019]. Spatially the anomalies of about 1-2°C are distributed almost homogeneously over Europe. Higher values of the anomalies are noted in some regions of Spain, Ukraine and the Arctic.

In winter of 2017 most significant (3-4°C) positive anomalies were observed over Scandinavia and the northern part of Russia. Winter colder than usual by 1-3°C was noted for the Balkan countries, Turkey and the Black Sea. Summer is characterized by anomalous heat over the central and the southern parts of Europe, while over Scandinavia summer temperatures were lower than normal.

Climatic mean annual precipitation sums are calculated for the period 1981-2010. In 2017 precipitation sums were close to climatic norm over most part of Europe (Fig. 3.2). The norm was exceeded up to 67% in the north-eastern part of Germany, northern Poland, a number of regions of Russia, southern Romania and southern Bulgaria. In Estonia, southern France, Italy, Spain and Portugal the precipitation made up 60-80% of the climatic norm.

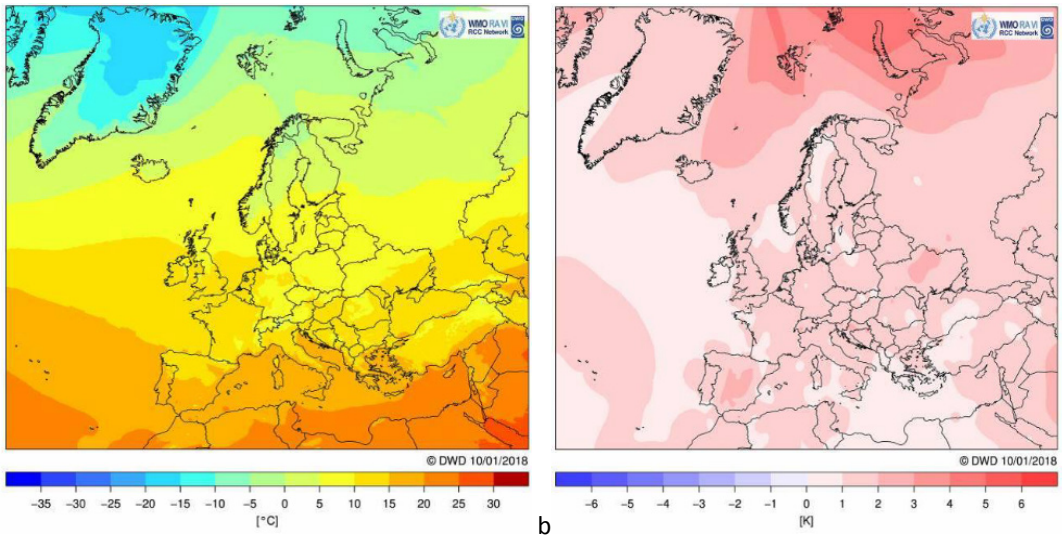

a b

Fig. 3.1. *Mean annual temperature in °C (a) and anomalies (b) for 2017 (reference period 1961-1990, source: http://www.dwd.de/rcc-cm).*

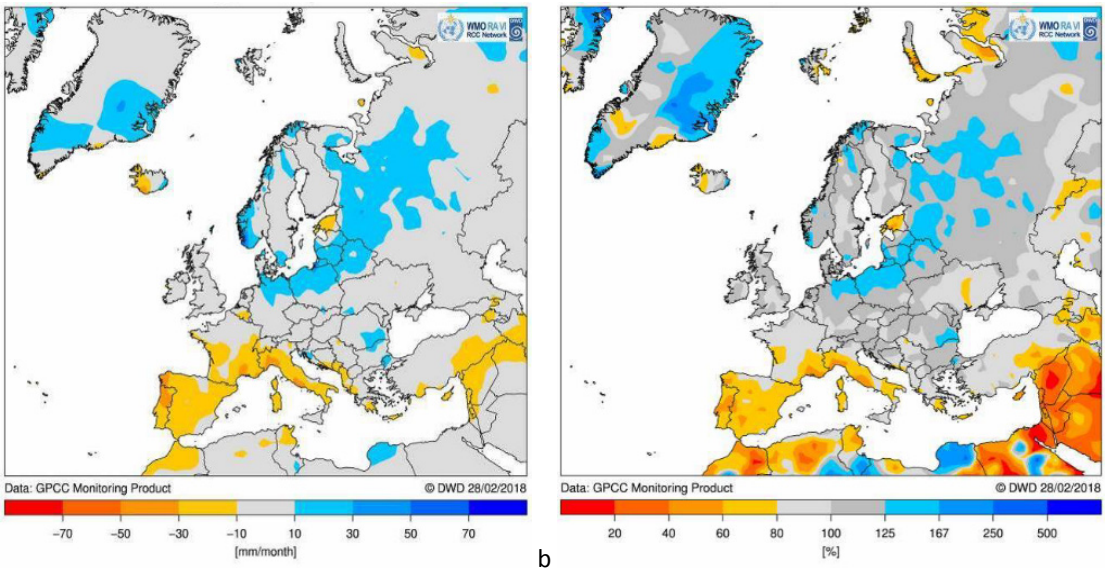

a b

Fig. 3.2. *Absolute (a, mm/month) and relative (b, %) anomaly of annual precipitation sums in 2017 relative to climatic mean value for the period from 1981 to 2010. Source: http://www.dwd.de/rcc-cm*

Winter of 2017 was dry over most part of western and southern Europe, the Balkans and Scandinavia, making up 40-60% of the climatic norm. Over most part of European Russia and the Norwegian coast precipitation were higher than normal by up to 67%. Dry summer conditions took place in Portugal, southern France, Italy, central Europe, southern regions of Eastern Europe. Over the northern part of Europe summer precipitation were presumably higher than normal.

Analysis of circulation indexes demonstrates that large-scale atmospheric circulation patterns in 2017 over Europe and Central Asia does not differ much from the climatic [*WMO*, 2019, *HMCR*, 2019]. However, in should be noted that on smaller scales the variability of meteorological conditions may affect transport patterns.

Precipitation sums in 2017 (Fig. 3.3) used in the modelling differ from those in 2016. The difference between precipitation in 2017 and 2016 is expressed in relative terms as difference between 2017 and 2016 divided by the value in 2016 and presented as percents. Therefore, positive values of this relative difference mean increase of precipitation in 2017, and negative – decrease. Increase of precipitation sums is noted for the Baltic Sea and most of Scandinavia, Germany, Poland, Belarus and the central part of Russian European area (Fig. 3.3b). The decrease of precipitation, compared to 2016, takes place over southern and south-western Europe, in the eastern European countries and central Asia.

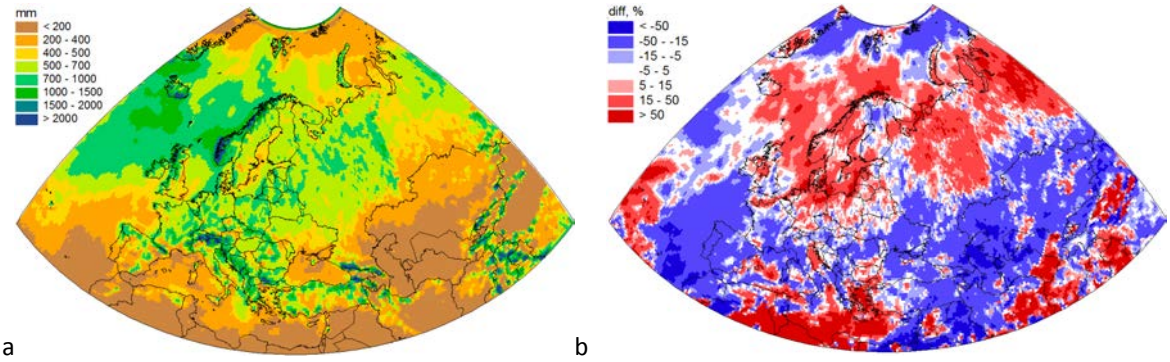

a b

Fig. 3.3. *Annual precipitation sums (a) and relative difference between precipitation in 2017 and 2016 (b). Positive values mean increase and negative – decrease of precipitation in 2017 relative to 2016*

Air temperature is important parameter affecting rates of chemical reactions. Since most of pollutants are emitted within the lower troposphere, it makes sense to consider mean temperature within atmospheric boundary layer. Annual mean air temperature in the EMEP region in 2017 averaged within atmospheric boundary layer (around 1 km) is shown in Fig. 3.4a, and the difference between the temperatures in 2017 and 2016 – in Fig. 3.4b. Over most part of the region the difference is within ±1°C, except for the Arctic and easternmost part of the EMEP region.

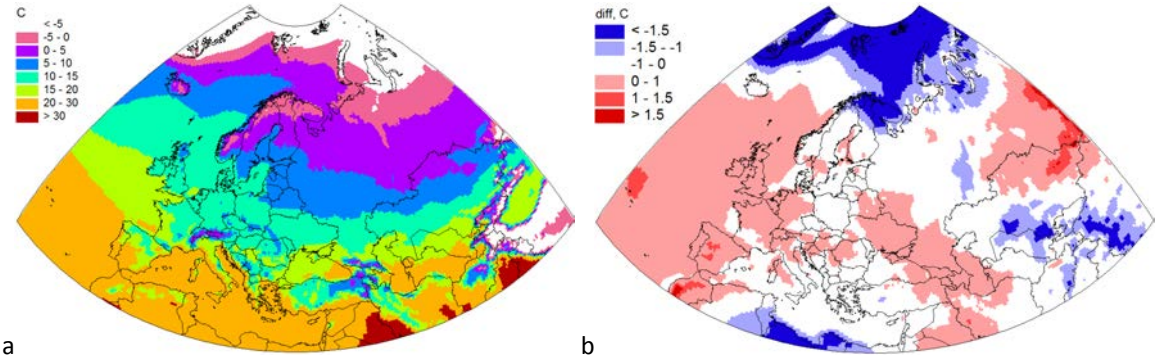

a b

Fig. 3.4. *Annual mean air temperature averaged over atmospheric boundary layer (~1 km) in 2017 (a) and difference between the temperatures in 2017 and 2016 (b)*

3.2. Model assessment of pollution levels

Assessment of heavy metal and POP pollution of the EMEP region is based on both modelling results and measurement data and includes evaluation of spatial patterns of pollution levels as well as transboundary transport in 2017. It is based on the most recent dataset of gridded heavy metal and POP emissions available at the moment of the study, which was prepared by CEIP for 2016 (Section 1.2.2). To evaluate changes in pollution levels due to inter-annual meteorological variability the assessment results are compared with previous estimates for 2016. This section contains a short summary and analysis of the assessment. More detailed information on evaluation of modelling results against measurements, transboundary pollution, deposition-specific deposition is available the Supplementary Data Reports for heavy metals [*Ilyin et al*., 2019] and POPs [*Gusev et al*., 2019].

3.2.1. Model setup

The operational model assessment of heavy metal and POP pollution in 2017 has been performed with the GLEMOS model, version v2.0. Description of the current stable version of the model is available at the MSC-E website (*http://en.msceast.org/index.php/j-stuff/glemos*). The simulations of transboundary pollution of the EMEP countries have been carried out over the new EMEP domain on the latitude/longitude projection (*https://www.ceip.at/ms/ceip_home1/ceip_home/new_emep-grid/*). Meteorological information for the model runs has been generated using a meteorological pre-processor based on the Weather Research and Forecast modelling system (WRF) [*Skamarock et al*., 2007] and fed by operational analysis data from the European Centre for Medium Range Weather Forecasts (ECMWF) [*ECMWF*, 2019]. Anthropogenic emissions data of all pollutants have been prepared for modelling based on the gridded emissions fields provided by CEIP (Section 1.2.1) and complemented by additional emission parameters required for model runs (Section 1.2.2). Data on wind re-suspension of particle-bound heavy metals (Pb and Cd) from soil and seawater has been generated using a dust pre-processor [*Gusev et al.*, 2006; 2007]. Concentrations of chemical reactants (O_3, OH, SO_2), particulate matter (PM2.5) and its organic constituents (OC, BC), which are required for Hg and POP chemistry, have been imported from the MOZART model [*Emmons et al.,* 2010]. Boundary conditions for the regional scale simulations of all considered pollutants have been obtained from the GLEMOS model run on a global scale (see for details Section 3.3.6). Initial conditions for the evaluation of pollution levels of long-living POPs (e.g. PCBs, HCB, and PCDD/Fs) in the EMEP region were prepared on the basis of long-term spin-up global model runs applying expert estimates of historical emissions.

3.2.2. Lead and cadmium

Levels of Pb and Cd atmospheric pollution are evaluated using results of the model simulations and measurements. Modelled concentrations and deposition were produced by the GLEMOS model using emission and meteorological data for 2017. Measurements of concentrations in air and wet deposition fluxes were carried out at the EMEP monitoring stations (Section 1.1.1).

Concentrations of Pb and Cd in air are distributed unevenly over the EMEP region. The highest levels are noted for Central Europe (southern Poland, west of Germany, Belgium, the Netherlands, north of Italy) (Fig. 3.5). In the eastern part of the EMEP region (EECCA countries and Russia) relatively high concentrations of Pb and Cd take place in the eastern part of Ukraine, the northern and south-western parts of Kazakhstan, Uzbekistan and Turkmenistan. Besides, areas or elevated Cd concentrations occur in the central and eastern parts of Russia. The lowest concentrations of the considered heavy metals take place in Northern Europe (Sweden, Finland, Norway, Iceland, north of Russia) and the Arctic.

In the most part of the EMEP region where measurement data are available, modelled concentrations match the observations. This statement is confirmed by statistical indicators: mean relative bias for concentrations of Pb is 1% and for Cd is 12%. Spatial correlation coefficients are 0.82 and 0.76, respectively. More detailed discussion on agreement between modelled and observed concentrations is given in Supplementary Data Report [*Ilyin et al*., 2019].

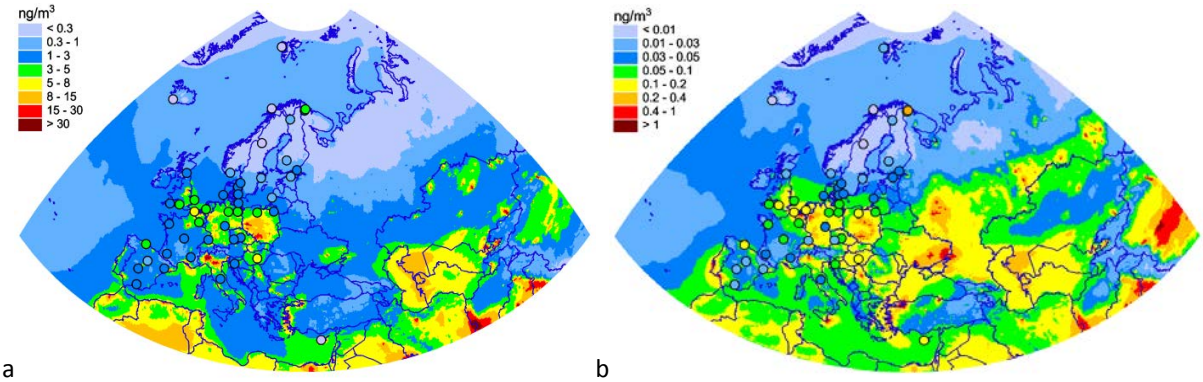

a b

Fig. 3.5. *Annual mean concentrations of Pb (a) and Cd (b) air concentrations in 2017. Circles show observed values in the same colour scale*

Spatial pattern of total deposition of Pb and Cd generally resembles that of air concentrations and to some extent reflects spatial distribution of emissions and wind re-suspension (Fig. 3.6). Unlike concentrations in air, deposition fluxes over most territory of Central Asia are relatively low due to dry climatic conditions and low precipitation amount. Besides, elevated precipitation at windward slopes of mountain regions favours increase of deposition. It results in higher deposition along the western part of Norway, the Alpine and Balkan regions, the south-eastern part of Kazakhstan and north of Kyrgyzstan (Tien Shan mountains).

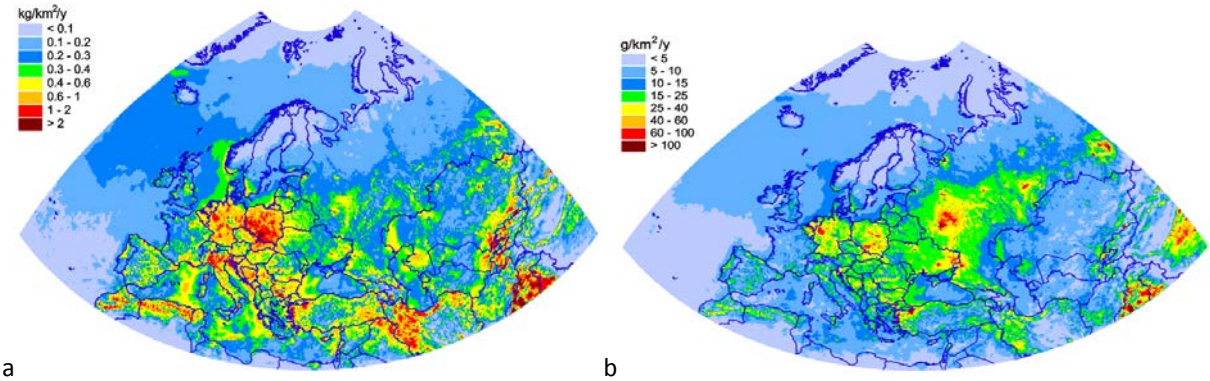

a b

Fig. 3.6. *Annual total deposition flux of Pb (a) and Cd (b) in 2017*

Total deposition is a sum of wet and dry deposition. In the EMEP countries wet deposition makes up about 70% and 80% of total deposition for Cd and Pb, respectively. Wet deposition is measurable parameter, which is regularly recorded by the EMEP stations. Spatial distribution of calculated wet deposition fluxes is generally confirmed by observations in the central part of Europe, the United Kingdom and southern Scandinavia. Modelled wet deposition of Cd and Pb underestimate the observed levels by about 40%, and spatial correlation coefficient is 0.5 – 0.6. However, the observed fluxes are significantly (2-5 fold) higher than the calculated levels in France, Spain, Latvia, Estonia and northern Scandinavia. These large discrepancies may be explained by various reasons such as uncertainties of the model parameterizations, emission data or measurements. More detailed comparison between modelled and observed levels is available in Supplementary Data Report [*Ilyin et al*., 2019].

Three groups of emission sources are responsible for heavy metal pollution levels in the EMEP region. These are EMEP anthropogenic emissions of considered year, wind re-suspension of dust particles containing heavy metals, and emissions from sources located outside the EMEP region (non-EMEP sources). Average contributions of EMEP anthropogenic sources, wind re-suspension and non-EMEP sources to total deposition of Cd amount to 66%, 24% and 10%, respectively. For Pb deposition the corresponding values are 42%, 42% and 16%. Therefore, for Cd the main contributor is presented by anthropogenic sources, while deposition of Pb is caused by anthropogenic sources and re-suspension in comparable proportions. However, it is important to note that uncertainty of modelled re-suspension is still high. Contribution of non-EMEP sources is relatively small for both Pb and Cd.

The ratios of these three components differ markedly among the EMEP countries (Supplementary Data Report [*Ilyin et al*., 2019]). For example, 79% of Cd deposition in Belgium comes from EMEP anthropogenic sources. In contrast, non-EMEP sources are the main contributor to Cd deposition in Cyprus that makes up 53% of total deposition. About three fourth of this deposition are caused by transport from desert areas of Africa and Asia. Sahara dust outbreaks are periodically recorded in Cyprus [*Nisantzi et al.,* 2015, *Mamouri et al*., 2016, *Kezoudi et al*., 2019, *Achilleos et al*., 2014].

Pollution levels in a country are produced by emission sources located both within the country (national sources) and due to transboundary transport from other countries (foreign sources). Contribution of foreign sources to total anthropogenic deposition of Pb and Cd in the EMEP countries

ranges from about 20% to almost 99%, while the remaining part is caused by national emission sources. The contribution of transboundary transport to Pb deposition exceeds 50% in 37 countries, and exceeds 75% - in 23 countries. For Cd deposition the corresponding values are 39 and 22 countries, respectively.

Countries act not only as receptors but also as sources of transboundary pollution. Pb and Cd emitted by country's sources deposit to own territories, to territories of other EMEP countries or outside the EMEP region. Magnitude of total deposition from national sources of the EMEP countries to other countries varies markedly depending on the country emission and geographical location. The highest Pb total deposition to the EMEP countries are noted for Kazakhstan (about 490 tonnes), followed by Poland (about 370 tonnes) and Russia (270 tonnes). Russia (80 tonnes), Ukraine (14 tonnes) and Poland (12 tonnes) produce the largest Cd deposition to the EMEP countries.

Pollution deposition to other countries as a fraction to total deposition in the EMEP countries is considered as a measure of transboundary export of pollution expressed in relative terms. For most of counties this fraction for Pb and Cd varies widely from about 40% to almost 100%. High fraction values typically take place for small countries (e.g., Monaco, Lichtenstein, Malta etc.) since almost all Cd and Pb emissions deposit outside their territories. Relatively small values (11-16%) were estimated for Russia and Iceland. Most of Pb and Cd emitted in Russia deposits within vast territory of this country and, hence, smaller part is deposited to neighbouring countries. In case of Iceland major part of the metals emitted by its sources is deposited to surrounding water surface of the Atlantic Ocean, and only minor part reaches territories of the EMEP countries. More detailed information on source-receptor relationships between the EMEP country in 2017 is available in Supplementary Data Report [*Ilyin et al.*, 2019] and at the MSC-E website (www.msceast.org).

Obtained estimates of Pb and Cd deposition in the EMEP region for 2017 were compared with previous estimates of the pollution levels for 2016. Since both studies use the same emissions dataset for 2016, the factors causing changes in modelling results include variability of meteorological conditions and updated model parameterisation of wind re-suspension. Detailed analysis of these factors and their effect on the modelling results is presented in Section 4.4. A brief outcome from the analysis is given below.

Figure 3.7 illustrates changes in Cd deposition between 2016 and 2017. Most significant absolute (Fig. 3.7a) and relative (Fig. 3.7b) differences are noted for the central and the western parts of the Mediterranean region. Relatively high absolute changes (-8 - -3 g/km^2/y) are seen over the eastern part of Europe, whereas relative changes over this regions are around -30%. Significant positive changes are noted for the Asian part of Russia, but absolute changes over this region are low (up to 3 g/km^2/y). Relative changes of Cd deposition induced by meteorological variability lie within ±15% range for majority of the EMEP countries. The highest decline between 2016 and 2017 noted for Ireland (-24%), Georgia (-22%) and Azerbaijan (-21%).

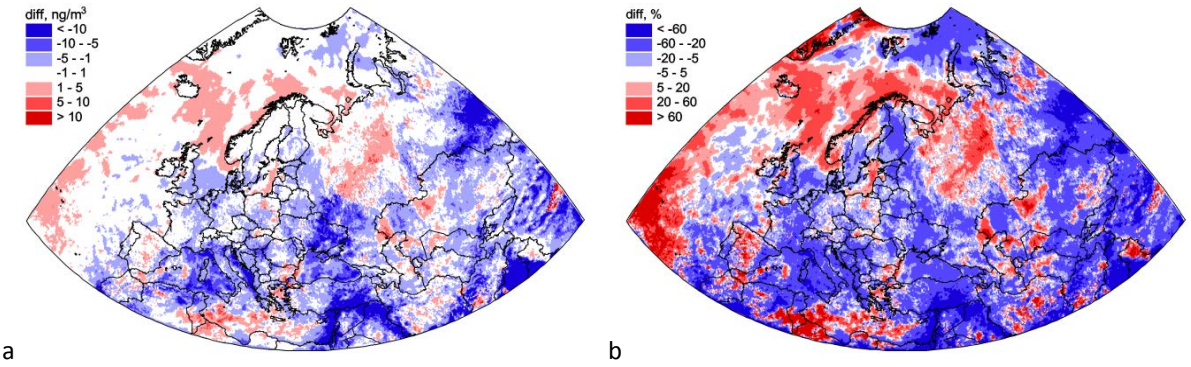

a b

Fig. 3.7. *Absolute (a) and relative (b) changes of Cd deposition between 2016 and 2017*

Changes of anthropogenic deposition in countries are accompanied by changes in relative contribution of national sources and transboundary transport. For example, the contribution of national sources to deposition of Cd in Ireland increased from 31% in 2016 to 40% in 2017 (Fig. 3.8a), while the contribution of the British sources decreased from 30 to 22%. The contribution of Germany remained around 10%. Changes expressed in absolute terms are shown in Fig. 3.8b. Deposition from national sources remains the same (66 kg), but deposition from the British sources reduced almost two-fold (from 65 to 35 kg) and from the German sources – from 24 to 14 kg.

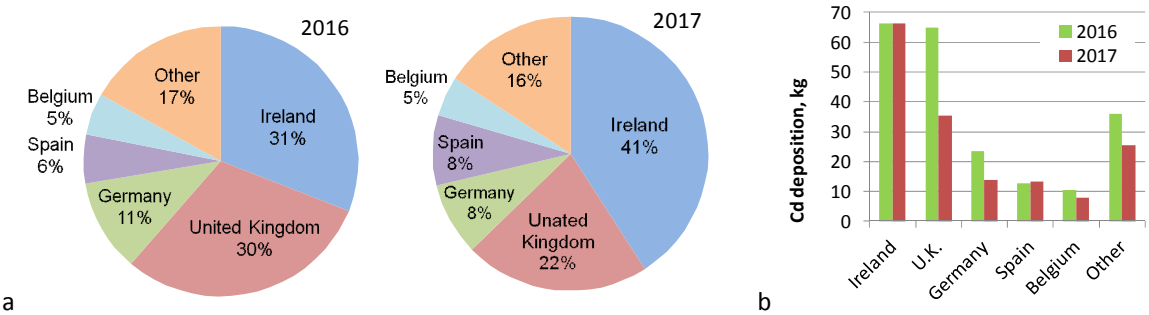

a b

Fig. 3.8. *Relative (a) and absolute (b) contribution of main source countries to Cd deposition in Ireland in 2016 and 2017*

Variability of meteorological conditions results in changes of deposition to the EMEP countries between 2016 and 2017 within ±15%. However, changes of transboundary contributions to deposition in the counties can be much greater. Besides, the changes in particular parts of a country can also differ markedly from the country-mean changes.

3.2.3. Mercury

Mercury differs from other heavy metals (e.g. Pb or Cd) by complex chemical cycling of its compounds in the atmosphere. The general character of the atmospheric dispersion of this pollutant is governed by the properties of particular physical and chemical forms. Emissions of short-lived oxidized Hg species, which occur in both gaseous and particulate forms, determine atmospheric Hg deposition in a country and transboundary pollution in the region. Whereas Hg emitted as long-lived

gaseous elemental Hg^0, it contributes to the global atmospheric transport and can deposit to other continents or travel around the globe and return back to the country. Mutual transformations of Hg species in the atmosphere also affect deposition patterns.

Simulated spatial pattern of Hg concentration in the EMEP region in 2017 is shown in Fig. 3.9a. Long residence time of Hg^0 in the atmosphere leads to relatively even distribution of its air concentration with insignificant spatial gradients. The concentration levels vary within ±20% from 1.3 ng/m^3 in remote areas of the Arctic and the Atlantic Ocean to 2 ng/m^3 in industrial and urban areas of Central, Southern and Eastern Europe. Simulated Hg^0 levels well agree with measurements at the sites of the EMEP monitoring network (Fig 3.9a). Deviation between the modelled and observed values does not exceed ±15%. Somewhat higher discrepancies are obtained for sites located in Poland and Estonia, which reported very low Hg^0 concentrations (below 1.2 ng/m^3). For more detailed evaluation of the modelling results against observations see Supplementary Data Report [*Ilyin et al*., 2019].

Mercury deposition is largely determined by oxidised Hg forms both emitted and produced chemically in the atmosphere. Therefore, the spatial pattern of Hg deposition is much more variable and reflects the effect of various factors including spatial distribution of emissions, areas of intensive atmospheric oxidation and precipitation pattern. Figure 3.9b shows spatial distribution of Hg net deposition (total deposition minus re-emission from snow and ice). This parameter is chosen instead of total deposition to characterise input and accumulation of the pollutant in the ecosystems, since significant amount of Hg deposited to snowpack is re-emitted to the atmosphere. As seen Hg deposition levels vary from a few g/km^2/y in the Arctic, northern Scandinavia, northern Russia and arid regions of Central Asia and Africa to more than 25-50 g/km^2/y in the Balkan countries, Central and Eastern Europe (Fig. 3.9b). Countries with the highest average deposition fluxes include Bosnia and Herzegovina, Slovakia, Liechtenstein, Poland, the Czech Republic, Montenegro and Slovenia (for more information see Supplementary Data Report [*Ilyin et al*., 2019]). Elevated levels of Hg deposition are also predicted in the high Arctic as a result of intensive Hg oxidation in springtime during the Atmospheric Mercury Depletion Events (AMDEs).

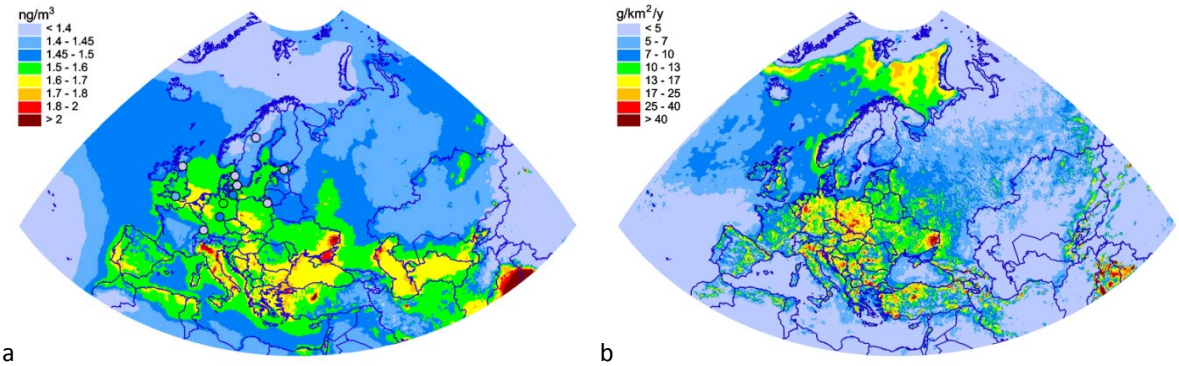

Fig. 3.9. *Spatial distribution of air concentration of Hg^0 (a) and net Hg deposition flux in the EMEP region in 2017. Circles show observed values in the same colour scale*

The model performance in simulating Hg deposition can be partly evaluated by comparison of modelled and measured wet deposition fluxes. The model evaluation against EMEP measurements demonstrates satisfactory agreement of modelled and observed values with high spatial correlation (0.81) and deviations being mostly within a factor of two (see Supplementary Data Report [*Ilyin et al.*, 2019]). However, the model tends to overestimate the observed values on average by 50%. This inconsistency is presumably connected with uncertainties of speciation of Hg anthropogenic emissions and incomplete knowledge on chemical transformations of Hg in the atmosphere. It should be noted that speciation of Hg emissions is not among the obligatory parameters included to the annual reporting by countries. Therefore, simplified expert estimates are used to prepare emission data for modelling (Section 1.2.2). Atmospheric chemistry of Hg is still actively investigated by the scientific community including identification of the major oxidation and reduction mechanisms, reaction kinetics and products (Section 4.2).

As it was mentioned above Hg deposition depends on both the pollutant emissions and variety of ambient meteorological parameters, which determine its dispersion in the atmosphere and removal to the ground. Figure 3.10 illustrates changes of Hg deposition pattern between 2016 and 2017 due to variability of meteorological parameters. Mercury deposition flux increased in temperate latitudes of the EMEP region (Denmark, the Netherlands, Germany, Poland, Slovakia, the Baltic countries, Russia), in the Northern Atlantic and the Arctic (the Barents Sea), over northern Africa. Deposition decreased in northern Scandinavia, Northern Russia, the Mediterranean Region, and Central Asia. These changes are largely caused by variation of the precipitation pattern (Section 3.1, Fig. 3.3), which lead to appropriate altering of Hg wet removal from the atmosphere. Significant increase of Hg deposition over the Barents Sea is caused by combination of two factors: lower air temperatures (Section 3.1, Fig. 3.4), which are responsible for more intensive Hg oxidation during AMDEs, and increased precipitation in this area.

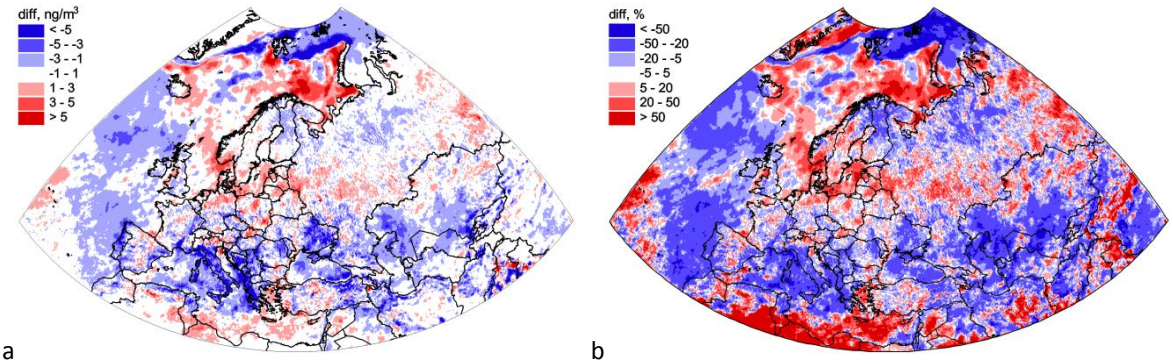

a b

Fig. 3.10. *Absolute (a) and relative (b) changes of Hg net deposition between 2016 and 2017 due to variation of meteorological parameters*

Mercury deposition to each EMEP country consists of contribution of various source types including national anthropogenic emissions of the country, transboundary transport from other EMEP countries, secondary and natural emissions of the region, and contribution of Hg global atmospheric circulation (Hg global pool) coming to the region across the boundaries. The share of these

components varies from country to country. National emissions along with emissions of other EMEP countries contribute on average 22% of Hg deposition in a country but this value varies from 1.7% for Iceland to 48% for Poland (Fig. 3.11). Contribution of Hg secondary and natural sources is insignificant and does not exceed a few percents. Emissions from these sources being in the Hg^0 form mostly contribute to the Hg global pool. In contrast, contribution of the Hg global pool is large and averages 76% of Hg deposition (50-97% in individual countries). However, it should be noted that the contribution the Hg global pool includes also some fraction of Hg from the EMEP sources (both anthropogenic and secondary/natural), which flew out through the boundaries, mixed up with other sources and returned back to the region. The more comprehensive source apportionment on a global scale demonstrates approximately equal contributions of regional sources and intercontinental transport to Hg deposition in Europe [*Ilyin et al.*, 2018].

As a part of transboundary pollution, the EMEP countries both receive Hg deposition from emission sources of other countries (import) and contribute to pollution of other countries (export). Fig. 3.12 shows statistics of the import to export ratios for the EMEP countries with respect to their pollution exchange with both other countries and the global pool. The median values for both categories are close to the unity indicating that the countries are almost equally distributed among importers and exporters of Hg pollution. The import/export ratio to/from the EMEP countries varies from 0.1-0.2 for Monaco and Portugal to 15 for Iceland and 28 for Belarus. The import/export ratio with respect to the Hg global pool varies from 0.05-0.25 for Monaco and Belgium to 18 for Norway and Iceland.

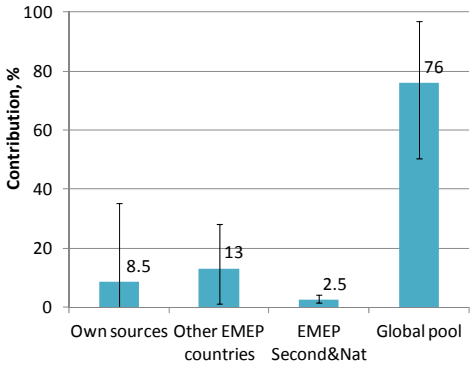

Fig. 3.11. *Contribution of various source types to Hg deposition in the EMEP countries. Bars show average contribution over all countries, whiskers present the range between minimum and maximum in individual countries.*

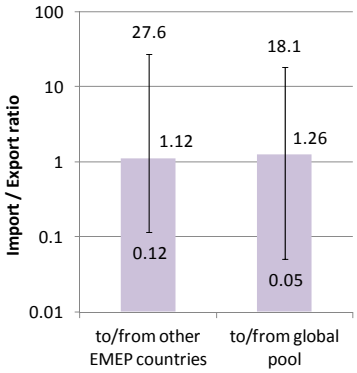

Fig. 3.12. *Import to export ratio of Hg atmospheric transport for the EMEP countries. Bars show the median ratio for all countries, whiskers present the range between minimum and maximum for individual countries.*

Mercury emitted by national sources partly deposits within a country's territory and partly contributes to transboundary pollution of other countries and regions. Contribution of a country to transboundary pollution depends on amount of national emissions, size and location of the country's territory. About 75% of Hg deposition in the EMEP countries is determined by major source countries – Ukraine, Russia, Kazakhstan, Poland, Turkey, Germany, and Italy. For most of these countries Hg deposition almost equally splits between deposition to own territory and territories of other

countries. Exceptions are Russia and Turkey, for which deposition to own territory exceeds contribution to transboundary transport by a factor of 6 and 2, respectively.

The effect of Hg transboundary transport on country pollution is characterised by relative contribution of national and foreign anthropogenic sources to Hg deposition in the country. The proportion of foreign sources varies from 15-20% for Turkey, Portugal, Italy and the UK to more than 95% for Malta, Belarus, Monaco and Liechtenstein. Mercury deposition from foreign sources exceeds deposition form national sources in 36 of 51 EMEP countries. Slovakia and the Czech Republic are among countries with high Hg deposition fluxes, which significantly affected by transboundary transport. On the other hand, high deposition levels in Bosnia and Herzegovina, Poland, Germany and Ukraine are largely determined by national sources. More detailed information on transboundary pollution for each EMEP country is available in Supplementary Data Report [*Ilyin et al*., 2019].

3.2.4. PAHs

Polycyclic Aromatic Hydrocarbons (PAHs) represent a group of chemicals that naturally occur in the environment and can be released to the atmosphere during incomplete combustion of fossil fuels and biomass burning. Being emitted to the atmosphere, PAH undergo complex interactions with other pollutants, including particulate matter and atmospheric reactants, and removal due to chemical transformations, dry and wet deposition [*Delgado-Saborit et al*., 2010; *Ravindra et al*., 2007].

Assessment of PAH pollution in the EMEP countries for 2017 was made for the 4 PAHs, namely, benzo(a)pyrene (B(a)P), benzo(b)fluoranthene (B(b)F), benzo(k)fluoranthene (B(k)F), and indeno(1,2,3-cd)pyrene (IP). Spatial distributions of annual mean modelled air concentrations of B(a)P and the sum of 4 PAHs in 2017 are presented in Fig. 3.13. The model predictions are combined on the maps with the values of observed air concentrations, reported by the EMEP monitoring stations. In general, the modelling results are consistent with the geographical pattern of observed air concentrations and reflect the main spatial gradients of PAHs in the EMEP region. In particular, elevated levels of B(a)P concentrations are seen in the countries of Central and Eastern Europe, e.g. in Poland, the Czech Republic, Hungary, northern Italy, as well as in some areas of Serbia, Spain, Romania, Macedonia, Montenegro, Turkey, and Russia. In some of these countries estimates of B(a)P air concentrations exceed air quality guidelines. More detailed information on the exceedances is given in the Section 3.3.3. Low levels of B(a)P concentrations are simulated for the UK, France, the Scandinavian countries, northern Russia, and the countries of Central Asia. Similar spatial distribution of air concentrations is obtained for the sum of 4 PAHs. At the same time, the gradients of concentrations are smoother and elevated levels of PAHs in the countries of Central and Eastern Europe are less pronounced comparing to B(a)P.

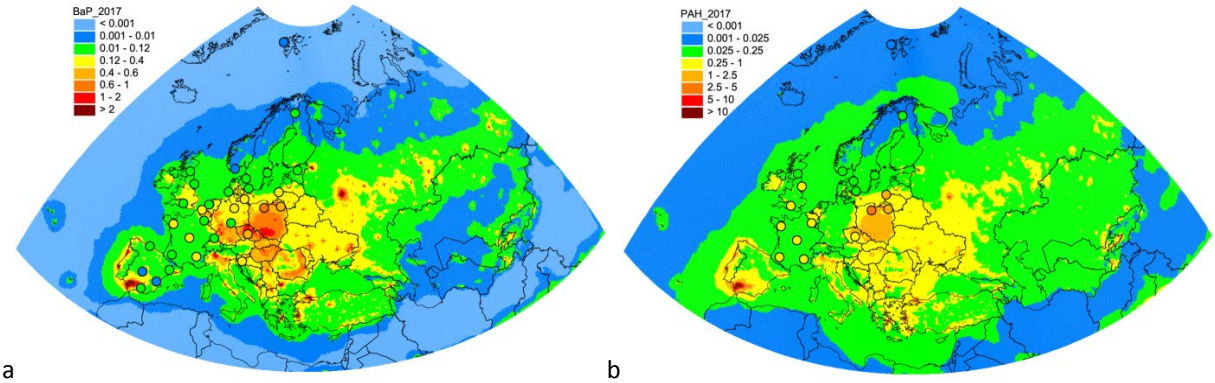

a b

Fig. 3.13. *Spatial distribution of the modelled and observed annual mean air concentrations of B(a)P (a) and of the sum of 4 PAHs (b) in the EMEP domain for 2017, ng/m^3*

Comparison of modelling results with the data of EMEP measurements generally shows reasonable agreement between modelled and observed concentrations. Co-located measurements of 4 PAHs in 2017 were performed at 18 monitoring sites in 8 EMEP countries. The model tends to under-predict annual mean air concentrations of the sum of 4 PAHs with mean relative bias about -17% and spatial correlation about 0.8. For almost 70% of selected monitoring sites the difference between the model estimates and measurements is within a factor of 2. For several monitoring sites, located in France, Finland, and Sweden, the differences between the model predictions and observed concentrations exceeded a factor of 2, with the largest discrepancies (under-prediction) for the monitoring sites in France.

Verification of modelling results for individual PAH compounds against the EMEP measurements indicates the under-prediction of observed B(a)P, B(k)F, and IP air concentrations, and over-prediction of observed B(b)F concentrations. In particular, the largest mean bias is obtained for B(k)F (about -40%), while for the other three PAHs discrepancies are about 20% or lower. Differences in model performance for individual PAH compounds may be explained by several reasons including uncertainties in the emission factors applied in national emission inventories for particular PAHs that might not match the distribution of PAHs in actual emissions, as well as the uncertainties in physical-chemical properties used in the model parameterization for these compounds. The model captures the spatial distribution of observed air concentrations of B(b)F, B(k)F, and IP with correlation coefficient about 0.7 - 0.8. At the same time spatial correlation between the model predictions and measurements for B(a)P is slightly lower (0.6).

Model predictions of PAH pollution in the EMEP countries for 2017 were also analyzed using the measurements of AIRBASE on the example of B(a)P. Observed annual mean air concentrations of about 210 background rural and suburban monitoring sites, performed in 27 European countries, were selected for the comparison. Amount of B(a)P measurements in the AIRBASE allows examining the level of agreement between modelled and observed air concentrations for the particular countries. Modelling results tend to under-predict annual mean observed B(a)P air concentrations by 39% for the rural and suburban monitoring sites. The most significant under-prediction is found for the monitoring sites in Poland, Slovakia, Austria, and France. At the same time, the model tends to over-predict B(a)P concentrations observed in Belgium, the Netherlands, and Sweden. The modelling

results reproduce the spatial distribution of observed B(a)P concentrations with correlation coefficient 0.5. In particular, the modelled concentrations reasonably well correlate with the observed pollution levels in Poland, Belgium, the Czech Republic, and Germany (with correlation coefficients about 0.5-0.8). At the same time, poor spatial correlation is found for Italy, Spain, France, the United Kingdom, and Austria. Different performance of the model with respect to bias and spatial correlation with observed concentrations for particular EMEP countries is most likely caused by several reasons including the uncertainties in the reported anthropogenic PAH emissions and their spatial distribution as well as possible uncertainties in model parameterizations used in the model simulations for PAHs. More detailed evaluation of modelling results against the monitoring data of EMEP and AIRBASE is given in Supplementary Data Report [*Gusev et al*., 2019].

Inter-annual variations of PAH pollution levels in the EMEP region between 2016 and 2017 are shown in Fig. 3.14 on the example of B(a)P annual mean air concentrations. The figure demonstrates the influence of inter-annual variability of meteorological conditions on the pollution levels, since modelling for these two years was carried out using the same set of emission data for 2016. The difference between B(a)P concentrations in 2017 and 2016 is shown in the figure both in relative and absolute values. As seen from Fig. 3.14a variability of B(a)P pollution between these two years is not significant. The largest changes in absolute values of concentrations are indicated for the central part of Europe which corresponds to relative differences of about ±25%. Comparing to the year 2016, increase of air concentrations in 2017 is estimated for the countries of Central and Eastern Europe, as well as for Russia and countries of Central Asia. At the same time decreasing concentrations are obtained for Western Europe.

The Fig. 3.14b demonstrates relative changes of B(a)P concentrations between the years 2016 and 2017. The most significant changes (about 50% or higher) are seen in the Northern Atlantic, Northern Africa, and Southeast Asia. These differences can be explained by inter-annual variability of background conditions obtained using global model simulations. However, the effect of these changes is likely not significant due to the low values of B(a)P concentrations in these areas.

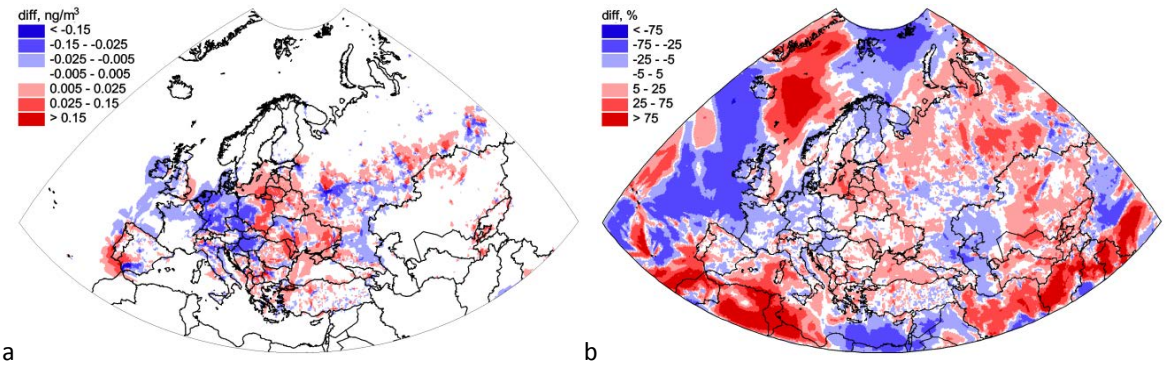

Fig. 3.14. *Absolute (a) and relative (b) changes of B(a)P air concentration between 2016 and 2017 due to inter-annual variation of meteorological conditions*

Relative differences of averaged annual mean B(a)P air concentrations in the EMEP countries between 2016 and 2017 are shown in Fig. 3.15. For more than a half of the EMEP countries the levels of B(a)P air pollution increased from 2016 to 2017. However, it can be seen that changes of concentrations do not exceed 20%. The largest increase of B(a)P air concentrations (about 10-20%) is obtained for Central Asian countries (Tajikistan, Uzbekistan, Kyrgyzstan, and Turkmenistan) as well as some European countries (Malta, Liechtenstein, Latvia, and Moldova). The most significant decrease of the concentrations (10-15%) is estimated for Ireland, the Netherlands, Luxembourg, and Slovenia.

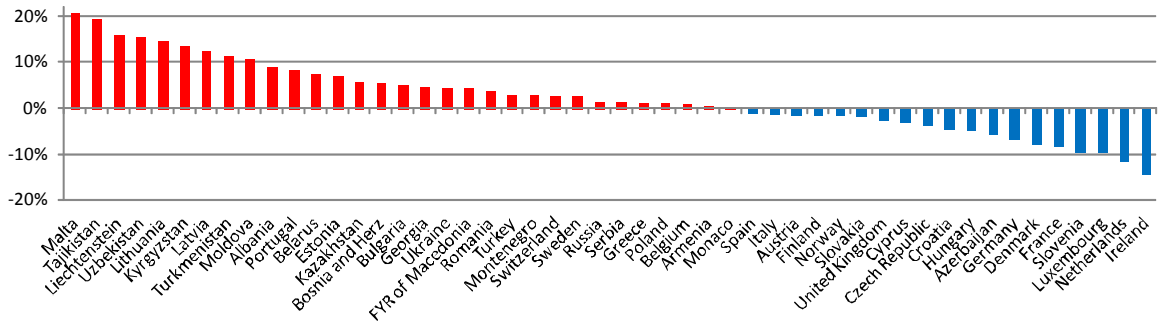

Fig. 3.15. *Relative difference between annual mean average B(a)P air concentrations in the EMEP countries simulated for 2017 and 2016, $(C_{2017}-C_{2016})/C_{2016}$ (in %)*

Long-range transport and annual total deposition of 4 PAHs within the EMEP region is evaluated for 2017 for each of the selected 4 PAHs. Source apportionment of PAH pollution is estimated taking into account contributions of anthropogenic emission sources of EMEP countries as well as contributions of emission sources located outside the model domain. Influence of non-EMEP emissions is taken into account through the application of global scale modelling on the basis of inventory of global PAH emissions developed by the research group of Peking University [*Shen et al.,* 2013].

Assessment of PAH distribution in the EMEP domain indicates importance of the long-range transport of pollution between the EMEP countries. Atmospheric transport of PAHs from the emissions of a particular country contributes to deposition over the country itself and deposition to the territories of other countries. The fraction of PAHs, emitted in the particular EMEP country and deposited to other EMEP countries is higher than the fraction, deposited to the country itself for 22 EMEP countries (43% of the countries). According to model estimates the largest contributions to the transboundary transport and deposition of PAHs in the EMEP region are made by the following countries with relatively high emissions, namely, Ukraine, Poland, the Russian Federation, Czech Republic, Romania, and Turkey.

Source apportionment of PAH deposition permits to compare estimates of the contribution of emission sources, located beyond their territories (contribution of transboundary transport), with contributions of their own national emissions to the pollution levels. In particular, for about a half of the EMEP countries the contribution of transboundary transport exceeded that of their national emissions. Model predictions of transboundary transport of pollution within the EMEP region provide also estimates of the influence of non-EMEP emission sources on the pollution in the EMEP countries.

The contribution of non-EMEP emission sources is accounted for about 1 - 10% with highest (30%) contribution for Iceland. Detailed information on source apportionment of PAH deposition for particular EMEP countries is available in the Supplementary Data Report [*Gusev et al.*, 2019].

3.2.5. HCB, PCDD/Fs and PCBs

HCB, PCDD/Fs and PCBs are unintentional by-products released into the environment during various anthropogenic activities. Along with anthropogenic emissions, additional contribution to the levels of pollution by these POPs can be made by the secondary emission sources, formed due to their long-term accumulation in and direct emissions to terrestrial and aquatic compartments. HCB, PCDD/Fs and PCBs are characterized by significant persistence in the environmental media (e.g. soil, water bodies) thus their presence in the environment long after the release pose risks to the ecosystems and human health.

To characterize the spatial variability of HCB, PCDD/F, and PCB pollution levels within the EMEP domain, analysis of model simulation results and measurement data of national monitoring networks is carried out. Spatial distributions of annual mean modelled air concentrations of HCB, PCDD/F, and PCB-153 in 2017 are presented in Fig. 3.16. Elevated levels of PCDD/F annual mean air concentrations (15-50 fg TEQ/m^3 and higher) are simulated for countries of Central Europe (Poland, Slovakia, and Hungary) as well as for Romania, Northern Italy, Russia, and Turkey.

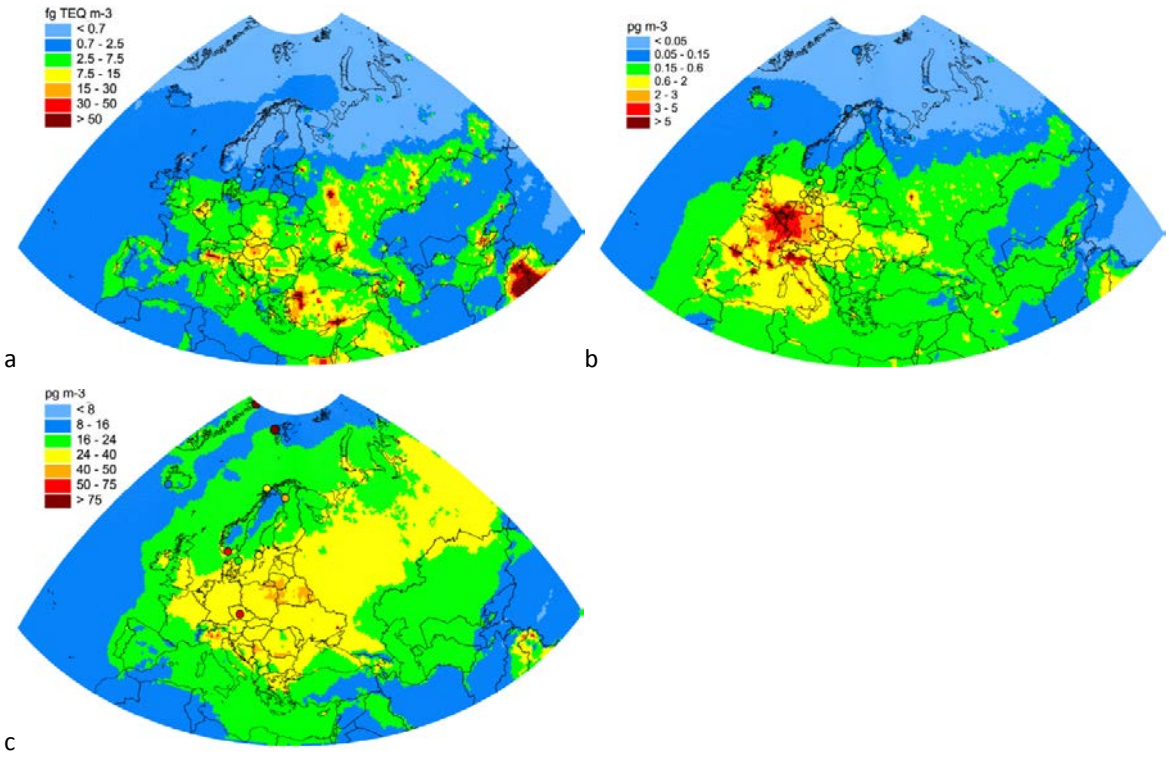

Fig. 3.16. *Spatial distribution of modelled and observed annual mean air concentrations of PCDD/Fs (a), PCB-153 (b), and HCB (c) in the EMEP domain for 2017*

For PCB-153 elevated annual mean air concentrations (0.6-5 pg/m^3 and higher) are indicated mostly for the countries of Western and partly Southern Europe (e.g. Germany, France, Belgium, Italy). At the same time Central and Northern Europe as well as the EECCA countries are characterized by lower levels of concentrations. Model estimates of HCB annual mean air concentrations are generally higher for the countries of Central, Southern, and Eastern Europe (about 25-50 pg/m^3). Other areas of the EMEP domain are characterized by low levels of HCB air concentrations. Contrary to PCDD/Fs and PCB-153 levels of HCB air pollution are relatively more homogeneous indicating its higher persistence in the atmosphere. Spatial distributions of annual deposition fluxes of HCB, PCDD/Fs, and PCB-153 are similar to that of air concentrations (see Supplementary Data Report [*Gusev et al*., 2019]).

In general, modelling results on PCB-153 for 2017 are consistent with measured pollution levels in the countries of Northern and Central Europe. Model estimates reasonably capture spatial gradients of PCB-153 concentrations observed at 11 EMEP monitoring sites in Czech Republic, Germany, Finland, Iceland, Norway, and Sweden with correlation coefficient about 0.8. For more than a half of monitoring sites the difference between measured and modelled concentrations is about or below a factor of 2. The most significant deviations, about a factor of 3-4, are found for three monitoring sites, namely, IS0091, NO0042, and NO0090.

The spatial pattern of observed HCB concentrations at 9 EMEP monitoring sites in Czech Republic, Denmark, Iceland, and Norway is characterized by noticeable variability of pollution levels with relatively high concentrations in the Arctic and in Central Europe (about 60-80 pg m^{-3}) which are not well captured by the model. There is a general tendency of under-prediction of observed HCB concentrations in modelling results with mean bias about -50%. Similar deviations of model predictions from measured HCB air concentrations were also mentioned in the previous Status Report [*Gusev et al*., 2018].

The under-prediction of observed HCB concentrations by the model and poor spatial correlation may indicate the influence of uncertainties in the officially reported emission data, in particular, inconsistencies in the methodologies and emission factors applied in the national inventories reported by the EMEP countries discussed in [*Gusev et al.,* 2018]. Besides, it can be attributed to possible underestimation of HCB long-range transport from the regions outside the EMEP domain in global model simulations due to underestimated emissions. Finally, the differences between the modelled and measured concentrations can be influenced by the uncertainties of the model parameterizations for HCB degradation and air-surface exchange. These uncertainties can lead to underestimation of its accumulation in the surface compartments and magnitude of secondary emission fluxes. To improve results of model assessment of HCB pollution specific research activities are planned that include refinement of GLEMOS model parameterizations related to soil compartment, scenario modelling of HCB accumulation in media and secondary emissions, and evaluation of modelling results using measurement data of HCB passive sampling campaign (see Section 4.3.2).

Monitoring of PCDD/F air concentrations in 2017 was carried out at two EMEP sites SE0012 and SE0014 for several months, namely, March, June, September and December. Seasonal variations of

measured and calculated air concentrations in general correspond to each other at both sites. At the same time, model predictions for 2017 are generally higher than measured PCDD/F air concentrations about a factor of 2-3. Analysis of measurement data shows that observed PCDD/F pollution levels in 2017 are noticeably lower comparing to the measurements for 2016. The difference in measured concentrations for 2016 and 2017 can be explained, in particular, by changes in emissions of PCDD/Fs in the considered years. However, this decrease of concentrations is not reflected by the model which can be attributed to the use of emission data for 2016 in model simulations for 2017. Thus further analysis of PCDD/F pollution levels is required using updated modelling results calculated with the emission data for 2017.

Similar to other pollutants considered above, year-to-year variations of HCB, PCDD/Fs, and PCB-153 between 2016 and 2017 were not significant. Difference between the annual mean concentrations for 2016 and 2017 is shown in Fig. 3.17 on the example of PCB-153. Model simulations for the two years were carried out using the same set of emission data for 2016. Thus, the figure demonstrates the effect of inter-annual variability of meteorological characteristics on calculated levels of concentrations. The most significant changes in absolute values of concentrations are seen for the countries of Western and Central Europe which are accounted for about ±25% or lower. In particular, increased air concentrations in 2017 are estimated for some areas in the countries of Central and Eastern Europe, as well as for Russia and countries of Central Asia. At the same time model estimates showed decreased concentrations in some areas of Western and Southern Europe as well as in the European part of Russia.

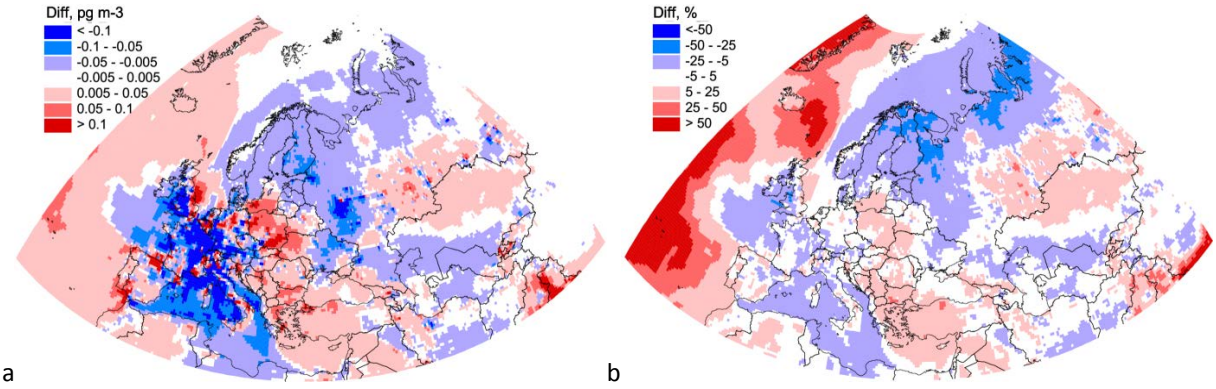

Fig. 3.17. *Spatial distribution of the difference between annual mean air concentrations of PCB-153 simulated for 2017 and 2016 in absolute values, C_{2017}-C_{2016} (a) and in relative values (C_{2017}-C_{2016})/C_{2016} in % (b)*

Relative differences between PCB-153 air concentrations in 2017 and 2016 are shown in Fig. 3.17b. The most significant relative increase of concentrations (about 50% or higher) is seen along the western boundary of the domain due to changes of background conditions. At the same time, decrease of concentrations (about 25-50%) is estimated for the Scandinavian countries and the northern part of Russia which can be explained by inter-annual variability of meteorological conditions.

Source apportionment of PCDD/F, PCB-153, and HCB pollution in the EMEP countries is made accounting for contributions of primary anthropogenic, secondary, and non-EMEP emissions. The

largest contribution of contemporary EMEP anthropogenic emissions is estimated for PCDD/Fs (39%), followed by PCB-153 (26%), and HCB (1%) (Fig. 3.18). Secondary emission sources of PCDD/Fs, PCB-153, and HCB contributed to deposition in the EMEP countries about 50% - 70%. The contribution of non-EMEP emission sources is about 8% for PCDD/Fs, 6% for PCB-153, and about 30% for HCB.

It is seen that for PCDD/Fs and PCB-153 distribution between the three considered source categories is quite similar. In case of HCB contributions of anthropogenic EMEP emission sources in 2017 is significantly lower (about 2%) whereas contributions of secondary sources (formed by anthropogenic emissions of previous years) and non-EMEP emission sources are close to 70% and 30%, respectively. Low contribution of HCB, emitted from EMEP anthropogenic sources in 2017, can be conditioned by possible underestimation of HCB emissions officially reported by countries.

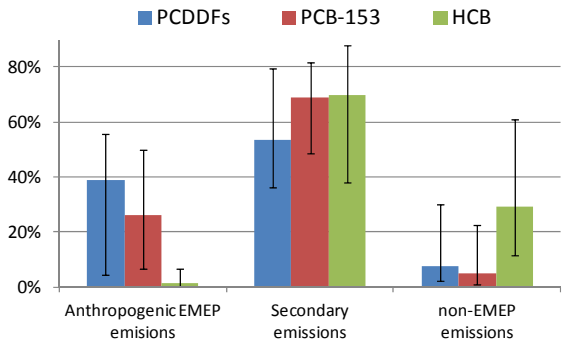

Fig. 3.18. *Contributions of three source groups (anthropogenic EMEP, non-EMEP and secondary emission sources) to deposition over the EMEP countries in 2017 for PCDD/Fs, PCB-153, and HCB. Whiskers denote the range of contributions across the EMEP countries*

Model evaluation of HCB, PCDD/F, and PCB-153 distribution in the EMEP domain indicates that long-range transport between the EMEP countries is an important source of pollution. POP emissions from the national sources of a given country undergo atmospheric transport and deposition as to the territory of a country itself and partly to the territories of other countries. The largest fraction of emissions contributed to deposition due to transboundary transport is estimated for HCB. For 26 countries of 51 (51% of the countries) the fraction of HCB, deposited to other EMEP countries is higher than the fraction, deposited to the country itself. For PCDD/Fs and PCB-153 similar estimates are lower accounting for 16 (31%) and 15 (29%) countries, respectively. Contributions of transboundary transport to the pollution levels in the EMEP countries can be compared with the contributions of their own national emission sources. Deposition due to transboundary transport is higher than the deposition from their national emissions in 38 of 51 countries for HCB, in 32 countries for PCB-153, and in 22 countries for PCDD/Fs. More detailed information on transboundary pollution for each EMEP country is available in Supplementary Data Report [*Gusev et al*., 2019].

3.2.6. Country-specific information

Dissemination of the assessment results and other relevant information aimed at support of political decisions is of high importance. Annual reports containing current status of heavy metals and POPs pollution within the EMEP region are supplemented by presentation of information on the web. It provides more flexible and targeted assistance to national experts and authorities with data required for the environment protection regulations.

Detailed information on heavy metals and POPs pollution is given for each individual EMEP country. This country-specific information includes variety of data on the model assessment for particular country collected in one place to make easier access to information and its analysis by national experts. Information is presented in the form of diagrams, maps and data files for all the EMEP countries at the MSC-E website (http://en.msceast.org/index.php/pollution-assessment/emep-countries-menu). In addition, the country-specific information for the EECCA countries is also available in Russian language (http://www.ru.msceast.org/index.php/pollution-assessment/eecca-countries-menu).

Country-specific information includes the following elements:

- Spatial distribution of pollution levels and their long-term changes;
- Transboundary pollution of a country;
- Contribution of national sources to transboundary transport;
- Pollutant (POPs) concentrations in other media (soil and vegetation)
- Ecosystem-specific deposition (17 land cover categories).

Detailed information on transboundary pollution of individual countries includes maps of total deposition flux to a country's territory (Fig. 3.19a) and relative contributions of foreign sources to anthropogenic deposition (Fig. 3.19b). Besides, source apportionment of anthropogenic deposition to the country's territory is presented (Fig. 3.19c). Each country contributes to atmospheric pollution of other EMEP countries. Spatial distribution of deposition caused by country's sources is available for the entire EMEP region. Besides, country's total deposition to main receptor regions and its fraction of deposition within the EMEP region are indicated (Fig. 3.19d).

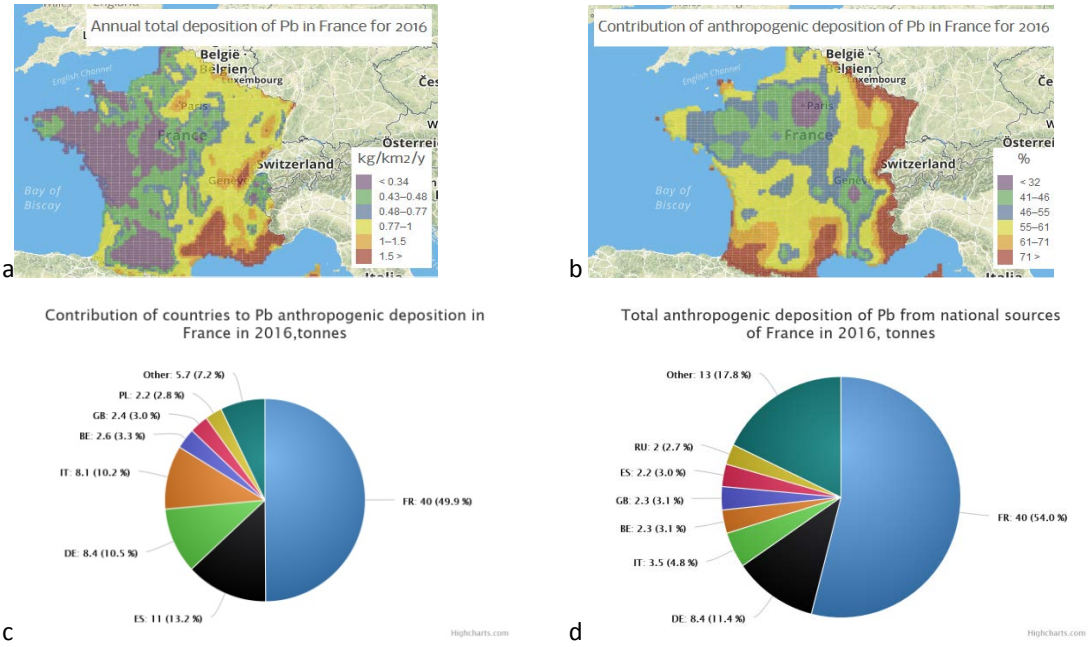

Fig. 3.19. *Characteristics of transboundary transport of Pb to France: (a) –deposition map, (b) – relative contributions of foreign sources; (c) – main contributors to anthropogenic deposition in the country; (d) main receptors of deposition from the country.*

Detailed information on source-receptor relationships between all EMEP countries is also available in the database at the website along with other data on HM and POP pollution of the EMEP domain (http://en.msceast.org/index.php/pollution-assessment/emep-domain-menu/data-hm-pop-menu).

3.3. Additional information products

Model assessment provides valuable information on air concentration and deposition fluxes of heavy metals and POPs as well as the source-receptor relationships within the scope of the EMEP domain to facilitate the policy making process within the LRTAP Convention (Section 1.4). Variety of additional information can be produced to support heavy metal and POP pollution assessment both within the Convention and in other international bodies. It includes evaluation of ecosystem-specific deposition, atmospheric loads to major regional watersheds, marginal seas and remote regions (the Arctic), estimates of air quality standards exceedances, and pollution assessment on a global scale.

3.3.1. Ecosystem-specific deposition

Evaluation of adverse effects of heavy metal and POP pollution on human health and ecosystems is among the priority tasks within the LRTAP Convention. To support the effects assessment MSC-E performs regular estimates of ecosystem-specific deposition of heavy metals to various types of land cover (forests, shrubs, grasslands, crops, water bodies, etc.) within the EMEP region. This information is used by the effects community (Working Group on Effects) for evaluation of critical load exceedances [*de Vries et al*., *2015a,b*]. Information on deposition of Pb, Cd and Hg to 17 types of ecosystems in the EMEP countries is available at the MSC-E website [*www.msceast.org*] (see also Section 1.4.6 and Supplementary Data Report [*Ilyin et al*., 2019]). Similar information on deposition of POPs will be available later.

Deposition fluxes vary significantly for different land cover types. For example, the highest fluxes of Hg are calculated for forested areas, varying from 17 g/km^2/y for deciduous broadleaf forests to almost 20 g/km^2/y for evergreen needleleaf forests (Fig. 3.20). The lowest deposition is estimated for water surfaces (8.4 g/km^2/y). Deposition flux to bare lands and areas with low vegetation is around 10-12 g/km^2/y, and deposition to urban areas is about 13 g/km^2/y. However, the maximum values of deposition relate to urban areas. It means that in some counties Hg deposition to urban land cover exceeds deposition to forests due to proximity of emission sources.

Spatial distribution of Cd deposition fluxes to croplands and forests (averaged over five forest types) in 2017 is shown in Fig. 3.21. Cadmium deposition flux to cropland surfaces varies from around 5 g/km^2/y in Scandinavia to about 50-100 g/km^2/y in the central part of Europe. However, it should be noted that atmospheric deposition is not the only source of cadmium in soils. Application of Cd-containing fertilizers could contribute similar or even higher mass of Cd to agricultural soils in Europe [*Six and Smolders,* 2014]. Deposition flux to forests is on average higher by a factor of 2 than deposition to croplands (Fig. 3.21b).

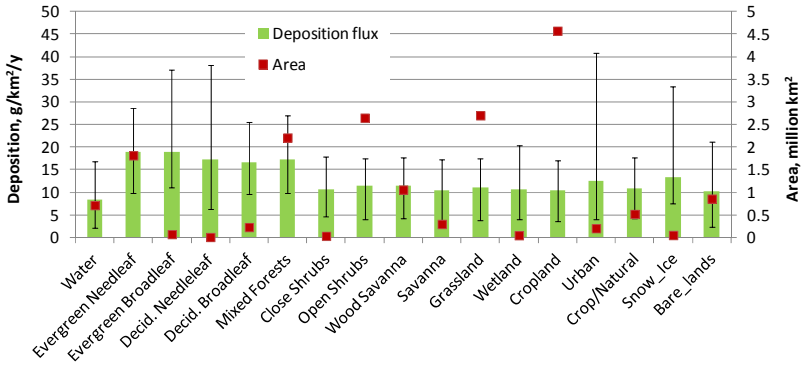

Fig. 3.20. *Deposition of Hg to various ecosystem types within the EMEP domain in 2017. Bars show average value for all EMEP countries; whiskers present range deposition flux variation among the EMEP countries*

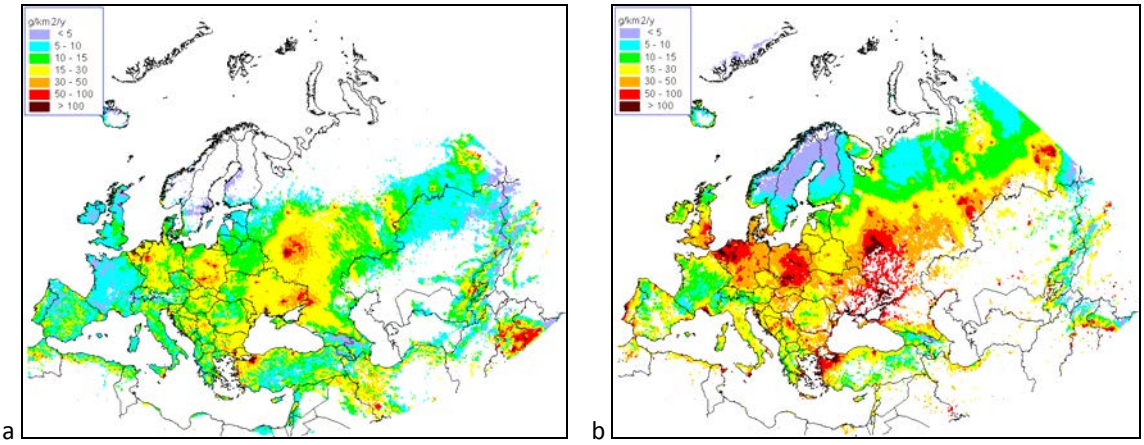

Fig. 3.21. *Annual deposition flux of Cd to croplands (a) and forests (b) in 2017*

It should be noted that the adverse effects assessment requires updated estimates of critical loads for heavy metals (and POPs). The most recent estimates available within the Convention relate to 2010 and cannot reflect the current pollution state [*de Wit et al*, 2015]. ***Therefore, more efforts of the effect community on evaluation of critical loads for heavy metals and POPs are needed.***

3.3.2. Heavy metal and POP deposition to watersheds

Aquatic ecosystems are among the most vulnerable receptors of heavy metals and POP pollution, which undergo long-term accumulation and bio-magnification of the contaminants. In many cases, direct atmospheric deposition to the water surface cannot completely characterize contamination of the water body due to additional input of the pollution with ground and surface water run-off from the adjacent territory. Therefore, evaluation of deposition to the entire watershed can provide more relevant information for assessment of the full pollution budget of the aquatic ecosystem.

Figure 3.22 shows spatial distribution of Hg deposition fluxes in the EMEP region and average Hg deposition in major regional watersheds. As seen the most loaded are watersheds of Central and Southern Europe as well as Turkey with the largest atmospheric deposition (above 20 g/km^2/y) to the

Vistula river watershed. Smaller amount of Hg deposits to rivers and lakes of Scandinavia, South-western Europe, and Eastern Russia. The lowest Hg deposition (below 4 g/km^2/y) fluxes are to watersheds of Central Asia and Northern Africa.

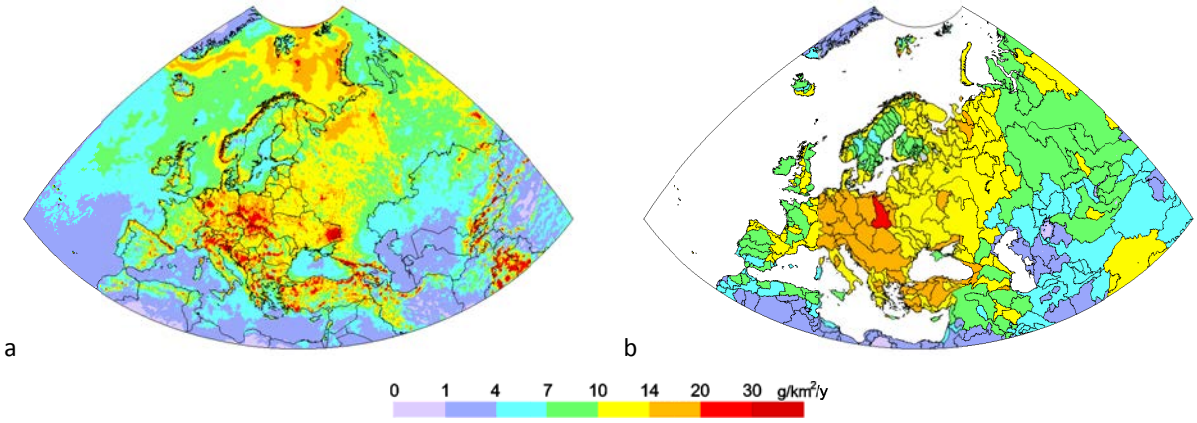

Fig. 3.22. *Spatial distribution of Hg deposition (a) and average Hg deposition over watersheds (b) in the EMEP region in 2017*

An example of detailed assessment is presented in Fig. 3.23 for the watershed of the Glåma river (Norway). Mercury deposition levels vary within the watershed territory from 2 g/km^2/y in the northern part to 12 g/km^2/y in the area close to the Oslo city (Fig. 3.23a). Besides, deposition also differs between the land-cover types. In total the major receptor of Hg deposition within the watershed is coniferous forest (45%) that is followed by shrubs (27%), grassland and wooden grassland (9% and 8%, respectively), and mixed forest (4%) (Fig. 3.23b). These ecosystems can differently contribute to Hg input with run-off to the river pollution and further export to the North Sea.

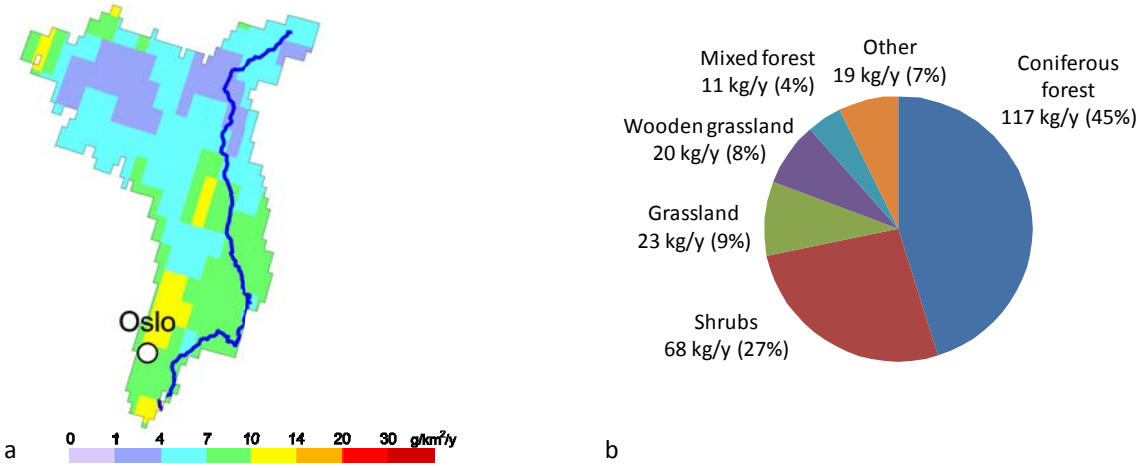

Fig. 3.23. *Spatial distribution of Hg deposition (a) and total Hg deposition to various ecosystems of the watershed of the Glåma river (Norway) in 2017*

Comparison of average heavy metal and POP deposition to watersheds of major rivers in Europe and Central Asia is shown in Fig. 3.24. The largest atmospheric load of Hg and B(a)P is to watersheds of

the Vistula and Oder rivers in Central Europe. In contrast, the watersheds of the Ugra and Oka rivers located in Russia are the most significantly affected by Cd deposition. Rivers whose watersheds also receive large deposition include Haliacmon, Adige, and Nestos for Hg; Vistula, Simav, and Meuse for Cd; Narew, Elbe, and Bug for B(a)P. In general, difference between the average values of Hg deposition to various watersheds is smaller than those of Cd and B(a)P due to considerable contribution of global sources to Hg pollution, which levels the deposition pattern in the region. Similar information is available for watershed-specific deposition of other heavy metals and POPs as well.

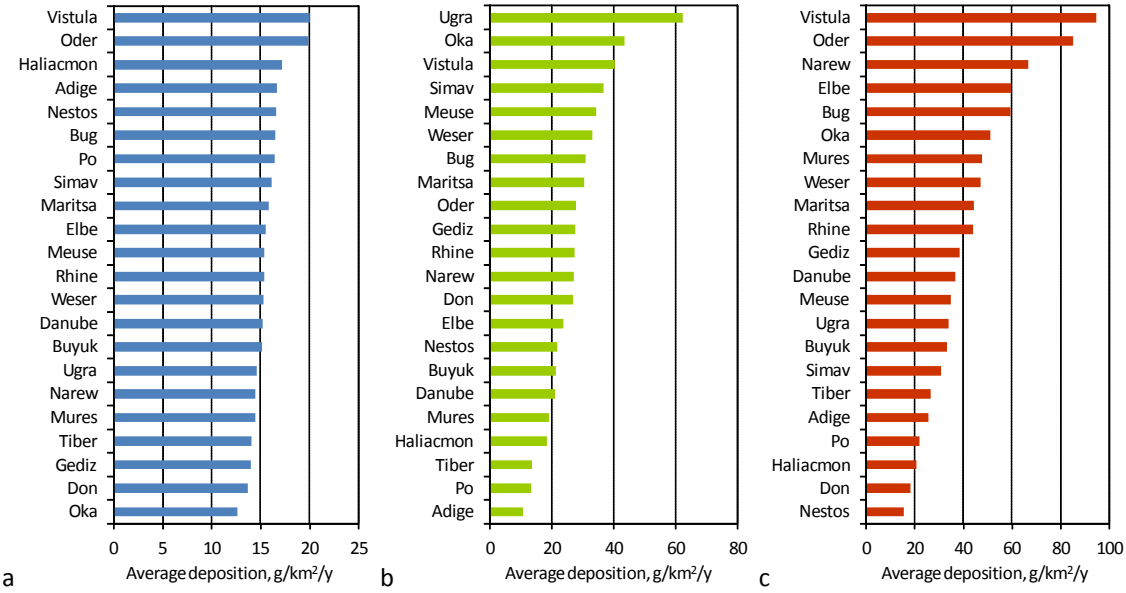

Fig. 3.24. *Average deposition flux of Hg (a), Cd (b) and B(a)P (c) to watersheds of rivers in Europe and Central Asia with significant atmospheric load of heavy metals in 2017*

3.3.3. Air pollution by PAHs: exceedances of air quality standards

Polycyclic Aromatic Hydrocarbons (PAHs) represent a group of semi-volatile organic compounds that are released into the environment mainly due to incomplete combustion processes of organic materials (e.g. biomass combustion, vehicular emissions). Some of the PAHs (e.g. Benzo(a)pyrene, B(a)P) are characterized by toxic properties and are considered as carcinogens, mutagens, and teratogens [*Theakston*, 2000]. In particular, B(a)P has been included in the list of carcinogens of category 1 by the International Agency for Research on Cancer (IARC) and has been classified as CMR substance (carcinogen, mutagen and reproductive toxicant) of category 1B[10] as well as aquatic toxicant of category 1. Taking into account possible risks for human health, the target value for B(a)P

[10] *Regulation (EC) No 1272/2008 of the European Parliament and of the Council of 16 December 2008 on the Classification, Labelling and Packaging of substances and mixtures, amending and repealing Directives 67/548/EEC and 1999/45/EC, and amending Regulation (EC) No 1907/2006.*

annual mean air concentrations equal to 1 ng/m^3 was set up by the European Union Ambient Air Quality Directive [*EU*, 2004]. Similar target level for B(a)P was also introduced as an air quality standard in a number of other countries of the EMEP domain (e.g. in the EECCA countries). Besides, the reference level of 0.12 ng/m^3 for B(a)P was defined by World Health Organization (WHO) as a level of air concentrations corresponding to the excess lifetime cancer risk level of 10^{-5} [*Theakston*, 2000].

Air pollution by toxic PAHs is recognized as a serious problem in areas of some of the EMEP countries [*EEA*, 2018]. Results of the model simulations for 2017 indicate high levels of annual mean B(a)P air concentrations, exceeding the EU target value (1 ng/m^3), in Turkey, Italy, Poland, Germany, Spain, the Czech Republic, Portugal, Greece, Hungary, Serbia, and Bulgaria (see Fig. 3.13a). Areas of high concentrations (above the EU target value) are also noted for some of the EECCA countries including Ukraine, the Russian Federation, Kyrgyzstan, Belarus, Georgia, and Armenia. However, these estimates are subject of higher uncertainties due to incompleteness of emission data for this part of EMEP region (see Chapter 1).

According to the modelling results, about 12% of total population of the EMEP countries in 2017 lived in areas with exceeded EU target level for annual mean B(a)P air concentrations (Fig. 3.25a). It can be seen that most of these exceedances took place for the population of urban areas.

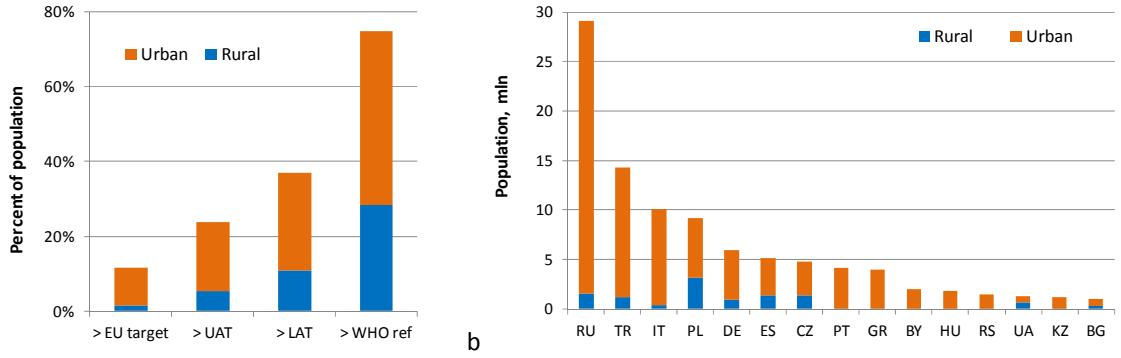

Fig. 3.25. *Percentage of urban and rural population of the EMEP countries in the areas with annual mean B(a)P air concentrations in 2017 above the EU limit values (EU target value for B(a)P – 1.0 ng/m^3, UAT – 0.6 ng/m^3, LAT – 0.4 ng/m^3), and WHO reference level 0.12 ng/m^3 (a) and population of selected EMEP countries in the areas with annual mean B(a)P air concentrations above the EU target value 1.0 ng/m^3 (b)*

The upper assessment thresholds (UAT) and lower assessment thresholds (LAT)[11] values were exceeded in the areas with 24% and 36% of population, respectively. In case of the WHO reference level for B(a)P, equal to 0.12 ng/m^3, only about 25% of population in the EMEP countries were in the conditions of the annual mean air concentrations below the reference level. Modelling results can be used to characterize exceedances of B(a)P limits in individual countries. Figure 3.25b shows estimates of population amount of selected EMEP countries living in areas with annual mean air concentrations

[11] *Directive 2004/107/EC of the European Parliament and of the Council of 15 December 2004*

above the EU B(a)P target level. The most significant part of population that can be exposed to elevated B(a)P air concentrations is estimated for Russia, Turkey, Italy, and Poland.

Evaluation of population exposure to elevated B(a)P air concentrations can be extended by the analysis of the effect of joint toxicity of PM chemical composition and evaluation of cumulative human health risk [*Liu et al.*, 2019; *Delgado-Saborit et al.*, 2011]. Along with B(a)P, atmospheric aerosol particles can be enriched by mixture of various toxic compounds including other POPs (e.g. other PAHs, PCDD/Fs, HCB) and heavy metals. In particular, toxicity of PAHs can be related to that of B(a)P using the WHO toxicity equivalency factors (TEFs) for individual PAHs [*ALS*, 2013]. These TEFs can be applied to characterize the carcinogenic potency of each considered PAH and calculate B(a)P equivalent concentration of total PAH mixture. Figure 3.26 shows spatial distribution of B(a)P equivalent concentrations of 4 PAHs (B(a)P, B(b)F, B(k)F, and IP), which represent the sum of concentrations of individual PAHs multiplied by corresponding values of TEFs. This information characterizes carcinogenic potency of the PAH mixture and can be further used in the risk assessment.

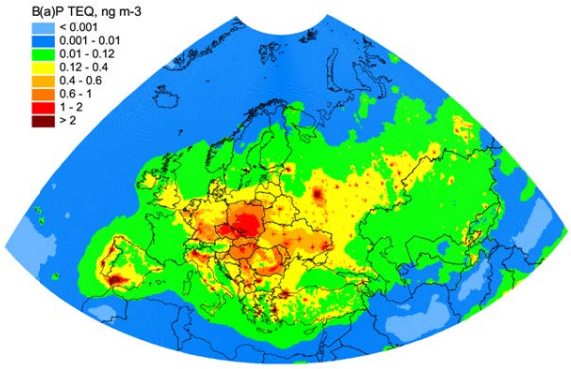

Fig. 3.26. *Spatial distribution of B(a)P equivalent concentrations of 4 PAHs (ng/m^3) in the EMEP domain based on the modelling results for 2017*

The information on exceedances of the EU and WHO air quality guidelines for B(a)P as well as data on B(a)P equivalent air concentrations of PAHs are expected to support activities of the Task Force on Health and Working Group on Effects with regard to the analysis of population exposure to toxic substances and their impacts on human health and ecosystems.

3.3.4. Atmospheric loads to the marginal seas

Protection of marine environment is an actual task targeted by a number of regional Conventions (HELCOM, OSPAR, Barcelona Convention, Bucharest Convention, and Tehran Convention). The marginal seas (Baltic, North, Mediterranean, Black, and Caspian) are the receptors of heavy metal and POP transboundary pollution. Information on heavy metal and POP deposition and source apportionment in 2017 was prepared. Some examples of the results are presented in this section. More detailed information is available in Supplementary Data Reports [*Ilyin et al*., 2019].

Mean deposition fluxes of heavy metals and POPs to water areas of the marginal seas within the EMEP region vary markedly depending on spatial distribution of emission sources and meteorological conditions. For example, mean deposition flux of B(a)P ranges from 0.7 g/km^2/y to the Caspian Sea to 9.7 g/km^2/y to the Baltic Sea (Fig. 3.27a). Most significant B(a)P emission sources are located next to the coast of the Baltic (Poland, Germany) and, hence, make significant contribution to B(a)P deposition over the sea. The Caspian Sea is surrounded by regions with relatively low B(a)P emissions (Section 1.2, Fig. 1.10d). Besides, this region is characterized by dry climatic conditions with relatively

low annual precipitation. Due to the same reason mercury deposition flux to the Caspian Sea is also the lowest (2.5 g/km^2/y) compared to the fluxes to other seas (Fig. 3.27b). The highest Hg deposition flux is noted for the North Sea (8.1 g/km^2/y).

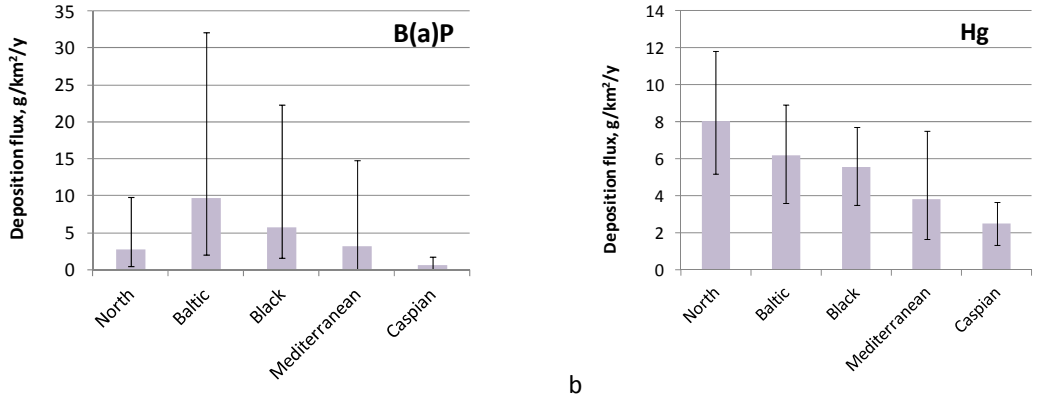

a b

Fig. 3.27. *Average deposition flux of B(a)P (a) and Hg (b) to marginal seas of the EMEP region in 2017*

Source apportionment of heavy metal and POP deposition differs for both different pollutants and seas. Contribution of the EMEP anthropogenic sources to total deposition of Cd varies from 15% over the Caspian Sea to 67% over the Baltic Sea (Fig. 3.28a). Contribution of Cd secondary sources is the largest over the Caspian (70%) and smallest over the Black and Baltic Seas (30%). Non-EMEP sources significantly affect Cd deposition over the Mediterranean Sea (35%). In contrast, anthropogenic deposition of PCDD/Fs is the largest over the Caspian and Black Seas (50%) and the smallest over the North Sea (30%). The North Sea is considerably affected by PCDD/Fs deposition from non-EMEP sources (22%).

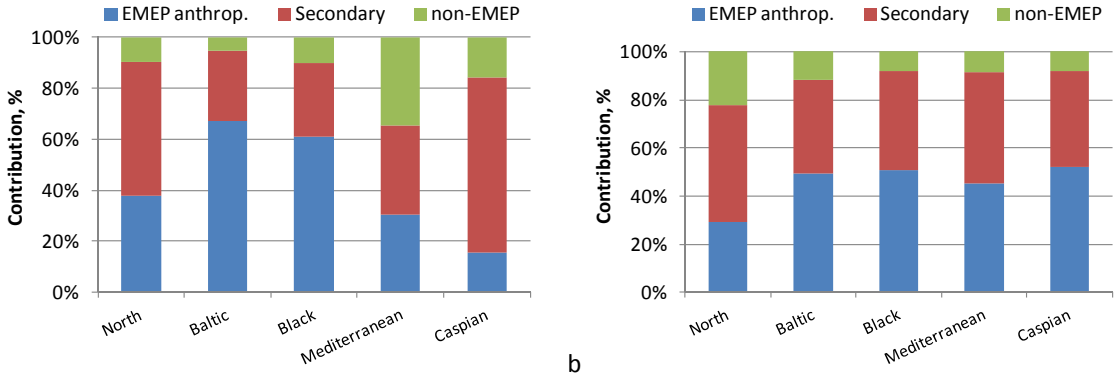

a b

Fig. 3.28. *Relative contribution of various source types to deposition of Cd (a) and PCDD/Fs (b) to the marginal seas of the EMEP region in 2017*

Atmospheric transport of the considered pollutants from various source types also determines spatial patterns of deposition over the sea reservoirs. For example, prevailing contribution of direct anthropogenic sources results in increasing gradient of B(a)P deposition towards the coast of Denmark, Germany and the Netherlands over the North Sea (Fig. 3.29a). The lowest fluxes take place

far from the coast in the northern part of the sea. In contrast, mercury deposition over the sea is affected by both spatial distribution of anthropogenic emissions and atmospheric oxidation chemistry, which converts long-lived Hg^0 to readily removed oxidized Hg forms. Besides, spatial distribution of atmospheric precipitation also affects Hg deposition. As a result, the highest Hg deposition flux is noted in the western coast of Norway and in the northern part of the North Sea (Fig. 3.29b). The lowest levels take place along the north-eastern coasts of the United Kingdom.

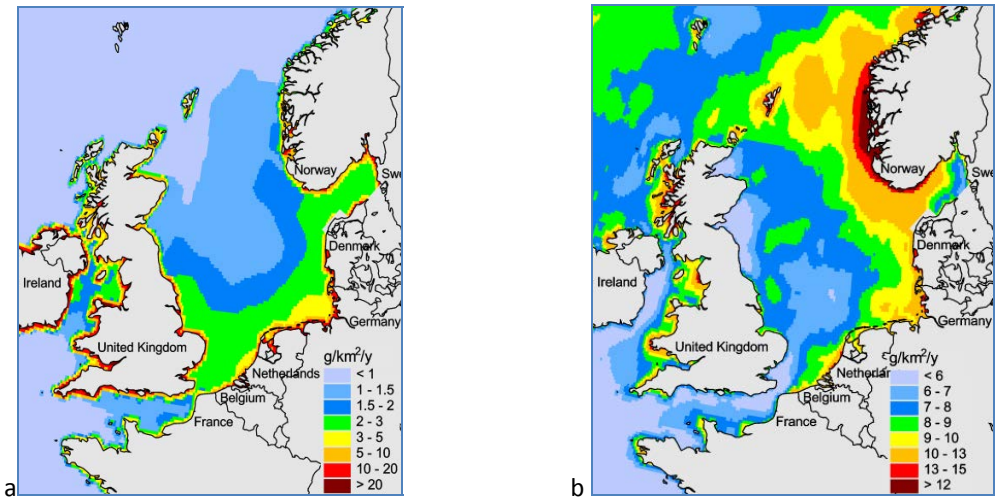

Fig. 3.29. *Total deposition of B(a)P (a) and Hg (b) over the North Sea in 2017*

3.3.5. Pollution of the Arctic

Following the agreement between the Convention and AMAP reached at the joint meeting held in Potsdam, Germany in 2016, MSC-E continued cooperation with AMAP in the field of analysis and assessment of heavy metal pollution in the Arctic region. Atmospheric deposition of heavy metals (Pb, Cd, Hg) and POPs (PAHs, PCDD/Fs, HCB, PCBs) were calculated to the Arctic within the scope of the EMEP domain. Besides, source-receptor relationships of the pollution in the Arctic were established for each of the considered pollutant.

The modelling results show that deposition fluxes of heavy metals and POPs to the Arctic are relatively low in comparison with the fluxes to other parts of the EMEP domain. It is explained by the remoteness of the Arctic from main emission sources. Besides, most part of the Arctic is characterized by relatively low annual precipitation sums compared to temperate regions of Europe.

For example, deposition fluxes of Pb in 2017 vary from about 50 g/km^2/y in Greenland, Spitsbergen and Franz-Josef Land to about 300 g/km^2/y in some coastal regions of Norway and Iceland (Fig. 3.30). Relatively high deposition fluxes in Norway and Iceland are caused by high precipitation amounts (Fig. 3.3) combined with significant contribution of secondary sources, namely re-suspension of Pb with marine aerosol from the sea surface. Similar spatial distribution is predicted for Cd. In contrast, relatively high Hg deposition takes place over wide areas of the Northern Atlantic and the Arctic Ocean because of atmospheric mercury depletion evens (AMDEs). However, it should be also taken

into account that major part of Hg deposited due to AMDE to ice or snow, is reduced and reemitted back to the atmosphere.

Spatial distribution of B(a)P deposition differs from that of heavy metals. First of all, a number of hot spots of B(a)P deposition takes place in the Russian part of the Arctic. These hot spots are explained by significant local emission sources in the Arctic. The second difference is that the increment of deposition fluxes along the coasts of Norway and Iceland is not as large as that of heavy metals due to less effective scavenging by precipitation. Besides, secondary emissions of B(a)P from the sea surface is less significant.

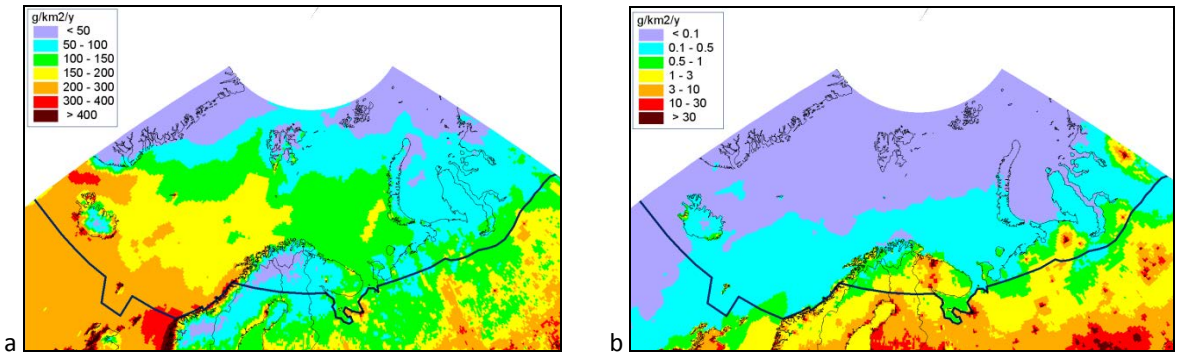

Fig. 3.30. *Total deposition fluxes of Pb (a) and B(a)P (b) to the Arctic (within the EMEP domain) in 2017. Dark line denotes the border of the Arctic region adopted by AMAP*

Deposition of heavy metals and POPs to the Arctic is caused by three groups of sources. The first group includes anthropogenic emissions of the EMEP countries. The second group covers secondary (historical) and natural sources. It means re-suspension of dust particles containing the pollutants (Pb, Cd) or re-volatilisation of substances (Hg, POPs) previously deposited from anthropogenic sources and accumulated in environmental media (soils, waters etc). Besides, in case of heavy metals, these sources also include natural component. The third group considers sources (anthropogenic and secondary) located outside the EMEP region but affecting the Arctic through intercontinental transport (non-EMEP sources).

Secondary sources (re-suspension from the sea surface) are the largest contributor to deposition of Pb in the Arctic, which input amounts to 54% of total deposition (Fig. 3.31). Main anthropogenic sources of Pb are located in the central, southern and south-eastern parts of Europe, while emissions in the Arctic are commonly low (Section 1.2, Fig. 1.10a). EMEP anthropogenic sources are dominant in pollution of the Arctic by Cd and B(a)P. Their contributions amount to 57% and 74%, respectively. Contributions of anthropogenic and secondary sources are comparable for PCDD/F deposition to the Arctic (31% and 41%, respectively). Contribution of non-EMEP sources is relatively small (from 4% to 20%) for considered pollutants except for Hg and PCDD/Fs. It contributes about 30% of PCDD/F deposition and up to 95% of Hg deposition to the Arctic. However, it should be noted that Hg emitted by the EMEP sources can leave the EMEP region getting involved into global scale transport and then enters the EMEP region as a part of the 'non-EMEP sources'. Therefore, the non-EMEP component of Hg deposition in fact includes considerable part of Hg emitted by EMEP sources.

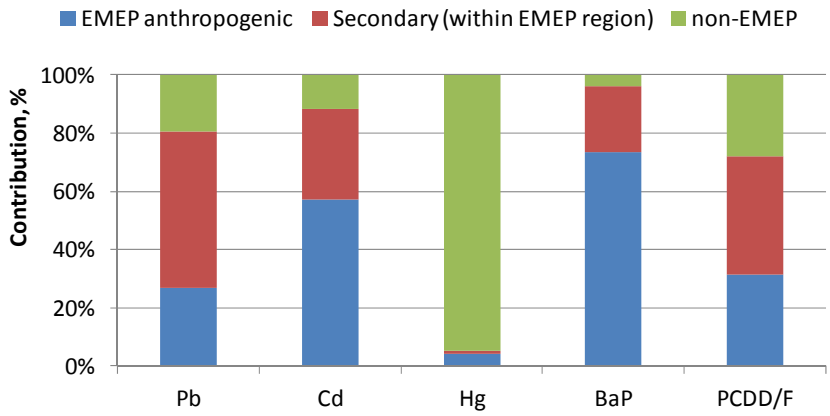

Fig. 3.31. *Relative contributions of the EMEP anthropogenic, secondary and non-EMEP sources to deposition in the Arctic (within EMEP domain) in 2017*

Contribution of particular countries to heavy metal and POP deposition to the Arctic depends on various factors such as proximity of a country to the receptor region, magnitude of national emissions of the country, patterns of atmospheric circulation, peculiarities of physical and chemical properties of the considered pollutants etc. For the considered heavy metals Russia and Kazakhstan are the main source countries of anthropogenic pollution in the Arctic. Contribution of Russian sources to the Arctic deposition ranges from 43% (Pb) to 84% (Cd) (Fig. 3.32). Kazakhstan contributes 3% of Cd, 11% of Hg and 22% of Pb to deposition in the Arctic. Russia is also the largest contributor of POPs to the Arctic atmospheric pollution. It makes around 70% of total B(a)P and PCDD/F deposition to the region. Other significant contributors include Poland and Scandinavian countries for B(a)P; and Turkey and Ukraine for PCDD/Fs.

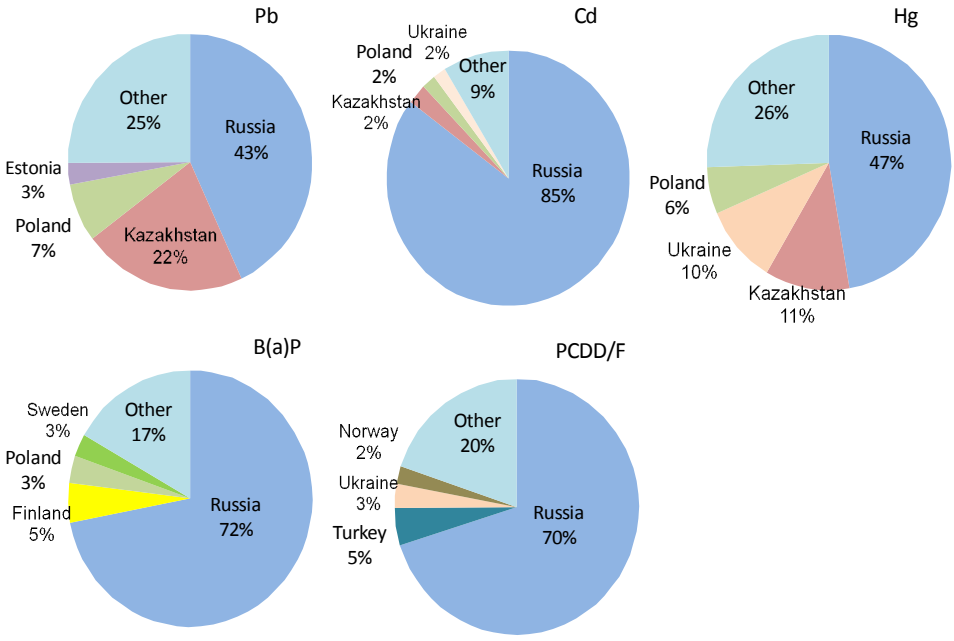

Fig. 3.32. *Source apportionment of heavy metal and POP anthropogenic deposition to the Arctic (within the EMEP domain) in 2017*

3.3.6. Global scale pollution by heavy metals and POPs

Heavy metals and POPs can be transported in the atmosphere over hundreds to thousands of kilometres from their emission sources. Therefore, the pollutants emitted in the other regions can reach the EMEP countries. It is particular relevant for Hg and some POPs (HCB, PCDD/Fs), which are characterized by long residence time in the atmosphere. To take into account the effect of inter-regional and intercontinental transport on pollution of the EMEP countries the regional model assessment was supported by global scale simulations using the GLEMOS multi-scale modelling system.

Simulated global distributions of Pb, Cd and Hg concentration in air are shown in Fig. 3.33. Concentrations of Pb and Cd are the highest in Southeast Asia (above 30 ng/m^3 for Pb and 1 ng/m^3 for Cd), mainly because of large emissions in China (Fig. 3.33a and 3.33b). Besides, elevated levels are predicted for arid areas of the south-western part of Asia, Middle East and Northern Africa. It is explained by significant dust suspension in these regions and, hence, large contribution of secondary emissions to atmospheric concentrations. The lowest levels occur over the Arctic and Antarctica.

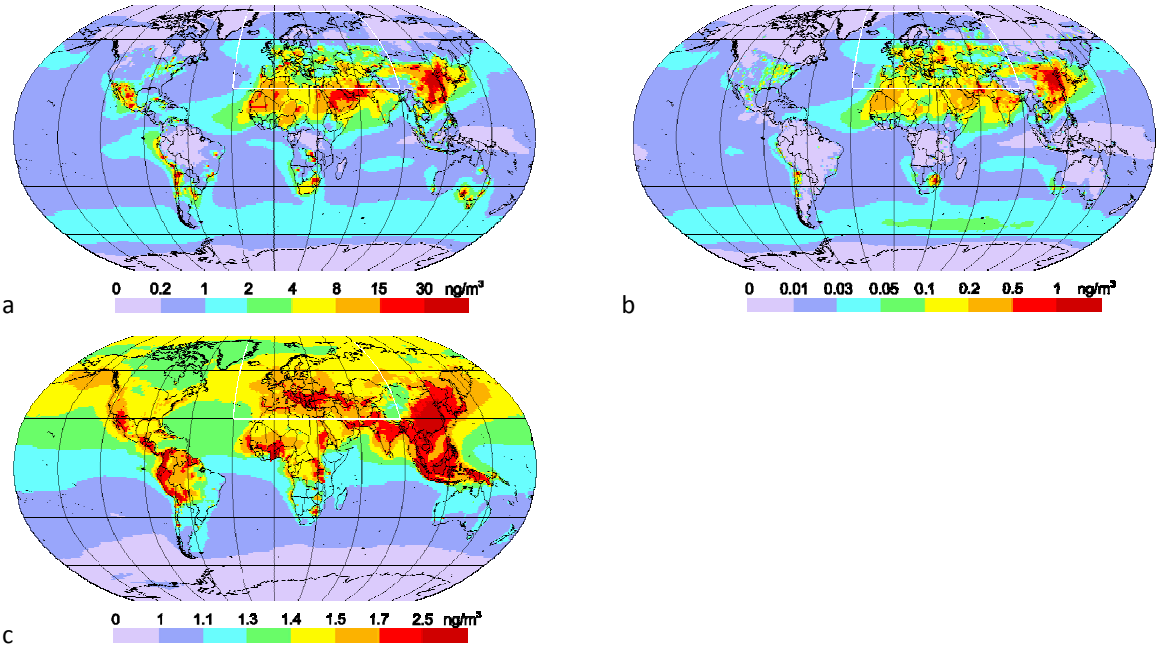

Fig. 3.33. *Global distribution of annual mean air concentration of Pb (a), Cd (b) and Hg (c) in 2017. White line depicts boundary of the EMEP region*

Mercury concentration in air is distributed relatively homogeneously over the globe with higher concentrations (1.3-2.5 ng/m^3) in the Northern Hemisphere and lower concentrations (0.8-1.3 ng/m^3) in the Southern Hemisphere (Fig. 3.33c). East and South Asia are characterized by highest Hg concentrations due to large anthropogenic emissions from power generation and industrial processes (above 2 ng/m^3). High concentration levels are also obtained for equatorial Africa, South America and Southeast Asia as a result of emissions from artisanal and small-scale gold mining in these regions. In addition, elevated Hg concentrations are found over Southern Europe and the western coast of North America caused by natural emissions from Hg-enriched soils. The lowest concentrations are simulated over the Southern Ocean and the Antarctica.

Spatial distributions of global-scale annual mean air concentrations of B(a)P, PCDD/Fs, PCB-153, and HCB simulated for 2017 are shown in Fig. 3.34. The highest levels of B(a)P concentrations, exceeding 1 ng/m^3, were estimated for the countries of East and South Asia (Fig. 3.34a). Relatively high concentrations (0.4-1 ng/m^3) were also obtained for the countries of Central and Eastern Europe. Other areas were characterized by relatively low pollution levels (below 0.4 ng/m^3).

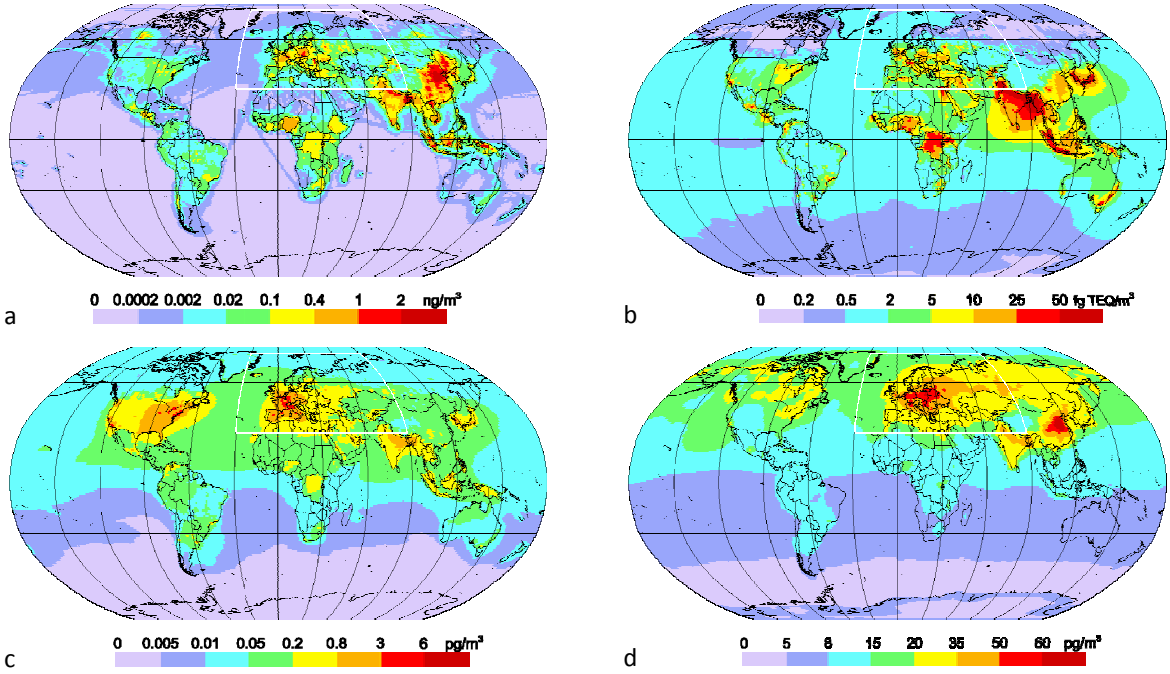

Fig. 3.34. *Global distribution of annual mean air concentration of B(a)P, ng/m^3 (a), PCDD/Fs, fg TEQ/m^3 (b), PCB-153, pg/m^3 (c), and HCB, pg/m^3 (d) in 2017. White line depicts boundary of the EMEP region*

The highest levels of PCDD/F are estimated for some of the regions in Southeast Asia (more than 50 fg TEQ/m^3) and Africa (25-50 fg TEQ/m^3) (Fig. 3.34b). Pollution levels in Europe, North and South America, and Australia are lower (5-25 fg TEQ/m^3). For PCB-153 elevated air concentrations are obtained for the European region and North America (0.8-6 pg/m^3) (Fig. 3.34c). For other regions less significant air concentrations are estimated (below 0.8 pg/m^3). Elevated HCB air concentrations are predicted for East and South Asia (24-80 pg/m^3), and for the European countries (about 24-60 pg/m^3) (Fig. 3.34d).

It should be pointed out that model estimates of heavy metal and POP levels on a global scale as well as evaluation of boundary conditions for the EMEP regional modelling strongly depend on availability of global-scale emissions inventories. However, no present-day gridded emissions data is currently available for Pb, Cd, HCB and PCDD/Fs. Assumptions and expert estimates used to construct appropriate emission fields (Section 1.2.2) lead to additional uncertainties of the modelling results both on a global scale and for the EMEP countries. ***Thus, improvement of the global scale assessment requires closer co-operation of the LRTAP Convention with other international bodies (UN Environment, Stockholm Convention, Minamata Convention) in order to facilitate development of global emissions inventories for heavy metals and POPs.***

4. RESEARCH ACTIVITIES

Research activities of MSC-E were carried out in accordance with the priorities of the long-term strategy for the Convention and were aimed at improvement of the pollution assessment quality and further development of the modelling tools. The main directions of the research included country-scale pollution assessments for B(a)P (France) and heavy metals (Germany), analysis of key emission sources and trends of B(a)P pollution, evaluation of a new mechanism of Hg photo-reduction in the atmosphere, and further development of the multi-media approach for POPs and Hg.

4.1. Country-scale pollution assessment

A series of country-scale studies of heavy metal and POP pollution in selected EMEP countries has been performed by MSC-E in close co-operation with national experts [*Travnikov et al*., 2018]. This activity is aimed at the analysis of uncertainties in the information on pollution levels and further improvement of modelling approach for the assessment of pollution in the EMEP region. This year the study for B(a)P has been continued both on regional and national scales analyzing major processes responsible for cycling of the pollutant in the environment. Besides, a new study has been initiated for Germany that will include detailed assessment of Hg, Pb and Cd pollution in the country during the period 2014-2016.

4.1.1. B(a)P pollution at regional and national scales

The B(a)P case study was initiated in 2017 following the recommendation of the 2nd joint session of the Working Group on Effects and the Steering Body to EMEP. The outcome of previous stages of this study is described in the POP Status Reports [*Gusev et al.*, 2017; 2018]. It comprises evaluation of sensitivity of model predictions to the uncertainties in the reported emission data using scenario modelling. Current stage of the study is focused on the analysis of modelling approach applied for B(a)P and evaluation of alternative approaches to describe most important processes. In particular, different model parameterizations for the evaluation of B(a)P degradation and gas-particle partitioning are tested. Model simulations are performed using the GLEMOS model and the CHIMERE model [*Menut et al.*, 2013]. Analysis of modelling results is carried out in close cooperation with national experts in B(a)P modelling from France and Spain. In this section summary of current progress in the case study activities is presented.

Emission data for modelling

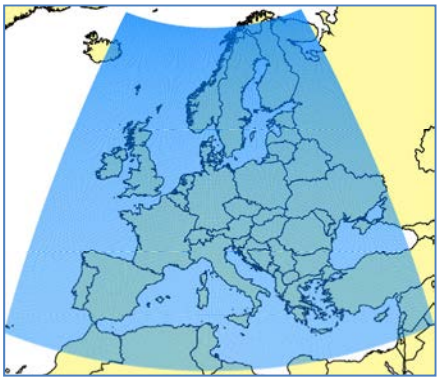

Fig. 4.1. *Spatial configuration of the EU02 modelling domain (0.2°x0.2°)*

Modelling of B(a)P pollution levels is carried out for the domain EU02 with spatial resolution 0.2°x0.2° (Fig. 4.1). Similar to previous stage of the case study the year 2015 is selected as a reference year for model simulations. Gridded emission data for B(a)P modelling were prepared on the basis of national emission inventories of Spain and France, defined on the basis of SNAP sectoral distribution. For other EMEP countries, within the geographical scope the EU02 modelling domain, annual emissions prepared by CEIP with spatial resolution 0.1°x0.1° were applied. To compile consistent emission dataset for modelling, gridded data of CEIP, defined for the NFR sectors, were transformed to the SNAP sectors. Seasonal variations of B(a)P anthropogenic emissions for the GLEMOS model were generated for each emission source sector using monthly temporal factors, based on the TNO estimates of the MACC project [*Denier van der Gon et al*., 2011a]. Temporal disaggregation of emissions in the CHIMERE model was done according to temporal factors of the GENEMIS project [*Ebel et al.*, 1997] defined for individual countries.

Model parameterizations of B(a)P processes

The most important processes, affecting B(a)P pollution levels in the atmosphere, include gas-particle partitioning and degradation due to the influence of atmospheric reactants. Additional effect on B(a)P air concentrations can have dry/wet deposition and air-surface gaseous exchange. The interaction of B(a)P with various components of aerosol particles including organic and inorganic sub-fractions as well as heterogeneous reactions of particle-bound B(a)P with ozone is associated with significant uncertainties due to complexity and incomplete knowledge of these processes. Brief overview of available approaches, developed for the description of gas-particle partitioning and degradation processes in the air quality models, is given below.

Partitioning of B(a)P between the gaseous and particle bound phases in the atmosphere comprises a combination of its absorption by organic matter, aerosol water and adsorption to black carbon and mineral part of the aerosol particles [*Lohmann and Lammel*, 2004; *Keyte et al*., 2013]. The process of partitioning depends on several factors, e.g. meteorological conditions, chemical composition of aerosol particles, and content of atmospheric reactants, as well as their spatial and temporal variations.

A number of approaches to describe partitioning of semi-volatile PAH compounds between the gaseous and particulate phases were developed and used to evaluate their long-range transport and air pollution levels. Earlier approaches include Junge-Pankow scheme based on adsorption of POPs onto the surface of aerosol particles [*Junge*, 1977; *Pankow*, 1987] and organic matter absorption scheme based on octanol-air partitioning coefficient [*Finizio et al.*, 1997; *Harner and Bidleman*, 1998].

Later on more complex approaches were elaborated which took into account chemical composition of aerosol particles and more detailed description of interaction between gaseous and sorbed phases of POPs. In particular, a parameterization based on combination of two processes, absorption by organic matter and adsorption to black carbon, was developed for the evaluation of PAH long-range transport [*Dachs and Eisenreich*, 2000; *Lohmann and Lammel*, 2004].

Another approach is based on the poly-parameter linear free energy relationships (ppLFER) [*Goss and Schwarzenbach*, 2001; *Shahpoury et al.*, 2016]. The ppLFER parameterization assumes adsorption of PAHs onto the surface of aerosol particles and absorption by inorganic and different organic matter sub-fractions of particulate matter. Evaluation of the latter two approaches showed in general better agreement of modelling results with measurements [*Efstathiou et al.*, 2016; *Shahpoury et al.*, 2016].

Degradation of B(a)P in the atmosphere can occur both in gaseous and particulate phase. In gaseous phase it can react with hydroxyl radical (OH), NO_3 and O_3. The latter two reactants are generally less effective comparing to the reactions with OH radical. However, the reactions with NO_3 can significantly contribute to the degradation of B(a)P in the atmosphere during the night-time [*Keyte et al.*, 2013].

Another important pathway of degradation is heterogeneous reactions of B(a)P in particulate phase with ozone. The rate of B(a)P degradation on various components of aerosol particles, namely organic matter, black carbon, aerosol water, and mineral fraction, is different and depends also on the air temperature and humidity. To describe multi-phase B(a)P degradation in the atmosphere a new kinetic multi-layer scheme ROI-T was recently developed and used in regional and global model simulations [*Mu et al.*, 2018]. The new scheme considers decomposition of ozone at aerosol surface to reactive oxygen intermediates (ROIs) and their reactions with B(a)P in surface and bulk layers of particles taking into account the effects of temperature and humidity. Model simulations of B(a)P long-range transport with the ROI-T scheme showed importance of considering B(a)P multi-phase degradation accounting for temperature/humidity variations.

To explore sensitivity of modelling results to changing of the model parameterizations three processes were selected, namely, gas-particle partitioning, degradation, and air-surface exchange. The following model parameterizations were chosen for testing: dual absorption/adsorption scheme for gas-particle partitioning process, and ROI-T multi-phase scheme for degradation process. The ppLFER scheme is planned to be tested on subsequent stage of this work. In addition, the effect of inclusion of air-surface gaseous exchange parameterization on modelling results is considered.

Setup of model simulations

Parameterizations of most of the processes, governing B(a)P transport and fate in the atmosphere, are based on similar approaches in the GLEMOS and CHIMERE models. In particular, dry deposition and removal of B(a)P from the atmosphere with precipitation are described similarly. Both models include description of air-surface gaseous exchange for B(a)P. In case of the CHIMERE model, gaseous exchange with the soil compartment only is considered, while in the GLEMOS model soil, vegetation, seawater, and freshwater compartments are included. Similar parameterizations of B(a)P degradation

in the gas-phase due to reactions with OH radical are used in the models. For B(a)P degradation in particulate phase, parameterization of heterogeneous reactions with O_3 without taking into account dependence on temperature and humidity variations is applied. For the latter degradation pathway different degradation rates of B(a)P, sorbed on the organic matter and black carbon, are used in the GLEMOS model, while the same rate is defined in the CHIMERE for both particulate fractions of B(a)P.

At the same time, different parameterizations of gas-particle partitioning process in the models are applied. In the CHIMERE model the Secondary Organic Aerosol Processor (SOAP) is used to describe formation of organic aerosol particles as well as partitioning of organic compounds between the gas and particle phases [*Couvidat and Sartelet*, 2015]. Description of the gas-particle partitioning in the GLEMOS model is based on combined approach using absorption into organic matter of atmospheric aerosol [*Harner and Bidleman*, 1998] and adsorption to black/elemental carbon according to [*Van Noort*, 2003].

The list of test model simulations performed by the GLEMOS and CHIMERE models is presented in Table 4.1. The reference case simulation assumes the use of native GLEMOS and CHIMERE model configurations without taking into account air-surface gaseous exchange. For each of the selected processes specific model simulation is performed with alternative parameterization. In addition, a model run with combined changes of gas-particle partitioning and degradation schemes as well as air-surface exchange is carried out.

Table 4.1. *Test model simulations to explore sensitivity of the modelling results to the inclusion or changing of the model parameterizations for gas-particle partitioning, degradation, and air-soil exchange of B(a)P*

Test simulation	***Description***
Reference model run	Model run with excluded gaseous exchange with soil
Gas-particle partitioning	Model run with dual OM&BC gas-particle partitioning scheme according to [*Mu et al.*, 2018]
Air-soil exchange	Model run with included gaseous exchange with soil
Degradation	Model run with degradation scheme according to [*Mu et al.*, 2018]: gas-phase degradation (OH, NO_3, O_3), particle phase degradation based on the results of ROI-T multi-phase scheme
All changes	Model run with combined changes of previous test simulations

Preliminary modelling results and their analysis

Preliminary model simulations of B(a)P pollution levels were performed for the EU02 domain. Figure 4.2 presents annual mean B(a)P air concentrations simulated by the GLEMOS and CHIMERE models for 2015. Both models predicted close pattern of B(a)P pollution levels for most of the regions in Europe.

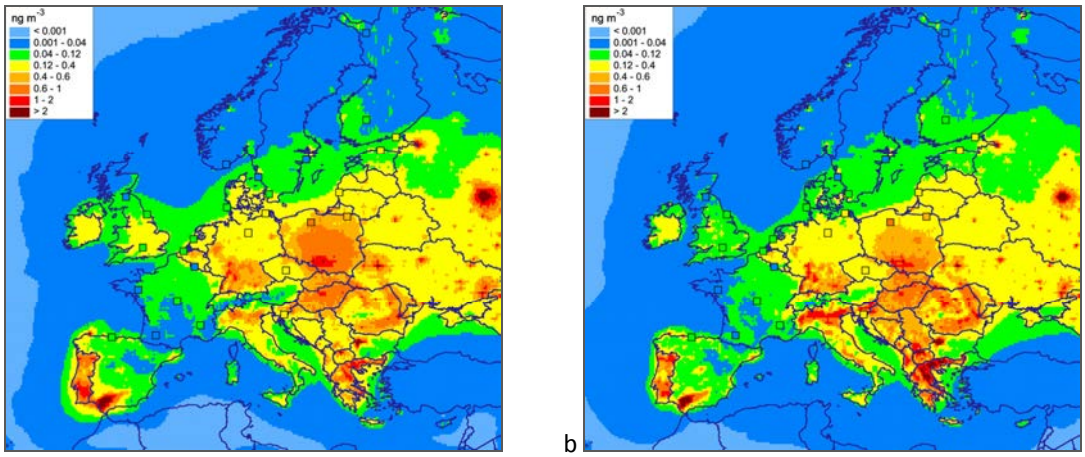

Fig. 4.2. *Annual mean B(a)P air concentrations in 2015 (ng/m^3), simulated by the GLEMOS (a) and CHIMERE (b) models for the* ***reference model run*** *(0.2°x0.2°); and B(a)P concentrations, observed at the EMEP monitoring sites, overlaid as coloured squares in the same scale as modelled values*

Evaluation of the model output against measurements for reference and test model runs was carried out using the data of 27 EMEP monitoring stations for 2015. Summary of statistical analysis of the agreement between the modelled and observed B(a)P air concentrations is presented in Table 4.2. In case of the reference model run both models reasonably reproduced the spatial pattern of observed B(a)P concentrations with correlation coefficients about 0.75-0.80. At the same time, the GLEMOS model tended to slightly over-predict observed B(a)P air concentrations (by 3%), while the CHIMERE model showed under-prediction by -16%. Results of both models were within the agreement of a factor of 2 with regard to measurements for about 60% of monitoring sites. However, for other monitoring sites the discrepancies were higher than a factor of 2, and in case of GLEMOS model higher than a factor of 3 for about 15% of sites.

Table 4.2. *Summary of statistical metrics, calculated on the basis of annual mean B(a)P air concentrations observed at EMEP monitoring stations (n=27) and estimated by GLEMOS and CHIMERE in the reference model run and test model runs for 2015*

Test simulations	***Model***	***Mean modelled (ng/m^3)***	***NMB^a (%)***	***R^a***	***RMSE^a (ng/m^3)***	***F2^a (%)***	***F3^a (%)***
Reference model run	GLEMOS	0.12	3.0	0.80	0.08	63	85
	CHIMERE	0.10	-16.2	0.75	0.10	59	100
Gas-particle partitioning	GLEMOS	0.14	14.3	0.81	0.09	67	81
	CHIMERE	0.11	-5.4	0.76	0.10	59	100
Air-soil exchange	GLEMOS	0.10	-13.2	0.78	0.07	59	85
	CHIMERE	0.09	-22.9	0.74	0.10	63	93
Degradation scheme	GLEMOS	0.04	-69.8	0.76	0.14	22	41
	CHIMERE	0.05	-55.8	0.70	0.13	48	74
All changes	GLEMOS	0.05	-57.4	0.78	0.13	33	52
	CHIMERE	0.09	-28.8	0.73	0.11	59	96

[a] *NMB is normalized mean bias; R is the spatial correlation between modelled and observed concentrations; RMSE is the root mean square error; F2 and F3 represent fractions of sites for which deviation between modelled and observed values are within a factor of 2 and 3, respectively.*

As seen from the table, inclusion of alternative parameterization of gas-particle partitioning and air-surface exchange do not have significant effect on the modelling results. Both models demonstrated slight improvement of spatial correlation between the model predictions and measurements in simulations with dual OM&BC partitioning scheme, whereas in simulations with air-surface exchange a bit lower spatial correlation was obtained comparing to the reference model run. Changes of other statistical metrics were different for the two models. At the same time, inclusion of alternative degradation scheme led to considerably lower predictions of B(a)P air concentrations and resulted in noticeably lower level of agreement with measurements.

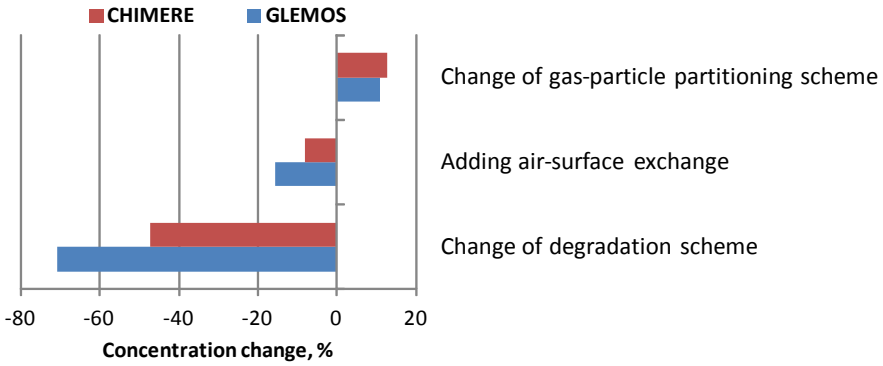

Fig. 4.3. *Relative changes of annual mean B(a)P air concentrations (ng/m^3), simulated by the GLEMOS and CHIMERE models, between the reference model run and test model runs*

Relative changes of modelled B(a)P air concentrations in the test model simulations in comparison with the reference model run are shown in Fig. 4.3. It is seen that GLEMOS and CHIMERE had similar response to changes of the model parameterizations. In particular, the substitution of gas-particle partitioning scheme resulted in average increase of the model predictions (about 10%) due to increased fraction of B(a)P in particulate phase and lower effect of B(a)P degradation in gaseous phase on total air concentrations compared to the reference model run. On the opposite, inclusion of air-surface gaseous exchange led to decrease of air concentrations (about 10-15%) due to transfer of B(a)P to the surface compartment.

The largest changes are seen in the simulations with alternative description of B(a)P degradation based on the results of ROI-T degradation scheme. Model predictions of GLEMOS and CHIMERE in test simulations are lower by 50-70% comparing to the reference case. Significant decrease of B(a)P air concentrations can be explained by more intensive degradation of B(a)P in particulate phase in the ROI-T scheme compared to the parameterizations applied in GLEMOS and CHIMERE.

Results of the test model simulations show critical role of parameterization of B(a)P degradation in the atmosphere for the evaluation of its long-range transport. Thus, further improvement of the model predictions of B(a)P air pollution levels can be associated with the refinement of parameterization of particle-bound B(a)P degradation. Particular attention should also be paid to the implementation of recent developments in the description of gas-particle partitioning process taking into account multi-phase content of aerosol particles in the atmosphere.

4.1.2. Heavy metal pollution in Germany

A new study of heavy metal pollution on a country scale has been started this year for Germany. The main objective of the study is generation of detailed information on levels and spatial distribution of atmospheric deposition of three heavy metals (Pb, Cd, Hg) in the country for the period from 2014 to 2016. Results of the study will be used by the German Environment Agency (UBA) for integrative evaluation of available information about heavy metal pollution of various ecosystems (i.e. comparison with metal concentrations in mosses, needles, leaves) and risk assessment.

The whole program of the study consists of a number of elements, which include preparation and analysis of input information required for the study (anthropogenic and secondary emissions, measurement data, meteorological fields, etc.), model simulations of heavy metal concentrations in air and deposition in the country, evaluation of modelling results against observations and analysis of discrepancies, formulation of recommendations for improvement of the assessment quality both on national and regional scales. This year activities include preparation of national emissions and monitoring data by experts of the country, collection and processing of other input information for modelling by MSC-E, pilot simulations of heavy metal pollution levels in the country, and preliminary evaluation against observations. First results of this work are briefly discussed below.

Information on anthropogenic emissions of Pb, Cd and Hg in 2014, 2015 and 2016 were prepared by the country's experts from UBA with spatial resolution 0.1°x0.1°. These data were generated as a part of the national tool GRETA (Gridding Emission Tool for ArcGIS) [*Schneider et al*., 2016]. The resulting fields of emissions spatial distributions in 2016 are shown in Fig. 4.4. As seen the highest emissions of the considered heavy metals take place in the western part of the country (North Rhine-Westphalia). Elevated emissions are also noted in areas around large cities – e.g., Berlin, Hamburg, Munich. Besides, relatively high emissions caused by large-point sources are scattered across the country. Emissions of other countries falling in the model domain were prepared by MSC-E using the EMEP gridded data produced by CEIP (Section 1.2.2).

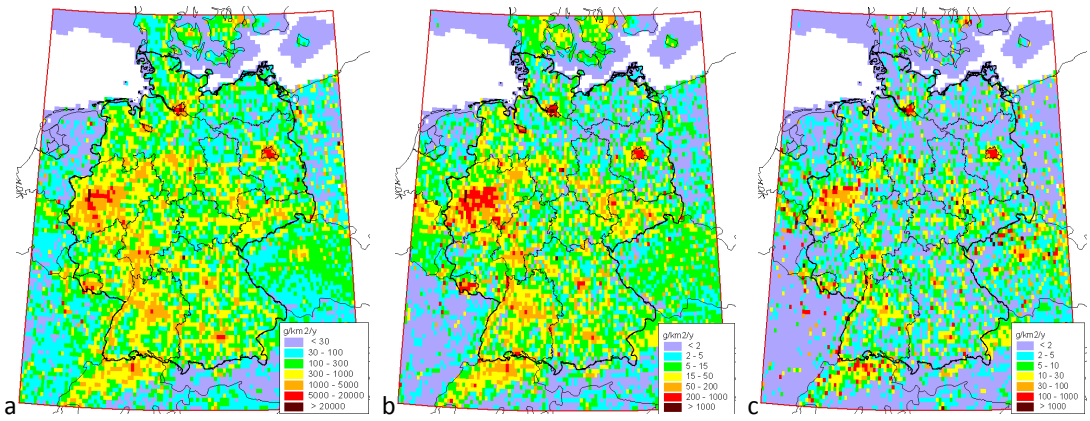

Fig. 4.4. *Spatial distribution of Pb (a), Cd (b) and Hg (c) emissions in 2016, g/km^2/y*

Emission data for Germany are split into several source categories in accordance with the GNFR (Gridded Nomenclature For Reporting) classification adopted in the Convention. The major part of Cd emission in Germany falls on sector *'Industry'*, which contributes about 70% to national total emission (Fig. 4.5). This sector is also an important contributor to emissions of Pb (37%) and Hg (30%). About 60% of Hg national emission comes from the sector '*Public power*'. Sector *'Road Transport'* is responsible for about 40% of Pb emissions.

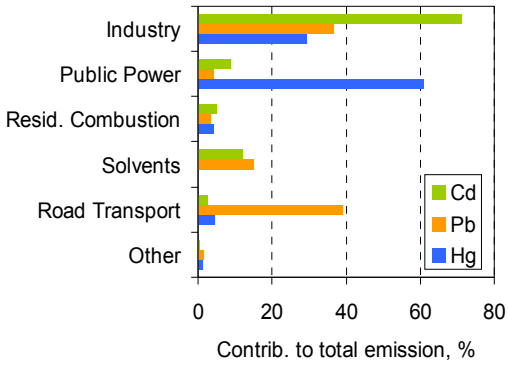

Fig. 4.5. *Contribution of GNFR emission sectors to total emissions of Pb, Cd and Hg in Germany in 2016*

Monitoring data used in the study are based on both the EMEP measurements and observations from the national monitoring network. Air concentrations and wet deposition fluxes of Pb and Cd are measured at 11 EMEP stations located in Germany, whereas Hg levels are observed at six EMEP sites. In addition, considerable amount of observed information comes from the national monitoring network. Measurements of air concentration and wet deposition of Pb and Cd are available at about 120 stations. Besides, information on Hg wet deposition fluxes is reported by 65 national stations.

Measurements of Pb and Cd collected for the study cover most parts of the country providing a good basis for evaluation and analysis of modelling results (Fig. 4.6a). In contrast, observations of Hg are available only at a few background EMEP sites and at other national sites located in the northern part of the country (Lower Saxony and Schleswig-Holstein) (Fig. 4.6b). This limited coverage restricts the evaluation capabilities for spatial patterns of Hg pollution in the country. However, some other types of measurements (e.g. in mosses) can be used for this purpose in future.

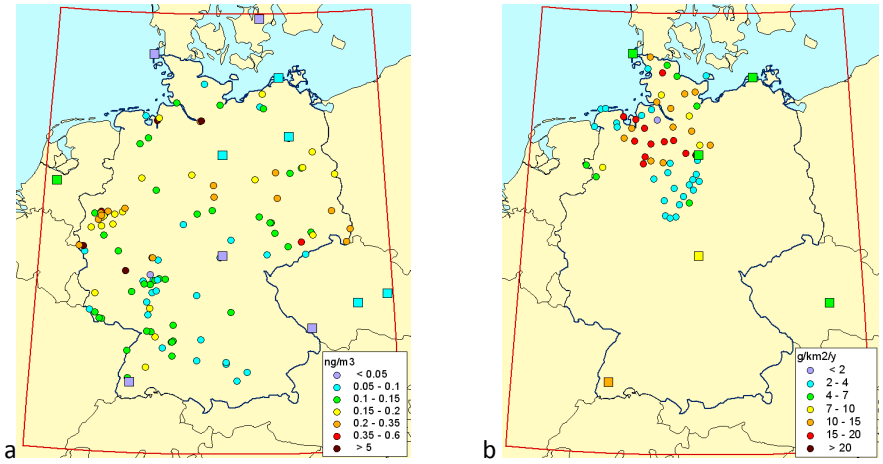

Fig. 4.6. *Observed concentrations of Cd in air (a), ng/m^3 and Hg wet deposition fluxes (b), g/km^2/y in 2016. Squares denote the EMEP stations, circles show stations from the national monitoring network*

The set of national monitoring data includes observations from sites of different types. The classification according to the site location distinguishes urban, suburban and rural stations. Besides, predominant influence of particular emission sources defines splitting into industrial, traffic and background stations. It should be noted that industrial stations are characterized by the highest concentrations of Pb and Cd. For instance, annual mean air concentrations averaged over sites of this type are 0.6 ng/m^3 for Cd and 32 ng/m^3 for Pb. Averaged values for other types are much lower and amount to 5-8 ng/m^3 for Pb and 0.1-0.2 ng/m^3 for Cd.

Special attention was paid by MSC-E to generation of meteorological data for the national-scale modelling domain. Fields of meteorological parameters were generated using the WRF pre-processor [*Skamarock et al.,* 2008] initialized by the operational analyses data from ECMWF [*ECMWF*, 2019]. The Centre made efforts to improve quality of the generated data testing various parameterizations of physical processes of the WRF pre-processor. In particular, a number of numerical tests were performed using different modelling schemes of cumulus convection, cloud microphysics and the air-soil interactions for refinement of simulated summer precipitation. Calculated values of precipitation sums were compared with observations from national network of synoptic stations of German Weather Service (DWD) [*DWD*, 2018]. The usage of updated set of WRF parameterizations favoured improvement of the calculated precipitation sums decreasing the mean relative bias (MRB) changed from 100% to -4% and increasing spatial correlation from 0.43 to 0.61 (Fig. 4.7).

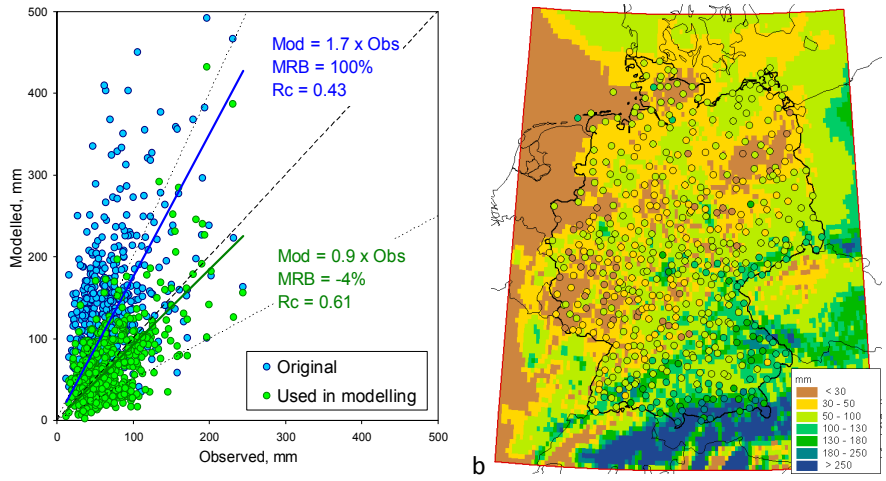

Fig. 4.7. *Comparison of observed and calculated (original and corrected for modelling purposes) precipitation sums in July (a) and spatial distribution of calculated (map) and observed (circles) precipitation sums in July (b)*

Pilot model simulations of Pb, Cd and Hg levels in Germany were carried out for the period 2014-2016. A multi-scale modelling approach was used for the simulations to take into account influence of national, regional and global sources on heavy metal pollution in various locations of the country (Fig. 4.8). This approach allows linking various spatial scales in an optimal manner combining wide coverage with fine resolution of the final domain for the country. An example of simulated spatial pattern of Pb concentration in Germany in 2016 is shown in Fig. 4.8. Elevated Pb concentrations (8-20 ng/m^3) are predicted in the western part of the country (North Rhine-Westphalia) in accordance with spatial distribution of emissions. It should be noted that similar spatial peculiarities were also

revealed for Cd and Hg. Relatively high Pb concentrations (5-8 ng/m^3) were also obtained for the eastern (Saxony, Berlin) and south-western (Baden-Württemberg, Hesse) parts of the country. In other parts of the country Pb levels do not exceed 5 ng/m^3. Generally, the simulated Pb concentrations agree well with available measurements.

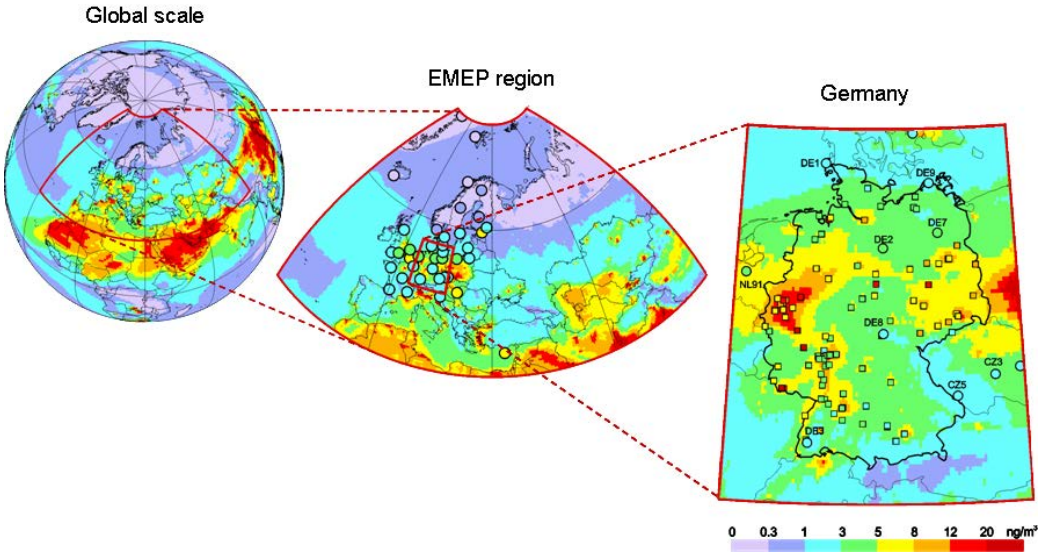

Fig. 4.8. *Modelled concentrations of Pb on a global, regional (EMEP) and country scales in 2016. Circles denote EMEP monitoring stations, and squares show national monitoring stations in Germany*

More detailed evaluation of the modelling results against observations is initiated. Preliminary analysis shows different model performance in different locations of the country. For example, the model well reproduces both magnitude and temporal changes of the observed concentrations over most considered period at a remote EMEP station DE2 (Waldhof) located in the central part of the country (Fig. 4.9a). In contrast, modelled Pb concentrations significantly exceed the observed ones at an urban background station DENW008 (Dortmund-Eving) situated in North Rhine-Westphalia, which is characterized by significant anthropogenic emissions. More thorough comparison of the modelling results with measurements as well as analysis of the discrepancies will be performed at later stages of the study.

a

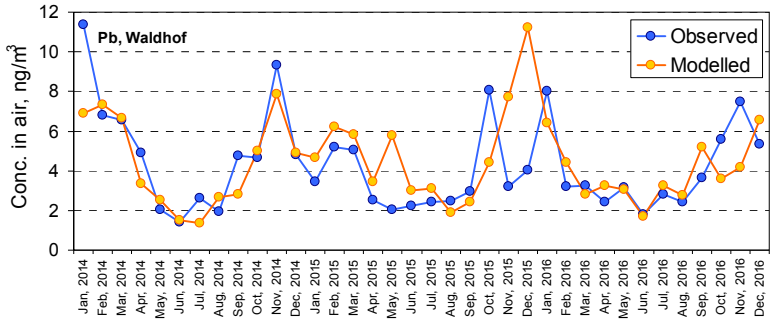

b

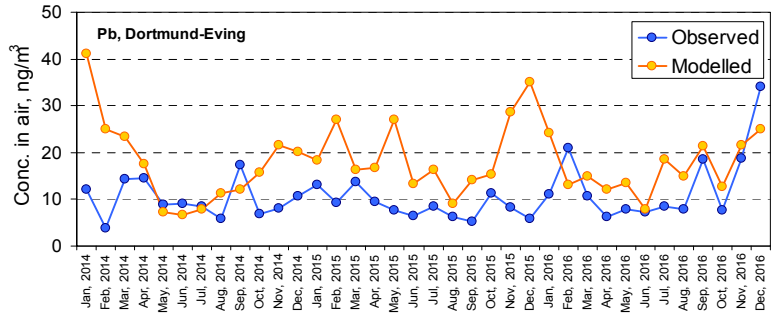

Fig. 4.9. *Monthly mean Pb concentrations in air at remote station Waldhof (a) and urban background station Dortmund-Eving (b) in 2014-2016.*

Further work within the country-scale study for Germany will include finalizing the model assessment of heavy metal pollution levels in the country, joint analysis of assessment results with national experts, evaluation of national emissions based on both modelling and measurement data, and formulation of recommendations for improvement of the assessment quality both on national and regional scales.

4.2. Model evaluation of Hg atmospheric chemistry: Photo-reduction of gaseous oxidized mercury

Mercury atmospheric chemistry is among the key factors, which governs its long-range transport in the atmosphere and deposition to the ground. It causes mutual transformations of long-lived elemental (Hg^0) and short-lived oxidized (Hg^{II}) Hg species and determines the overall Hg residence time in the atmosphere and its potential to long-range transport from emission sources. In spite of significant improvements in understanding of Hg oxidation and reduction mechanisms, current knowledge on Hg atmospheric chemistry remains incomplete [*Subir et al*., 2011; 2012; *Gustin et al*., 2015; *Ariya et al*., 2015].

Gas-phase oxidation of Hg^0 by reactive halogens, in particular, by atomic bromine (Br) is considered as an important or even dominant pathway of Hg oxidation in the atmosphere [*Donohoue et al*., 2006; *Hynes et al*., 2009; *Goodsite et al*., 2012; *Gratz et al*., 2015; *Coburn et al*., 2016]. The two-step Br-initiated mechanism of Hg^0 oxidation with participation of various secondary oxidants (e.g. OH, Br, BrO, NO_2, HO_2) is intensively studied by the scientific community [*Dibble et al.,* 2012; 2013, 2014*; Wang et al*., 2014; *Jiao and Dibble,* 2015; 2017]. The newly found secondary reactions imply

relatively short life-time of Hg^0 with respect to oxidation and low atmospheric concentrations that conflict with available observations [e.g. *Horowitz et al*., 2017]. This phenomenon was investigated in detail in a study reported in HM Status Report 2018 [*Ilyin et al*., 2018]. In particular, it was shown that application of the Br-initiated mechanism for simulations of the Hg atmospheric cycle leads to strong overestimation of Hg oxidation and unrealistically low Hg^0 concentrations in the atmosphere. However, theoretical studies point out a possibility of Hg^{II} reduction mechanisms, which could take place in air, cloud water, or heterogeneously at the surface of atmospheric aerosol [*Ariya et al*., 2015]. A new mechanism of Hg^{II} photo-reduction in gaseous phase was recently suggested by *Saiz-Lopez et al*. [2018]. To investigate possibility and importance of the new mechanism the GLEMOS chemical transport model was applied for test simulations on a global scale. Major results of the model simulations are discussed below. More details of the study are available in [*Saiz-Lopez et al*., 2018].

For the sake of the study the most recent form of the two-step Br oxidation mechanism was implemented in the GLEMOS model [*Ilyin et al*., 2018; *Saiz-Lopez et al.,* 2018]. An experimental version the model considers six Hg chemical species in the atmosphere: Hg^0, unstable intermediate Hg^IBr and four Hg^{II} species ($HgBr_2$, HgBrOH, HgBrOOH, HgBrONO). The Hg^{II} species are simulated in both gaseous and particulate state using the parameterisation of gas-particle partitioning from [*Amos et al.*, 2012]. Details of the chemical mechanism implemented in the model as well as the reaction rate constants are given in Table 4.3. In addition to the oxidation reactions we also included gas-phase photo-reduction of $HgBr_2$, HgBrOH, HgBrOOH, HgBrONO using the photolysis rates calculated by the CAM-Chem model [*Saiz-Lopez et al*., 2018]. Six-hourly concentration fields of Br were archived from a GEOS-Chem simulation [*Parrella et al.,* 2012], whereas OH, HO_2, NO_2 and particulate matter (PM2.5) fields were imported from MOZART [*Emmons et al*., 2010].

Table 4.3. *Experimental chemical mechanism for atmospheric Hg in GLEMOS*

N	Reaction	Rate, molecule cm^{-3} s^{-1}	Reference
R1	$Hg^0 + Br + M \rightarrow Hg^IBr + M$	$1.5 \times 10^{-32} (T/298)^{-1.86}$ $[Hg^0][Br][M]^{(a)}$	*Donohoue et al*. [2006]
R2	$Hg^IBr + M \rightarrow Hg^0 + Br + M$	1.6×10^{-9} exp(-7801/T) [HgBr][M]	*Dibble et al*. [2012]
R3	$Hg^IBr + Br \rightarrow Hg^0 + Br_2$	3.9×10^{-11} [HgBr][Br]	*Balabanov et al*. [2005]
R4	$Hg^IBr + Y \overset{M}{\rightarrow} Hg^{II}BrY$ Y = Br, OH, NC_2, HO_2	Y = Br, OH : $2.5 \times 10^{-10} (T/298)^{-0.57}$ [HgBr][Y] Y = NO_2, HO_2 : k_Y ([M],T)[HgBr][Y]	*Goodsite et al*. [2004] *Jiao and Dibble* [2017]
R5	$Hg^{II}BrY \overset{h\nu}{\rightarrow} Hg^0 + products$ Y = Br, OH, NC_2, HO_2	k_{photo} [HgBrY]	*Saiz-Lopez et al*. [2018]
R6	$Hg^{II}BrY \overset{h\nu}{\rightarrow} Hg^IBr + products$ Y = Br, OH, NC_2, HO_2	k_{photo} [HgBrY]	*Saiz-Lopez et al.* [2018]

[(a)] All concentrations in brackets are in molecule cm^{-3}; [M] is the number density of air

We performed a number of test model runs for the period 2007-2013 using anthropogenic emissions for 2010 [*AMAP/UNEP*, 2013]. The first 6 years of the period were used for the model spin up to achieve the steady-state Hg concentrations in the troposphere. The model results are presented as

annual averages for 2013. The list of the test model simulations is given in Table 4.4. Run #1 corresponds to model simulation with the Br oxidation chemistry and no Hg^{II} reduction. This simulation scenario has been already studied in detail and described in [*Ilyin et al*., 2018]. Since products of Hg^{II} photo-dissociation are unknown we considered two different chemical scenarios of the photolysis reaction. The first scenario (Run #2) includes photo-reduction of Hg^{II} species directly to Hg^0, whereas the second scenario (Run #3) considers monohalide HgBr as the main product of the reaction (see *Saiz-Lopez et al*. [2018] for the chemical explanation). Results of the model simulations were evaluated against a collection of ground-based measurements from at various regional and global monitoring networks described in [*Travnikov et al*., 2017].

Table 4.4. *Model test runs for different atmospheric Hg^{II} reduction scenarios in the GLEMOS model*

Run ID	Scenario
Run #1	No Hg^{II} reduction (reactions R1-4)
Run #2	Gas phase Hg^{II} photo-reduction to Hg^0 (reactions R1-4, R5)
Run #3	Gas phase Hg^{II} photo-reduction to $Hg^{I}Br$ (reactions R1-4, R6)

Figure 4.10 shows global distributions of Hg^0 surface concentration simulated in different test runs as well as ground-based measurements at various monitoring sites. As seen all three spatial patterns reflect the inter-hemispheric gradient of Hg^0 concentration and similar areas of elevated concentrations related to major emissions regions (South and East Asia, Europe, North America, Equatorial Africa and South America). As it was mentioned in [*Ilyin et al*., 2018] the model simulation with no Hg^{II} reduction (Run #1) leads to significant underestimation of measured Hg^0 concentrations, particularly, in remote regions of the Southern Hemisphere, where the effect of the atmospheric chemistry is the most pronounced (Fig. 4.10(a)).

Application of the photo-reduction mechanism with direct production of Hg^0 (Run #2) leads to insufficient net oxidation of Hg^0 in the atmosphere. It results in very long residence time and overestimated steady-state Hg^0 air concentrations in comparison with observations (Fig. 4.10(b)). In contrast, the other version of the mechanism with photo-reduction to HgBr (Run #3) provides more realistic levels and spatial distribution of Hg^0 concentration on a global scale (Fig. 4.10(b)).

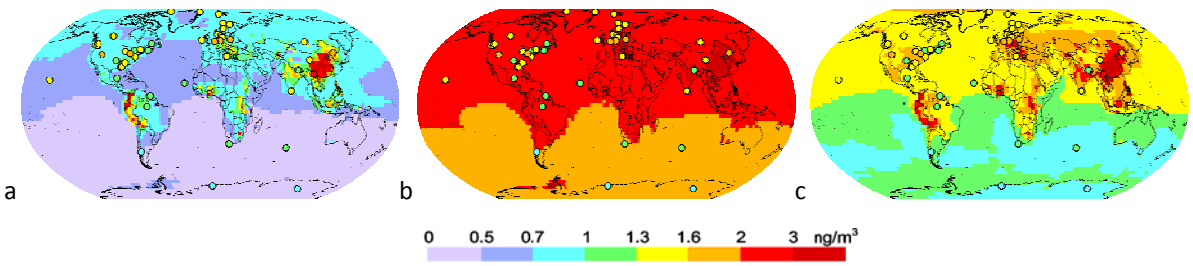

Fig. 4.10. *Spatial distribution of Hg^0 surface concentration for different tests: (a) – Run #1; (b) – Run #2; (c) – Run #3. Circles show observed values in the same color scale. The measurement dataset is the same as in Travnikov et al. [2017].*

More detailed evaluation of the modelling results against observations is shown in Fig. 4.11. The model Run #1 underestimates the observed Hg^0 air concentrations by 40% on average (Fig. 4.11a). It is accompanied by slight overestimation of measured Hg wet deposition (Fig. 4.11b). It indicates unrealistically strong oxidation capacity of the atmosphere. Run #2 demonstrates twofold overestimation of Hg^0 measurements and almost 80% underestimation of observed wet deposition. In its turn, it implies the lack of Hg^0 oxidation in the atmosphere. Run #3 provides relatively good agreement of modelling results with measurements still containing 20% overestimation of Hg^0 air concentration and 20% underestimation of Hg wet deposition.

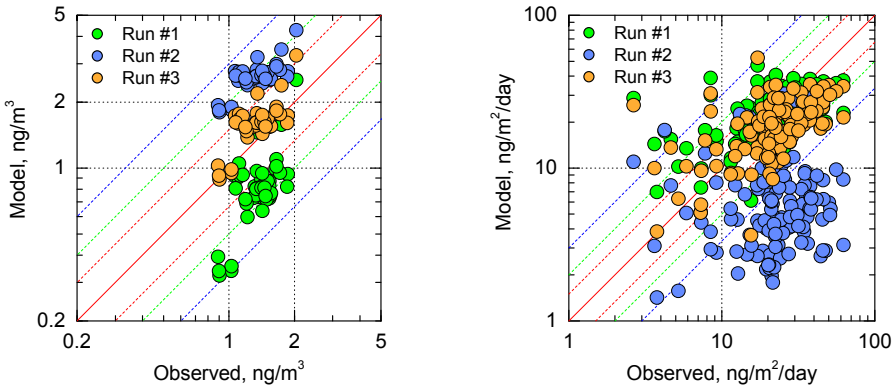

a b

Fig. 4.11. *Comparison of simulated Hg^0 air concentration (a) and Hg wet deposition (b) with measurements in 2013. The measurement dataset is the same as in Travnikov et al. [2017]*

More understanding of the oxidation and reduction processes can be obtained from analysis of the Hg chemical budget in the atmosphere (Fig. 4.12). Model estimates of the global atmospheric reservoir of Hg^0 are 1600, 7400 and 3800 Mg for the test Runs #1, #2 and #3, respectively. Only the last value is comparable with the previous estimates of 4000 Mg for the total atmosphere [e.g. *Travnikov et al.*, 2009; *Holmes et al.*, 2010] and 3500 Mg for the troposphere [*Horowitz et al*., 2017].

The gas-phase oxidation by atomic Br leads to transformation of Hg^0 to a unstable intermediate HgBr, which decomposes back to Hg^0 or reacts further with various atmospheric compounds (e.g. Br, OH, HO_2, NO_2) to form Hg^{II} (Fig. 4.12a). Oxidized Hg^{II} species can photo-dissociate back to Hg^0 or to HgBr. Direct photolysis of Hg^{II} to Hg^0 shifts the redox equilibrium to the reduction direction leading to very high steady-state level of Hg^0 and low levels of Hg^{II} (Fig. 4.12b). In contrast, the photo-reduction pathway through photolysis of Hg^{II} to HgBr is limited by the following decomposition of HgBr to Hg^0. It results in slower rates of overall Hg^{II} reduction and higher atmospheric levels of the Hg^{II} species (Fig. 4.12c). The simulated Hg^{II} species in this model test (Run #3, Fig. 4.12c) are dominated by $HgBr_2$, which contributes 77% of total atmospheric Hg^{II}. The second largest Hg^{II} species is HgBrONO (15%), which is followed by HgBrOH (8%). Contribution of HgBrOOH is negligible.

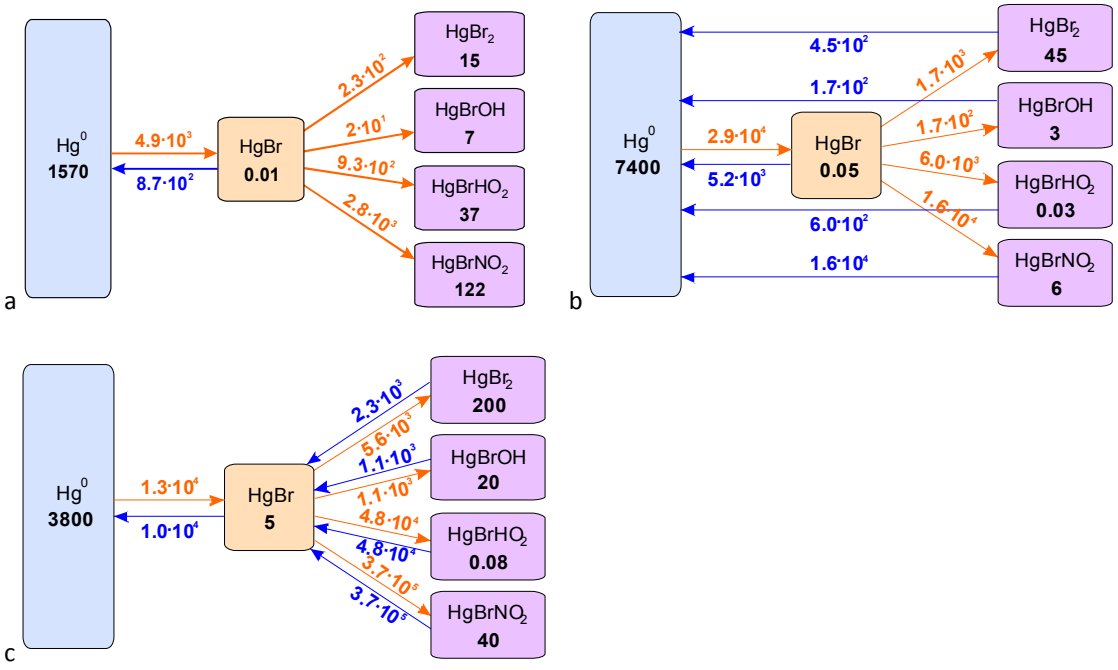

Fig. 4.12. *Global budget of Hg chemical cycling in the atmosphere for different tests: (a) – Run #1; (b) – Run #2; (c) – Run #3. The mass estimates are in Mg of Hg, the fluxes are in Mg of Hg per year*

The process of formation of the Hg^{II} species in the most realistic Run #3 is illustrated in Fig. 4.13 The figure shows distribution of average mixing ratios of $HgBr_2$, HgBrOH, HgBrOOH, and HgBOrNO in the atmosphere along with net production rates (production minus decomposition) of these species in appropriate reactions (R4 and R7, Table 4.3). The production rates depend on local concentrations of monohalide HgBr, concentration of appropriate oxidants (Br, OH, HO_2, NO_2), and air temperature. The decomposition rates are determined by the photolysis rate, which is a function of solar radiation, and concentration of Hg^{II} species. The dominant Hg^{II} species $HgBr_2$ is largely produced in the upper troposphere at high and temperate latitudes of both hemispheres and next to the surface at high latitudes of the Southern Hemisphere (Fig. 4.13a). Due to absence of removal factors Hg^{II} produced in the upper troposphere has long residence time that leads to its accumulation and high concentrations aloft. The lower atmosphere, particularly, of the tropical zone is characterized by net decomposition and lower concentrations of $HgBr_2$.

The second important Hg^{II} species, HgBrONO, is also mostly produced in the upper troposphere at high latitudes of the Southern and, in particular, Northern Hemispheres (Fig. 4.13d). These regions are also characterized by relatively high concentrations of the species in the free troposphere. HgBrOH has a maximum of the production rate in the upper troposphere of the tropics, where elevated concentrations of these species occur (Fig. 4.13b). The production and decomposition of HgBrOOH mostly compensate each other resulting in very low net production rates throughout the whole atmosphere with some shift to production in the upper atmosphere and to decomposition in the lower atmosphere. Therefore, the steady-state concentrations of this Hg^{II} species is very low (Fig. 4.13c). All Hg^{II} species are depleted in the low troposphere of the Intertropical Convergence Zone due to intensive scavenging by precipitation.

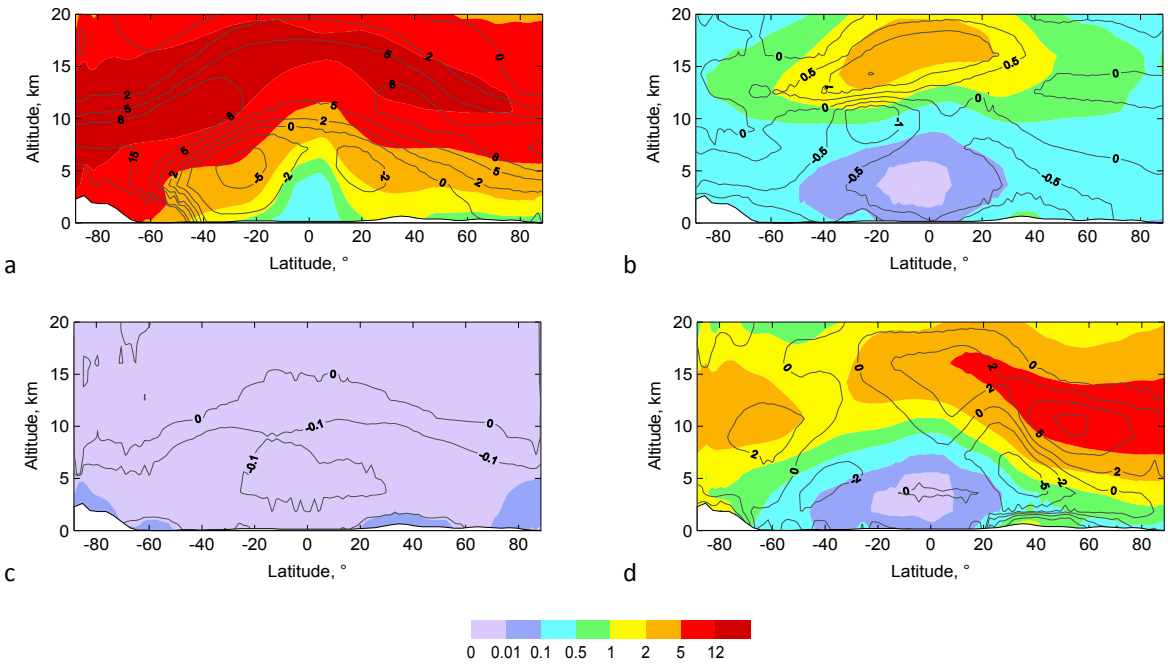

Fig. 4.13 *Annual zonal mean volume mixing ratios (colour palette, ppqv Hg) of $HgBr_2$ (a), HgBrOH (b), $HgBrHO_2$ (c), HgBrONO (d) for test Run #4. Isolines show net production rates (10^2 molecules cm^{-3} s^{-1}) for appropriate Hg species according to reactions R4 and R6 from Table 4.3. Positive values correspond to net production of Hg^{II}, negative values show net dissociation to HgBr.*

The photo-reduction mechanism significantly affects Hg global deposition pattern. Comparison of spatial distribution of Hg deposition simulated with no reduction (Run #1) and with the considered gaseous-phase photolysis (Run #3) is shown in Fig. 4.14. The photo-reduction mechanism decrease air concentrations of Hg^{II} and increase concentrations of Hg^0. It leads to decrease of dry and wet deposition of HgII all over the globe. In contrast, it increases dry deposition of Hg0, mostly, due to interaction with vegetation. Thus, effect of the photo-reduction consists of decreased Hg deposition over the ocean and increased deposition terrestrial vegetated areas. An exception is Hg deposition over the Southern ocean, where intensive Hg^0 oxidation largely prevails over Hg^{II} reduction and general increase of Hg^0 concentration leads to increased Hg deposition.

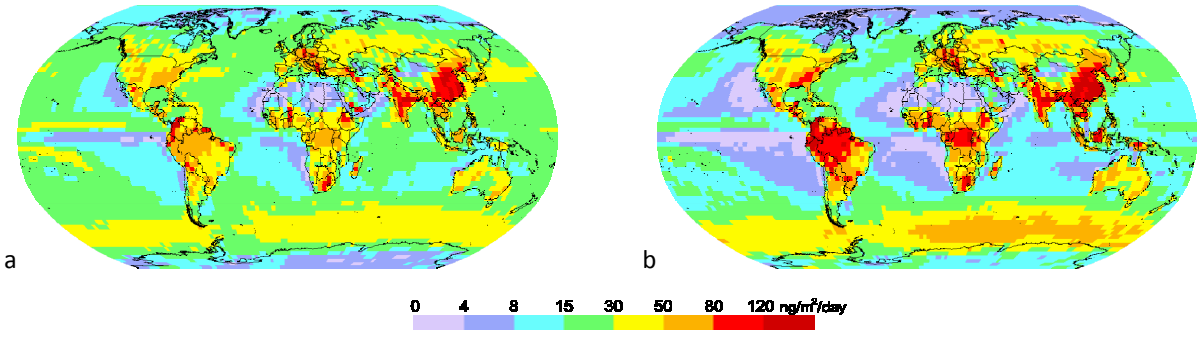

Fig. 4.14. *Spatial distribution of Hg total deposition for different tests: (a) – Run #1; (b) – Run #2; (c) – Run #3*

Thus, the analysis shows that the new gaseous photo-reduction mechanism applied along with the Br-initiated oxidation chemistry provides reasonable agreement of modelling results with observations. However, remaining discrepancies of modelling results with measurements require further in-depth study of the Br oxidation/reduction chemistry.

4.3. Model assessment of POP and Hg multi-media dispersion

Environmental dispersion of some POPs (HCB, PCDD/Fs, PCBs) and Hg is characterized by intensive cycling between various media (atmosphere, ocean, soil, vegetation). For instance, a pollutant deposited to soil can undergo physical or chemical transformations and be re-emitted back to the atmosphere or be leached by ground water to a lake or a river with following run off to the ocean. The cycling of these pollutants between the environmental media determines a complex character of their dispersion and leads to legacy effect of historical emissions on contemporary pollution levels. To take this phenomenon into account a multi-media modelling approach has been developed by MSC-E for a long period. It has been successfully applied for simulation of POP pollution both on regional and global scales. Besides, it is developed and tested for Hg. This section contains a short overview of the multi-media approach implemented in the GLEMOS model and discussion of new developments for HCB and Hg.

4.3.1. Overview of GLEMOS multi-media approach

GLEMOS is an up-to-date multi-scale multi-pollutant simulation platform developed for operational and research applications within the EMEP programme. The framework allows modelling of dispersion and cycling of different classes of pollutants (e.g. mercury and other heavy metals, POPs, tracers) in the environment with a flexible choice of the simulation domain (from global to national scale) and spatial resolution. One of unique features of the GLEMOS system is support of multi-media description of pollutants' cycling in the environment. Due to the physical and chemical properties Hg and POPs are predominantly global scale multi-media pollutants, characterized by dynamic exchange between the atmosphere, water, soil, and vegetation compartments. Besides, they may be accumulated in the media like soil, seawater, and sediments forming the secondary sources of pollution.

Three pollutant groups have been included into the current version of the model – POPs, Hg, and particle-bound heavy metals (Pb, Cd). The multi-media approach is implemented in the GLEMOS modelling system using a modular architecture. It implies possibility to construct the suitable model configuration for particular application by means of including, removing or replacing some modules with other ones. It also allows considering different number of environmental media depending on a pollutant properties. Parameterizations of atmospheric processes of heavy metals and all media processes of POPs are largely based on the previous well developed and extensively tested models MSCE-HM [*Travnikov and Ilyin*, 2005] and MCSE-POP [*Gusev et al*., 2005].

In order to evaluate transport and fate of POPs in the environment several modules describing processes in the atmosphere, the ocean, soil, and vegetation have been elaborated along with the module of inter-media exchange. The structure and processes included in the current GLEMOS version are illustrated in Fig. 4.15. Different phases of POPs are considered in each medium, which are involved in different physical and chemical processes, which include transport, phase partitioning, degradation, and the inter-media exchange. Three dimensional advective transport and diffusion of POPs is considered in the atmosphere and the ocean compartment. In addition, vertical

transport of POPs in soil is implemented in the model. The inter-media exchange module describes the following processes: dry and wet deposition of aerosol and gaseous species and bi-directional exchange between the atmosphere and the ocean, soil, and vegetation surfaces, vegetation-soil exchange with litterfall and run-off from soil to the ocean.

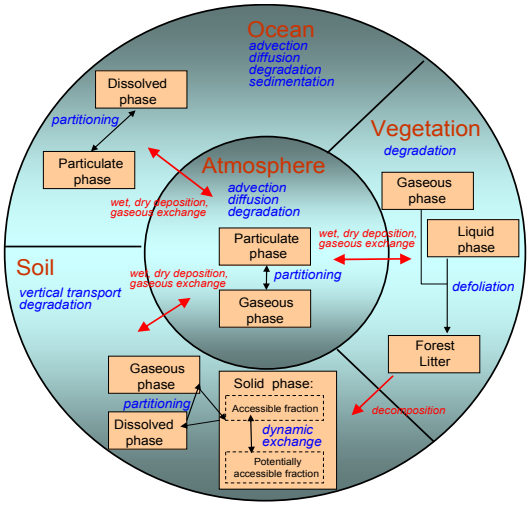

Fig. 4.15. *The scheme of the main processes related to POPs in the current version of the GLEMOS model*

The multi-media version of GLEMOS was applied to study regional and global scale transport of several POPs and evaluated against available measurements. Results of model simulations and their analysis can be found in the MSC-E reports [*Travnikov and Jonson*, 2011; *Jonson and Travnikov*, 2012; *Shatalov et al.*, 2014; *Shatalov et al.*, 2015]. Some examples of the modelling results for PCB-153, illustrating multi-media dispersion of POPs and evaluation against measurements, are shown below. Simulations of long-term fate of PCB-153 in the environment for the period 1930-2010 were based on the global inventory of historical PCB emissions [*Breivik et al.*, 2007] (Fig. 4.16). Dynamics of PCB-153 accumulation in the environmental media are shown in Figs. 4.16 and 4.17. Results show that the soil compartment accumulates maximum amount of PCB-153 emissions (87% by the end of the period). The shares of PCB-153 in the ocean and atmosphere compartments are smaller and equal to 13% and 1%, respectively. The soil compartment was characterized by the most significant inertness among others. Maximum total mass of PCB-153 in this medium took place in 1985 (Fig. 4.16) that was 10 years after the emissions maximum in 1975.

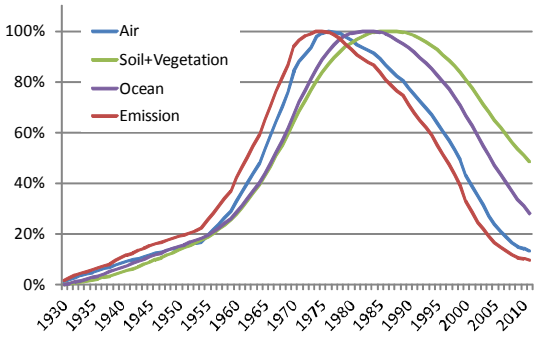

Fig. 4.16. *Normalized long-term changes of global anthropogenic emissions and total content of PCB-153 in the environmental media*

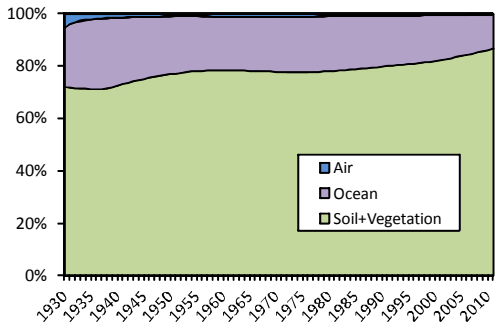

Fig. 4.17. *Share of PCB-153 mass between the environmental media for the period 1930-2010*

Spatial distribution of PCB-153 concentrations in the surface water simulated for the year 2010 is shown in Fig. 4.18. There is an evident latitudinal dependence of pollution levels with the highest concentration values at high-latitudes of the Northern Hemisphere. This pattern of concentrations

can be attributed to the distribution of most PCB-153 emissions in the Northern Hemisphere as well as to the strong temperature dependence of the gaseous flux from the atmosphere to water that increases for lower air temperatures. Measurement of PCB-153 concentrations in seawater from different campaigns [*AMAP*, 1998; *AMAP*, 2004; *Schulz-Bull et al*., 1991; *Iwata et al*., 1993; *Kannan et al*., 1998; *PWGSC*, 2003] were employed for validation of the oceanic module of GLEMOS. For the purpose of comparison observations were divided into three groups according to the latitude of measurement sites and averaged zonally within the groups (40°N: Japan Sea; 50°N: North Sea, Bering Sea; and 70°N: Norwegian Sea, Barents Sea, Beaufort Sea, Chukchi Sea). As seen from Figs. 4.19, the model was able to reasonably reproduce the measured latitudinal trend of PCB-153 concentration in seawater.

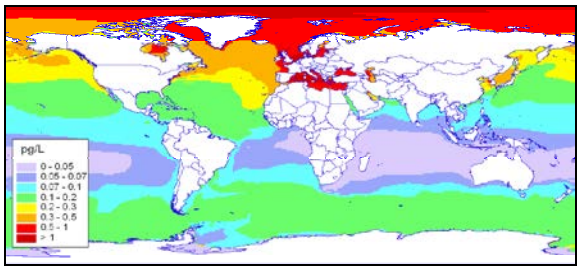

Fig. 4.18. *Spatial distributions of PCB-153 annual mean concentration in seawater for 2010, pg/L*

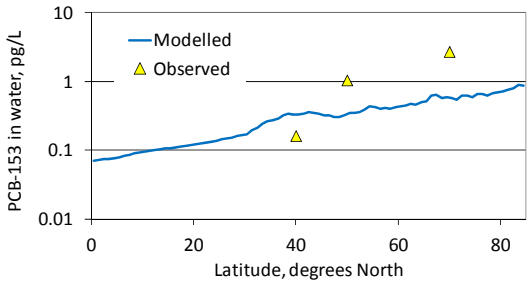

Fig. 4.19. *Zonally averaged meridional profiles of measured and modelled PCB-153 concentrations in seawater, pg/L*

Global distribution of simulated annual mean PCB-153 concentrations in the top 5 cm layer of soil are shown in Fig. 4.20. Elevated levels of PCB-153 in soil are estimated for the regions with high anthropogenic emissions (Europe and Northern America) with maximum concentration level in Central Europe. Modelled PCB-153 concentrations in the upper soil layer were compared with measurements performed at 191 background sites worldwide [*Meijer et al*., 2003]. In general, model predictions tend to under-estimate measured values (Fig. 4.21). At the same time, there is significant spatial correlation between measured and modelled values.

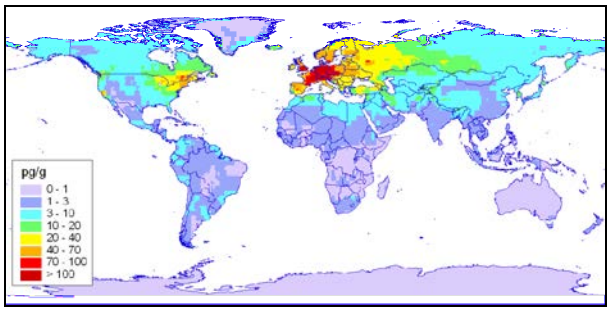

Fig. 4.20. *Spatial distributions of PCB-153 annual mean concentration in the top 5 cm of soil for 2010*

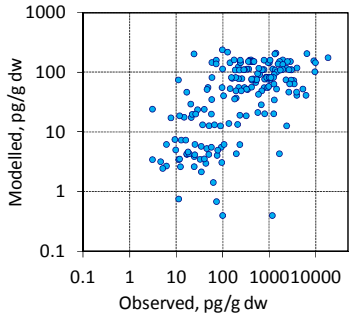

Fig. 4.21. *Scatter plot of modelled soil concentrations of PCB-153 in the upper soil level and measured soil concentrations of PCB-153/132 [Meijer et al., 2003] (dw – dry weight of soil)*

4.3.2. Refinement of HCB pollution assessment

Hexachlorobenzene (HCB) is known as a pollutant of global concern due to significant potential to long-range transport, persistence in the environment, bioaccumulation, and harmful effects both for human health and for the ecosystems. It is classified as a carcinogen of the group 1B under the Regulation (EC) No 1272/2008 (CLP), which defines it also as a toxicant for specific organs under repeated exposure. In addition, HCB is classified as hormonal disruptor [*Starek-Świechowicz et al*., 2017] and as a very toxic compound to aquatic organisms according to CLP. Major route for population exposure to HCB is through the ingestion of food (92%) [*WHO*, 2004] while inhalation and drinking of water are less important (7% and 1%, respectively). Analysis of monitoring of HCB content in human adipose tissue and milk generally shows reduction of HCB exposure of general population since the 1970s [*Fürst*, 2006; *Guerranti et al.*, 2011]. Nevertheless, the Long-Term Strategy of the Convention is paying particular attention to this pollutant indicating that HCB pollution levels are still a concern and are associated with long-term risks.

HCB was widely used for agricultural purposes from the 1940s until 1970s as a pesticide and fungicide [*EEA*, 2006]. After restrictions and banning of HCB application in agriculture starting from 1970s, its production and use have been substantially declined, leading to the decrease of its content in the environment. Contemporary levels of HCB pollution are likely supported by industrial and combustion emission sources and to significant extent by the secondary releases from the environmental media previously polluted due to agricultural or industrial activities [*Barber et al.*, 2005]. While global concentrations of HCB has decreased significantly due to restrictions of its use, local levels of HCB in some countries of the polar region do not decrease [*Toft,* 2015; *Pouch et al*., 2018]. Some other studies also believe that the Arctic region can be a sink for HCB [*Macdonald et al*., 2005; *Wania*, 2003].

This section presents the progress in the activity related to the refinement of HCB pollution levels assessment. At previous stages of this work [*Gusev et al.*, 2017; *Gusev et al.*, 2018] it was indicated that the model assessment of HCB pollution was associated with considerable uncertainties due to incomplete information on contemporary and historic anthropogenic HCB emissions as well as to uncertainties of the modelling approach applied. At current stage, a review of scientific literature was performed to refine information on HCB physical-chemical properties and to update the model parameterizations of processes controlling HCB concentrations in media. Test model simulations of HCB long-term accumulation in media were carried out to analyse the effect of changes in parameterizations on the agreement of the model predictions with measurements. In addition, the information on sources of HCB emissions and routes of population exposure was collected and reviewed to contribute to the analysis of HCB adverse effects.

HCB emission sources

HCB does not occur naturally, it can be produced for various applications or released as unintentional by-product in course of manufacturing of chlorinated compounds. Although production of HCB is prohibited in Europe, small amounts are unintentionally formed from a number of sources. For instance, various incineration processes, leaks from old landfills, non-compliance to strictly controlled conditions of manufacturing processes and disposal of wastes from the manufacture and use of several chlorinated compounds, including chlorinated solvents and pesticides could be mentioned [*EFSA*, 2006]. In addition, HCB can be formed as by-product in different industrial processes or as unintentional impurity in some products, for example, in number of pigments based on tetrachlorophthalic anhydride [Government of Japan, 2007] .

According to the study [*Thomsen et. al*., 2009], residential wood combustion as well as a diffuse sources and waste incineration processes, are believed to be the most probable sources of HCB emission. Industrial combustion processes, for example, in metal industry, petroleum refineries and emission from energy sector can be assumed to be of minor importance. In addition, various kinds of wastes and by-products, including petroleum residues, solid and liquid waste and industrial wastewater, waste from generation of energy can be significant source of HCB to water and soil. Contribution of waste management processes depends on final disposal methods and recovery of waste. Whereas the amount of generated waste is significant, this source of HCB emission may be important.

Some studies show that one of the major sources of HCB is re-emission of “old” HCB from the environmental media [e.g. *Barber et al.,* 2005]. Importance of secondary HCB emissions was considered in several previous studies performed by MSC-E [*Shatalov et al*., 2010; *Gusev et al*., 2011]. It was concluded that further improvement of the evaluation of HCB pollution levels in the EMEP countries could be achieved by the refinement of officially reported HCB emissions and historical releases of HCB to the environment. Other recent studies also supposed that the main source of HCB is recycling from soil, sediments, snow and ice. *Wang et al*. [2012] investigated air-soil exchange of HCB and other POPs of the Tibetan Plateau and showed that the Tibetan soils may appear to be secondary sources of HCB. In addition, it was found out that concentrations of HCB in soil were correlated with content of organic carbon in soil.

HCB can also be found as a component of different kinds of products, including ammunition, fireworks, and synthetic rubber. Thus, *Schmid et al*. [2014] investigated contribution of HCB emission from fireworks. Measurements carried out during the Swiss National holiday showed that HCB is contained as an additive in fireworks. It was estimated that HCB from fireworks can contribute up to 10% to the total emissions in Switzerland. Such hypothesis was studied also by the Chemical Legislation European Enforcement Network (CLEEN) on the basis of data for Denmark (2008–2010) and Austria (2009–2010). It was shown that concentrations of HCB in fireworks can amount up to 4.4 wt% [*CLEEN*, 2012]. It should be noted that HCB concentrations were above the Limit value (50 mg/kg) in approximately 10% of 439 samples which have been tested during this project.

Environmental fate of HCB

HCB undergoes very little biodegradation in the environment, for this reason it has long half-live in the different environmental media including biota [*Niimi*, 1987]. It is important to note that availability of HCB for organisms is reduced due to its strong binding to soils and sediments [*Barber et al*., 2005]. Consequently, historical HCB contamination of soils and sediments can remain for long time after cessation of its emissions. HCB has been found at relatively high air concentrations in remote polar regions, both the Arctic and Antarctic, that can be due to long-range atmospheric transport from temperate regions [*Euro Chlor*, 2002].

Table 4.5. *Estimates of HCB half-live in the different environmental media*

Compartment	**Half-life, years**					
	Euro Chlor [2002]	*Beyer et al.* [2000]	*Mackay et al*., [1992]	*Pouch et al.* [2018]	*Barber et al*. [2005]	*EFSA* [2006]
Air	5	0.84	2.7 - 6		1.76	0.43 - 6.28
Freshwater	6	6.3	2.7 - 6			2.7-5.7 (surface water) 5.3-11.4 (ground water)
Sea water	12	6.3	2.7 - 6			
Sediment	3.7	6.3		17 - 31		3 - 6
Soil	6.2	6.3	> 6		2.7 - 22	2.7 - 5.7 (aerobic) 10.6-22.9 (anaerobic)

Being released to the atmosphere HCB can exist in the vapour phase or be associated with particles [*Eisenreich et al*., 1981; *WHO*, 2004; *EFSA*, 2006]. Measurements have showed that generally the vapour phase is prevalent whereas content of HCB in association with particles is under 5 percent [*Ballschmiter and Wittlinger*, 1991; *Lane et al*., 1992, *WHO*, 2004]. In the troposphere HCB can undergo slow photolytic degradation. Measured rate constant for the gas-phase reactions of the hydroxyl radical with HCB at 298 K was about $0.27 \cdot 10^{-13}$ cm^3 s^{-1} which is equivalent of 940 days of HCB atmospheric lifetime [*Brubaker and Hites*, 1998].

In water, both abiotic and biotic degradation of HCB are very slow [e.g. *EFSA*, 2006]. The half-life value of HCB is estimated to range from 2.7 to 12 years (Table 4.5). Hydrolysis reactions are not relevant for HCB but slow photolytic degradation is possible [*Mill and Haag*, 1986; *Barber at al*., 2005]. *Ji et al*. [2015] suppose that HCB can undergo microbial degradation under anaerobic conditions resulting in its transformation to low-chlorobenzene compounds. Major fate processes of HCB leading to its removal from water are volatilisation from the water surface, which is moderately rapid, and adsorption to particulates and sedimentation [*Oliver*, 1984; *Oliver and Charlton*, 1984; *EFSA*, 2006]. Half-life value of HCB in sediments is estimated to be up to 30 years due to its strong adsorption to particulates and long persistence [*Pouch et al*., 2018]. In addition, after sedimentation HCB can accumulate on the bed and later can became locked up under overlying sediments [*Oliver and Nicol*, 1982].

The main process for HCB removal from the surface soil layer is its volatilisation [*Barber et al*., 2005; *Schwarzenbach et al*., 1983; *Nash and Gish*, 1989]. At lower soil horizons aerobic and anaerobic biodegradation processes are more important [*Beck and Hansen*, 1974; *Howard et al*., 1991]. Processes of desorption of HCB from soil and sediments are slow but they lead to secondary emission of HCB to the environment [*EFSA*, 2006; *Oliver et al*., 1989].

Persistence of HCB, its mobility and bioaccumulation properties result in its world-wide distribution. Taking into account historical application of HCB, soil is the main environmental compartment which was contaminated by HCB. According to expert estimates [*Mukesh Kumar et al*., 2013] mass of HCB in soil is much greater than its content in the atmosphere despite significant difference between the global volume of soil and air (Fig. 4.22). HCB content in sediments and water in total do not exceed 3%. Low concentrations of HCB in water could be explained by its low solubility [*Barber et.al*, 2005].

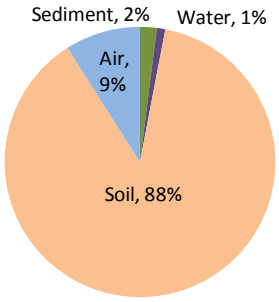

Fig. 4.22. *Global distribution of HCB in various environmental compartments*

Model assessment of HCB pollution: refinement of the model parameterization

Assessment of HCB transport and fate is performed on the basis of officially reported emission data and expert estimates of emissions using the combined global and regional model simulations. Previous studies of HCB pollution levels in the EMEP region [*Gusev et al.,* 2017, 2018] indicated under-prediction of observed air concentrations in the EMEP countries. The under-prediction was attributed to several reasons, namely, incompleteness of reported inventories of national HCB emission sources, underestimation of HCB emissions in other regions of the world outside the EMEP domain (e.g. in Southeast Asia), and uncertainties of the applied modelling approach. Major attention at this stage is paid to the analysis of the model parameterizations of HCB processes in media and air-surface exchange.

Current version of the GLEMOS model includes the following processes for the soil compartment: gaseous exchange with the atmosphere, partitioning of the pollutant between various phases, vertical transport due to diffusion and convective water fluxes, bioturbation, and degradation. Several phases of POPs within the soil are considered in the model: gaseous phase, dissolved phase, pollutant sorbed on the dissolved organic carbon, and on organic carbon within the solid soil fraction (Fig. 4.23). To take into account the dynamic character of the redistribution of POPs between the solid soil fraction and other phases, total content of solid organic carbon (OC) is split into two separate fractions: easily accessible and potentially accessible fractions [*Vassilyeva and Shatalov*, 2002]. The model assumes that all POP phases in soil are in instantaneous equilibrium with the exception of POP sorbed on potentially accessible soil OC fraction for which dynamic exchange with easily accessible fraction is implemented.

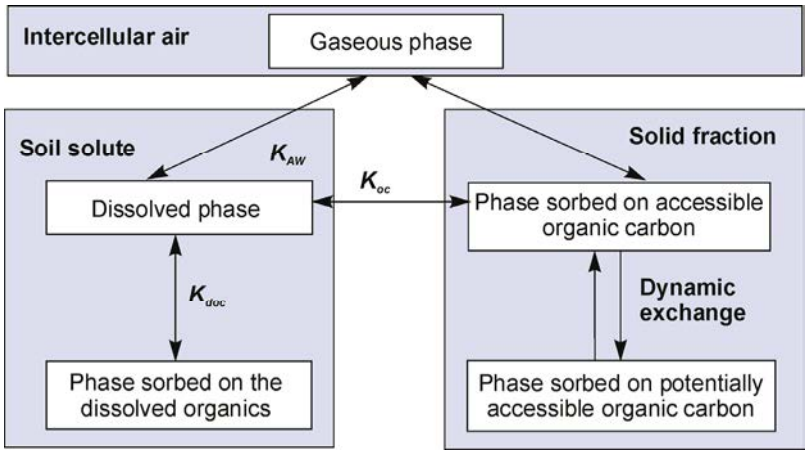

Fig. 4.23. *Partitioning of POPs between different phases in soil and partitioning coefficients*

Taking into account under-estimation of the observed HCB concentrations in the atmosphere and soil by the model [*Gusev et al.,* 2017; 2018], analysis of model parameterizations is focused on the soil compartment. The processes related to HCB accumulation in soil include gaseous air-surface exchange, phase partitioning and degradation. Parameterizations of these processes depend on a number of parameters for which different estimates are available in scientific literature. These are octanol-water partition coefficient K_{ow}, describing sorption of POPs on the organic matter, and rate of degradation of POPs in soil. Compared to the currently used values of these parameters in the model, higher estimate of K_{ow} coefficient is given in [*Ballschmitter and Wittlinger*, 1991; *Manz et al.*, 2001]. In addition, estimate of slower rate of HCB degradation in soil is available in [*Beyer et al.*, 2000]. These estimates might lead to more significant accumulation of HCB in soil and subsequently to more intensive re-volatilization to the atmosphere. In addition to the selected parameters, the value of accessible fraction of POP sorbed on solid phase OC is considered.

In order to evaluate the effect of changed values of K_{ow} coefficient, degradation rate, and accessible fraction on modelling results, test model runs (Table 4.6) with coarse spatial resolution 3°x3° for the period 1945-2017 were carried out using the GLEMOS model. Model simulations were based on the expert estimates of historic HCB emissions developed earlier [*Shatalov et al.*, 2010] and prolonged to the year 2017.

Table 4.6. *Test model simulations to evaluate model response to changes of parameters of HCB degradation and partitioning in soil compartment. Along with modified values of parameters previously used estimates in standard model parameterization are given*

Test simulation	***Description***
Base case (BASE)	Model run with the set of parameters used for standard calculations
K_{ow} partition coefficient (KOW)	Model run with modified K_{ow} partition coefficient, K_{ow} = $1.6x10^6$ at 10° Celsius, previous value K_{ow} = $3.54x10^5$
Degradation (DEGR)	Model run with modified HCB degradation rate in soil, k_s = $3.5x^9$ s^{-1} , previous value k_s = $5.24x^9$ s^{-1}
Accessible fraction (ACCFR)	Model run with modified accessible fraction of POP sorbed on organic carbon in solid phase in soil, 0.6 , previous value 0.3

Fig. 4.24 illustrates the differences in the dynamics of HCB content in the atmospheric compartment between the results of long-term test model simulations. The largest effect of changes in the model parameterizations on the modelling results can be seen for K_{ow} partition coefficient. In particular, slower increase of HCB content in air in the period of emission growing (1945-1978) is obtained for the KOW model simulation. The end of calculation period (2000-2017) is characterized by the highest HCB content in air in case of the KOW model simulation and the lowest one in case of the ACCFR model simulation. Results of the DEGR model simulation are rather close to the BASE model simulation results. The difference between the test simulations can be explained by more intensive accumulation of HCB in soil compartment under the KOW simulation and more intensive air-surface exchange due to increased accessible fraction of HCB sorbed on the solid phase OC in soil in case of the ACCFR model run.

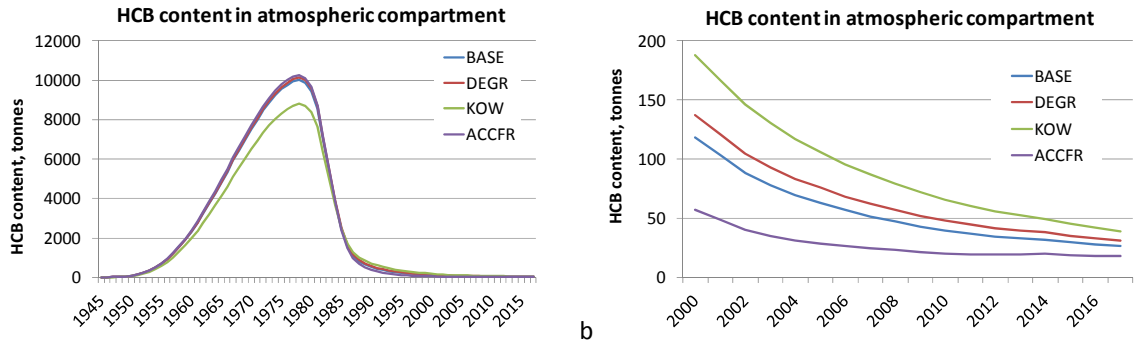

***Fig. 4.24**. Long-term changes of HCB content in the atmosphere in period 1945-2017 (a) and in the end of calculation period 2000-2017 (b) on the basis of the test model simulations (see Table 4.5)*

Similar dynamics of HCB content can be seen in the modelling results for soil compartment shown in Fig. 4.25a. The largest amount of accumulated HCB in soil is obtained in the KOW model simulation while the lowest one in the ACCFR model simulation. Increase of K_{ow} partition coefficient leads to significantly higher accumulation of HCB in soil compared to other test model simulations.

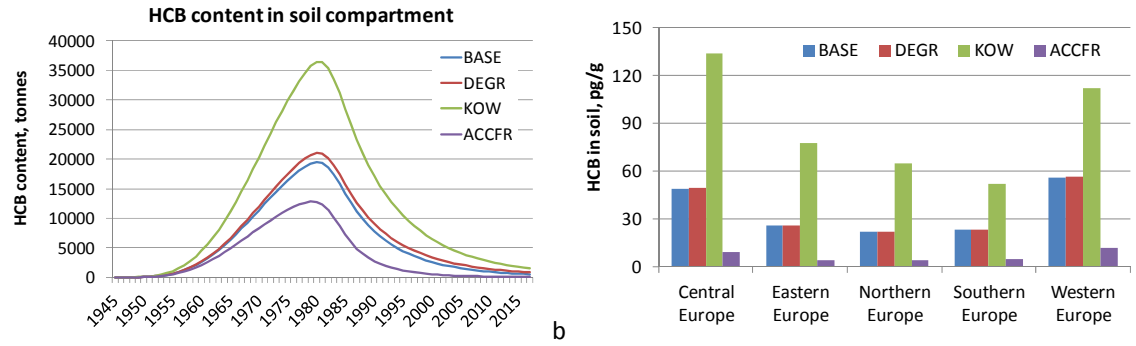

***Fig. 4.25**. Long-term changes of HCB content in soil compartment in period 1945-2017 (a) and averaged annual mean modelled HCB concentrations in soil (b) in the European countries for 2017 on the basis of the test model simulations (see Table 4.5)*

In Fig. 4.25b comparison of averaged annual mean HCB soil concentrations, estimated for the year 2017, is shown for the countries of Central, Eastern, Northern, Southern and Western Europe. It can be seen that the results of the model calculations are mostly sensitive to change of K_{ow} partition coefficient and accessible fraction of POP sorbed on solid OC in soil, while change of HCB degradation in soil has small effect on HCB levels in soil. In both cases the difference with results of the BASE model run exceeds a factor of 2.

To evaluate the effect of parameterization changes on the agreement of the model predictions with measurements, results of the test model simulations were compared with the available EMEP measurements for 2017. Annual mean HCB air concentrations measured in 2017 are available at 7 monitoring sites in the Czech Republic, Finland, Iceland, Norway, and Sweden.

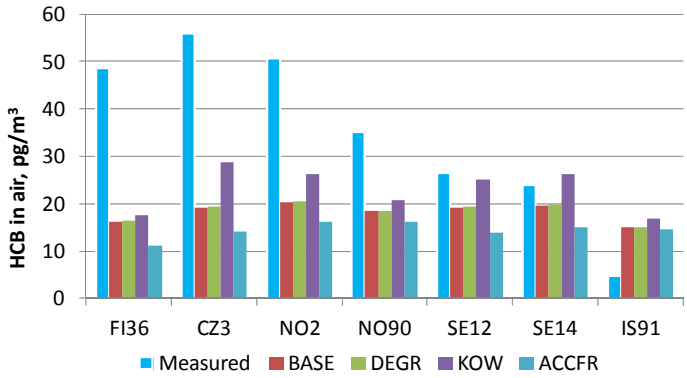

***Fig. 4.26**. Comparison of annual mean HCB air concentrations observed at EMEP monitoring stations in 2017 and model predictions based on test simulations (see Table 4.6).*

Comparison of the model predictions based on the test model simulations with measurements is shown in Fig. 4.26. It is seen from the figure that increase of K_{OW} parameter leads to the improvement of agreement with measurements whereas change of HCB degradation rate has no effect and enlargement of accessible fraction results is worsening the agreement. Statistical parameters of the comparison are summarized in Table 4.7. In general, the model tends to under-predict observed concentrations. The spatial correlation of the modelled and observed concentrations in most of test cases is about 0.5. In case of the KOW test run the model shows somewhat lower bias and more significant number of stations where modelled concentrations are within a factor of 2 with regard to measurements.

***Table 4.7.** Statistical parameters of the comparison of the test model simulations results with measurements of EMEP monitoring sites for 2017.*

Parameter	***Normalized mean bias (%)***	***Correlation***	***Factor 2 (%)*** [(a)]
Base case (BASE)	-48	0.46	43
K_{ow} partition coefficient (KOW)	-34	0.44	71
Degradation (DEGR)	-47	0.47	43
Accessible fraction (ACCFR)	-59	-0.18	29

[(a)] *Factor 2 represents a fraction of sites, for which deviation between modelled and observed values are within a factor of 2.*

The test model simulations show significant sensitivity of the modelling results to the changes of parameters of processes, affecting HCB fate in soil compartment. Thus, further analysis and refinement of the model parameterization of HCB soil processes is of importance. Particular attention should be paid to the refinement of phase partitioning of HCB in soil and values of K_{OW} coefficient and accessible fraction of HCB sorbed on solid OC in soil. In addition, refinement of information on distribution of organic carbon in soil in different phases is needed.

The model evaluation of long-term HCB fate in media and analysis of sensitivity of the model results to changes of process parameterizations will be continued. In addition, the model predictions of contemporary HCB pollution levels will be compared with the results of EMEP passive sampling campaign performed for HCB in 2016.

4.3.3. Development of Hg multi-media modelling

Mercury dispersion in the environment has complex character including transport in the atmosphere and the ocean, chemical transformations in air, soil and seawater, as well as continuous exchange between the environmental media. This aspect should be taken into account in assessment of Hg pollution levels and, in particular, long-term changes of Hg contamination – historical trends and future scenarios. A pilot multi-media version of the GLEMOS model for Hg has been developed and tested previously [*Travnikov et al.*, 2009]. The model includes three environmental media – atmosphere, ocean and soil – with appropriate exchange fluxes. Major distinctions of the experimental multi-media version from the regular GLEMOS model include low spatial resolution (20°×20°), simplified atmospheric and oceanic dispersion schemes and use of averaged meteorological and oceanic driving fields presenting 'climatic' conditions. All these simplifications allow application of the model for very long-term time periods (centuries) to evaluate the pollutant accumulation and cycling in the environment.

The experimental version uses the same atmospheric module as that of the regular GLEMOS version except for the driving meteorological fields and parameterization of the atmospheric dispersion. The atmospheric model domain consists of 13 irregular model layers and covers global atmosphere up to 30 km altitude. Atmospheric dispersion and other processes are driven by meteorological fields based on the ECMWF ERA-40 re-analysis (http://data-portal.ecmwf.int/data/d/era40_daily/) averaged over a long period in order to obtain 'climatic' conditions. Atmospheric dispersion is presented by simple upwind scheme with bi-directional fluxes between the gridboxes. Mercury is presented in the atmosphere by two gaseous forms (elemental and oxidized), oxidized particulate form and aquatic forms in cloud water (dissolved elemental, mercury ion, sulfate and chloride complexes).

The oceanic model domain covers the open ocean and coastal waters as well as some inland seas (Baltic, Mediterranean, Black, Caspian, Red Seas, etc.) and consists of 6 irregular layers down to 1.2 km depth. Oceanic processes are driven by sea currents and other data based on ECMWF ORA-S3 ocean re-analysis (http://www.ecmwf.int/products/forecasts/d/charts/ocean/) using averaging procedure similar to that for meteorological data. Mercury in seawater is presented by three major

forms – aqueous elemental, oxidized and non-reactive mercury. The model considers the following processes governing mercury fate in seawater: dispersion with sea currents as well as upwelling and downwelling exchange with the deep ocean; reduction of oxidized mercury to elemental form and conversion to non-reactive form; gas exchange of dissolved elemental mercury with the atmosphere; settling non-reactive mercury to the deep ocean with suspended particles.

Soil is presented in the model by a one 20 cm depth layer. It is assumed that Hg occurs in soil in two forms – solid and dissolved in ground water. Solid form, in its turn, is divided into mercury content in mineral and organic soils. We expect that mercury in mineral soil has natural origin and is characterized by strong binding. Mineral Hg concentration is assumed to be constant and non-zero only at the mercuriferrous belts location. In contrast, Hg content in organic soils reflects accumulation of mercury mostly from atmospheric deposition and varies both spatially and temporally. The model considers the following processes governing mercury fate in soil: partitioning of the dissolved and solid Hg forms; gaseous exchange of Hg dissolved in ground water with the atmosphere; run-off of Hg dissolved in ground water to the ocean; volatilization of solid phase Hg to the atmosphere.

For the research purpose, we performed rough estimates of historical Hg emission trend. Modern anthropogenic emissions were taken from the recent global mercury emission inventory for 2010 [*AMAP/UNEP*, 2013]. Since much of global mercury emission is originated from coal and other fuels combustion we approximated historical evolution of Hg emission by scaling modern emission levels by a factor derived from historical trend of CO_2 emissions from fossil fuel combustion. Besides, in order to estimate the effect of one of the most important historical Hg emission episodes on we considered emission of the pollutant from the gold and silver mining in North America. Contribution of this source was evaluated based on estimates of Hg emission from North American gold rush in 1870-1880 [*Strode et al.*, 2009] and the primary mercury production in North America as the temporal scaling factor [*Hylander and Meili,* 2003]. It should be noted that the developed emissions trend does not reflect historical evolution of Hg emissions from other important sources including metal and cement production, waste incineration and artisanal gold mining.

Pre-industrial conditions were simulated by reaching the steady-state with zero anthropogenic emissions (over 10000 years). After that a 200-years simulation was performed from the beginning of 19th century to nowadays using historical anthropogenic emissions discussed above. Figure 4.27 shows simulated changes of total mercury burden in the atmosphere, soil and the ocean as well as atmospheric deposition. The total mercury burden in the atmosphere has increased more than twice since the pre-industrial period till nowadays, mercury in the ocean – by about 25%, and about 10% increase was obtained for mercury in soil. It should be noted, that increase of mercury concentrations in the upper layers of soil and the ocean is more significant than in the whole media and can reach a factor of two. The largest enrichment due to anthropogenic activity was obtained for atmospheric deposition: it was enlarged by a factor 2.3. Besides, the deposition increase varies between different regions and continents. For example, in Asia it exceeds a factor of 3 whereas is South America it is around a factor of 2 (Fig. 4.28).

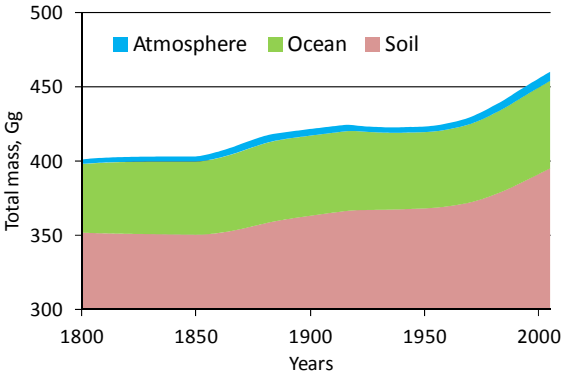

Fig. 4.27. *Simulated evolution of total Hg burden in the three main environmental media since 1800 till 2010*

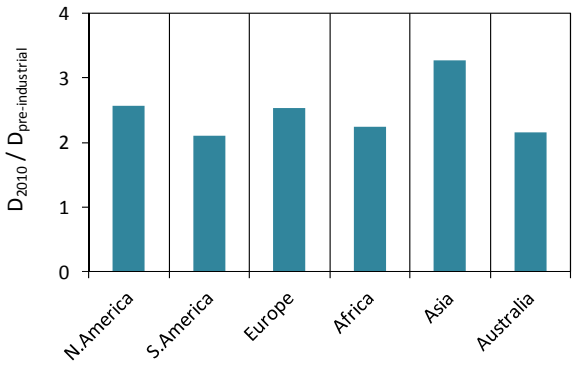

Fig. 4.28. *Average increase of Hg atmospheric deposition in various continents since 1800 till 2010*

Figure 4.29 shows spatial distribution of simulated present-day concentrations of Hg in the atmosphere and the ocean. For comparison, available Hg measurements in air (Travnikov et al., 2017) and seawater (Zhang et al., 2014) are also shown in the figure. As seen simulated Hg air concentration generally reproduces the observed values, but somewhat underestimate concentrations in the Northern Hemisphere and the south-to-north gradient due to low spatial resolution and too intensive inter-hemispheric exchange (Fig. 4.29a). Concentrations of total mercury in seawater are high in coastal waters adjacent to industrial regions and zones with significant upwelling (Fig. 4.29b).

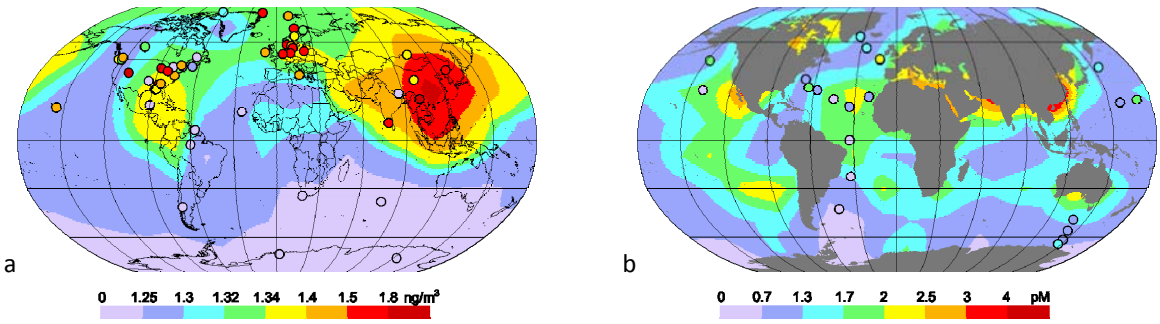

Fig. 4.29*. Simulated present-day air concentration of* Hg^0 *(a) and concentration of total Hg in seawater (b). Circles present measurements data in the same colour scale [Travnikov et al., 2017; Zhang et al., 2014]*

4.4. Analysis of factors affecting heavy metal pollution changes between 2016 and 2017

Pollution levels of heavy metals in the EMEP region in a particular year are formed by the influence of various factors. The first factor is anthropogenic emissions. Another important factor is meteorological conditions changing from year to year. Besides, changes of meteorological conditions affect wind re-suspension of dust particles containing heavy metals. In addition to this, changes of the model parameterizations also lead to changes of calculated pollution levels.

In order to analyze the effects of these factors on deposition changes taken place between 2016 and 2017 three sets of calculations were carried out (Table 4.8). All calculations were carried out using the same data on anthropogenic emissions. Therefore, the changes in the results are driven by changes of meteorological conditions (Section 1.3), which affect transport of pollutants and their removal from the atmosphere as well as changes of wind re-suspension. Besides, some changes regarding wind re-suspension parameterization were made in the model.

Table 4.8. *Model runs performed for the analysis of changes between 2016 and 2017*

	Run#1	*Run#2*	*Run#3*
Emission data	2016	2016	2016
Meteorological conditions	2016	2017	2017
Wind re-suspension	Original, 2016.	Original, 2017	Corrected, 2017

Changes between deposition were expressed in relative (percent) and absolute (g/km^2/year) terms with regard to results for 2016 (Run #1). Positive value of the change means that deposition in 2017 is higher than that in 2016, and vice versa. Results of the analysis of the changes are exemplified by Cd. Maps of Cd total deposition fluxes in 2016 (Run #1) and 2017 (Run #2) are demonstrated in Fig. 4.30. The maps of spatial distribution of the fluxes in 2016 and 2017 are similar. Spatial distribution of the fluxes reflects mainly spatial distribution of anthropogenic emissions in the EMEP region. Areas of the highest fluxes noted for the Benelux region, western Germany, Poland, the central parts of Russia and the eastern parts of Ukraine are associated with relatively high Cd emissions in the corresponding regions.

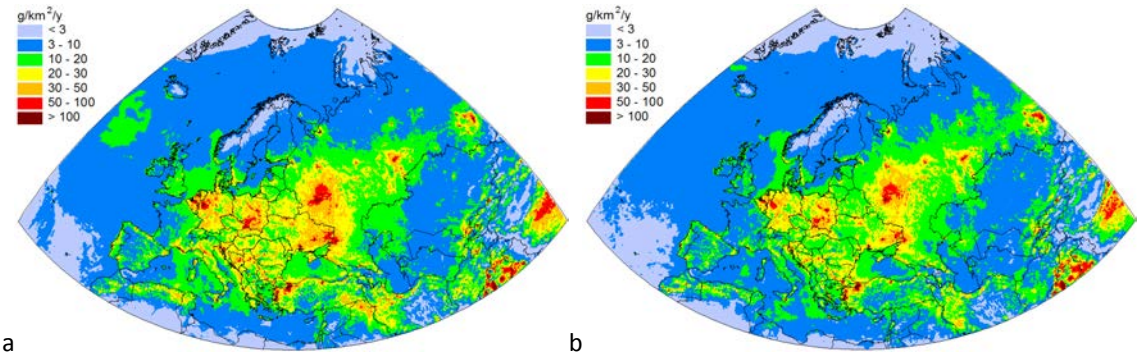

a b

Fig. 4.30. *Total deposition of Cd in 2016 (Run#1, a) and 2017 (Run#3, b)*

Most significant absolute (Fig. 4.31a) and relative (Fig. 4.31b) differences between deposition fluxes in 2016 and 2017 are noted for the central and the western parts of the Mediterranean. Relatively high absolute changes (-8 - -3 g/km^2/y) are seen over the eastern part of Europe, whereas relative change over this region is around -30%. Significant positive change is noted for the Asian part of Russia, but the absolute change over this region is low (up to 3 g/km^2/y).

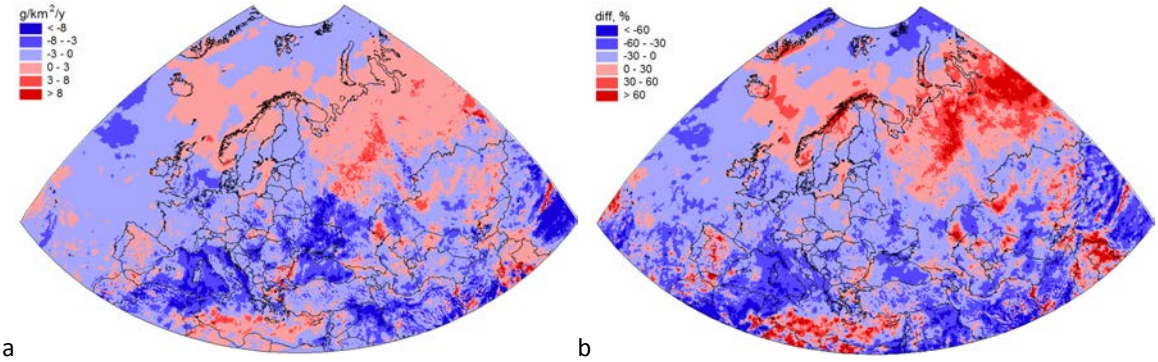

a b

Fig. 4.31. *Absolute (a) and relative (b) difference between Cd total deposition fluxes in 2016 and 2017*

The differences shown in Fig. 4.31 reflect overall effect of changes of various factors. In order to derive the effect of meteorological conditions it is worth comparing deposition fluxes caused by anthropogenic sources. Since in all considered model calculations anthropogenic emissions are the same, the changes in anthropogenic deposition between 2016 and 2017 are caused only by inter-annual meteorological variability. Over most parts of the EMEP countries the relative difference, caused by meteorological variability, lies within ±30% (Fig. 4.32a). Relatively high increase in the eastern part of the domain is associated with small absolute changes (Fig. 4.32b).

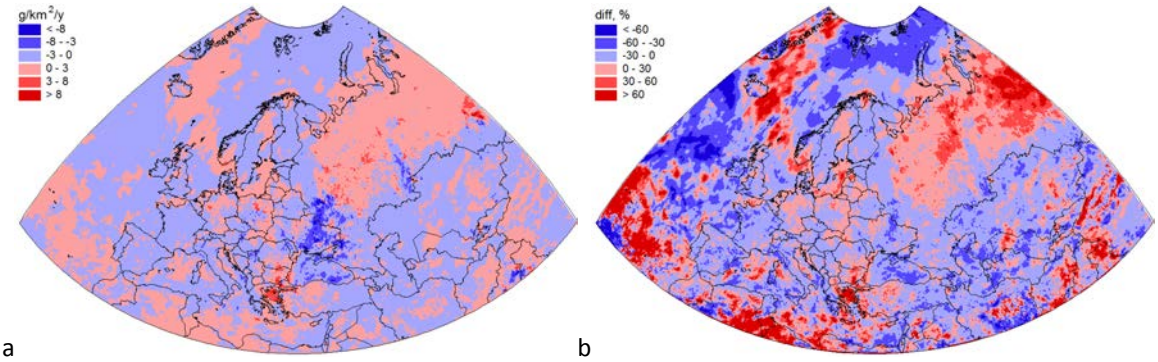

a b

Fig. 4.32. *Absolute (a) and relative (b) difference between Cd total anthropogenic deposition fluxes in 2016 and 2017*

Changes of total anthropogenic deposition to the EMEP countries between 2016 and 2017 vary from -24% (Iceland) to 16% (Bulgaria) (Fig. 4.33). For 85% of countries the changes lie within ±15% limits. In a number of countries the increase or decrease of the deposition in 2017 compared to 2016 can be explained by the corresponding changes of atmospheric precipitation. For example, in the countries of Transcaucasia region (Georgia, Azerbaijan and Armenia) Cd deposition in 2017 are 22%, 21% and

14% lower than the deposition in 2016. The corresponding change of country-mean calculated precipitation amount was 11%, 29% and 28%. Decline of precipitation amounts is confirmed by the results of station-based meteorological observations which record 8% decline in this region [*GSOD*, 2019]. The same can be noted for a number of countries where increase of deposition takes place. For example, increase of deposition in the Netherlands, Malta and Bulgaria by 8%, 13% and 16%, respectively, is accompanied by the corresponding increase of precipitation amounts by 17%, 27% and 10%.

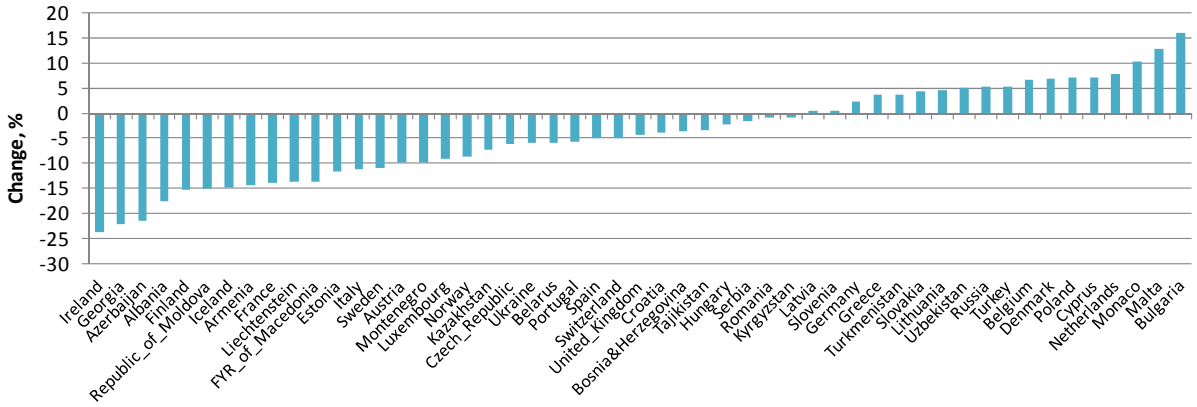

Fig. 4.33. *Changes of total anthropogenic Cd deposition to the EMEP countries between 2016 and 2017. Positive values mean increase, and negative – decrease in 2017 compared to 2016*

However, in a number of countries the sign of deposition change does not coincide with the sign of precipitation change. For example, country-mean precipitation increased in Sweden by 13% and in Norway – by 15% between 2016 and 2017. According to the data from synoptic stations, the increase of observed precipitation amounted to 14% in Sweden and 9% in Norway [*GSOD*, 2019]. However, Cd deposition in these countries declined by 8% and 11%, respectively. In order to explain this, it is important to consider source-receptor relationships for these countries.

Main transboundary contributors of Cd deposition to territory of Sweden in 2017 are Germany (18%), Poland (16%) and Russia (12%) (Fig. 4.34a). National emission sources contribute about 14% to total anthropogenic deposition in Sweden. The ratios between the county's contributions look similar for 2016 and 2017. However, comparison of absolute contributions allows seeing the changes induced by meteorological variability. Deposition of Cd from national sources to Sweden increased by 14 kg (7%). It is agreed with the increase of atmospheric precipitation by 13%. However, atmospheric inputs from Germany, Poland and Russia declined by 31 kg (10%), 44 kg (15%) and 105 kg (37%), respectively (Fig. 4.34b). Over territories of Germany and Poland average increase of precipitation between 2016 and 2017 made up 26 and 11%, respectively. It resulted to 8% increase of Cd deposition from national sources to territories of Germany and Poland. Therefore, less amount of Cd, emitted in Germany and Poland, could participate in transboundary transport and affect neighbouring countries, such as Sweden. Change of deposition from Russian sources to Sweden is much higher than that of precipitation, especially in regions where main emission sources are located. Therefore, changes in transport patterns have to be taken into account.

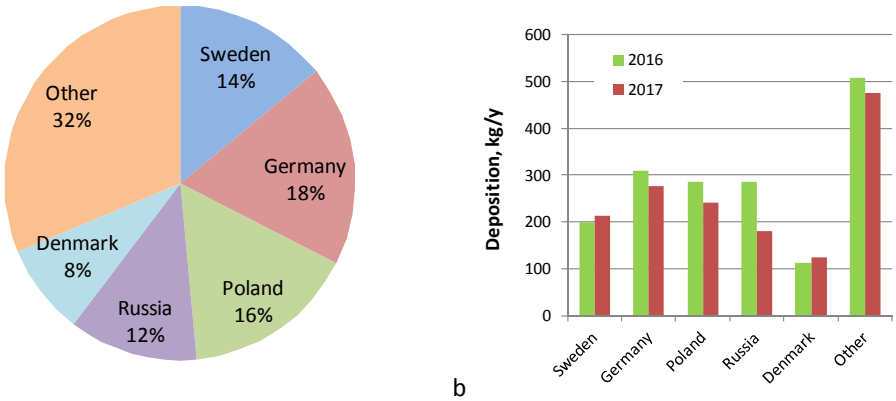

a b

Fig. 4.34. *Main contributors to Cd deposition to Sweden (a) in 2017 and Cd deposition of main contributors to Sweden in 2016 and 2017 (b)*

Atmospheric transport of Cd from main contributors to pollution in Sweden (Germany and Poland) to other EMEP countries also changed from 2016 to 2017. Main countries-receptors of Cd emitted by German sources are Poland, France, the Czech Republic and Russia. From 2016 to 2017 contribution of German emissions to deposition in countries located to the west of Germany (France) declined by almost 40%, while the contributions to counties eastward from Germany (Poland, the Czech Republic and Russia) increased by 25%, 12% and 10%, respectively. The same tendency is noted for Poland: contribution of the Polish sources to deposition in Germany (westward from Poland) declined by 45%, while the contribution to countries located to the east of Poland (Russia, Ukraine, Belarus) increased by 11%, 13% and 18%, respectively.

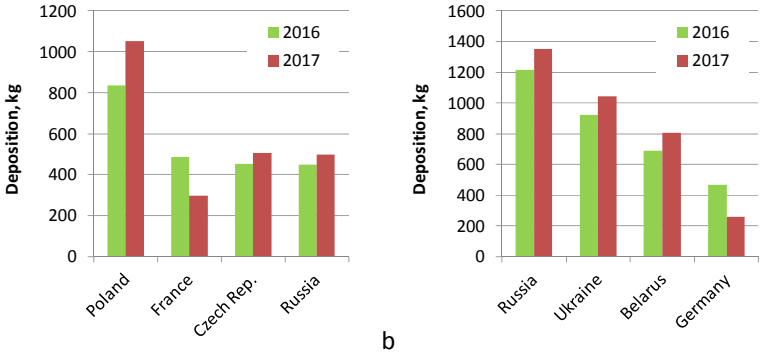

a b

Fig. 4.35. *Main countries-receptors of Cd deposition from sources of Germany (a) and Poland (b) in 2016 and 2017*

Analysis of the example of transboundary pollution aspects in Sweden and its neighboring countries demonstrates that changes in meteorological conditions considerably affect parameters of long-range transport such as import from and export to other countries and deposition from national sources.

Brief overview of changes in heavy metal deposition induced by meteorological factors is exemplified by countries in Scandinavia (Sweden) and Transcaucasia (Armenia, Georgia, Azerbaijan). It is shown that inter-annual meteorological variability considerably affects both total magnitude of atmospheric deposition and contributions of different emission sources to pollution levels in the EMEP countries.

As seen in Section 1.4.2 and Supplementary Data Report [*Ilyin et al*., 2019], significant contribution to deposition in the EMEP countries is caused by secondary sources. Changes of atmospheric input to country's territories from secondary sources are induced by changes of meteorological conditions and changes of parameterizations.

Absolute change of Cd deposition fluxes produced by wind re-suspension in the EMEP region between 2016 and 2017 lies within ±3 g/km^2/y over most part of the modelling domain (Fig 4.36a). Spatial distribution of relative changes is more diverse. The deposition diminished markedly in Finland, the western part of Russia, Belarus, over the Baltic region, Turkey and Caucasus region (Fig. 4.36b). Significant increase is noted for the vast areas of the Asian and some European parts of Russia, Kazakhstan, some regions of Poland, Germany and Spain.

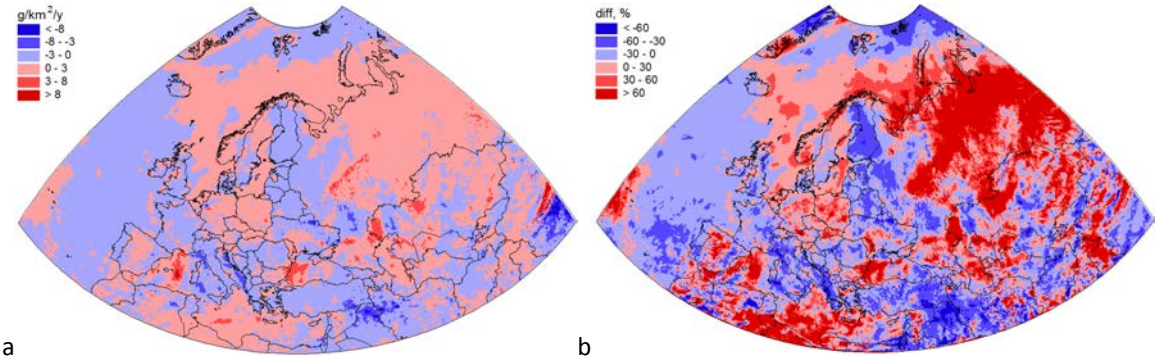

a b

Fig. 4.36. *Absolute (a) and relative (b) difference between Cd deposition fluxes caused by wind re-suspension (original parameterization) in 2016 and 2017*

This spatial distribution of absolute and relative changes of deposition from secondary sources is a result of complex processes of dust suspension, atmospheric transport and scavenging. The main meteorological driving factors for re-suspension are wind velocity and soil moisture. On one hand, due to lack of precipitation soil becomes dry, which favours the re-suspension. On the other hand, precipitation removes pollutants from the atmosphere including those which were previously re-suspended during dry conditions. That is why the increase of precipitation over central (e.g., Germany, Poland) and northern (Norway, Sweden) Europe is accompanied with the increase of deposition of re-suspended Cd. Most likely, this Cd was blown from soils of other regions and reached the central and northern parts of Europe because of long-range transport.

Comparison of modelled and observed concentrations of lead and cadmium revealed that in some parts of Europe (e.g., Belgium, the Netherlands) the model substantially (1.5-2.7 fold) overestimates the observed concentrations. This overestimation was linked with overpredicted contribution of wind re-suspension. In order to reach better agreement between modelled and observed air concentrations, soil enrichment factor was corrected. The correction favoured decrease of the

discrepancies between modelled and observed concentrations. For Cd the mean relative bias changed from 47% to 18%, and for Pb – from 21% to 2% (Fig. 4.37). Correlation coefficients (around 0.8) changed insignificantly.

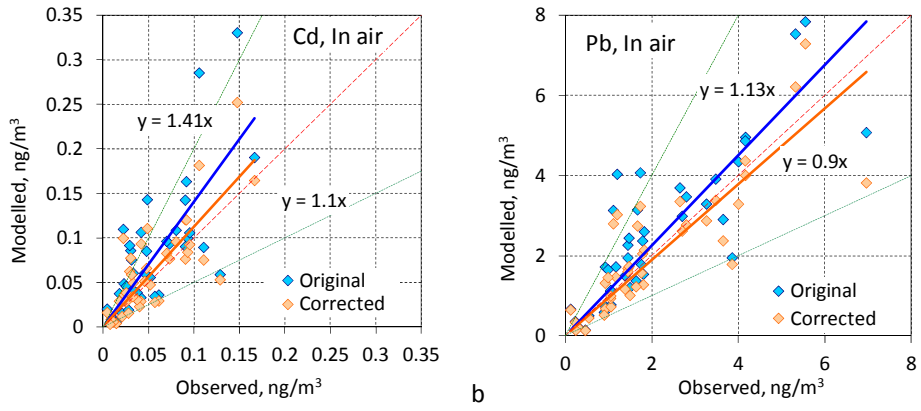

Fig. 4.37. *Modelled and observed mean annual concentrations in air of Cd (a) and Pb (b) at the EMEP stations in 2017*

Correction of soil enrichment factors led to general decline of Pb and Cd deposition from 2016 to 2017. In absolute terms the decline of Cd deposition made up around 3 g/km^2/y over most of the modelling domain (Fig. 4.38a). Relative decline of re-suspension component varied from 30% to 60% over the western and the eastern parts of Europe, while over the central and the southern parts it can exceed 60% (Fig. 4.38b).

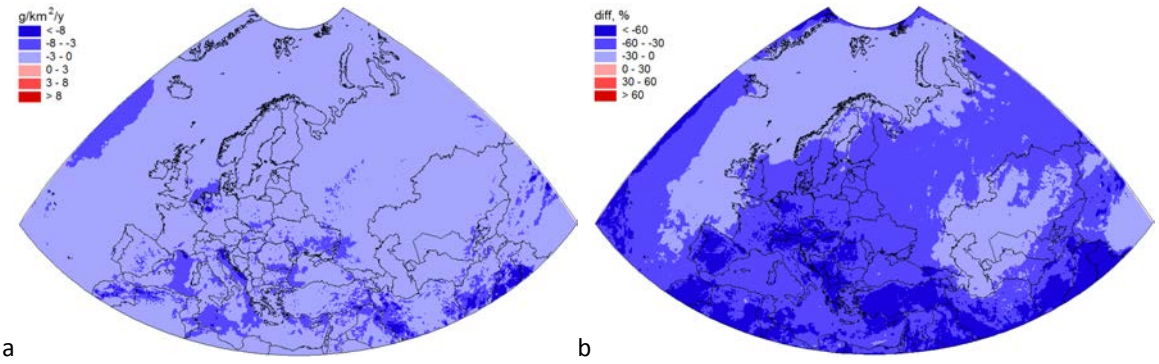

Fig. 4.38. *Absolute (a) and relative (b) difference between Cd deposition fluxes caused by correction of wind re-suspension parameterization from 2016 to 2017*

A third group of sources affecting pollution levels in the EMEP region includes sources (both anthropogenic and secondary) located outside the EMEP domain. In order to take into account these emissions global-scale modelling is performed (see section 3.3.6.). Although Pb and Cd does not tend to disperse globally like Hg, non-EMEP sources make noticeable contribution to Cd and Pb total deposition, especially in countries situated near the borders of the modelling domain.

Absolute changes of Cd deposition from non-EMEP sources between 2016 and 2017 lie within ±3 g/km^2/y over most part of the EMEP region (Fig. 4.39a). Stronger negative change is noted for the eastern part of the Mediterranean region. However, relative differences are more contrasting: over the southern, western, central and the northern parts of Europe, the eastern part of Central Asia as well as over the eastern part of the Mediterranean Sea strong positive change, sometimes exceeding 60%, takes place. Significant negative change (below -60%) of this component is noted for the west of Mediterranean Sea, Italy, south-eastern Europe and the western part of Central Asia (Fig. 4.39b).

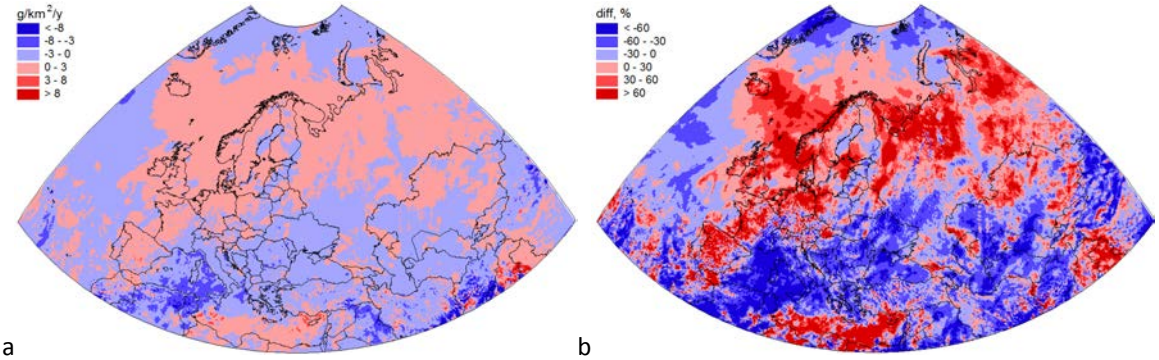

a b

Fig. 4.39. *Absolute (a) and relative (b) difference between Cd deposition fluxes caused non-EMEP sources in 2016 and 2017*

It is important to state that neither model parameterization no emission data has been changed for calculations of 2016 and 2017. Therefore, the changes are caused by variability of meteorological conditions outside the EMEP region. Boundary concentrations of Cd are presented by anthropogenic and re-suspension components. The main component of deposition from non-EMEP sources is re-suspension from bare lands, namely deserts of Africa (Sahara), Arabia and eastern Asia (Gobi). Comparison of global spatial distributions of dust fluxes from these deserts indicates smaller dust suspension in 2017 compared to 2016. Further it would be important to study the sensitivity of the modelling results to boundary concentrations for the new EMEP grid in more detail.

Changes of country –averaged components of Cd deposition fluxes as well as total fluxes over each EMEP country are summarized in Fig. 4.40. In most of the countries the change of deposition relative to total value in 2016 varies from +16 to -30%. As a rule, the changes are induced by inter-annual variability of meteorological conditions which affects deposition from wind re-suspension, anthropogenic or non-EMEP sources. In the majority of the countries decline of deposition is noted. The lowest decline between 2016 and 2017 is noted for Monaco (-67%) followed by Albania (-40%) and Italy (-36%). The decline in these countries and some other countries of Central Asia and southern Europe is mostly caused by decline of contribution of non-EMEP sources. Besides, significant reduction of deposition in Belgium and the Netherlands is explained by correction of wind re-suspension parameterization. The highest relative increase of Cd deposition occurred in Cyprus (around 40%) due to stronger effect of transport of re-suspended Cd from bare lands in 2017 compared to 2016.

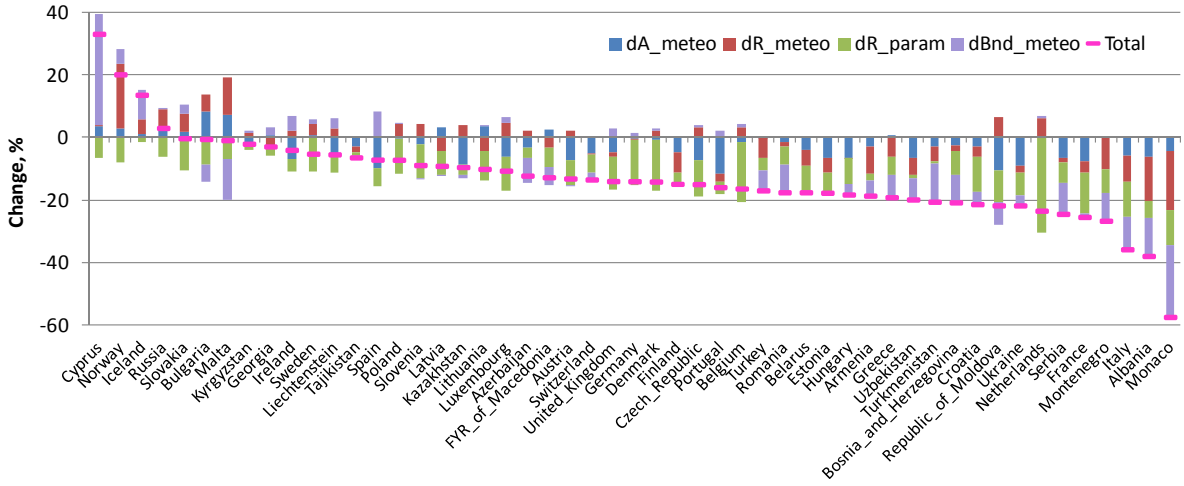

Fig. 4.40. *Changes of total (pink stripes) Cd deposition and its components (bars) relative to total deposition in 2016 between 2016 and 2017. dA_meteo, dR_meteo, dBnd_meteo – changes due to meteorological variability of anthropogenic, re-suspension and non-EMEP components; dR_param – changes because of correction of re-suspension parameterization, Total – total change*

The analysis of pollution changes between 2016 and 2017, exemplified by Cd, demonstrates that ***even in case of constant anthropogenic emissions the overall change of deposition to country as a whole ranges within ±30% over most of the EMEP countries due to variability of meteorological conditions.*** In particular parts of the counties the changes can be even higher. In the central and northern parts of Europe the main changes are related to anthropogenic and re-suspension component. In a number of countries of Central Asia, Caucasus and southern Europe significant contribution to the change is made by non-EMEP component. The role of this component in the pollution of the EMEP countries by heavy metals requires more detailed investigation.

4.5. Analysis of key emission sources and trends of B(a)P pollution in the EMEP countries

High levels and lack of decrease of PAH air concentrations in the EMEP countries during two recent decades have been indicated as an important issue in the Long-term strategy of the Convention. Specific attention in this respect is paid to residential combustion and biomass burning as prevailing PAH emission source categories. The strategy highlights importance of continued scientific research that can support additional efforts for the reduction of unintentional releases of PAHs in the EMEP region and especially for countries of Eastern Europe, the Caucasus and Central Asia. In this respect MSC-E is carried out the analysis of temporal variations of observed B(a)P concentrations, reported national emission data, and model estimates of pollution levels. An overview of the results of this work is presented in this section. The information on trends in B(a)P pollution levels as well as on exceedances of air quality guidelines for B(a)P can be used as a contribution to the activities of the Task Force on Technical and Economic Issues (TF TEI) with regard to the analysis of effectiveness of measures on reduction of PAH pollution.

Evaluation of temporal changes of observed B(a)P pollution levels during the recent decade was performed on the basis of monitoring data of AIRBASE for the period 2007–2017. Statistical approach applied for the analysis of these measurements is described in [*Gusev et al.*, 2017]. In particular, linear regression for the time-series of each site, which reported more than three values of annual mean measured concentrations, was calculated. In order to test statistical significance of B(a)P concentrations changes, 95% confidence intervals for slopes of linear regression (for each monitoring site) were evaluated. In case when all the values of regression slopes from the confidence interval for a given site were positive, it was assumed that statistically significant increase of concentrations at this site took place. On the opposite, when all the values of regression slopes were negative, statistically significant decrease was assumed for the considered site. Preliminary results of the analysis are presented below. More detailed evaluation of temporal changes in the observed and modelled concentrations as well as in the emission data will be presented on further stages of this activity.

Distribution of monitoring sites indicating increase or decrease of annual mean observed B(a)P air concentrations in period 2007-2017 is presented in Fig. 4.41a,b. It can be seen that decreasing B(a)P air concentrations are observed in most of the countries provided measurements of B(a)P pollution levels. At the same time, in four areas, namely, the UK and Ireland, Spain, Northern Italy as well as Poland, Czech Republic, Germany, and Austria increasing levels of B(a)P concentrations can be seen.

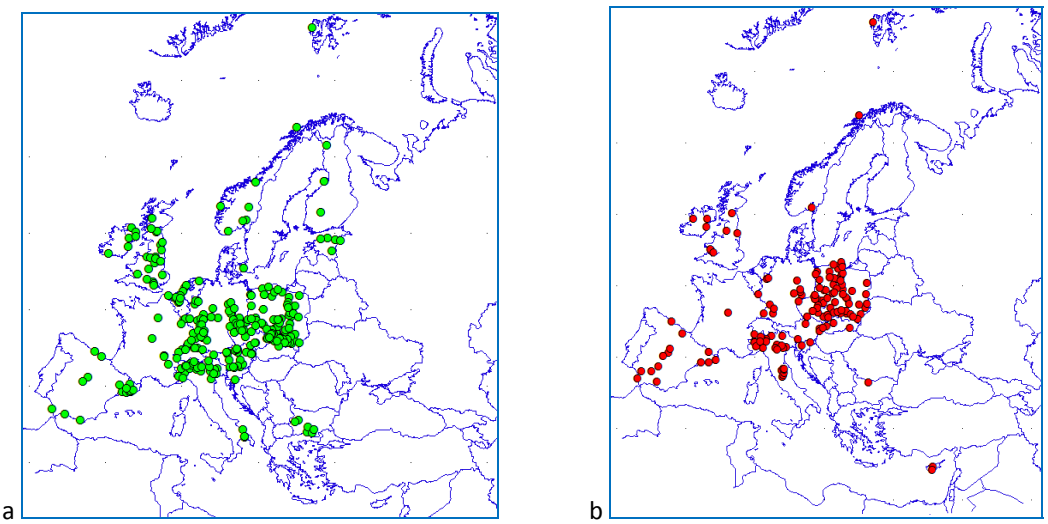

Fig. 4.41. *Locations of AIRBASE monitoring sites, reported decreasing (a) or increasing (b) trends of annual mean B(a)P air concentrations in period 2007-2017 (decrease is shown using green color, increase is shown using red color)*

Number of monitoring sites reported increasing or decreasing trends of annual mean B(a)P air concentrations in period 2007-2017 is presented in Fig. 4.42. Data of about 67% of the sites indicate declining of B(a)P concentrations in the EMEP countries. For about 46% of the sites these changes can be considered as statistically significant. At the same time, about 33% of the sites reported increasing B(a)P concentrations and 22% of them can be considered as statistically significant. Among

the three different types of monitoring site locations, slightly higher amount of increasing pollution levels was reported by the rural monitoring sites (Fig. 4.42a).

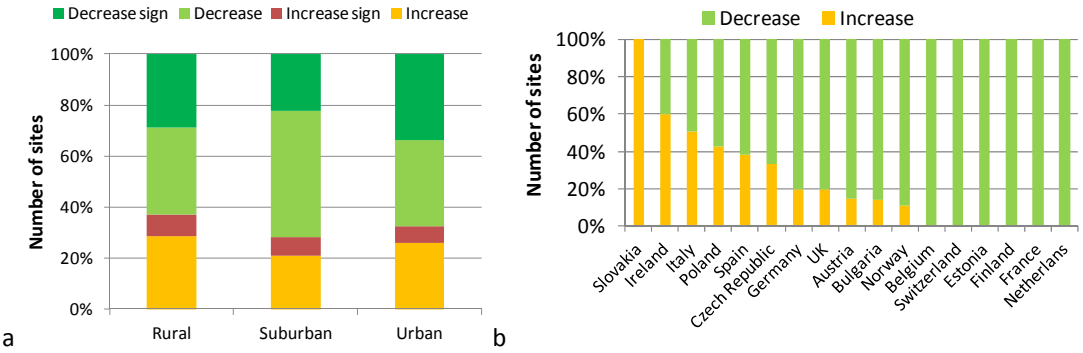

Fig. 4.42. *Number of AIRBASE monitoring sites (in %), indicated increase (light red) or decrease (light green) of annual mean B(a)P air concentrations in European countries in period 2007-2017 differentiated by site type (a) and by countries (b). Amount of sites indicated statistically significant changes is shown in bright green/red colours*

In Fig. 4.42b the fractions of growing and declining concentrations is shown for selected European countries. According to these data in most of the countries both decreasing and increasing tendencies in the reported B(a)P concentrations can be seen. In the majority of countries the levels of B(a)P concentrations are declining. However, in some of the countries, for example, in Slovakia, Ireland, Italy, Poland, Spain, and the Czech Republic a percentage of time-series with increasing pollution levels is relatively high (more than 20%).

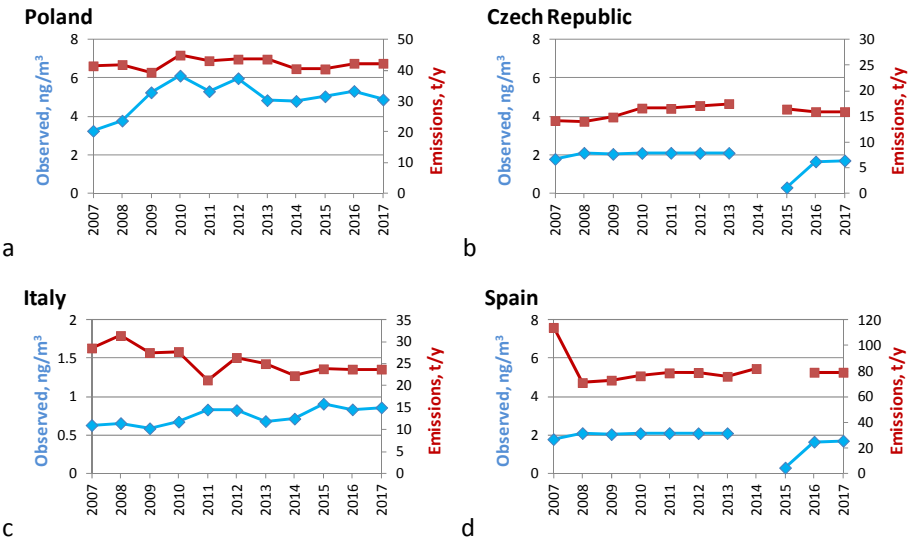

Fig. 4.43. *Temporal variations of averaged B(a)P annual mean air concentrations in the selected EMEP countries in period 2007-2017 in comparison with variations of annual emissions*

Time-series of observed B(a)P air concentrations in the EMEP countries can be compared with temporal variations of the officially reported national emission data. To achieve comparability of the regression analysis results for measurements and emissions, data on emissions were used for the same years as available data on observed B(a)P concentrations. In Fig. 4.43 temporal variations of averaged B(a)P annual mean air concentrations in the selected EMEP countries are compared with the variations of annual emissions. It can be seen that the period from 2007 to 2017 is generally characterized by relatively small temporal variations of both observed B(a)P concentrations and emissions. In particular, B(a)P emissions in the countries of Central Europe, for example, Poland and the Czech Republic, were mostly on the same level or slightly increased from 2007 to 2017. According to the reported emission data the releases of B(a)P in Italy and Spain tended to decrease during this period. At the same time time-series of the observed concentrations indicate the increase of concentrations in Italy and almost no changes in concentrations for Spain.

Preliminary model evaluation of long-term changes of B(a)P pollution levels in the EMEP countries was performed for the same period of time on the basis of the most recent data on B(a)P emissions. In Fig. 4.44 the model predictions for the locations of AIRBASE monitoring sites are illustrated with indications of increasing or decreasing annual mean observed B(a)P air concentrations in period 2007-2017. The modelling results are generally comparable with temporal variations of the observed B(a)P air concentrations (see Fig. 4.41).

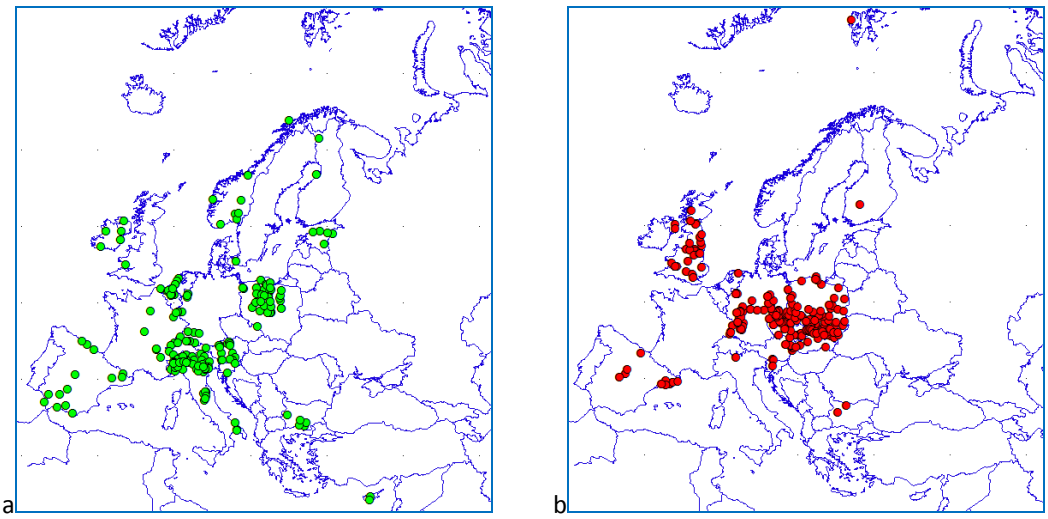

Fig. 4.44. *Locations of AIRBASE monitoring sites for which model simulations indicated decrease (a) or increase (b) of B(a)P air concentrations in the period 2007-2017. (Decrease of concentrations is shown using green color, and increase of concentrations is shown using red color).*

In particular, for most of the countries the decline of B(a)P air concentrations in the locations of monitoring sites is simulated. The increase of concentrations is estimated for the countries of Central Europe, Germany, the UK, and Spain.

Statistical analysis of model predictions in comparison with the measurement data is given in Table 4.9 and exemplified by four countries, namely, Poland, the Czech Republic, Italy, and Spain. It can be

seen that the number of site locations, showing increase of B(a)P concentrations according to calculation results, is higher than that according to measurement data (with the exception of Italy). Particularly, the model predictions indicated increasing B(a)P concentrations for larger amount of monitoring site locations in Germany and the UK. In case of Italy, contrary to monitoring data, the model results for most of monitoring sites indicate decrease of B(a)P concentrations. The latter discrepancy can be explained by the difference between the observed trends in B(a)P concentrations and temporal variations of emissions in the corresponding grid cells as well as effect of temporal variations of transboundary transport from other emission sources.

Table 4.9. *Comparison of number of locations of monitoring sites for which increase or decrease of modelled and observed B(a)P air concentrations in period 2007-2017 for the selected EMEP countries is evaluated*

Country	***Total number of sites***	***Increase Observed***	***Modelled***	***Decrease Observed***	***Modelled***
Poland	126	54	86	72	40
Czech Republic	33	11	33	22	0
Spain	34	13	20	21	14
Italy	57	29	1	28	56

Thus, changes of the PAH levels in the EMEP countries taken place in the last decade requires further analysis. First of all, special attention has to be paid to the modelled and observed changes at the particular monitoring stations taking into account statistical significance of the changes. Source-receptor apportionment is another aspect which should be accounted for in the analysis. In particular, contributions national and foreign emissions as well as emission sectors to PAH pollution levels will be evaluated to carry out more detailed analysis of temporal trends in PAH air concentrations.

5. COOPERATION

Scientific co-operation is an important part of MSC-E activities aimed at support and improvement of heavy metal and POP pollution assessment within EMEP as well as dissemination of the assessment results to wider international audience. For this purpose the Centre collaborates with Subsidiary bodies to the Convention and other international organizations.

5.1. Subsidiary bodies of the Convention

Co-operation with Subsidiary bodies of the Convention includes collaborative work with the Task Force on Measurements and Modelling (TFMM) and the Task Force on Techno-Economical Issues (TF TEI).

5.1.1. Task Force on Measurements and Modelling

MSC-E continued cooperation with TFMM. The Centre participated in the TFMM meeting held in May, 2019 in Madrid, Spain. Information on recent activities of MSC-E in the field of the model assessment of heavy metals and POPs was presented. In particular, progress in the atmospheric Hg chemistry research and the results of the model study of Hg atmospheric chemistry were demonstrated. Different mechanisms of Hg oxidation and photo-reduction were tested. Besides, approaches of multi-media modelling with regard to Hg global cycling aimed at improvement of assessment of Hg levels in the EMEP region were outlined.

Analysis of heavy metal pollution levels in hot spots of the EMEP region, using modelling results and monitoring data was undertaken. Modelled concentrations in air were compared with the available EMEP data, monitoring results from AIRBASE data base, and modelling results simulated by other regional-scale models. Special attention was paid to the contribution of main emission sectors to simulated concentrations in air. Furthermore, initial steps of country-scale study of heavy metal pollution levels in Germany were overviewed. Information on national emission and monitoring data provided by German experts was analyzed. Pilot results of multi-scale (global, regional, national) modelling were presented. Further steps of the country-scale study were announced with focus on detailed evaluation of the modelling results and analysis of the discrepancies between modelled and observed levels.

The outcome of country-specific case study on B(a)P pollution in Europe, performed in co-operation with national experts of France and Spain, was shown. Current stage of the study was focused on the analysis of modelling approach applied for B(a)P and evaluation of alternative model parameterizations. In particular, different gas-particle partitioning and degradation schemes were tested using the models GLEMOS and CHIMERE. Results of the test model simulations showed critical role of parameterization of B(a)P degradation in the atmosphere for the pollution assessment. Thus, further improvement of the model predictions of B(a)P concentrations can be associated with the refinement of the model description of B(a)P degradation. Besides, particular attention should also be given to the description of gas-particle partitioning process taking into account multi-phase

content of aerosol particles in the atmosphere. Further activities in the framework of B(a)P case study will include country-scale assessment of B(a)P pollution in Poland and multi-model analysis of B(a)P long-range transport within the EMEP EuroDelta-Carb intercomparison exercise in co-operation with national experts and TFMM.

In the framework of cooperation with the WGE new types of the model output information were proposed to facilitate evaluation of the effects. This output includes deposition of heavy metals and POPs to watersheds and information on enrichment of atmospheric particulate matter with toxic pollutants (heavy metals and POPs). Finally, plans of future work in the fields of research and development, country-specific studies in EMEP countries, and cooperation with the effects community for 2020/2021 were formulated.

5.1.2. Task Force on Techno-Economical Issues

Analysis of effectiveness of measures on reduction of PAH pollution is an important activity under Convention that is performed by the Task Force on Technical and Economic Issues (TF TEI). The Long-term Strategy of the Convention emphasized the need of continued scientific research that can support additional efforts for the reduction of unintentional releases of PAHs in the EMEP region and especially for countries of Eastern Europe, the Caucasus and Central Asia. MSC-E carried out evaluation of temporal trends in the observed B(a)P concentrations and reported national emission data. Besides, model assessment of temporal variations of PAH pollution levels and contributions of key groups of emission sources is being performed. An overview of the results of this work is presented in this report. The information on trends in B(a)P pollution levels as well as on exceedances of air quality guidelines for B(a)P in the EMEP region can be used as a contribution to the activities of TF TEI.

In the framework of co-operation with TF TEI MSC-E took part in the TF TEI Workshop aimed at promoting ratification of the CLRTAP Protocols by the EECCA countries. The Centre informed the countries about variety of information products on emissions, monitoring, and modelling generated within EMEP and aimed at support of national activities in pollution reduction and implementation of the Protocols. In particular, available information on transboundary pollution by heavy metals and POPs of the EMEP countries was illustrated with focus on the countries of the EECCA region. Problems and challenges of the pollution assessment in this region were formulated.

5.2. International organizations

The Centre actively participates in cooperation with other international organizations and programmes to facilitate information exchange and improve quality of the pollution assessment both in the EMEP region and on wider scales. This year international co-operation was focused on scientific collaboration with the Arctic Monitoring and Assessment Programme as well as with the Stockholm and Minamata Conventions.

5.2.1. Arctic Monitoring and Assessment Programme

EMEP has successful experience of long-term co-operation with the Arctic Monitoring and Assessment Programme (AMAP), which includes participation in joint assessments and projects. Specifically, MSC-E took part in a number of the AMAP Assessments of the Arctic pollution with heavy metals and POPs [*AMAP*, 2004, 2005; 2011]. Besides, joint collaboration with the UN Environment on the Global Mercury Assessments was among priority directions of both international bodies.

Currently, MSC-E participates in two new AMAP Assessments on the Arctic pollution by Hg and POPs providing the results of model simulations and contributing to preparation of the reports. Figure 5.1 illustrates information on Hg pollution of the Arctic, which is based on the multi-model simulations performed as a part of the Global Mercury Assessment 2018 [*UN Environment*, 2019]. Four chemical transport models took part in the study – GLEMOS (EMEP/MSC-E), GEOS-Chem (Massachusetts Institute of Technology, USA), GEM-MACH-Hg (Environment and Climate Change Canada, Canada), ECHMERIT (Institute of Atmospheric Pollution Research, Italy). Mercury deposition levels in the Arctic vary from 12 g/km^2/y in Northern Scandinavia, Alaska and the Labrador Sea to less than 1 g/km^2/y over central Greenland (Fig. 5.1a). Generally, Hg deposition over the Arctic Ocean is lower than deposition over terrestrial territories. In total, Hg deposition to the Arctic consists of almost equal contributions of direct anthropogenic sources (46%) and natural/legacy sources (54%). The largest anthropogenic contribution is made by industrial sources (21%), which are followed by artisanal and small-scale gold mining (ASGM, 16%), power generation (6%), and internal use and product waste (3%).

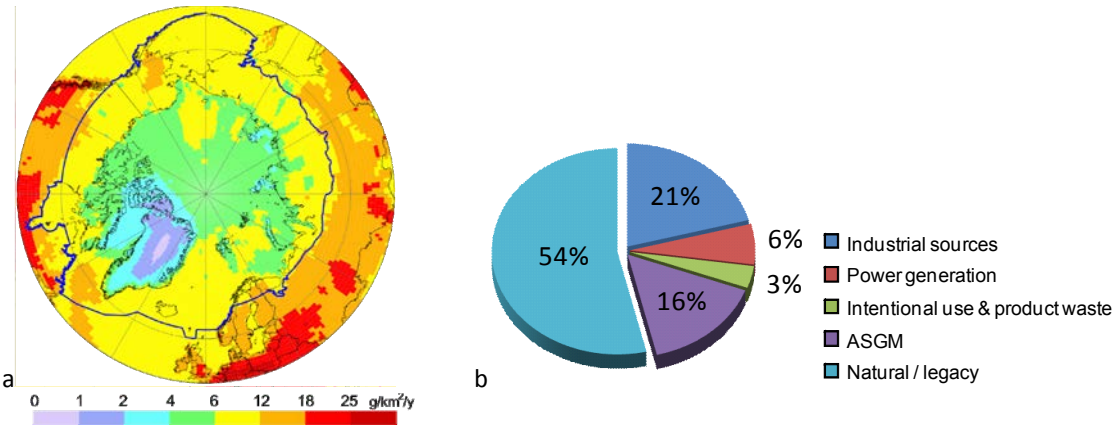

Fig. 5.1. *Spatial distribution (a) and sectoral composition of Hg deposition (b) in the Arctic in 2013*

A meeting of AMAP POPs expert group was held in Stockholm (Sweden) in April 2019 to scope updating of the AMAP assessment of POPs in the Arctic and their interactions with climate change. Participants of the meeting provided updated information on studies of POPs and emerging compounds in the Arctic region. MSC-E presented results of model evaluation of long-range transport of selected POPs and contributions of the EMEP countries to deposition in the Arctic region. Besides, possible topics of further co-operation between MSC-E and AMAP were outlined and

discussed. Results of the model assessment of the Arctic region pollution by selected POPs are planned to be included to the being prepared AMAP POP assessment.

5.2.2. Helsinki Commission

In the framework of cooperation with the Helsinki Commission, MSC-E performs regular evaluation of airborne pollution load of heavy metals and POPs to the Baltic Sea. This work is carried out in accordance with the Memorandum of Understanding between the Baltic Marine Environment Protection Commission (HELCOM) and the United Nations Economic Commission for Europe (UN ECE) and is based on the long-term EMEP/HELCOM contract.

This year long-term variations of Cd, Hg, B(a)Pm and PCB-153, deposition fluxes to the Baltic Sea were estimated for the period 1990-2016. Along with this, source apportionment of annual deposition was carried out for 2016. Results of the assessment were summarized in the Joint report of the EMEP Centres for HELCOM [*Gauss et al*., 2018] and presented in the indicator fact sheets, published on the HELCOM website [*http://www.helcom.fi*].

Anthropogenic emissions of Cd, Hg, B(a)P, and PCB-153 in the HELCOM countries declined from 1990 to 2016 by 37%, 45%, 38%, and 78%, respectively. Russia, Poland, and Germany were the main contributors to the emissions among the HELCOM countries in 2016. Their share in total emission of the HELCOM countries exceeded 75% for PCB-153 and 90% for the other three pollutants. The most noticeable drop of Cd, Hg, and B(a)P emissions took place in the beginning of 1990s, while during the subsequent period of time the changes were less significant and were almost levelled off (Fig. 5.2a). Contrary to this, decline of PCB-153 emissions was more substantial and took place during the whole period 1990-2016.

Model assessment of long-term variations of pollution indicated considerable decrease of atmospheric deposition of B(a)P (by 67%), Cd (by 61%), and PCB-153 (by 61%) to the Baltic Sea in the period 1990-2016, whereas Hg deposition declined within this period by only 34% (Fig. 5.2b). It is seen that deposition of selected pollutants are subject of noticeable inter-annual variations that reflects the influence of changes of meteorological conditions from year to year (e.g. changes of atmospheric transport pathways, precipitation amount). The decrease of deposition varies substantially among different sub-basins of the Baltic Sea. In particular, the largest changes of Cd deposition took place in the Bothnian Bay sub-basin (by 70%), Hg deposition in the Sound sub-basin (by 60%), B(a)P and PCB-153 in the Western Baltic sub-basin (by 70%).

Anthropogenic emission sources of the HELCOM countries contributed to annual Cd, Hg, B(a)P, and PCB-153 deposition to the Baltic Sea in 2016 about 38%, 13%, 73%, and 37%, respectively. Russia, Poland, and Denmark were the main contributors of anthropogenic Cd, Hg, and B(a)P deposition to the Baltic Sea, whereas for PCB-153 most significant contributions were made by Sweden and Finland. Along with anthropogenic emissions significant contribution (more than 50%) to Cd, Hg, and PCB-153 deposition to the Baltic Sea was made by secondary emission sources (e.g. re-emission from soil and sea water compartments) as well as by the long-range transport from the emission sources located outside the HELCOM countries.

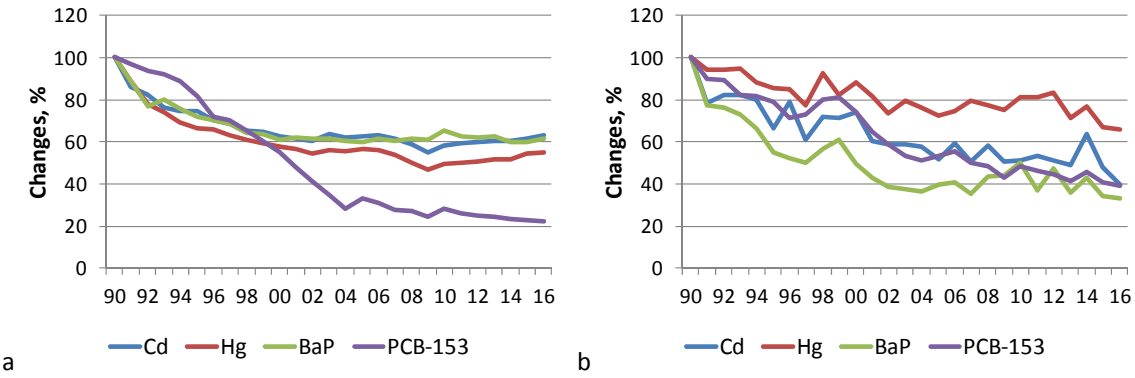

Fig. 5.2. *Relative changes of annual total emissions of HELCOM countries (a) and annual atmospheric Cd, Hg, B(a)P, and PCB-153 deposition to the Baltic Sea in the period 1990-2016 (b)*

The information on airborne input of Cd, Hg, benzo(a)pyrene and PCB-153 to the Baltic Sea was presented and discussed during the Ninth Meeting of the Working Group on Reduction of Pressures from the Baltic Sea Catchment Area (HELCOM PRESSURE 9-2018) held in Riga, Latvia, in October 2018. In particular, it was noted that airborne deposition of Hg remained one of the main pathway of this contaminant to the Baltic Sea environment that required further assessment of their sources and long-term changes.

5.2.3. UN Environment and Minamata Convention

MSC-E continuously co-operates with the United Nations Environment Programme (UN Environment) on Hg pollution assessment. Mercury is a global pollutant that causes increasing public concern about the adverse effects on human health and biota. To support the international negotiation process aimed at Hg pollution reduction the UN Environment coordinated preparation of a series of Global Mercury Assessments (GMA) [*UNEP*, 2002; *AMAP/UNEP*, 2008; *AMAP/UNEP*, 2013; *AMAP/UNEP*, 2015; *UN Environment*, 2019]. MSC-E has been involved in all the assessments sharing information on Hg pollution and coordinating activities on global scale modelling. The work on the most recent Global Mercury Assessment 2018 has come to the end this year leading to the public release of the Summary Report that contains the main findings on current status and changes of Hg pollution on a global scale [*UN Environment*, 2019]. MSC-E took part in the assessment coordinating activities of the international group of experts on modelling of Hg fate and transport in the atmosphere and pollution on global and regional scales.

In addition, MSC-E contributed to the work of the Ad hoc Technical Expert Group on Effectiveness Evaluation of the Minamata Convention providing information on relevant activities and gained experience within the LRTAP Convention. In particular, the Centre submitted information on approaches used within CLRTAP to assess Hg atmospheric pollution in the EMEP region by means of monitoring and modelling and support evaluation of the adverse effects on human health and biota.

5.2.4. Stockholm Convention

MSC-E continued co-operation and data exchange with the Stockholm Convention on POPs. Collection and refinement of national POP emission inventories under the Stockholm Convention provides additional information for the evaluation of emissions of the EMEP countries as well as data for the updating of the scenario of global PCDD/F emission. In the framework of this activity MSC-E analysed and implemented the data on PCDD/F emissions, compiled under the Stockholm Convention (SC), for the assessment of their environmental pollution on the global scale.

In particular, updated emission scenario of PCDD/F emissions was constructed applying the methodology of [*Wang et al.*, 2016] as described in [*Gusev et al.*, 2018]. The methodology is based on the regression analysis of PCDD/F releases to the environmental media (atmosphere, soil) and the following factors, namely, gross national input, country area, gross national input per capita, and CO2 emissions per million of gross national product. Scenario of gridded annual PCDD/F emissions was used for the evaluation of global scale transport and fate of PCDD/Fs for 2017. The Fig. 5.3 illustrates spatial distribution of global scale PCDD/F emissions and model estimates of PCDD/F deposition fluxes for 2017.

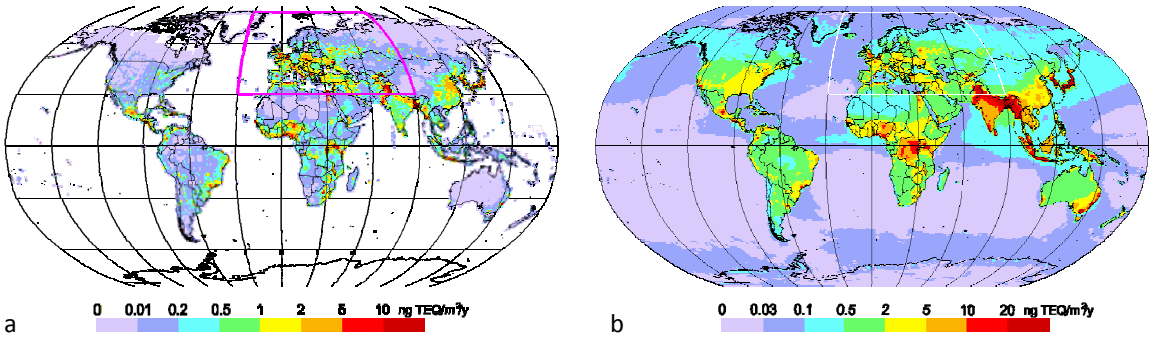

Fig. 5.3. *Spatial distribution of global annual emissions of PCDD/Fs used for global scale model simulations (a) and annual modelled deposition fluxes of PCDD/Fs estimated for 2017 (b)*

Collaboration with experts, involved in the UNEP Stockholm Convention Global Monitoring Plan (GMP) activities on global-scale monitoring of POP concentrations in air and other compartments, is another important activity for the evaluation of POP intercontinental transport and long-term changes of pollution. Possible topics of further co-operation in this field were discussed between MSC-E and GMP experts during the meeting of AMAP POP expert group held in Stockholm (Sweden) in April 2019.

6. MAIN CHALLENGES AND DIRECTIONS OF FUTURE RESEARCH

The Status Report summarizes EMEP activities in the field of heavy metal and POP pollution assessment in 2019. It contains information on heavy metal and POP pollution levels, transboundary transport, ecosystem-specific deposition, atmospheric loads to watersheds etc. It also discusses research and development activities aimed at improvement of the modelling tools, cooperation with national experts of the EMEP countries, CLRTAP Subsidiary Bodies, and international organizations. Main challenges of heavy metal and POP pollution assessment and directions of future research are outlined below.

- Downscaling of pollution assessment from regional to national and local scales is performed within a framework of country-specific studies in co-operation with national experts and involving variety of national data. A new study has been initiated for Germany that will include detailed assessment of Hg, Pb and Cd pollution in the country during the period 2014-2016, evaluation of national emissions using modelling results and observations, development of recommendations for improvement of the assessment quality both on national and regional scales. Besides, detailed assessment of PAH pollution in Poland will be launched with emphasis on evaluation of exceedances of air quality guidelines and testing of the country's emissions.

- Air pollution by toxic PAHs is recognized as a serious problem in some EMEP countries, especially, in Central and Eastern Europe. To further improve the quality of PAH model assessment, a multi-model analysis for B(a)P pollution is planned in the framework of the EMEP EuroDelta-Carb intercomparison exercise in co-operation with TFMM and national experts. Detailed assessment of contributions of key emission source categories and exceedances of the EU and WHO target levels in the EMEP region will be continued to support activities of TF Health and WGE as well as to contribute to the analysis of the effectiveness of the POP Protocol in co-operation with TFTEI.

- Mercury pollution remains to be a topic issue both in the EMEP countries and at the broader international level. The general concern about the Hg pollution problem is accompanied by incomplete knowledge on Hg behaviour and cycling in the environment. In particular, there are gaps in understanding of Hg chemical transformations in the atmosphere. Therefore, the major mechanisms of Hg oxidation and photo-reduction in the atmosphere will be further studied and evaluated to improve quality of Hg pollution assessment. Besides, the multi-media approach to Hg simulations in GLEMOS will be further developed.

- Mercury and some POPs (HCB, PSDD/Fs, PCBs) are characterized by long-residence time in the atmosphere as well as by cycling and accumulation in various environmental media. Therefore, assessment of Hg and POP pollution in the EMEP countries should take into account contribution of global and secondary sources along with direct anthropogenic emissions from regional sources. Besides, relative importance of these source types can change in time dramatically due to reduction of anthropogenic emissions. Attribution of long-term changes of Hg and POP pollution to regional and extra-regional (global and secondary) sources will be performed using the multi-media modelling system (GLEMOS) and available global Hg and POP emissions inventories (e.g. EDGAR, UNEP).

- Evaluation of adverse effects of heavy metal and POP pollution on human health and ecosystems is of high importance. MSC-E will continue long-term co-operation with WGE focusing on joint analysis of heavy metal measurements in moss in co-operation with ICP-Vegetation, support of ICP-Waters with information on Hg deposition to water bodies/watersheds, data exchange with TF Health on B(a)P pollution levels and exceedances of air quality guidelines.

REFERENCES

Aas W., Breivik K., Nizzetto P.B. [2019] Heavy metals and POP measurements. EMEP/CCC-Report 3/2019.

Achilleos S., Evans J.S., Yiallouros P.K., Kleanthous S., Schwartz J., and Koutrakis P. [2014]. PM10 Concentration levels at an urban and background site in Cyprus: The impact of urban sources and dust storms. *Air Waste Manag Assoc*. 2014 December , 64(12): 1352–1360.

ALS [2013] Benzo(a)pyrene toxic equivalence quotient (TEQ) and aggregate organochlorine pesticides parameters, *EnviroMail* No. 59 Re-Release, July, 2013.

AMAP [2004] Persistent Toxic Substances, Food Security and Indigenous Peoples of the Russian North. Final Report. Arctic Monitoring and Assessment Programme (AMAP), Oslo, 2004. https://www.amap.no/documents/doc/persistent-toxic-substances-food-security-and-indigenous-peoples-of-the-russian-north.-final-report/795

AMAP [2005] AMAP Assessment [2002] Heavy Metals in the Arctic. Arctic Monitoring and Assessment Programme (AMAP), Oslo, Norway. xvi + 265 pp.

AMAP [2005] AMAP Assessment Report: Arctic pollution Issues. Arctic Monitoring and Assessment Programme (AMAP), Oslo, Norway. xvi + 859 pp.

AMAP [2011] AMAP assessment 2011: mercury in the Arctic. Oslo, Norway: Arctic Monitoring and Assessment Programme (AMAP); (pp. xiv +193).

AMAP/UNEP [2008] Technical Background Report to the Global Mercury Assessment. Arctic Monitoring and Assessment Programme / UNEP Chemicals Branch. 159 pp. http://www.unep.org/chemicalsandwaste/LinkClick.aspx?fileticket=gwLbyNhGtn8%3d&tabid=3593&language=en-US. Accessed on June 28, 2016.

AMAP/UNEP [2013] Technical Background Report for the Global Mercury Assessment 2013a. Arctic Monitoring and Assessment Programme, Oslo, Norway / UNEP Chemicals Branch, Geneva, Switzerland, vi + 263 pp., available at: http://www.amap.no/documents/download/1265 (last access: 10 April 2018).

AMAP/UNEP [2015] Global Mercury Modelling: Update of Modelling Results in the Global Mercury Assessment 2013. Arctic Monitoring and Assessment Programme, Oslo, Norway/UNEP Chemicals Branch, Geneva, Switzerland. iv + 32 pp.

Amos H.M., Jacob D.J., Holmes C.D., Fisher J.A., Wang Q., Yantosca R.M., Corbitt E. S., Galarneau E., Rutter A. P., Gustin M.S., Steffen A., Schauer J.J., Graydon J.A., Louis V.L. St., Talbot R.W., Edgerton E.S., Zhang Y. and Sunderland E.M. [2012] Gas-particle partitioning of atmospheric Hg(II) and its effect on global mercury deposition, *Atmos. Chem. Phys.,* 12, 591–603, doi:10.5194/acp-12-591-2012.

Ariya P.A., Amyot M., Dastoor A., Deeds D., Feinberg A., Kos G., Poulain A., Ryjkov A., Semeniuk K., Subir M. & Toyota K. [2015] Mercury Physicochemical and Biogeochemical Transformation in the Atmosphere and at Atmospheric Interfaces: A Review and Future Directions, *Chemical Reviews* 115(10), 3760-3802.

Balabanov N., Shepler B., Peterson K. [2005] Accurate global potential energy surface and reaction dynamics for the ground state of HgBr2, *J. Phys. Chem*. A, 109, 8765—8773.

Ballschmlter K. and R. Wlttllnger [1991] Interhemisphere Exchange of Hexachlorocyclohexanes, Hexachlorobenzene, Polychlorobiphenyls, and 1 ,I ,I-Trichloro-2,2-bis(p -chlorophenyl)ethane in the Lower Troposphere. *Environ. Sci. Technol*., 25, 1103-1111.

Barber J.L., Sweetman A.J., van Wijk D., Jones K.C. [2005] Hexachlorobenzene in the global environment: emissions, levels, distribution, trends and processes. *Science of the Total Environment*. 349:1–44. doi: 10.1016/j.scitotenv.2005.03.014.

Beck J. and Hansen K.E. [1974] The degradation of quintozene, pentachlorobenzene, hexachlorobenzene and pentachloroaniline in soil. *Pestic Sci* 5: 41-48.

Beyer A., D. MacKay, M. Matthies, F. Wania, and E. Webster [2000] Assessing Long-Range Transport Potential of Persistent Organic Pollutants. *Environ. Sci. Technol*., 2000, 34(4), 699-703.

Blunden J., D.S. Arndt and G. Hartfield, Eds. [2018]. State of the Climate in 2017. *Bull. Amer. Meteor. Soc*., 99 (8), Si–S310, doi:10.1175/2018BAMSStateoftheClimate.1.

Bogdal C., C. E. Müller, A. M. Buser, M. Quante, Z. Wang, M. Scheringer, A. C. Gerecke, P. Schmid, M. Zennegg, M. MacLeod, K. Hungerbühler [2014] Emissions of Polychlorinated Biphenyls, Polychlorinated Dibenzo-p-dioxins, and Polychlorinated Dibenzofurans during 2010 and 2011 in Zurich, Switzerland. *Environ. Sci. Technol., 48, 482−490*.

Breivik K., R. Alcock, Y.-F.Li, R. E. Bailey, H. Fiedler, J.M. Pacyna [2004] Primary sources of selected POPs: regional and global scale emission inventories. *Environmental Pollution,* 128, 3–1.

Breivik K., Sweetman A., Pacyna J.M., Jones K.C. [2007] Towards a global historical emission inventory for selected PCB congeners - A mass balance approach-3. An update. *Science of the Total Environment*, vol. 377, pp. 296-307.

Brubaker, W.W. and Hites, R.A. [1998] OH reaction kinetics of gas-phase б- and r- hexachlorocyclohexane and hexachlorobenzene. *Env Sci Technol* 32: 766-769.

CLEEN [2012] Euro POP Final Report. Published by the EUROPOP Working Group. Chemical Legislation European Enforcement Network. http://www.cleen-europe.eu/file/download/120/Dokument1.pdf.

Coburn S., B. Dix, E. Edgerton, C. D Holmes, D. Kinnison, Q. Liang, A. Ter Schure, S. Wang, and R. Volkamer [2016] Mercury oxidation from bromine chemistry in the free troposphere over the southeastern US, *Atmospheric Chemistry and Physics*, 16(6), 3743–3760, doi:10.5194/acp-16-3743-2016.

Couvidat F. and K. Sartelet [2015] The Secondary Organic Aerosol Processor (SOAP v1.0) model: a unified model with different ranges of complexity based on the molecular surrogate approach. *Geosci. Model Dev*., 8, 1111–1138. doi:10.5194/gmd-8-1111-2015.

Dachs J. and S. J.Eisenreich [2000] Adsorption onto Aerosol Soot Carbon Dominates Gas-Particle Partitioning of Polycyclic Aromatic Hydrocarbons. *Environ. Sci. Technol*. 2000, 34, 3690-3697.

De Vries W, Groenenberg J.E. and Posch M. [2015b] Mass balance approaches to assess critical loads and target loads of metals for terrestrial and aquatic ecosystems. pp. 207-222. In: Critical loads and dynamic risk assessments. Nitrogen, acidity in terrestrial and aquatic ecosystems. Edited by W. de Vries, J-P. Hettelingh and M. Posch. *Envitornmental pollution* 25, Springer.

De Vries W., Posch M., Sverdrup H.U., Larssen T., de Wet H.A., Bobbink R. and Hettelingh J-P. [2015a] Geochemical indicators for use in the computation of critical loads and dynamic risk assessment. pp 15-58. In: Critical loads and dynamic risk assessments. Nitrogen, acidity in terrestrial and aquatic ecosystems. Edited by W. de Vries, J-P. Hettelingh and M. Posch. *Envitornmental pollution* 25, Springer.

De Wit H.A., Hettelingh J-P., and Harmens H. [2015] Trends in ecosystem and health responses to long-range transported atmospheric pollutants. Norwegian Institute for Water Research, 92p.

Delgado-Saborit J.M., C. Stark, R.M. Harrison [2011] Carcinogenic potential, levels and sources of polycyclic aromatic hydrocarbon mixtures in indoor and outdoor environments and their implications for air quality standards. *Environment International* 37 (2011), 383–392.

Denier van der Gon H.A.C., Hendriks C., Kuenen J., Segers A. and Visschedijk A. [2011a] Description of current temporal emission patterns and sensitivity of predicted AQ for temporal emission patterns. EU FP7, MACC, deliverable report D_D-EMIS_1.3. TNO.

Dibble T.S., M.J. Zelie and Y. Jiao [2014] Quantum chemistry guide to PTRMS studies of as yet undetected products of the bromine atom initiated oxidation of gaseous elemental mercury. *Journal of Physical Chemistry* A, 118:7847-7854.

Dibble, T.S., M.J. Zelie and H. Mao [2012] Thermodynamics of reactions of ClHg and BrHg radicals with atmospherically abundant free radicals. *Atmospheric Chemistry and Physics*, 12:10271-10279.

Dibble, T.S., M.J. Zelie and H. Mao [2013] Corrigendum to "Thermodynamics of reactions of ClHg and BrHg radicals with atmospherically abundant free radicals" published in Atmospheric Chemistry and Physics, 12:10271-10279, 2012. *Atmospheric Chemistry and Physics*, 13:9211-9212.

Dickhut R.M., Cincinelli A., Cochran M., Ducklow H.W. [2005] Atmospheric concentrations and air-water flux of organochlorine pesticides along the Western Antarctic Peninsula. *Environ. Sci. Technol*. 39, 465–470. doi:10.1021/es048648p.

Donohoue D., Bauer D., Cossairt B., and Hynes A. [2006] Temperature and pressure dependent rate coefficients for the reaction of Hg with Br and the reaction of Br with Br: A pulsed laser photolysispulsed laser induced fluorescence study, *J. Phys. Chem*. A, 110, 6623–6632, doi:10.1021/jp054688j.

DWD [2018] DWD Climate Data Center (CDC): Historical daily station observations (temperature, pressure, precipitation, sunshine duration, etc.) for Germany, version v006, 2018. www.dwd.de, accessed in September, 2018.

Ebel A., Friedrich R., and Rodhe H. [1997] Tropospheric Modelling and Emission Estimation. Transport and Chemical Transformation of Pollutants in the Troposphere, chapter. GENEMIS: Assessment, Improvement, and Temporal and Spatial Disaggregation of European Emission Data, Springer, Berlin, Germany.

ECMWF [2019]. European Centre for Medium-Range Weather Forecasts. https://apps.ecmwf.int/archive-catalogue/. Accessed in September, 2018.

EEA [2006] Atmospheric Emission Inventory Guidebook. A joint EMEP / CORINAIR Production Prepared by the EMEP Task Force on Emission Inventories https://www.eea.europa.eu/publications/EMEPCORINAIR4/sources_of_HCB.pdf/view .

EEA [2018] Air quality in Europe — 2018 report, EEA Report No 12/2018, European Environment Agency.

EEA/CEIP Review Report [2019] S.Gaisbauer, K. Mareckova, M. Pinterits, B. Ullrich, R. Wankmueller: Inventory Review 2019. Review of emission data reported under the LRTAP Convention and NEC Directive, Stage 1 and 2 and review, Status of gridded and LPS data. Technical Report CEIP 4/2019. Available at: http://www.ceip.at/review_proces_intro/review_reports.

EFSA (Food Safety Authority EFSA) [2006] Opinion of the Scientific Panel on contaminants in the food chain on a request from the Commission related to hexachlorobenzene as undesirable substance in animal feed. *The EFSA Journal,* 402, 1 – 49.

Efstathiou C.I., J. Matejovicová, J. Bieser, and G. Lammel [2016] Evaluation of gas-particle partitioning in a regional air quality model for organic pollutants. *Atmos. Chem. Phys*., 16, 15327–15345.

Eisenreich S.J., Looney B.B. and Thornton J.D. [1981] Airborne organic contaminants in the Great Lakes ecosystem. *Environ Sci Tech* 15(1): 30-38.

EMEP/EEA Guidebook [2013] EMEP/EEA air pollutant emission inventory guidebook – 2013. EEA Technical report No 12/2013. Available at: https://www.eea.europa.eu/publications/emep-eea-guidebook-2013.

EMEP/EEA Guidebook [2016] EMEP/EEA air pollutant emission inventory guidebook – 2016. EEA Technical report No 21/2016. Available at: https://www.eea.europa.eu/publications/emep-eea-guidebook-2016.

Emmons L. K., Walters S., Hess P.G., Lamarque J.-F., Pfister G.G., Fillmore D., Granier C., Guenther A., Kinnison D., Laepple T., Orlando J., Tie X., Tyndall G., Wiedinmyer C., Baughcum S.L., and Kloster S. [2010] Description and evaluation of the Model for Ozone and Related chemical Tracers, version 4 (MOZART-4), *Geosci. Model Dev*., 3, 43–67, doi:10.5194/gmd-3-43-2010.

EU [2004] Directive 2004/107/EC of the European Parliament and of the Council of 15 December 2004 relating to arsenic, cadmium, mercury, nickel and polycyclic aromatic hydrocarbons in ambient air (OJ L 23,

26.1.2005, pp. 3-16) (http://eur-lex.europa.eu/LexUriServ/LexUriServ.do?uri=OJ:L:2005:023:0003:0016:EN:PDF).

Euro Chlor [2002] Euro Chlor Risk Assessment for the Marine Environment OSPARCOM Region - North Sea. Hexachlorobenzene.

Fiedler H. [2007] National PCDD/PCDF release inventories under the Stockholm Convention on Persistent Organic Pollutants, *Chemosphere,* 67, S96–S108.

Finizio A., D. Mackay, T. Bidleman, and T. Harner [1997] Octanol–air partition coefficient as a predictor of partitioning of semi-volatile organic chemicals to aerosols. *Atmos. Environ.*, 31, 2289–2296, doi:10.1016/S1352-2310(97)00013-7.

Fürst P. [2006] Dioxins, polychlorinated biphenyls and other organohalogen compounds in human milk – levels, correlations, trends and exposure through breast feeding. Mol Nutr Food Res 50: 922-933.

Gauss M., J. Bartnicki, A. Gusev, W. Aas, H. Klein [2018] Atmospheric Supply of Nitrogen, Cadmium, Mercury, Benzo(a)pyrene, and PCB-153 to the Baltic Sea in 2016. MSC-W Technical Report 1/2018. https://emep.int/publ/helcom/2018/index.html.

Goodsite M.E., Plane J.M.C., and Skov H. (2012] Correction to A Theoretical Study of the Oxidation of Hg0 to HgBr2 in the Troposphere, *Environ. Sci. Technol*., 46, 5262, doi:10.1021/es301201c.

Goss K.-U. and R. P. Schwarzenbach [2001] Linear free energy relationships used to evaluate equilibrium partitioning of organic compounds. *Environ. Sci. Technol.*, 35, 1–9, doi:10.1021/es000996d.

Government of Japan (2007] Submission to COP3: Assessment Committee on BAT Levels for Reduction of a Specified Chemical as a Contaminant By-product. April 2007. https://www.meti.go.jp/policy/chemical_management/kasinhou/files/information/report/hcb/hcb_bat_Report_2_eng.pdf

Gratz L.E., Ambrose J.L., Jaffe D.A., Shah V., Jaegle L., Stutz J., Festa J., Spolaor M., Tsai C., Selin N.E., Song S., Zhou X., Weinheimer A.J., Knapp D.J., Montzka D.D., Flocke F.M., Campos T.L., Apel E., Hornbrook R., Blake N.J., Hall S., Tyndall G.S., Reeves M., Stechman D., and Stell M. [2015] Oxidation of mercury by bromine in the subtropical Pacific free troposphere, *Geophysical Research Letters*, 42, 10.1002/2015gl066645.

GSOD [2019]. Global Surface Summary of the Day – GSOD. https://data.noaa.gov/dataset/dataset/global-surface-summary-of-the-day-gsod. Accessed on June 11, 2019.

Guerranti, C., Palmieri, M., Mariottini, M., & Focardi, S. E. [2011] Persistent Organic Pollutants in Human Milk from Central Italy: Levels and Time Trends. *ISRN Toxicology,* 1–6. doi:10.5402/2011/107514.

Gusev A., Ilyin I., Rozovskaya O., V. Shatalov, O.Travnikov, I.Strijkina [2019] Assessment of transboundary pollution by toxic substances: Heavy metals and POPs. Supplementary materials for POPs. MSC-E Data Report 4/2019.

Gusev A., O.Rozovskaya, V.Shatalov, N.Vulykh, W. Aas, K. Breivik, F. Couvidat, and M.G. Vivanco [2018] Persistent Organic Pollutants: assessment of transboundary pollution on global, regional, and national scales. EMEP Status Report 3/2018.

Gusev A., O.Rozovskaya, V.Shatalov, N.Vulykh, P. Nizzetto, K. Breivik, and W.Aas [2017] Transboundary transport of Persistent Organic Pollutants with emphasis on PAHs: regional and national scale assessment and transition to the new EMEP grid. EMEP Status Report 3/2017.

Gusev A., V.Shatalov, and O.Rozovskaya [2014] PilotModelling of PCDD/F Transport and Fate on Global Scale and within the European Region. *Organohalogen Compounds*. Vol. 76, 958-961.

Gusev A., S.Dutchak, O.Rozovskaya, V.Shatalov, V.Sokovykh, N.Vulykh [2011] Persistent Organic Pollutants in the Environment. EMEP Status Report 3/2011.

Gusev A., O.Rozovskaya, V. Shatalov [2007] Modelling POP long-range transport and contamination levels by MSCE-POP model. EMEP/MSC-E Technical Report 1/2007.

Gusev A., I. Ilyin, L.Mantseva, O.Rozovskaya, V. Shatalov, O. Travnikov [2006] Progress in further development of MSCE-HM and MSCE-POP models (implementation of the model review recommendations) EMEP/MSC-E Technical Report 4/2006.

Gusev A., E.Mantseva, V.Shatalov, B.Strukov [2005] Regional Multicompartment Model MSCE-POP, EMEP/MSC-E Technical Report 5/2005.

Gustin M.S., H.M. Amos, J. Huang, M.B. Miller, and K. Heidecorn [2015] Measuring and modelling mercury in the atmosphere: a critical review, *Atmospheric Chemistry and Physics*, 15(10), 5697–5713, doi:10.5194/acp-15-5697-2015.

Harmens H., Mills G., Hayes F., Sharps K., Frontasyeva M. and the participants of the ICP Vegetation [2016]. Air Pollution and Vegetation. ICP Vegetation Annual Report 2015/2016. 35 p.

Harner T. and T. F. Bidleman [1998] Octanol-air partition coefficient for describing particle/gas partitioning of aromatic compounds in urban air. *Environ. Sci. Technol.*, 32, 1494–1502, doi:10.1021/es970890r.

HMCR [2019]. Hydrometeorological Centre of Russia. The main peculiarities of atmospheric circulation and weather in the northern hemisphere. https://meteoinfo.ru/circulation-review. Accessed on April 30, 2018.

Holmes, C. D., Jacob, D. J., Corbitt, E. S., Mao, J., Yang, X., Talbot, R., and Slemr, F. [2010] Global atmospheric model for mercury including oxidation by bromine atoms, *Atmos. Chem. Phys*., 10, 12037–12057, doi:10.5194/acp-10-12037-2010.

Horowitz H.M., D.J. Jacob, Y. Zhang, T.S. Dibble, F. Slemr, H.M. Amos, J.A. Schmidt, E.S. Corbitt, E.A. Marais and E.M. Sunderland [2017] A new mechanism for atmospheric mercury redox chemistry: Implications for the global mercury budget. *Atmospheric Chemistry and Physics Discussions*, 1-33, 10.5194/acp-2016-1165.

Howard P.H., Boethling R.S., Jarvis W.F., Meylan W.M. and Michalenko E.M. [1991] In:Taup, H. ed. Handbook of environmental degradation rates. Chelsea, Michigan, Lewis Publishers.

Hylander L.D., Meili M. [2003] 500 years of mercury production: global annual inventory by region until 2000 and associated emissions. *Science of the Total Environment* 304, 13–27.

Hynes A.J., Donohoue D.L., Goodsite M.E., and Hedgecock I.M. [2009] Our Current Understanding of Major Chemical and Physical Processes Affecting Mercury Dynamics in the Atmosphere and At the Air-Water/Terrestrial Interfaces, in: Mercury Fate and Transport in the Global Atmosphere, edited by: Pirrone, N., and Mason, R., Springer Science Business Media, LLC, 427–457.

Ilyin I., Gusev A., Rozovskaya O., V. Shatalov, O.Travnikov, I.Strijkina [2019] Assessment of transboundary pollution by toxic substances: Heavy metals and POPs. Supplementary materials for heavy metals. MSC-E Data Report 3/2019.

Ilyin I., O.Rozovskaya, O.Travnikov, W. Aas, K.A. Pfaffhuber [2018] Assessment of heavy metal transboundary pollution on global, regional and national scales. EMEP Status Report 2/2018.

Iwata H., Tanabe S., Sakai N., and Tatsukawa R. [1993] Distribution of persistent organochlorines in the oceanic air and surface seawater and the role of ocean on their global transport and fate. Environmental Science and Technology, 27:1080-1098.

Ji X., Lin W., Zhang W., Yin F., Zhao X., Wang C., … Liu S. [2015] A comprehensive review of the process on hexachlorobenzene degradation. MATEC Web of Conferences, 22, 04007. doi:10.1051/matecconf/20152204007.

Jiao Y. and Dibble T. S. [2017] First kinetic study of the atmospherically important reactions BrHg + NO2 and BrHg + HOO, *Phys. Chem. Chem. Phys*., 19, 1826–1838, doi:10.1039/c6cp06276h.

Jiao Y. and T.S. Dibble [2015] Quality structures, vibrational frequencies, and thermochemistry of the products of reaction of BrHg• with NO2, HO2, ClO, BrO, and IO. Journal of Physical Chemistry A, 119:10502-10510.

Jonson J.E., Travnikov O. [2012] Global scale modelling within EMEP: Progress report. Join MSC-E/MSC-W Report EMEP/MSC-E Technical Report 1/2012.

JRC [2016]. European Commission, Joint Research Centre (JRC)/Netherlands Environmental Assessment Agency (PBL): Emission Database for Global Atmospheric Research (EDGAR), Global Emissions EDGAR v4.3.1. http://edgar.jrc.ec.europa.eu.

Junge C. E. [1977] Fate of pollutants in the air and water environment, edited by: Suffet, I. H., Wiley, New York.

Kallenborn R., Breivik K., Eckhardt S., Lunder C.R., Manш S., Schlabach M., Stohl A. [2013] Long-term monitoring of persistent organic pollutants (POPs) at the Norwegian. Troll station in Dronning Maud Land, Antarctica. *Atmos. Chem. Phys*. 13, 6983–6992.doi:10.5194/acp-13-6983-2013.

Kannan N., Yamashita N., Petrick G., and Duinker J.C. (1998) Polychlorinated Biphenyls and Nonylphenols in the Sea of Japan, Environ. Sci. Technol., vol. 32, No.12, pp. 1747 - 1753.

Keyte I.J., R.M. Harrisonz, and G. Lammel [2013] Chemical reactivity and long-range transport potential of polycyclic aromatic hydrocarbons – a review. *Chem. Soc. Rev.*, DOI: 10.1039/c3cs60147a.

Kezoudi M., Tesche M., Smith H., Ulanowski J., Tsekeri A., Baars H., Siomos N., Estellés V., Miladi L., Müller D., Amiridis V. and Weinzierl B. [2019] Mineral dust size distributions in the eastern Mediterranean from balloon-borne optical particle counter and validation with aircraft measurements and remote-sensing retrievals. *Geophysical Research Abstracts*, Vol. 21, EGU2019-123.

Lane D.A., Johnson N.D., Hanley M.J.J., Schroeder W.H. and Ord D.T. [1992] Gas- andparticle-phase concentrations of alpha-hexachlorocyclohexane, gamahexachlorocyclohexane, and hexachlorobenzene in Ontario air. *Environ Sci Technol*, 26:126-133.

Larssen S., Sluyter R. and Helmis C. [1999]. Criteria for EUROAIRNET. The EEA Air Quality Monitoring and Information network. Technical Report no. 12. EEA, Copenhagen, 43 p.

Lequy E., Saby N.P.A., Ilyin I., Bourin A., Sauvage S., Leblond S. [2017] Spatial analysis of trace elements in a moss bio-monitoring data over France by accounting for source, protocol and environmental parameters. *Sci Total Environ*. vol. 590-591, pp 602-610.

Liu X., H. Zhang, W. Pan, Q. Xue, J. Fu, G. Liu, M. Zheng, A. Zhang [2019 A novel computational solution to the health risk assessment of air pollution via joint toxicity prediction: A case study on selected PAH binary mixtures in particulate matters. *Ecotoxicology and Environmental Safety* 170 (2019), 427–435.

Lohmann R. and G. Lammel [2004] Adsorptive and Absorptive Contributions to the Gas-Particle Partitioning of Polycyclic Aromatic Hydrocarbons: State of Knowledge and Recommended Parametrization for Modeling. *Environ. Sci. Technol.*, 38, 14, 3793-3803, DOI: 0.1021/es035337q

Ma J.M., Hung H.L., Tian C., Kallenborn R. [2011] Revolatilization of persistent organic pollutants in the Arctic induced by climate change. *Nature Climate Change* 2011, 1, (5), 255-260.

Macdonald R.W., Harner T., & Fyfe J. [2005] Recent climate change in the Arctic and its impact on contaminant pathways and interpretation of temporal trend data. *Science of the Total Environment*, 342, 5–86. https://doi.org/10.1016/j.scitotenv.2004.12.059.

Mackay D., Shiu W.Y., & Ma K.C. [1992] Illustrated handbook of physical-chemical properties and environmental fate for organic chemicals. Volumes 1 and 2. Monoaromatic Hydrocarbons, Chlorobenzenes and PCBs. Chelsea, MI: Lewis Publishers.

Mamouri R-E., Ansmann A., Nisantzi A., Solomos S., Kallos G., and Hadjimitsis D.G [2016] Extreme dust storm over the eastern Mediterranean in September 2015: satellite, lidar, and surface observations in the Cyprus region. *Atmos. Chem. Phys*., 16, 13711–13724.

Manz M., K.-D. Wenzel, U. Dietze, G. Schuurmann [2001] Persistent organic pollutants in agricultural soils of central Germany.

Meijer S.N., Ockenden W.A., Sweetman A., Breivik K., Grimalt J.O., and Jones K.C. [2003] Global Distribution and Budget of PCBs and HCB in Background Surface Soils: Implication for Sources and Environmental Processes. *Environ. Sci. Technol*. vol. 37, pp. 667-672.

Menut L., B. Bessagnet, D. Khvorostyanov, M. Beekmann, N. Blond, A. Colette, I. Coll, G. Curci, G. Foret, A. Hodzic, S. Mailler, F. Meleux, J.-L. Monge, I. Pison, G. Siour, S. Turquety, M. Valari, R. Vautard, and M. G. Vivanco [2013] CHIMERE 2013: a model for regional atmospheric composition modelling. *Geosci. Model Dev*., 6, 981–1028.

Mill T. and Haag, W. [1986] The environmental fate of hexachlorobenzene. In: Morris, C.R.and Cabral, J.R.P. ed. Hexachlorobenzene: Proceedings of an International Symposium. Lyon, International Agency for Research on Cancer. IARC Sci Publ 77: 61-66.

Mu Q., M. Shiraiwa, M. Octaviani, N. Ma, A. Ding, H. Su, G. Lammel, U. Pöschl, and Y. Cheng [2018] Temperature effect on phase state and reactivity controls atmospheric multiphase chemistry and transport of PAHs. *Sci. Adv.*, 4: eaap7314, 1-8.

Mukesh Kumar D.J., S. Dinesh Kumar, D. Kubendran, P.T. Kalaichelvan [2013] Hexachlorobenzene - sources, remediation and future prospects. *International Journal of Current Research and Review*. 05, 1-12.

Nash R.G. and Gish T.J. [1989] Halogenated pesticide volatilization and dissipation from soil under controlled conditions. *Chemosphere* 18: 2353-2362.

Nickel S., Schröder W., Wosniok W., Harmens H., Frontasyeva M. V., Alber R., Aleksiayenak J., Barandovski L., Blum O., Danielsson H., de Temmermann L., Dunaev A. M., Fagerli H., Godzik B., Ilyin I., Jonkers S., Jeran Z., Karlsson G. P., Zechmeister H. G. [2017] Modelling and mapping heavy metal and nitrogen concentrations in moss in 2010 throughout Europe by applying Random Forests models. *Atmos. Environ*., 156, 146–159.

Niimi A.J. [1987] Biological half-lives of chemicals in fishes. *Rev. Environ. Contam. Toxicol*. 99, 1-46.

Nisantzi A., Mamouri R.E., Ansmann A., Schuster G.L. and Hadjimitsis D.G. [2015] Middle East versus Saharan dust extinction-to-backscatter ratios. *Atmos. Chem. Phys*., 15, 7071–7084.

Oliver B.G. [1984] Distribution and pathways of some chlorinated benzenes in the Niagara River and Lake Ontario. *Water Pollut Res* J Can 19: 47-59.

Oliver B.G. and Charlton M.N. [1984] Chlorinated organic contaminants on settling particulates in the Niagara River vicinity of Lake Ontario. *Environ Sci Technol* 18: 903- 908.

Oliver B.G. and Nicol K.D. [1982] Chlorobenzenes in sediments, water, and selected fish from Lakes Superior, Huron, Erie, and Ontario. *Environ Sci Technol* 16: 532-536.

Oliver B.G., Charlton M.N. and Durham R.W. [1989] Distribution, redistribution, and geochronology of polychlorinated biphenyl congeners and other chlorinated hydrocarbons in Lake Ontario sediments. *Environ Sci Technol* 23: 200-208.

Pankow J. F. [1987] Review and comparative analysis of the theories on partitioning between the gas and aerosol particulate phases in the atmosphere, *Atmos. Environ*., 21, 2275–2283, doi:10.1016/0004-6981(87)90363-5.

Parrella J.P., Jacob D.J., Liang Q., Zhang Y., Mickley L.J., Miller B., Evans M.J., Yang X., Pyle J.A., Theys N., and Van Roozendael M. [2012] Tropospheric bromine chemistry: implications for present and pre-industrial ozone and mercury, *Atmos. Chem. Phys.,* 12, 6723–6740, doi:10.5194/acp-12-6723-2012.

Pouch A., Zaborska A., & Pazdro K. [2018] The history of hexachlorobenzene accumulation in Svalbard fjords. Environmental Monitoring and Assessment, 190(6).doi:10.1007/s10661-018-6722-3.

Pulles T., H. Kok, U. Quass [2012] Application of the emission inventory model TEAM: Uncertainties in dioxin emission estimates for central Europe. *Atmospheric Environment,* 40, 2321–2332.

Pulles T., Kok H., Quass U., Juery C., Matejovicova J. [2005] Dioxin emissions in candidate countries. TNO Report R&I-A R 2005/054. Available at: http://ec.europa.eu/environment/archives/dioxin/pdf/rapport_2005.pdf.

PWGSC (2003) Canadian Arctic Contaminants Assessment Report II - Physical Environment. Minister of Public Works and Government Services Canada, Ottawa, Canada (www.ainc-inac.gc.ca)

Ravindra K., R. Sokhia, R. Van Grieken [2007] Atmospheric polycyclic aromatic hydrocarbons: Source attribution, emission factors and regulation. *Atmospheric Environment,* Volume 42, Issue 13, April 2008, Pages 2895-2921.

Regulation (EC) No 1272/2008 (CLP) of the European Parliament and of the Council of 16 December 2008 on classification, labelling and packaging of substances and mixtures, amending and repealing Directives 67/548/EEC and 1999/45/EC, and amending Regulation (EC) No 1907/2006.

Saiz-Lopez A., Sitkiewicz S.P., Roca-Sanjua¡n D., Oliva-Enrich J.M. , Da¡valos J.Z. , Notario R., Jiskra M., Xu Y., Wang F., Thackray C.P., Sunderland E.M., Jacob D.J., Travnikov O., Cuevas C.A., Acuana A.U., Rivero D., Plane J.M.C., Kinnison D.E., Sonke J.E. [2018] Photoreduction of gaseous oxidized mercury changes global atmospheric mercury speciation, transport and deposition. *Nature Comm*. 9, 4796, doi: 10.1038/s41467-018-07075-3.

Schmid P., Bogdal C., Wang Z., Azara V., Haag R., & von Arx U. [2014] Releases of chlorobenzenes, chlorophenols and dioxins during fireworks. *Chemosphere*, 114, 158–164. doi:10.1016/j.chemosphere.2014.03.088.

Schneider C., Pelzer M., Toenges-Schuller N., Nacken M. and Niederau A. [2016] ArcGIS basierte Lösung zur detaillierten, deutschlandweiten Verteilung (Gridding) nationaler Emissionsjahreswerte auf Basis des Inventars zur Emissionsberichterstattung. Im Auftrag des Umweltbundesamtes. ISSN 1862-4804. Dessau-Roßlau, November 2016. http://www.umweltbundesamt.de/publikationen. 233 p.

Schroder W., S. Nickel, S. Schonrock, M. Meyer, W. Wosniok, H. Harmens, M.V. Frontasyeva, R. Alber, J. Aleksiayenak, L. Barandovski, A. Carballeira, H. Danielsson, L. de Temmermann, B. Godzik, Z. Jeran, G.P. Karlsson, P. Lazo, S. Leblond, A.J. Lindroos, S. Liiv, S.H. Magnusson, B. Mankovska, J. Martinez-Abaigar, J. Piispanen, J. Poikolainen, I.V. Popescu, F. Qarri, J.M. Santamaria, M. Skudnik, Z. Spiric, T. Stafilov, E. Steinnes, C. Stihi, L. Thoni, H.T. Uggerud, H.G. Zechmeister [2015]. Spatially valid data of atmospheric deposition of heavy metals and nitrogen derived by moss surveys for pollution risk assessments of ecosystems. *Environmental Science and Pollution Research*, vol 23, pp 10457–10476.

Schulz-Bull D.E., Petrick G., Duinker J.C. (1991) Polychlorinated biphenyls in North Sea water, Marine Chemistry, vol. 36, pp. 365 - 384.

Schwarzenbach R.P., Giger W., Hoehn E. and Schneider J.K. [1983] Behaviour of organic compounds during infiltration of river water to groundwater. Field studies. *Environ Sci Technol* 17: 472-479.

Secretariat of the Stockholm Convention [2012] Guidance for Strengthening the Regulatory Framework to Enable Regular Monitoring of Products and Articles that may Contain New POPs.

Shahpoury P., G. Lammel, A. Albinet, A. Sofuoglu, Y. Dumanoglu, S. C. Sofuoglu, Z. Wagner, and V. Zdimal [2016] Evaluation of a conceptual model for gas-particle partitioning of polycyclic aromatic hydrocarbons using poly-parameter linear free energy relationships. *Environ. Sci. Technol.*, 50, 22, 12312-12319.

Shatalov V., A. Gusev, S. Dutchak, O. Rozovskaya, V. Sokovykh, and N. Vulykh [2010] Persistent Organic Pollutants in the Environment. EMEP Status Report 3/2010.

Shatalov V., Ilyin I., Gusev A., Rozovskaya O., Travnikov O. [2015] Heavy Metals and Persistent Organic Pollutants: development of multi-scale modeling and trend analysis methodology. EMEP/MSC-E Technical report 1/2015.

Shatalov V., Ilyin I., Gusev A., Rozovskaya O., Travnikov O. [2014] Heavy Metals and Persistent Organic Pollutants: Model Assessment of Pollution and Research Activities. EMEP/MSC-E Technical report 4/2014.

Shen H., Huang Y., Wang R., Zhu D., Li W., Shen G., Wang B., Zhang Y., Chen Y., Lu Y., Chen H., Li T., Sun K., Li B., Liu W., Liu J., Tao S. [2013] Global atmospheric emissions of polycyclic aromatic hydrocarbons from 1960 to 2008 and future predictions, *Environ. Sci. Technol*., 47, 6415–6424.

Six L. and Smolders E. [2014]. Future trends in soil cadmium concentration under current cadmium fluxes to European agricultural soils. *Science of the Total Environment* 485–486 (2014) 319–328.

Skamarock W.C., Klemp J.B., Dudhia J., Gill D.O., Barker D.M., Duda M.G., Huang X-Y., Wang W. and Powers J.G. [2008]. A Description of the Advanced Research WRF Version 3. NCAR/TN–475+STR NCAR TECHNICAL NOTE

Starek-Świechowicz B., Budziszewska B., & Starek A. [2017] Hexachlorobenzene as a persistent organic pollutant: Toxicity and molecular mechanism of action. Pharmacological Reports, 69(6), 1232–1239.doi:10.1016/j.pharep.2017.06.013.

Strode S., Jaeglé L., Selin N.E. [2009] Impact of mercury emissions from historic gold and silver mining: Global modelling. *Atmos. Environ*. 43(12), 2012-2017.

Subir M., Ariya P.A., and Dastoor A.P. [2011] A review of uncertainties in atmospheric modeling of mercury chemistry I. Uncertainties in existing kinetic parameters – Fundamental limitations and the importance of heterogeneous chemistry, *Atmos. Environ.,* 45, 5664–5676, doi:10.1016/j.atmosenv.2011.04.046.

Subir M., Ariya P.A., and Dastoor A.P. [2012] A review of the sources of uncertainties in atmospheric mercury modeling II. Mercury surface and heterogeneous chemistry – A missing link. *Atmos. Environ*. 46, 1-10.

Theakston F. [2000] Air quality guidelines for Europe. Second edition. WHO Regional Publications, European Series, No. 91, ISBN 92 890 1358 3.

Thomsen M., Nielsen O., Illerup Jytte Boll [2009] Unintentional formation and emission of the persistent organic pollutants HCB and PCBs in the Nordic Countries: documentation of existing informtion regarding sources and emissions to air, water and soil, with focus on reporting obligations according to the Stockholm Convention, The UNECE POP protocol, and PRTR registers. Tema Nord, Vol. 518, 2009, p. 1-139.

Tista M., R.Wankmueller, Mareckova K. [2018a] Methodologies applied to the CEIP GNFR gap-filling 2018. Part I: Heavy Metals (Pb, Cd, Hg). Technical report CEIP 02/2018.

Tista M., Wankmueller R. and K.Mareckova [2018] Methodologies applied to the CEIP GNFR gap-filling 2018. Part II: Persistent organic pollutants (Benzo(a)pyrene, Benzo(b)fluoranthene, Benzo(k)fluoranthene, Indeno(1,2,3-cd)pyrene, Dioxin and Furan, Hexachlorobenzene). Technical report CEIP 01/2018.

Toft G. [2015] Organochlorines and the Effect on Female Reproductive System. Reference Module in Earth Systems and Environmental Sciences. doi:10.1016/b978-0-12-409548-9.09543-9.

Travnikov O., Gusev A. and Ilyin I. [2018] Detailed assessment of heavy metal and POP pollution in the EMEP countries: An overview of case studies. PART I. EMEP/MSC-E Technical Report 4/2018. 30 p.

Travnikov O., Angot H., Artaxo P., Bencardino M., Bieser J., D'Amore F., Dastoor A., De Simone F., Diéguez M. D. C., Dommergue A., Ebinghaus R., Feng X. B., Gencarelli C. N., Hedgecock I. M., Magand O., Martin L., Matthias V., Mashyanov N., Pirrone N., Ramachandran R., Read K. A., Ryjkov A., Selin N. E., Sena F., Song S., Sprovieri F., Wip D., Wängberg I., and Yang X. [2017] Multi-model study of mercury dispersion in the atmosphere: atmospheric processes and model evaluation, *Atmos. Chem. Phys*., 17, 5271-5295, doi:10.5194/acp-17-5271-2017.

Travnikov O. and Jonson J.E. (Eds.) [2011] Global scale modelling within EMEP: Progress report. Joint MSC-W/MSC-E Report. EMEP/MSC-E Technical Report 1/2011.

Travnikov O., Jonson J.E., Andersen A.S., Gauss M., Gusev A., Rozovskaya O., Simpson D., Sokovyh V., Valiyaveetil S., and Wind P. [2009] Development of the EMEP global modeling framework: Progress report, EMEP/MSC-E Technical Report 7/2009, Meteorological Synthesizing Centre – East of EMEP, Moscow, 44 pp.

Travnikov O. and I.Ilyin [2005] Regional Model MSCE-HM of Heavy Metal Transboundary Air Pollution in Europe. EMEP/MSC-E Technical Report 6/2005, 59 pp.

UN Environment [2019] Global Mercury Assessment 2018. UN Environment Programme, Chemicals and Health Branch Geneva, Switzerland.

UNECE [1979] The 1979 Geneva Convention on Long-range Transboundary Air Pollution. United Nations Economic Commission for Europe. http://www.unece.org/env/lrtap/lrtap_h1.html.

UNECE [2009] EMEP monitoring strategy. ECE/EB.AIR/GE.1/2009/15.

UNECE [2014] Guidelines for reporting emission data under the Convention on Long-range Transboundary Air Pollution (ECE/EB.AIR/130). Available at: http://www.ceip.at/fileadmin/inhalte/emep/2014_Guidelines/ece.eb.air.125_ADVANCE_VERSION_reporting_guidelines_2013.pdf.

UNEP [2002] Global Mercury Assessment 2002. UNEP Chemicals. 258 pp. http://www.unep.org/chemicalsandwaste/Portals/9/Mercury/Documents/final-assessment-report-25nov02.pdf. Accessed on June 28, 2016.

Van Noort P.C.M. [2003] A thermodynamis-based estimation model for asorption of organic compounds by carbonaceous materials in environmental sorbents. *Environ. Toxicol. Chem*., vol. 22, pp. 1179-1188.

Vassilyeva G. and V. Shatalov [2002] Behaviour of persistent organic pollutants in soil. MSC-E Technical Note 1/2002.

Wang B., H. Fiedler, J. Huang, S. Deng, Y. Wang, G. Yu [2016] A primary estimate of global PCDD/F release based on the quantity and quality of national economic and social activities. *Chemosphere*, 151, 303 – 309.

Wang F. Saiz-Lopez A., Mahajan A.S., Gómez Martín J.C., Armstrong D., Lemes M., Hay T., and Prados-Roman C. [2014] Enhanced production of oxidised mercury over the tropical Pacific Ocean: A key missing oxidation pathway. *Atmos. Chem. Phys*. 14, 1323–1335.

Wang X., Sheng J., Gong P., Xue Y., Yao T., & Jones K.C. [2012] Persistent organic pollutants in the Tibetan surface soil: Spatial distribution, air–soil exchange and implications for global cycling. *Environmental Pollution*, 170, 145–151.doi:10.1016/j.envpol.2012.06.012.

Wania F. [2003] Assessing the Potential of Persistent Organic Chemicals for Long-Range Transport and Accumulation in Polar Regions. Environmental Science & Technology, 37(7), 1344–1351.doi:10.1021/es026019e.

Wania F., Daly G.L. [2002] Estimating the contribution of degradation in air and deposition to the deep sea to the global loss of PCBs. *Atmospheric Environmen*t 2002, 36, (36-37), 5581-5593.

Wania F., Mackay D. [1996] Tracking the distribution of persistent organic pollutants. *Environ. Sci. Technol*. , 30, (9), A390-A396.

WHO [2004] Hexachlorobenzene in drinking-water. Background document for preparation of WHO Guidelines for drinking-water quality. Geneva, World Health Organization (WHO/SDE/WSH/03.04/100).

WMO [2019] Annual Bulletin on the Climate in WMO Region VI - Europe and Middle East - 2017 . Ed. by Deutscher Wetterdienst. Responsible Mächel H. https://www.dwd.de/DE/leistungen/ravibulletinjahr/bulletin_2017.pdf,jsessionid=FB49DAFE415EAE6932E5A46DC080353.live11051?__blob=publicationFile&v=3. Accessed on April 30, 2018.

Zhang, Y., L. Jaeglé, and L. A. Thompson [2014] Natural biogeochemical cycle of mercury in a global three-dimensional ocean tracer model, *Global Biogeochem. Cycles*, 28, 553–570.

APPENDIX A1

Reporting of EECCA countries

Table A1. *Reporting of main heavy metals (Pb, Cd, Hg) of the EECCA countries within the last five years*

Reporting of main heavy metals (Pb, Cd, Hg)					
EECCA countries	***2015***	***2016***	***2017***	***2018***	***2019***
Armenia	2008 - 2013 (only Pb, only a few sectors)	2014		2016	2017
Azerbaijan	1990 - 2013 (only Hg, only a few sectors)	1990-2014 (Pb, Cd: 1995-2014)	1990 - 2015 (Pb, Cd: 1995-2015)	1990 - 2016 (Pb, Cd: 1995-2016)	1995-2017 (Hg1990-2017)
Belarus	2013			2014-2016	2017
Georgia	2007 - 2013 (no Hg)	2007-2014 (Cd, Hg: 2013-2014)	2007 - 2015	2007-2016	2007-2017
Kazakhstan		2013-2014	1990, 2000, 2005, 2010 - 2015	1990 - 2016	
Kyrgyzstan		2014 (only Hg)	2015 (only Hg)		2017
Republic of Moldova	2013	1990-2014 (no emissions calculated for the waste sector)	1990 - 2015		
Russian Federation					
Ukraine	2013	2014	2015	2016	2017

Table A2. *Reporting of POPs (PCDD/Fs, PAHs, HCB, PCBs) of the EECCA countries within the last five years*

Reporting of POPs (PCDD/Fs, PAHs, HCB, PCBs)					
	2015	**2016**	**2017**	**2018**	**2019**
Armenia		2014		2016 (only PCDD/Fs)	2017 (No HCB, no PCBs)
Azerbaijan	1995-2013	1995-2014 (no HCB, no PCBs)	1995-2015	1995-2016	1995 -2017 (HCB, PCBS no data for 2000)
Belarus	2013			2014-2016	2017
Georgia	2007-2013 (no HCB)	2007-2014 (PCDD/Fs) 2013-2014 (PAHs, HCB, PCBs)	2007-2015	2007-2016 (HCB only 2013-2016)	2007-2017
Kazakhstan		2013-2014	1990, 2000, 2005, 2010-2015	1990-2016	
Kyrgyzstan					2017
Republic of Moldova	2013	1990-2014 (no emissions calculated for the waste sector)	1990-2015		
Russian Federation					
Ukraine	2013 (no PCDD/Fs)				2017

APPENDIX A2

Emission changes between 2016 (reported in 2018) and 2017 (reported in 2019) over ±15 % (data sets used for gridding)

Data values represent the 'total national totals'. The column 'data sources' in the table below indicates the following four cases:

- *"reported"*: both 2016 and 2017 data are reported by country.
- *"gapfilled":* both 2016 and 2017 data are gap-filled with expert estimates
- *"new gapfilled":* 2016 data was reported by country and 2017 data had to be gap-filled by expert estimates (because it was not reported by country)
- *"new reported":* 2016 data was gap-filled, 2017 data is as reported by country.

The indicator *"new"* in column *"Change (%)"* indicates that the value has been either reported or gap-filled for the first time.

Component	Country	Data sources	2017 value (t)	2016 value (t)	Change (%)	Change (t)
B(a)P	AZ	new gapfilled	0.396	0.200	98%	0.197
B(a)P	BY	reported	6.861	8.875	-23%	-2.014
B(a)P	ES	gapfilled	41.518	79.038	-47%	-37.520
B(a)P	GR	gapfilled	27.168	7.652	255%	19.516
B(a)P	HR	reported	1.920	2.286	-16%	-0.367
B(a)P	IS	reported	0.014	0.017	-19%	-0.003
B(a)P	MC	New reported	0.000	0.032	-100%	-0.032
B(a)P	MK	reported	1.890	2.848	-34%	-0.959
B(a)P	MT	reported	0.008	0.006	34%	0.002
B(a)P	NL	reported	1.949	1.652	18%	0.297
B(a)P	RU	gapfilled	68.651	86.900	-21%	-18.249
B(a)P	RUE	gapfilled	18.249	25.703	-29%	-7.454
B(a)P	SK	New reported	1.150	5.212	-78%	-4.062
B(b)F	AT	gapfilled	2.581	3.038	-15%	-0.458
B(b)F	AZ	new gapfilled	0.420	0.282	49%	0.138
B(b)F	BY	reported	13.457	17.471	-23%	-4.014
B(b)F	DE	reported	1.909	1.373	39%	0.536
B(b)F	ES	gapfilled	45.109	99.102	-54%	-53.992
B(b)F	GR	gapfilled	70.335	10.001	603%	60.334
B(b)F	IS	reported	0.042	0.063	-32%	-0.020
B(b)F	LT	reported	3.366	2.867	17%	0.499
B(b)F	MC	New reported	0.000	0.029	-100%	-0.029
B(b)F	MK	reported	2.069	3.095	-33%	-1.026
B(b)F	MT	reported	0.028	0.013	116%	0.015

Component	Country	Data sources	2017 value (t)	2016 value (t)	Change (%)	Change (t)
B(b)F	NL	reported	1.882	1.520	24%	0.362
B(b)F	RU	gapfilled	74.589	108.960	-32%	-34.370
B(b)F	RUE	gapfilled	19.828	32.228	-38%	-12.400
B(b)F	SE	New reported	3.583	4.451	-19%	-0.867
B(b)F	SK	New reported	1.207	6.728	-82%	-5.522
B(k)F	AT	gapfilled	1.035	1.318	-21%	-0.283
B(k)F	AZ	new gapfilled	0.353	0.223	59%	0.131
B(k)F	BY	reported	3.769	4.722	-20%	-0.953
B(k)F	DE	reported	1.243	1.052	18%	0.192
B(k)F	ES	gapfilled	18.097	42.993	-58%	-24.896
B(k)F	FI	gapfilled	1.342	1.620	-17%	-0.278
B(k)F	GR	gapfilled	30.733	3.436	794%	27.297
B(k)F	IT	gapfilled	10.570	12.930	-18%	-2.361
B(k)F	KG	gapfilled	3.222	2.565	26%	0.657
B(k)F	LT	reported	1.304	1.104	18%	0.200
B(k)F	MC	New reported	0.000	0.039	-100%	-0.039
B(k)F	MK	reported	1.145	1.732	-34%	-0.588
B(k)F	MT	reported	0.008	0.006	27%	0.002
B(k)F	NL	reported	1.007	0.799	26%	0.207
B(k)F	NO	reported	0.978	0.571	71%	0.408
B(k)F	PL	reported	14.347	11.991	20%	2.356
B(k)F	RU	gapfilled	29.924	47.269	-37%	-17.346
B(k)F	RUE	gapfilled	7.954	13.981	-43%	-6.027
B(k)F	SE	New reported	1.281	1.644	-22%	-0.363
B(k)F	SK	New reported	1.062	2.813	-62%	-1.751
Cd	AZ	reported	0.100	0.170	-41%	-0.070
Cd	BE	reported	1.344	2.768	-51%	-1.423
Cd	ES	reported	4.221	7.038	-40%	-2.817
Cd	GB	reported	4.049	3.493	16%	0.556
Cd	GR	gapfilled	1.398	2.000	-30%	-0.602
Cd	LU	reported	0.070	0.084	-16%	-0.014
Cd	MC	New reported	0.000	0.001	-65%	-0.001
Cd	MT	reported	0.001	0.006	-84%	-0.005
Cd	NL	reported	0.765	0.653	17%	0.112
Cd	PT	reported	4.602	3.583	28%	1.018
Cd	UA	gapfilled	3.696	16.340	-77%	-12.644
PCDD/F	CY	reported	0.000	0.000	46%	0.000
PCDD/F	HR	reported	0.000	0.000	-21%	0.000
PCDD/F	HU	reported	0.000	0.000	-17%	0.000

Component	Country	Data sources	2017 value (t)	2016 value (t)	Change (%)	Change (t)
PCDD/F	IS	reported	0.000	0.000	94%	0.000
PCDD/F	KG	gapfilled	0.000	0.000	41%	0.000
PCDD/F	LU	reported	0.000	0.000	-22%	0.000
PCDD/F	LV	reported	0.000	0.000	16%	0.000
PCDD/F	MC	New reported	0.000	0.000	-100%	0.000
PCDD/F	MK	reported	0.000	0.000	-27%	0.000
PCDD/F	MT	reported	0.000	0.000	2141%	0.000
PCDD/F	PT	reported	0.000	0.000	-47%	0.000
PCDD/F	RO	reported	0.000	0.000	22%	0.000
PCDD/F	RU	gapfilled	0.001	0.001	-21%	0.000
PCDD/F	RUE	gapfilled	0.000	0.000	-29%	0.000
PCDD/F	UA	gapfilled	0.001	0.000	135%	0.000
PCDD/F	UZ	gapfilled	0.000	0.000	22%	0.000
HCB	AZ	new gapfilled	0.000	0.000	-73%	0.000
HCB	BE	reported	0.035	0.006	531%	0.030
HCB	BY	reported	0.001	0.001	35%	0.000
HCB	ES	reported	0.002	0.001	52%	0.001
HCB	FI	reported	0.034	0.059	-43%	-0.026
HCB	GB	reported	0.036	0.031	17%	0.005
HCB	IE	reported	0.002	0.002	19%	0.000
HCB	IT	reported	0.011	0.022	-49%	-0.011
HCB	KZT	new gapfilled	0.001	0.001	39%	0.000
HCB	LU	reported	0.000	0.001	-24%	0.000
HCB	MC	New reported	0.000	0.000	-100%	0.000
HCB	ME	gapfilled	0.002	0.003	-45%	-0.001
HCB	MK	reported	0.007	0.006	20%	0.001
HCB	MT	reported	0.000	0.000	4489%	0.000
HCB	PL	reported	0.004	0.005	-18%	-0.001
HCB	PT	reported	0.059	0.049	21%	0.010
HCB	RU	gapfilled	0.005	0.007	-24%	-0.002
HCB	RUE	gapfilled	0.002	0.002	-24%	-0.001
HCB	SK	reported	0.003	0.001	150%	0.002
Hg	FR	reported	3.795	3.227	18%	0.567
Hg	BE	reported	1.050	1.374	-24%	-0.324
Hg	BY	reported	0.270	0.198	36%	0.072
Hg	GR	gapfilled	1.647	2.148	-23%	-0.500
Hg	HU	reported	1.342	1.167	15%	0.175
Hg	LT	reported	0.146	0.105	38%	0.040
Hg	LU	reported	0.063	0.120	-48%	-0.058

Component	Country	Data sources	2017 value (t)	2016 value (t)	Change (%)	Change (t)
Hg	MC	New reported	0.004	0.002	183%	0.003
Hg	MT	reported	0.026	0.004	518%	0.022
Hg	SK	reported	1.250	1.726	-28%	-0.476
Hg	UA	gapfilled	5.394	24.164	-78%	-18.769
IP	AT	gapfilled	1.838	1.531	20%	0.307
IP	AZ	new gapfilled	0.080	0.226	-65%	-0.146
IP	BA	gapfilled	1.185	1.414	-16%	-0.229
IP	BY	reported	3.937	5.100	-23%	-1.163
IP	ES	gapfilled	32.125	49.935	-36%	-17.810
IP	FI	gapfilled	2.382	1.881	27%	0.500
IP	GR	gapfilled	21.600	5.498	293%	16.102
IP	HR	reported	1.068	1.287	-17%	-0.219
IP	IS	reported	0.010	0.018	-44%	-0.008
IP	IT	gapfilled	18.763	15.018	25%	3.745
IP	KG	gapfilled	2.716	4.055	-33%	-1.339
IP	MC	New reported	0.000	0.014	-99%	-0.014
IP	MK	reported	1.205	1.829	-34%	-0.624
IP	MT	reported	0.007	0.006	26%	0.001
IP	NL	reported	0.944	0.808	17%	0.136
IP	SE	New reported	1.625	2.361	-31%	-0.737
IP	SK	New reported	0.667	3.846	-83%	-3.179
PAH	BY	reported	28.024	36.168	-23%	-8.144
PAH	DE	new gapfilled	32.816	181.621	-82%	-148.805
PAH	ES	reported	136.850	271.067	-50%	-134.217
PAH	GR	gapfilled	149.837	26.587	464%	123.250
PAH	IS	reported	0.092	0.130	-29%	-0.038
PAH	MC	New reported	0.000	0.114	-100%	-0.114
PAH	MK	New reported	6.367	9.504	-33%	-3.137
PAH	MT	reported	0.051	0.030	66%	0.020
PAH	NL	reported	5.783	4.779	21%	1.003
PAH	RU	gapfilled	226.283	298.031	-24%	-71.748
PAH	RUE	gapfilled	60.151	88.150	-32%	-27.999
PAH	SE	reported	10.286	12.581	-18%	-2.294
PAH	SK	reported	4.059	18.599	-78%	-14.540
Pb	AM	New reported	3.710	5.034	-26%	-1.324
Pb	AZ	reported	2.065	2.936	-30%	-0.870
Pb	CH	reported	14.939	19.183	-22%	-4.244
Pb	CY	reported	18.454	26.794	-31%	-8.339
Pb	ES	reported	100.099	153.004	-35%	-52.905

Component	Country	Data sources	2017 value (t)	2016 value (t)	Change (%)	Change (t)
Pb	GB	reported	94.614	64.429	47%	30.184
Pb	GR	gapfilled	8.202	14.659	-44%	-6.458
Pb	IE	reported	5.084	13.400	-62%	-8.316
Pb	LV	reported	3.453	2.674	29%	0.779
Pb	MC	New reported	0.015	0.012	24%	0.003
Pb	MT	reported	0.187	0.751	-75%	-0.563
Pb	PL	reported	305.490	418.318	-27%	-112.828
Pb	RS	reported	54.804	38.574	42%	16.229
Pb	UA	New reported	102.434	85.464	20%	16.971
PCB	BE	reported	0.003	0.006	-52%	-0.003
PCB	BG	reported	0.004	0.003	21%	0.001
PCB	BY	reported	0.009	0.012	-22%	-0.003
PCB	EE	reported	0.005	0.004	20%	0.001
PCB	FI	New reported	0.026	0.000	NEW	0.026
PCB	GE	New reported	0.380	0.000	NEW	0.380
PCB	KG	gapfilled	0.005	0.000	NEW	0.005
PCB	LT	reported	0.002	0.001	32%	0.000
PCB	MC	New reported	0.000	0.000	21044%	0.000
PCB	MK	reported	0.025	0.008	234%	0.018
PCB	MT	reported	0.000	0.000	3573%	0.000
PCB	NL	New reported	0.000	0.000	NEW	0.000
PCB	PT	reported	0.096	1.095	-91%	-1.000
PCB	RO	reported	0.019	1.095	-98%	-1.077
PCB	UA	New reported	0.001	0.000	NEW	0.001

APPENDIX A3

Overview of gap-filling in 2019

	Cd	Hg	Pb
Albania	X	X	X
Armenia	X	X	X
Aral Lake	-	-	-
Asian Areas	X	X	X
Austria	X	X	X
Atlantic Ocean	-	-	-
Azerbaijan	X	X	X
Bosnia and Herzegovina	X	X	X
Baltic Sea	-	-	-
Belgium	X	X	X
Bulgaria	X	X	X
Black Sea	-	-	-
Belarus	X	X	X
Caspian Sea	-	-	-
Switzerland	X	X	X
Cyprus	X	X	X
Czechia	X	X	X
Germany	X	X	X
Denmark	X	X	X
Estonia	X	X	X
Spain	X	X	X
Finland	X	X	X
France	X	X	X
United Kingdom	X	X	X
Georgia	X	X	X
Greece	X	X	X
Croatia	X	X	X
Hungary	X	X	X
Ireland	X	X	X
Iceland	X	X	X
Italy	X	X	X

	Cd	Hg	Pb
Kyrgyzstan	X	X	X
Kazakhstan	X	X	X
Liechtenstein	X	X	X
Lithuania	X	X	X
Luxembourg	X	X	X
Latvia	X	X	X
Monaco	X	X	X
Republic of Moldova	X	X	X
Montenegro	X	X	X
Mediterranean Sea	-	-	-
North Macedonia	X	X	X
Malta	X	X	X
Netherlands	X	X	X
Norway	X	X	X
North Africa	X	X	X
North Sea	-	-	-
Poland	X	X	X
Portugal	X	X	X
Romania	X	X	X
Serbia	X	X	X
Russian Federation	X	X	X
Russian Federation in the extended EMEP domain	X	X	X
Sweden	X	X	X
Slovenia	X	X	X
Slovakia	X	X	X
Tajikistan	X	X	X
Turkmenistan	X	X	X
Turkey	X	X	X
Ukraine	X	X	X
Uzbekistan	X	X	X

X	*Reported (also in previous years!)*
X	*Partly replaced*
X	*Replaced*
X	*Partly expert estimates/reported data*
X	*Expert estimates only*